SYNTHESIS AND CHARACTERIZATION OF MAGNETORHEOLOGICAL (MR) FLUID FOR DIFFERENT ENGINEERING APPLICATIONS

Thesis
Submitted in partial fulfillment of the requirements for the degree of

DOCTOR OF PHILOSOPHY

by

SUBASH ACHARYA

DEPARTMENT OF MECHANICAL ENGINEERING
NATIONAL INSTITUTE OF TECHNOLOGY KARNATAKA,
SURATHKAL, MANGALORE – 575025
October 2021

SYNTHESIS AND CHARACTERIZATION OF MAGNETORHEOLOGICAL (MR) FLUID FOR DIFFERENT ENGINEERING APPLICATIONS

Thesis

Submitted in partial fulfillment of the requirements for the degree of

DOCTOR OF PHILOSOPHY

by

SUBASH ACHARYA

Under the guidance of

Dr. Hemantha Kumar

Associate Professor

DEPARTMENT OF MECHANICAL ENGINEERING

NATIONAL INSTITUTE OF TECHNOLOGY KARNATAKA,

SURATHKAL, MANGALORE – 575025

October 2021

DECLARATION

I hereby *declare* that the Research Thesis entitled **"SYNTHESIS AND CHARACTERIZATION OF MAGNETORHEOLOGICAL (MR) FLUID FOR DIFFERENT ENGINEERING APPLICATIONS"** which is being submitted to the **National Institute of Technology Karnataka, Surathkal** in partial fulfillment of the requirements for the award of the Degree of **Doctor of Philosophy** in **Department of Mechanical Engineering** is a *bonafide report of the research work carried out by me.* The material contained in this Research Thesis has not been submitted to any University or Institution for the award of any degree.

Register Number   : **165127ME16F19**

Name of the Research Scholar   : **Subash Acharya**

Signature of the Research Scholar   : *Subash*

Department of Mechanical Engineering

Place   : **NITK, Surathkal**

Date   : 05|10|2021

C E R T I F I C A T E

This is to *certify* that the Research Thesis entitled "SYNTHESIS AND CHARACTERIZATION OF MAGNETORHEOLOGICAL (MR) FLUID FOR DIFFERENT ENGINEERING APPLICATIONS" submitted by **Mr. Subash Acharya (Register Number: 165127ME16F19** as the record of the research work carried out by him, is *accepted as the Research Thesis submission* in partial fulfillment of the requirements for the award of degree of **Doctor of Philosophy.**
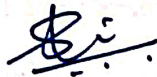
Research Guide

05/10/2021

Dr. Hemantha Kumar

Associate Professor

Department of Mechanical Engineering

NITK, Surathkal

Chairman - DRPC

ACKNOWLEDGEMENTS

Subash Acharya

ABSTRACT

Magnetorheological fluid (MRF) are suspensions of iron particles in a carrier oil. They are controllable smart fluid whose rheological properties change under the application of magnetic field. The design of Magnetorheological (MR) device and the composition of MR fluid used in it have a significant effect on its performance. In this study, MRF composition suitable for MR damper, MR brake and MR beam were determined based on optimization. Initially, the key ingredient of MRF, that is, iron particles of different average sizes, were characterized to determine their morphology, particle size distribution and magnetic properties. The morphology of iron particles were observed using Field Emission Scanning Electron Microscope. The particle size distribution was measured using particle size analyzer. The magnetic properties of different iron particles were measured using vibrating sample magnetometer.

In the first part of this study, optimal dimensions of MR damper and composition of MRF suitable for MR damper were determined. A shear mode monotube MR damper was designed by using optimization technique. A damper was manufactured in accordance with the optimized size and was filled with commercially available commercial MR fluid, MRF 132DG (Lord Corporation) to determine its damping characteristics using damper testing machine. Experimentally determined values were validated with computational ones. Further, six MR fluid samples (MRFs) were prepared composed of combination of three different particle mass fractions and two sizes of iron particles. Rheological tests were conducted on these samples to determine the flow curves at off-state and on-state magnetic field conditions and they were compared with those of commercial MR fluid, MRF 132DG (Lord Corporation). In addition, the sedimentation stability of prepared fluid were examined. These MRFs were filled in the MR damper and their damper characteristics were determined. The area bounded by the force-displacement graphs was used to calculate the energy dissipated which was then used to calculate equivalent damping coefficient. Finally, using multi-objective genetic algorithm (MOGA) optimization, based on maximization of on-state damping coefficient and minimization of off-state damping coefficient, the optimal mass fraction and particle size was determined.

iii

In the next part of the study, optimal dimensions of MR brake and composition of MRF suitable for MR brake were determined. At first, optimum dimensions of MR brake were computed considering the properties of commercially available MRF132DG fluid using MOGA optimization. Maximization of field induced braking torque and minimization of off-state torque were chosen as the objectives. This was performed in MATLAB software coupled with magnetostatic analyses in ANSYS APDL software. The braking torque of designed and fabricated MR brake utilizing commercial MR fluid, MRF 132DG (Lord Corporation) was experimentally determined and validated with computational ones. Selection of optimal composition of MRF was done considering In-house MR fluid samples composed of different combinations of particle mass fractions, mean particle diameters and base oil viscosities. A design of experiments technique was employed and braking torque corresponding to the synthesized MRFs at different speeds and current supplied along with the variation of shaft speed during braking process were measured. Based on the experimental results, MOGA optimization technique was used to determine optimal MR fluid composition with the objectives of maximizing field induced braking torque and minimizing off-state torque.

Further, the effect of particle size and mass fraction of iron powder in the MRF on the vibration behaviour of MRF sandwich beams were studied. Six MRFs composed of combination of two particle sizes and three mass fractions of carbonyl iron powder were prepared and their viscoelastic properties were measured. The MRFs were used to fabricate different MRF core aluminium sandwich beams. Additionally, a sandwich beam with commercially available commercial MR fluid, MRF 132DG (Lord Corporation) as core was fabricated. The modal parameters of the cantilever MRF sandwich beams were determined at different magnetic fields. Further, sinusoidal sweep excitation tests were performed on these beams at different magnetic fields to investigate their vibration suppression behaviour. Finally, optimal particle size and mass fraction of iron powder suitable for sandwich beam were determined based on maximization of damping ratio and minimization of mass of MRF.

Keywords: MR fluid, MR damper, MR brake, MR sandwich beam, Magnetostatic analyses, Multi-objective GA Optimization, Damping ratio, Vibration control.

CONTENTS

x

LIST OF FIGURES

xiv

LIST OF TABLES

ABBREVIATIONS & NOTATIONS

MR	Magnetorheological
MRF	Magnetorheological fluid
MRFs	Magnetorheological fluid samples
AWG	American wire gauge
CIP	Carbonyl iron powder
DC	Direct Current
FESEM	Field Emission Scanning Electron Microscope
DOE	Design of Experiments
ANOVA	Analysis of variance
GA	Genetic Algorithm
MOGA	Multi-Objective Genetic Algorithm
DAQ	Data Acquisition
ER	Electrorheological
PAO	Polyalphaolefin
Lp	Length of piston (m)
L	Piston Flange height (m)
w	Mean circumference of shear gap (m)
Dp	Diameter of piston (m)
t	MR fluid shear gap thickess (m)
μ	Apparent viscosity without magnetic field (Pa-s)
τ_y	Dynamic yield stress (Pa)
d_r	Diameter of piston rod (m)
Q	Volumetric flow rate (m^3/s)
v	Relative velocity between piston and cylinder (m/s)
A_p	Piston area (m^2)
K_d	Dynamic range
F	Total damping force (N)
F_μ	Viscous damping force (N)
F_τ	Field induced damping force (N)

T_B	Total braking torque (Nm)
T_η	Off-state or viscous torque (Nm)
T_{MR}	Controllable field induced torque (Nm)
η	Apparent viscosity of the fluid (without magnetic field)
n	Number of surfaces in contact with MR fluid
ω	Angular velocity of the disc (rad/s)
$\tau(H,r)$	Yield stress as a function of magnetic field intensity in the MR fluid and disc radius (Pa)
r_o	Brake disc radius (m)
r_2	MR Brake bobbin radius (m)
r_1	MR brake casing radius (m)
ω_n	Natural frequency (rad/s)
ζ	Damping ratio
G*	Complex shear modulus

Chapter 1

INTRODUCTION

Smart materials are progressively implemented in many technologies due to their inherent advantages over their conventional counterparts. Smart devices are designed to use the properties of smart materials in such a way that they respond to variations in external conditions such as such as temperature, magnetic field, electric field, light, stress field, etc. in a predetermined controllable manner. The different types of smart materials include biomatic polymers and gels, controllable magnetorheological (MR) and Electrorheological (ER) fluids, MR elastomers, MR composites, shape memory alloys and polymers, piezoelectric polymers, electro-active polymers, piezoelectric and electrostrictive ceramics, magnetostrictive materials, liquid crystals, etc. Smart materials have a great potential in applications such as semi-active vibration control, noise reduction, shape control, smart machines, health monitoring and micro-mechanical systems with spectacular engineering applications in motor industry, aircraft, aerospace,mechanical engineering, civil structures, medical technology, micro-system technology, etc (Gołdasz and Bogdan 2014).

MR fluid and ER fluid are smart materials consisting of solid particles in a non-conductive carrier fluid which respond to magnetic and electric fields respectively. MR fluid and ER fluid were first reported by Rabinow (1948) and Winslow (1947) respectively who discovered changes in the rheological properties with external field and made efforts to implement in various devices. Commercialization of the same was hindered due to technological limitations and cost factors. However, from the year 1990 onwards, a plethora of research were undertaken which lead to their successful implementation in several devices with more applications using MR fluid due to their advantages over ER fluid. ER fluid require higher voltage for their operation and there is electrical breakdown at high voltages while MR fluids operate at a lower voltage. ER fluid are more sensitive to temperature while MR fluid are less temperature dependent and more stable. Moreover, MR fluid generate much higher yield stresses than that of ER fluid.

1.1 MAGNETORHEOLOGICAL FLUID

Magnetorheological fluid are suspensions of micron sized, non-colloidal, low-coercivity magnetizable particles in a carrier fluid. When subjected to an external magnetic field, they change from a liquid to that of a semi-solid and the changes are reversible and occurs in a fraction of a second. Instantaneous controllable MRF properties upon application of external magnetic field have been exploited in broad spectrum of engineering applications such as seat dampers, shock absorbers, brakes, clutches, engine mounts, polishing devices, valves, robotics, dampers for vibration control and many more potential applications (Ahamed et al. 2018; Bicchi et al. 2005; Klingenberg 2001; Muhammad et al. 2006; Seung-Bok Choi 2013; Wang and Meng 1948). Although there are plethora of research and publications pertaining to MR devices, very few have been successfully commercialized such as MR dampers for suspensions, seats, mounts, prosthetics, brakes, beams, and tactile feedback device (Gilbert and Jackson 2005; Spaggiari et al. 2019). MR brakes are one of the MR devices which have grabbed the attention of researchers in the recent past owing to their bright potential in replacing conventional brakes in several applications. Though the first patent on MRF and MR brake was filed by Jacob Rabinow (Jacob 1951), it took several decades for the first commercialization of MR brake in aerobic exercise equipment due to its lower cost compared to its counterpart (Webb 1998). Nevertheless, tremendous torque requirement, temperature rise in the fluid and In-use thickening of MRFs (Carlson 2002) pose a major impediment for implementation of MR brakes in various applications.

The iron particles are randomly distributed in the MR fluid in the absence of magnetic field as shown in figure 1.1 (a). However, when magnetic field is applied by placing permanent magnets or using electromagnet, the iron particles acquire a dipole moment aligned with the external field and form chain like structure as depicted in figure 1.1 (b). This chain formation causes a yield stress in the MR fluid. Also, MR fluid yield stress is continuously and instantaneously controllable as it responds to the magnitude of the magnetic field applied. This leads to quick response and continuously varying force of devices employing MR fluid.

(a) Without magnetic field   (b) Under magnetic field
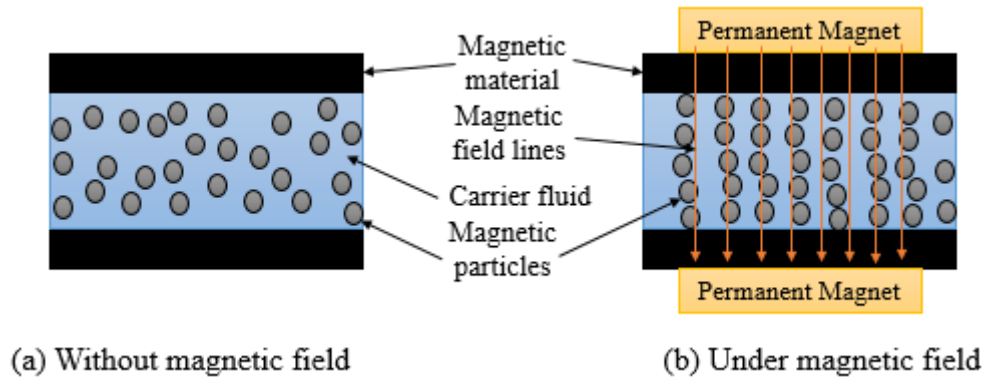
Figure 1.1 MR fluid behavior with and without magnetic field (Courtesy: Choi and Han 2012)

In the absence of magnetic field, the behavior of MR fluid can be described as Newtonian, while it exhibits distinct non-Newtonian behavior (Bingham) in the presence of magnetic field. Rheology of MR fluid is characterized into two regimes: pre-yield and post-yield conditions whose constitutive equations are given by the following (Jolly et al. 1999):

$$\tau = G^{*}.\gamma , \qquad\qquad \tau < \tau_y \qquad\qquad (1.1)$$

$$\tau = \tau(B) + \mu .\dot{\gamma}, \qquad \tau > \tau_y \qquad\qquad (1.2)$$

where, γ is shear strain, is shear rate, $\tau(B)$ is field dependent or dynamic yield stress, μ is post-yield viscosity, B is magnetic flux density, G* is complex shear modulus and τ is shear stress of MR fluid.
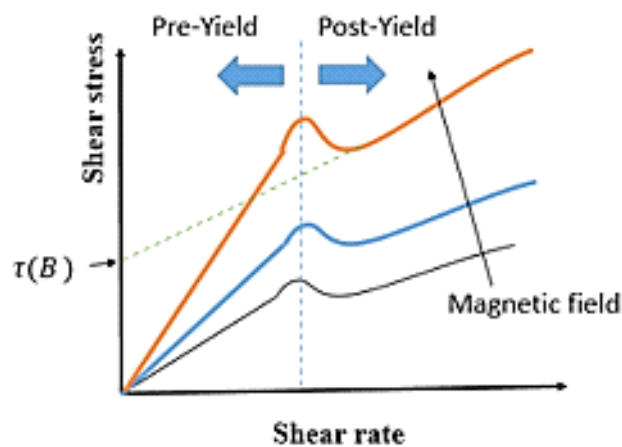
Figure 1.2 Flow curves for different magnetic flux densities

(Courtesy: Choi and Han 2012)

The dynamic yield shear stress increases with increment in magnetic field. In the absence of magnetic field, the shear stress of the fluid is due to its own viscosity and is termed as viscous-induced shear stress. In the presence of magnetic field, the fluid shear stress comprises of two components, namely, viscous-induced shear stress and field-dependent yield shear stress. The field-dependent yield shear stress of MR fluid is evaluated by adopting two rheological regimes of MR fluid as shown in figure 1.2. In the pre-yield region, MR fluid behaves like a linear viscoelastic material, a non-linear viscoelastic material in the yield region and a plastic material in the post-yield region. The rheological property in the post-yield region namely field-dependent dynamic yield shear stress is considered in the design of MR fluid devices like dampers, brakes, clutches, etc. In the design of smart structures such as MR fluid sandwich beams and MR elastomer sandwich beams for vibration control, the field-dependent complex modulus in the pre-yield region is the significant property considered. (Choi and Han 2012).

1.1.1 MR fluid components
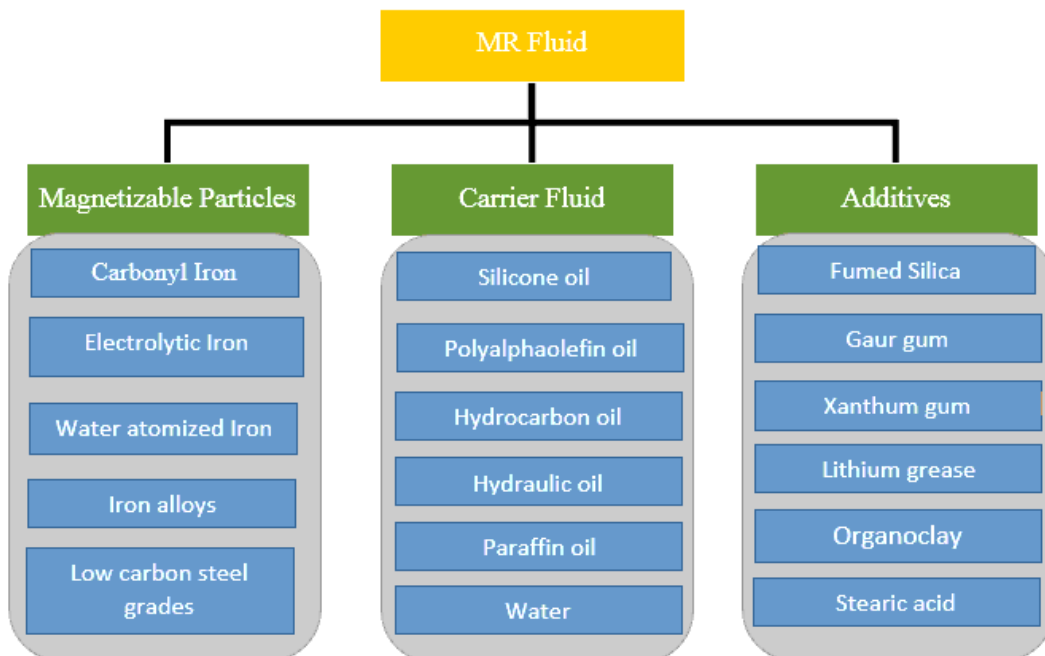
Figure 1.3 MR fluid Constituents

MR fluid consists of three main components, namely carrier fluid, magnetizable particles and additives. The magnetisable particles are suspended in the carrier fluid. The carrier fluid is selected with respect to its rheological characteristics temperature stability, magnetorheological effect, compatibility with magnetic particles and chemical stability. Petroleum based oils, mineral oils, silicone oil, polyalphaolefin oil, polyester, polyether, water, industrial hydrocarbon oils and synthetic oils are some of the most commonly used carrier fluid for preparation of MR fluid. Magnetizable materials are used as dispersed phase in the preparation MR fluid. Magnetizable particles used are ferrite-polymer, iron–cobalt alloy, carbonyl iron, water atomized iron, electrolytic iron, nickel–zinc ferrites, iron and its compounds. Carbonyl iron particles and its alloys have the high saturation magnetization and cost effective compared to other particles. These particles demonstrate a low magnetic coercivity which is very essential for reversibility of MR effect. The volume fraction of magnetizable particles is usually in the range from 20–50 %. A combination of small percentage of additives are added to the MR fluid suspension to prevent particle settling due to gravity, increase redispersibility of particles, enhance lubrication, reduce oxidation and produce a stable suspension. Commonly used additives include fumed silica, gaur gum, Xanthum gum, lithium grease, organoclay, stearic acid, etc. Figure 1.3 shows the some of the important constituents of MR fluid (Ashtiani et al. 2015).

1.1.1 MR Fluid operation modes

The MR fluid can be used with four different operating modes for different engineering applications which are flow mode, shear mode, squeeze mode and pinch mode (Jolly et al. 1999).

(a) Flow Mode   (b) Shear mode
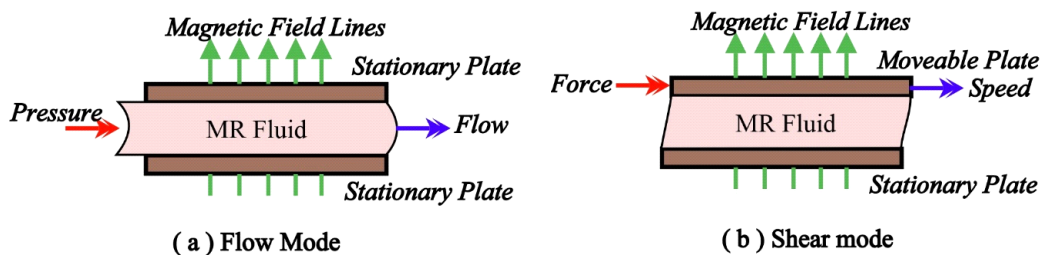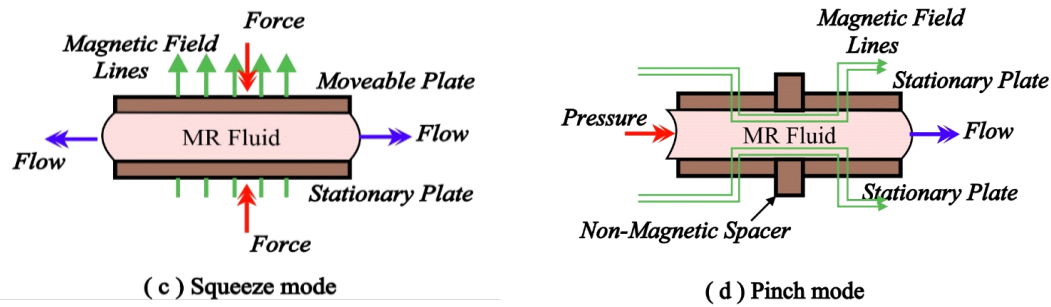
Figure 1.4 MR fluid operation modes (a) Flow mode, (b) Shear mode, (c) Squeeze mode and (d) Pinch mode (Courtesy: De Vicente et al. 2011)

The MR fluid flows due a pressure difference between two stationary planar or concentric surfaces in flow mode of operation as shown in figure 1.4 (a). The magnetic field is applied normal to the fluid flow direction which causes changes in the rheological properties of the fluid. MR dampers for vehicle suspensions are designed to operate in flow mode due to greater force which can be attained. Figure 1.4 (b) shows shear mode of operation of MR fluid in which fluid flows between two surfaces which move relative to each other and the magnetic field is perpendicular to the fluid flow direction. Rotary dampers, brakes, clutches and steering dampers are examples of devices which use this mode. Figure 1.4 (c) shows MR fluid operating in Squeeze mode in which the MR fluid is contained between two planar parallel surfaces. Based on predetermined displacement or force input, the distance between the surfaces is varied. It is used in applications in which magnitude of vibration is small. Devices utilizing this mode include MR mounts and high force small stroke linear dampers. In pinch mode, the MR fluid flows between two surfaces as in the case of valve mode while the application of magnetic field is almost parallel to the direction of fluid flow as shown in figure 1.4 (d). The poles are arranged axially along the flow path and separated by a non-magnetic spacer. This design leads to application of highly non-uniform magnetic field inside the MR fluid as compared to other modes of operation (Gołdasz and Bogdan 2014). When field is applied, the fluid solidifies only near the walls which causes a change in the effective orifice diameter through which it flows instead of throughout the valve length as in case of valve mode (Goncalves and Carlson, 2009).

6

1.2 MAGNETORHEOLOGICAL DAMPER

Dampers are used to absorb or dissipate the energy of undesirable vibration induced in a variety of applications. There are three types of dampers, namely, passive, active, and semi-active, which are used in accordance with the cost, safety, comfort among other criteria. Passive dampers are presently used to a larger extent as they are cheaper, though they have many limitations. The characteristics of a passive damper are constant which are designed by based on application requirements. However, an active damper controls the vibration by adding or dissipating energy from the system using actuator which is actuated by a controller based on sensor signal. An external energy source is required to supply large amount of power to the actuator which significantly adds to products cost. The limitations of passive and active dampers are overcome by a semi-active damper which is cost effective, requires less energy to function and yet has good performance compared to them. A semi-active device requires smaller amount of external power to control the level of damping and to operate controller and sensors. A magnetorheological damper is widely used semi-active device which alters the damping coefficient by application of magnetic field in accordance with the control strategy of the controller. The MR damper consists of piston reciprocating in a cylinder similar to conventional damper. It uses MR fluid in place of oil and the piston is incorporated with electromagnetic coil which obtains control current from a controller. The MR fluid's viscosity is varied by inducing magnetic field due to application of current in real time. Using control strategy, desired magnitude of current is provided to the coil so that magnetic field produced will induce necessary damping force in the system.

1.3 TYPES OF MR DAMPER

The MR dampers are classified mainly into three types based on their construction, namely:

- Mono tube damper
- Twin tube damper and
- Twin rod single tube damper
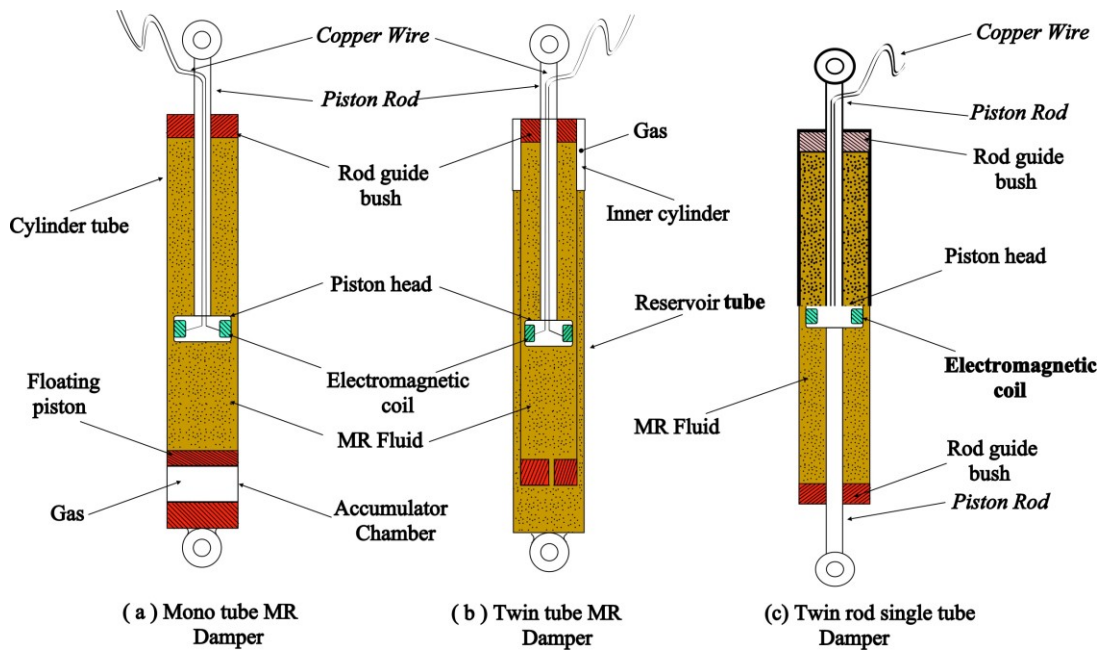
Figure 1.5 Types of MR Damper (Courtesy: Moghadam 2020)

The mono tube MR damper consists of single cylinder for piston, MR fluid and an accumulator for accommodating volume changes during piston rod movement. There is a floating piston which separates the MR fluid from the accumulator chamber which consists of high-pressure nitrogen gas as shown in figure 1.5(a). An annular gap between piston and cylinder permits fluid to flow between the chambers while piston is in motion. When current is supplied to piston coil, the MR fluid in the shear gap is subjected to magnetic field due to which it offers more resistance to fluid flow thus inducing more damping force. To avoid cavitation, high pressure gas is necessary in accumulator below the floating piston. However, it requires very high surface finish on cylinder inner surface, sealing requirements and friction. The twin tube MR damper shown in figure 1.5 (b) consists of two tubes, one mounted inside the other. MR fluid is completely filled in the inner tube while it is partially filled in the space between inner and outer tube. Either air at atmospheric pressure or some inert gas at high pressure occupies the remaining space in outer tube. A base valve separates the inner and outer tubes. Inner tube houses the piston and the volume changes occurring during the piston rod movement is accommodated by the MR fluid moving from inner tube to outer tube through the base valve. This configuration does not require high precision machining as in the case of

monotube MR damper. In twin rod single tube MR damper as depicted in figure 1.5(c), piston has piston rods on either side of it and protrudes from either ends of damper cylinder. It does not need an accumulator as there is no volume changes during piston movement. It finds applications in Gun recoil mechanism, bicycle applications, building applications to protect it from earthquake and wind flow.

Table 1.1. Comparison of different types of MR dampers

	Mono tube MR damper	Twin tube MR damper	Twin rod single tube MR damper
Construction	Consists of single cylinder and hence compact.	Consists of two cylinders one inside the other.	Consists of single cylinder but has piston rods on either side of piston.
Accommodating Volume changes	Accumulator chamber is provided below floating piston which consists of high-pressure nitrogen gas	MR fluid moving from inner tube to outer tube through the base valve.	It does not need an accumulator as there is no volume changes during piston movement.
Manufacturing considerations	It requires very high surface finish on cylinder inner surface, sealing requirements and friction.	This configuration does not require high precision machining as in the case of monotube MR damper.	This configuration does not require high precision machining as in the case of monotube MR damper.

1.4 MAGNETORHEOLOGICAL BRAKE

Conventional hydraulic brakes are the commonly used type of brakes in many mechanical systems. However, it has limitations such as brake pad wear necessitating periodic replacement, low braking performance in high speed, also high temperature effect, bulky size, heavy weight, delayed response time of 200-300 milliseconds owing to pressure build up in the hydraulic lines (Karakoc et al. 2008a). On the other hand, MR brakes when compared to conventional hydraulic brakes have quicker response, easier implementation of a new controller, lesser maintenance since there is no material wear and lower weight as it does not require additional auxiliary components. Hence, MR brakes have a great potential in replacing Conventional hydraulic brakes due to their benefits.
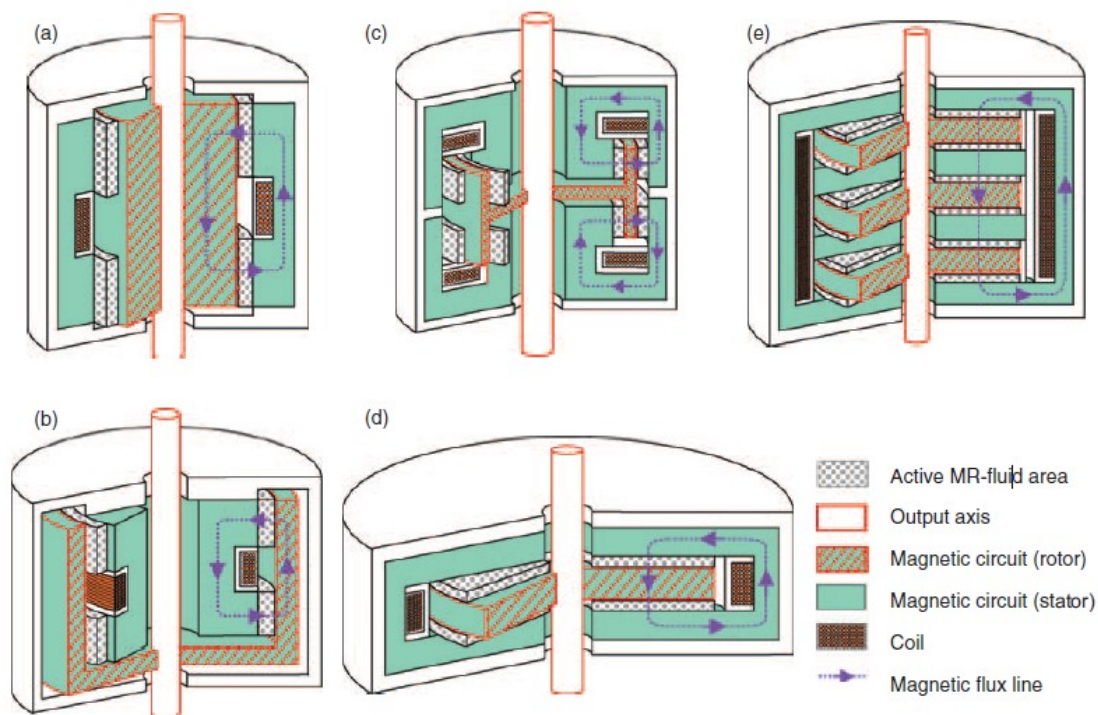
Figure 1.6 Different MR brake designs: (a) drum, (b) inverted drum, (c) T-shaped rotor, (d) disk, and (e) multiple disks (Avraam et al. 2010)

A MR brake consists of four main components namely rotor, housing or stator, electromagnetic coil and MR fluid. MR fluid is filled between rotor disk and stator with electromagnetic coil embedded or wound on the stator. When braking is to be applied,

current is supplied to the coils in the brake which sets up a magnetic field around it causing a change in the viscosity of the MR fluid, thus causing a braking action on the rotor surface. Different configurations of MR brakes such as single disk brakes, multi-disk brakes, drum brakes, inverted drum brakes and T-shaped rotor brakes with various coil designs have been designed by many researchers as shown in figure 1.6 (Avraam et al. 2010). However, single disk MR brakes are compact, lighter in weight and very easy to manufacture. Drum brake shown in figure 1.6 (a) has rotor of cylindrical shape and is easier to manufacture but has larger inertia and low torque to volume ratio. Figure 1.6 (b) shows inverted drum brakes which are more compact and have hollow rotor which houses the coil and reduces the rotor inertia compared to drum brakes. The T-shaped rotor brake shown in figure 1.6 (c) produces higher torque due to larger area of MR fluid subjected to MR effect at the periphery of rotor. However, it is complex and hence difficult to manufacture. Simple disk MR brakes shown in figure 1.6 (d) are preferred as they are compact, lighter in weight and very easy to manufacture. It was first application of MR fluid published by Rabinow when he had invented MR fluid. Multiple disk brakes shown in figure 1.6 (e) consists of many disks and are used in systems where high torque to volume or torque to weight ratios are required such as prosthetics, orthotics and automotive applications. Nevertheless, they are complex to manufacture.

1.5 MAGNETORHEOLOGICAL FLUID SANDWICH BEAM

Vibration occurs when a system is displaced from its stable equilibrium position and creates undesirable changes to the characteristics of systems as they produce stresses, energy losses, wear, fatigue and induce human discomfort. They occur in machines, dynamic systems and structures. The reduction of such undesirable noise and vibration is important in mechanical systems. Present technologies in machines and structures adopt lighter materials for better performance but, due to this there has been reduction in damping in the system. Therefore, increase in damping is highly necessary for the systems at higher operating speeds utilising the modern lightweight materials. The increase in damping also helps in reducing the resonance of the system for better dynamic performance. For structures general materials were preferred in previous decades, but in recent year there has been adoption of sandwich structures for

automobile, aerospace and construction applications. In addition to these, laminated sandwich structures have been implemented in marine and space vehicles due to their high strength, less weight, cost effective, durable and less maintenance costs. When the structures are under the continuous external dynamic forces, they tend to lose their strength and undergo fatigue which finally leads to failure of the system. The natural frequency of the system should be determined, then the effect of resonance can be reduced using different damping methods. The structural vibration can be controlled by modifying properties like stiffness, mass, shape and by providing passive, active or semi-active counter forces. Passive damping methods in the form of viscoelastic layer were the only way to reduce the undesirable effects of external forces and vibration. But it had limitations such as variable stiffness effect and damping properties. The use of active vibration control techniques has its own set of properties to develop damping continuously for variation in external forces. But, this process is very complicated and expensive to operate.

Vibration in structures such as beams can be damped using a damping layer, i.e. either on the surface or sandwiched between two or more layers of the beam. Surface damping techniques are another form of damping methods which are very easy to operate and are widely used to solve such problems. This method is classified into two configurations, one is unconstrained or surface layer damping and the other is constrained layer damping. In unconstrained layer damping, the damping layer is put on the outside layer of the system, therefore when the system is subjected to continuous force, the damping layer undergoes tensile or compressive deformation. For constrained layer damping the damping layer is placed between two elastic layers. When the forces are applied to the structure, the damping layer undergoes shear deformation. Constrained layer damping (CLD) approach is considered to be one of the effective methods to reduce the vibration. Various constrained layer damping techniques can be implemented to minimize the vibration of the system, using viscoelastic damping layer viz. elastic core, elastomer between the two layers, viscoelastic layers in the form of smart fluids like electrorheological fluids (ERF), magnetorheological fluids (MRF) and magnetorheological elastomer (MRE). The constrained damping layers are the main materials used in semi-active damping system. The semi-active damping control

method are used for various structural vibration control applications. They offer better performance than the active damping method with minimal maintenance and complexity. Widely used semi-active controllable fluids are electro-rheological (ER) fluid and magneto-rheological (MR) fluids because of their controllable rheology and damping properties with less power input. MR fluids have better dynamic yield strength, better temperature stability and contaminants compared to ER fluids. In this study, MR fluid based semi active control technique is studied. A magnetorheological fluid sandwich structure consists of a MR fluid sandwiched between two metallic or non-metallic face plates as shown in figure 1.7.
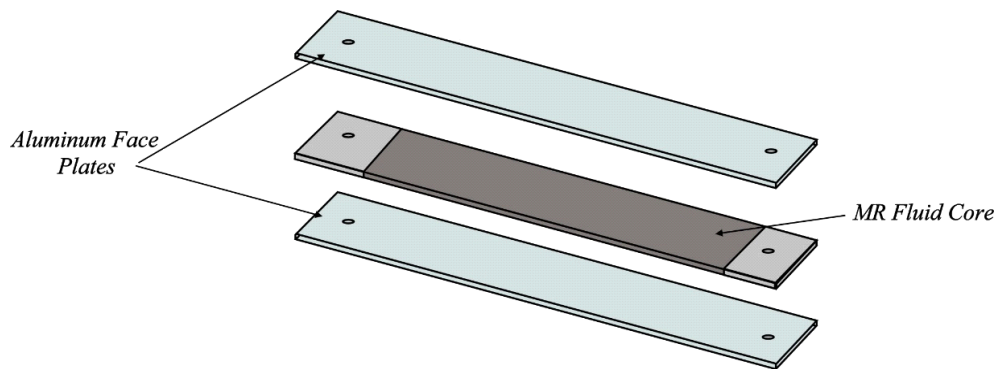
Figure 1.7 MR fluid sandwich Beam (Srinivasa et al. 2020)

1.6 ORGANIZATION OF THESIS

There are totally six chapters in this thesis namely Introduction, Literature review, Optimal Composition of MRF for Damper, Optimal MRF for MR Brake, Optimal MRF for MRF Core Sandwich Beam and Conclusions. In the first chapter, brief introduction to MR fluid, Constituents of MR fluid, MR fluid operation modes, MR damper, MR brake and MR fluid core sandwich beam are discussed. Chapter 2 provides literature review on preparation and characterization of MR fluid of different compositions, Different applications of MR fluid, design and characterization of MR damper, design and characterization of MR brake and damping and vibration suppression capabilities of MR fluid core sandwich beam. Further, motivation for research are deliberated, followed by defining the objectives and scope of research. The research methodology followed in this research for synthesis and characterization of

MR fluid, determination of optimal composition of MR fluid for MR damper, MR brake and MRF core sandwich beam are briefly described.

Chapter 3 discusses the optimal design and fabrication of MR damper and its characterization using commercial MR fluid, MRF 132DG (Lord Corporation), Validation of experimental results with analytical ones, Characterization of iron powders, Preparation and characterization of In-house prepared MR fluid for MR damper, Damping Characteristics of MR Damper for Prepared MR fluid and determination of Optimal MRF composition for damper.

Chapter 4 discusses the Optimal design and fabrication of MR brake and its characterization using commercial MR fluid, MRF 132DG (Lord Corporation), Validation of experimental results with analytical ones, Characterization of iron powders, Preparation and characterization of MR fluid for MR brake, Torque characteristics of MR brake for prepared MRF and determination of Optimal MRF composition for brake.

Chapter 5 discusses the characterization of iron powders, preparation and characterization of MR fluid for MR fluid core sandwich beams, fabrication of MR fluid core sandwich beams, determination of natural frequencies and damping ratios of MRF Sandwich Beams, determination of forced vibration characteristics of the MRF Sandwich Beams and Determination of Optimal MRF composition for MRF sandwich beam. In chapter 6, conclusions drawn from the present study, contributions of this study and scope for future work have been presented.

CHAPTER 2

LITERATURE REVIEW

2.1 INTRODUCTION

Devices employing MR fluid have grabbed the attention of research community, due to their adjustable damping capacity, simplicity, lower current requirements, quick response and ease of control. These type of semi-active devices are controlled using magnetic field in accordance with the dynamic responses of the system. Literature related to synthesis and characterization of magnetorheological fluid, applications of MR fluid in different engineering applications, characterization of MR damper, design and performance evaluation of MR brake and vibration analysis of MR fluid sandwich beams have been discussed in this chapter.

2.2 MAGNETORHEOLOGICAL FLUID

The composition of MR fluid namely the iron particle size, mass fraction and its magnetic properties, carrier fluid type and its viscosity, additives and its quantity have a major effect on the rheological properties and sedimentation stability of MR fluid. Hence, a plethora of research has been undertaken by many researchers to enhance the properties of MR fluid. The effect of carrier fluid and additives on the properties of MR fluid have been studied by many researchers. Sukhwani and Hirani (2007) synthesized polyalphaolefin based MR fluid with electrolytic iron powder (EIP) and four different additives and compared their MR effect and stability. It was concluded that EIP based MR fluid significantly reduced the cost of MR fluid without any major reduction in MR effect. The coating of environment friendly guar gum and xanthan gum additives has negligible effect on the saturation magnetization of Iron particles and subsequently, on the MR effect. Also, they provided best sedimentation stability of MR fluid. Turczyn et al. (2008) prepared carbonyl iron powder based MR fluid composed of different carrier oils such as silicone oil, mineral oil and synthetic oils and additives such as Aerosil (fumed silica), Arsil and Arabic gum with various concentrations. The MR effect and sedimentation stability of the prepared MR fluid

were studied and it was concluded that MR effect did not reduce due to presence of additives while the sedimentation stability of MR fluid increased due to presence of additives. Also, it was found that Aerosil gave maximum stability. Swaminathan et al. (2016) prepared MR fluid using different carrier fluid, iron powder of different sizes and additives and studied the effect of particle size, type and amount of additives on viscosity and stability of fluid. The carrier fluid used are paraffin oil, silicone oil and synthetic oil and additives are Aerosil (fumed silica) and Grease. It was concluded that fumed silica provided higher sedimentation stability. Use of additives and their amount increased the stability of fluid. MR fluid with smaller sized iron powder resulted in higher viscosity and MR effect. Zuzhi et al. (2016) synthesized a MR fluid optimized through an orthogonal experimental design by using silane coupling agent and bentonite as additives at appropriate contents. Sedimentation ratio, apparent viscosity and yield stress were measured to evaluate the performance of the MR fluid by using an optimized process. Cheng et al. (2016) prepared different MRF samples with different volume fractions of CIP varying from 10 to 50% dispersed in silicone oil and analysed the sedimentation stability of MRF. It was determined that MRF with lower volume fractions of CIP settled faster than those in higher volume fractions. Zhang et al. (2021) investigated the rheological properties and sedimentation performance of MRF with different additives. The additives used were Sodium Dodecyl Sulfate (SDS), stearic acid, and their mixture. It was found that the shear stress of the samples with stearic acid was higher than that of the MRF with SDS for same mass fractions. Also, the settling stability of the MRF with the mixture of stearic acid and SDS was better than that of the MRF with other additives.

Phulé et al. (1999) synthesized and characterized magnetic particles of iron and nickel zinc ferrite with nano-scale additives and concluded that these novel MR fluid particles had improved stability and redispersibility. Lim et al. (2004) determined that submicron-sized fumed silica particles added to the CI based MR fluid inhibited sedimentation of CI particles without affecting magneto-sensitive flow properties. López-López et al. (2005) found that the magnetorheological behaviour of iron suspensions stabilized by aluminium stearate surfactant gave larger MR response compared to that containing gel-forming silica nanoparticles and also explained the

field dependence of yield stress. Lim et al. (2005) prepared MR fluid with and without organoclay additive and concluded that organoclay additive inhibited the sedimentation of the CIP without affecting their magnetic properties. López-López et al. (2008) synthesized and characterized iron particles dispersed in kerosene and stabilized by addition of organoclay. They found that the addition of clay slowed down particle settling and eased the redispersion of particles without affecting their magnetorheological properties. Zhang et al. (2009) synthesized and determined sedimentary stability, off-state viscosity and shear yield stress of MR fluid based on carrier fluid such as special shock absorption fluid and transformer oil with seven different additives. Kim et al. (2012) characterized the rheological behaviour of CIP dispersed in a mixture medium of grease and kerosene and concluded that both yield stress and relaxation modulus exhibit solid-like characteristics. Iglesias et al. (2012) determined that nanoscale magnetite added as additive provided excellent MR response, sedimentation stability and redispersibility of CIP dispersed in mineral oil. Fei et al. (2015) studied the effect of single and multiple surfactants and their proportions on the sedimentation ratio and zero-field viscosity of MR fluid. They determined surfactants compounding type and content which gave maximum MR response. Ashtiani and Hashemabadi (2015) investigated the effect of adding magnetite and fumed silica nano particles to CI powder dispersed in silicone oil. The MR effect increased up to six times when using magnetite in comparison to nano particle–free MR fluid while fumed silica made the suspension highly stable. Kamble et al. (2015) prepared MR fluid based on Honge and Castor oils with fine lithium grease added as additive and carried out a comparative study on the properties like shear stress, strain, shear rate, dynamic viscosity, angular frequency, storage modulus, loss modulus and loss factor. Yang et al. (2016) studied the effects of oleic acid and dimer acid on the shear viscosity, thixotropic behaviour, sedimentation stability and temperature dependence of MR fluid. Wu et al. (2016) studied the influence of compounding of surfactants, concentrations and their adding order, stirring times, stirring temperature, stirring speed and determined their optimum values by measuring sedimentation ratio and zero-field viscosity. Portillo and Iglesias (2017) concluded that addition of magnetic nanoparticles improves the dispersibility characteristic and magnetorheological behaviour compared to fluid containing stabilizing and thickening

additives. Xu et al. (2018) used fumed silica (FS) as thixotropic agent in MR polishing fluid with ten different weight fractions to find the proper additive amount for good rheological and sedimentation properties. They suggested that 0.6 % weight fraction of FS was the most promising additive proportion for proper rheological and sedimentation properties, while a further increase in FS weight fraction greatly increased apparent viscosity and decreased yield stress undesirably.

The effect of particle size and volume fraction of iron powder on the characteristics of MR fluid were examined. According to Ginder et al. (1996), the maximum yield stress of an MR fluid depends mainly on the volume fraction of the solid magnetic material and the magnetic saturation of the material. Phule and Ginder (1998) summarized that the particle size, size distribution, shape of the magnetic phase, the carrier phase and different additives affect the stability and redispersibility of MR fluid. Genc and Phule (2002) examined the effects of dispersed phase saturation magnetization and applied magnetic fields on the rheological properties of MR fluid of different average particle sizes. The results show that the decrease in yield stress for finer particle based MR fluid is due to the relatively smaller magnetization of the finer particles. Chiriac and Stoian, (2009) determined that higher yield stresses and consequently better MR effect were obtained in the case of MR fluid with narrow particle size distribution compared to particles with broader particle size distributions. Kolekar et al. (2014) synthesized and characterized silicon oil based MR fluid of different volume fractions of CIP and found that higher the volume fraction of iron particles, higher will be the storage modulus and loss factor. Wu et al. (2016) studied the influence of the particle size on the rheological property of magnetite nanospheres based MR fluid by the experimental and computer simulation methods. It was found that the MRFs with larger particle size gave better MR effect. Zhang et al. (2016) determined the morphology, off state yield stress and sedimentation stability of MR fluid of three different sizes before and after wear of iron particles and concluded that small size particles are good for improving the wear property of MR fluid. Mangal and Sharma (2017) considered carrier fluid, particle size, percentage of iron particles, concentrations of additives as parameters for multi-parameter optimization for maximization of field induced yield stress and viscosity.

Coating of iron particles with different materials have proved to increase the sedimentation stability and redispersibility of MR fluid. Jang et al. (2005) examined the MR behaviours and sedimentation characteristics of MR fluid with and without poly vinyl butyral coating on CIP. The PVB coated CIP not only improved the sedimentation behaviour with a decreased particle density but also maintained yield behaviours with constant shear stresses on a broad range of shear rates. Fang et al. (2005) prepared MR fluid by ball-milling the guar gum powder together with CIP. By forming a coating layer over the ground CIP, the guar gum improves the sedimentation stability and thixotropy of the MR fluid without reducing the MR effect. Wu et al. (2006) found that inducing a guar gum coating on CIP not only greatly improved the sedimentation stability but also strengthened the yield stress of the MR fluid. Bombard et al. (2009) concluded that redispersibility of MRF is strongly dependent on both CIP coating and choice and concentration of dispersing additives. Liu et al. (2013) synthesized and characterized the behaviour of three samples of MR fluid with different volume fractions with coated and uncoated CIP and found that the MRF with the volume fraction of 20% CIP gave good overall properties. Lee and Choi (2018) synthesized and characterized MR fluid consisting of particles coated with conducting polydiphenylamine (PDPA), which possesses outstanding chemical stability, heat resistance and convenience of processing. It was found that in the presence of a magnetic field, the coated MR fluid showed slightly lower rheological properties than the pristine CIP based MR fluid while its sedimentation stability was significantly improved.

Improved properties of MR fluid were observed by using different shapes of iron particles. Jiang et al. (2011) synthesized and characterized dimorphic MR fluid by adding wire-like iron nano-structures into the conventional carbonyl iron based fluid. They found that the iron wire additives greatly enhanced the stress strength and the sedimentation stability of the dimorphic MR fluid. Vicente et al. (2012) investigated the effect of spherical, plate-like and rod-like magnetic particles on MR performance using silicone based MR fluid. They found that rod-like particle based MR fluid exhibited a larger storage modulus and yield stress and the effect of particle shape is found to be negligible at large particle content or magnetic field strengths. Sarkar and

Hirani (2015) concluded that with increase in volume fraction of iron particles, the MR fluid synthesized using mixed sized particles show better shear stress compared to the MR fluid containing smaller sized spherical shaped particles and larger sized flaked shaped particles at higher shear rate.

Many researchers have observed that use of larger and smaller sized iron particles in the synthesis of MR fluid yielded significant improvement in its properties. Wereley et al. (2006) determined the optimal composition of MRF made of micron sized and nano sized particles that provide the best combination of high yield stress and low settling rate based on sedimentation stability and rheological tests. Ngatu and Wereley (2007) synthesized MRF made of micron sized iron and nano sized particles of various concentrations to examine trade-off between increasing suspension stability versus decreasing yield stress as nanoparticles were substituted for micro particles. Dodbiba et al. (2008) synthesized and characterized MR fluid made of various concentrations of large and small sized CI particles dispersed in Ionic fluid and determined the optimum proportions of the particles for highest MR effect. Park et al. (2009) examined the flow behaviours at a steady shear mode of micron sized CIP with and without nano-sized CIP under varying magnetic field strength. The MR fluid with magnetic iron nanoparticle demonstrated slightly higher yield behaviours. Rosenfeld and Wereley (2010) synthesized magnetorheological fluid based on nanometer-sized powders, micron-sized powders and mixtures of the two and compared their yield stress and plastic viscosity. Patel (2011) prepared bidisperse MR fluid and concluded nano particles restrict the aggregation of micron sized particles which gives more stability than the commercially available monodispersed MR fluid. Bombard and Teodoro (2011) synthesized a ternary blend of water atomized iron particles and CIP of two different sizes dispersed in polyalphaolefin. They found that the blend viscosity was ten-fold lower than that of MRF based on only each powder alone. Shah et al. (2012) reported that larger sized nano magnetite particles provide fifteen times higher yield stress compared to that of the small sized nano particles. Further, they also reported that on mixing smaller and larger particles with different weight fractions, the yield stress value increases by a factor of three compared to that of the larger sized particle ferrofluid. Chand et al. (2014) characterized MR fluid containing micro and nano

particles of various concentrations and found that the addition of nanoparticles to MR fluid increases the viscosity as well as the fluid stability under a magnetic field. Leong et al. (2016) incorporated nanoparticles in different types of MR materials which are MR fluid, MR grease and MR elastomer and indicated that it remarkably improved the stability and re-dispersion of the particles and also enhanced the rheological and viscoelastic properties. Gurubasavaraju et al. (2017) determined optimal volume concentration of dispersed particles for synthesis of MRF utilizing response surface method and particle swarm optimization technique with the objectives of maximizing the shear stress and damping force. They considered constituents of MRF, annular gap and DC current as parameters for optimization. Zhu et al (2021) performed rheological characterization and sedimentation stability tests of bimodal MR fluid comprising of CIP mixed with different proportions of iron nano particles. It was concluded that sedimentation stability of the bimodal MR fluid improved significantly with the increase in the proportion of iron nanoparticles. Further, bimodal MR fluid with a small proportion of iron nanoparticles can achieve an improvement in both rheological property and sedimentation stability compared with CIP based magnetorheological fluids.

Rabbani et al. (2015) investigated the sedimentation stability and rheological properties of a MRF of CIP in silicone oil within a temperature range of 10 to 85 ℃. The effect of adding stearic and palmitic acids on the stability and magnetorheological effect of a suspension were also studied. 3% weight fraction of stearic acid in the MR fluid demonstrated a relatively low off-state viscosity, high shear stress and superior sedimentation stability. Also, there was a significant decrease in the shear stress with increase in temperature. Kumar et al. (2019) provided a review of challenges and solutions in the preparation and use of magnetorheological fluids such as sedimentation Stability, formation of hard cake, clumping effect, oxidation of particles, temperature effects, sealing issues, time response, In-use thickening (IUT) and interior wall incrustation. Morillas and Vicente (2020) gave state of the art recent developments in the field of MR fluid and MR elastomers. The experimental characterization, challenges and applications of these materials have been discussed. Plachy et al. (2018) investigated the effect of effect of oxidation of carbonyl iron particles on magneto-

rheological behavior of MR fluid. It was observed that there was significant decrease in the magnetization saturation of the oxidised CIP particles and lower rheological properties of MR fluid. Utami et al. (2018) investigated the rheological properties of MR fluid after long term cyclic operation use in damper. It was found that on-state and off-state damping force increased with number of cycles and particle size and shape changed.

2.3 MR FLUID APPLICATIONS

While MR fluids were first reported by Rabinow more than 70 years ago, applications of MR fluids have only recently become popular. MR fluid has found applications in many devices which require semi-active control such as shock absorbers, brakes, clutches, bearings, mounts, landing gear, haptic devices, prosthetic knee, gun recoil, stay cables, seat suspension and many more potential applications. Some of the devices have seen successful implementation while some are under research stage.

2.3.1 Magnetorheological fluid Bearings

The dynamic characteristics of the bearings significantly affects the reliable functioning of rotor systems. The damping and stiffness of the bearings are improved by suitable design of bearings. Magnetorheological fluid have a great potential in the vibrations control and overall performance improvement of the journal bearings. By means of squeeze film type and disk type MR fluid dampers, Zhu et al. (2001) demonstrated that the rotor vibrations could be effectively controlled. By application of current to the damper, the support damping and stiffness can be controlled for every vibration modes of the rotor. Hesselbach and Abel-Keilhack (2003) experimentally demonstrated the use of MR fluid in hydrostatic bearings for maintaining a constant bearing gap whenever there is variation in payload. They concluded that the drawbacks of conventional hydrostatic bearing namely the stiffness and response time can be overcome by the use of MR fluid in hydrostatic bearings. Forte et al. (2004) performed numerical analysis and experimental study of MR fluid squeeze film damper. It was concluded that the rotor dynamic characteristics were effectively controlled due to the dampening effect of MR fluid in the presence of current. Gertzos et al. (2008) derived

hydrodynamic journal bearing characteristics for several bearing length to diameter ratios and dimensionless shear numbers of MR fluid. They found a good agreement between computational fluid dynamic analysis and experimental results and recommended the method for design of MR fluid based journal bearings. Bompos and Nikolakopoulos (2016) studied the performance of journal bearing employing Newtonian, MR fluid and nano MR fluid using coupled finite element and CFD analysis. It was concluded that MR fluid containing particles of nano size significantly improved the static and dynamic performance of journal bearing. Bompos and Nikolakopoulos (2016) designed and manufactured a MR bearing as shown in figure 2.1 and evaluated its performance for Newtonian fluid and non-Newtonian MR fluid. The dynamic behaviour of bearing employing MR fluid resulted in better vibration control.

Figure 2.1 MR fluid based bearing (Bompos and Nikolakopoulos 2014)

2.3.2 Magneto-rheological fluid clutches

Magneto-rheological fluid clutches are used in several automotive systems such as auxiliary engine devices, active differentials, and automatic transmissions. The purpose of developing the magnetic clutch is to overcome the mechanical friction that happens to the conventional clutch. Due to its inherent advantages over conventional clutch, MR fluid clutch has attracted the attention of researchers in recent past. Herold et al. (2010) designed, fabricated and tested a magnetorheological fluid clutch. They experimentally characterized the static and dynamic characteristics of the clutch in order to validate the clutch design and provide a basis for the clutch model

development. Bucchi et al. (2014) fabricated a permanent magnet excited MR clutch for the disengagement of the vacuum pump used with the power-brake in diesel engine vehicles. The MR clutch having hybrid geometry consisting of a disc and a cylinder exhibited a fail-safe operation with negligible power consumption, reduced size and absence of axial loads compared with electromagnetic clutches. Bucchi et al. (2015) expressed the temperature dependence of torque characteristic of a permanent magnet magnetorheological clutch by Arrhenius law and found a loss of transmitted torque for increasing temperature. They also obtained an approximate dependence of MR fluid shear stress on temperature. Bucchi et al. (2017) worked on geometry optimization of a magnetorheological clutch based on fluid gap shapes and coil positions. They computed the magnetic flux using a lumped parameter model was validated using 2D FE models for four different designs of MR clutch. The results of were in good agreement with finite element model results. Pisetskiy and Kermani (2018) designed, manufactured and tested multi-disk MR clutch for a 5 degree of freedom (DOF) robot as shown in figure 2.2. They found a good correlation between simulation and experimental results.
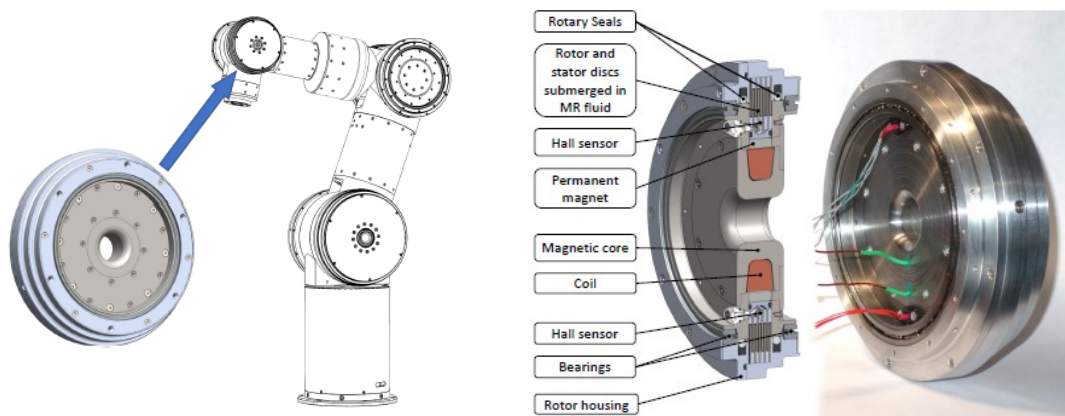
Figure 2.2 MR fluid clutch for a 5 DOF robot (Pisetskiy and Kermani 2018)

2.3.3 Magneto-rheological fluid mounts

The isolation of engine vibration to chassis is a topic of interest to automotive engineers. This could be done by means of mount and it should possess low stiffness during high-frequency low-amplitude excitations and high stiffness during low-

frequency high-amplitude excitations. Conventional rubber mounts have constant stiffness and damping and it cannot meet these contradictory requirements. However, hydraulic mounts which has rubber and fluid for controlling damping characteristics can satisfy these requirements. The controllability and performance of hydraulic mounts can enhanced by use of MR fluid. Hong and Choi (2005) demonstrated through experiments that vibration levels of structural system employing controller can be effectively reduced by means of MR mounts. Nguyen et al. (2009) determined optimal dimensions of mixed mode MR mount involving flow and squeeze mode. The performance of MR mount was experimentally determined and matched well with the prediction of theoretical analytical model. Zhang et al. (2011) performed dynamic testing and modeling of MR fluid squeeze mount and found a good match between the mathematical and test results. Do and Choi (2015) reviewed the design and other aspects of different configurations of high load MR mounts which operate in flow mode, shear mode and squeeze mode. One of the design configuration of MR mount is shown in figure 2.3. The authors provided guidelines for designing an MR mount having combination of flow and shear modes which has several benefits as compared to one operating single mode.
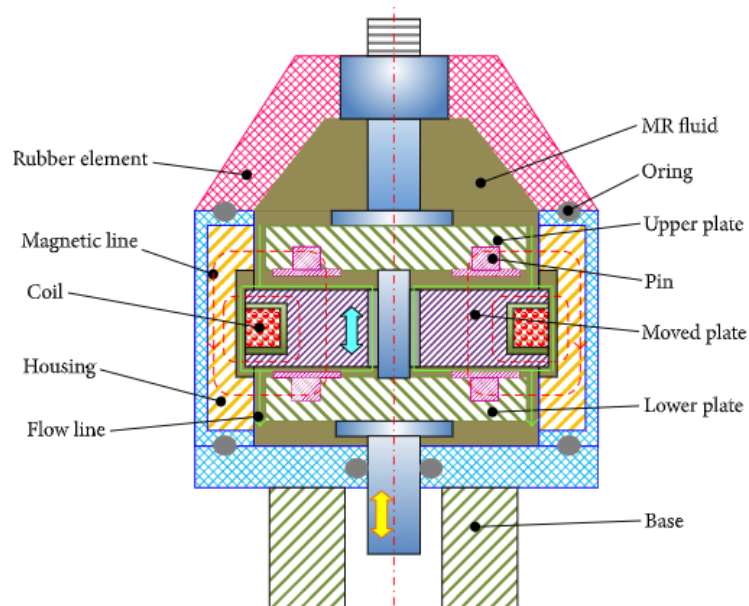
Figure 2.3 Magnetorheological mount (Courtesy: Do and Choi 2015)

2.3.4 Magneto-rheological fluid aircraft landing gear

The landing gear of an aircraft is subjected to impact during landing due to which there is impact stress, structural fatigue damage and passenger discomfort. Hence, several landing gear designs have been presented by researchers among which use of MR fluid has also been attempted. Batterbee et al. (2007) presented procedure for optimal design of MR damper for landing gear considering dynamic ratio and magnetic circuit performance as objectives with space constraints. In another work, Batterbee et al. (2007a) described the design and fabrication of MR landing gear shock strut in place of existing passive landing gear. The quasi-static and sinusoidal response of the strut were measured to validate the MR fluid parameters in the dynamic model of MR strut. Lee et al. (2009) concluded from a series of simulations and experiments that a MR damper employing skyhook controller can effectively reduce vibrations of landing gear system. Powell et al. (2013) synthesized MR fluid with three different hydraulic oils as carrier fluid and iron powder of different sizes and weight fractions. The rheology of these fluid were measured under different magnetic fields and compared with commercial Lord MR fluid. Further, the performance of damper filled with synthesized and commercial fluid under sinusoidal excitations and impact testing were determined. It was concluded that the damper filled with synthesized and commercial fluid produced closer performance and hence feasible for use in helicopter landing gear. Yoon et al. (2020) designed a MR landing gear having dimensions same as that of commercially available landing gear strut, while the dimensions of magnetic core were obtained to maximize the field induced damping force. The configuration of MR landing gear is shown in figure 2.4. A new control logic was proposed and significant performance improvement of damper was observed under drop simulations.
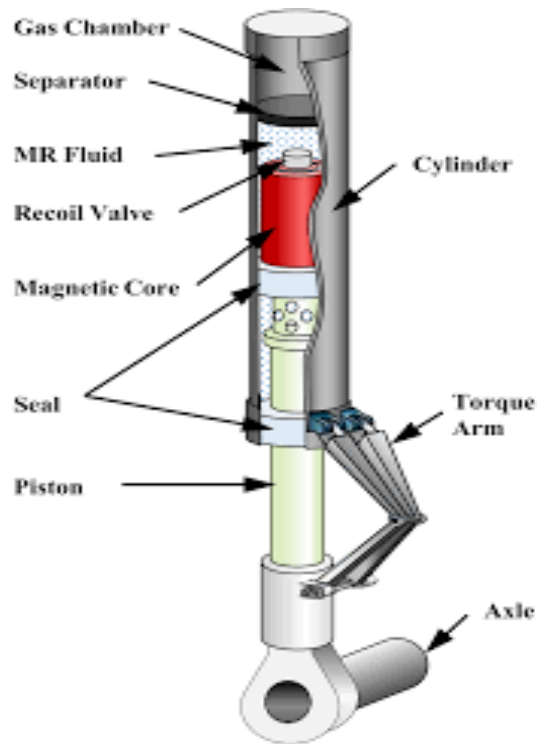
Figure 2.4 Configuration of a MR landing gear (Yoon et al. 2020)

2.3.5 Magneto-rheological fluid prosthetic knee

A MR prosthetic knee consists of MR actuator, sensors and artificial intelligence. The viscosity of MR fluid is varied by application of magnetic field and hence its flexion resistance. When the amputee walks, the stiffness of knee can be varied in real time. Due to its inherent advantages compared to hydraulic based prosthetic knees, it is being manufactured and marketed. Jonsdottir et al. (2009a) performed parametric study of a MR prosthetic knee which is a product of Ossur Inc. The effect of changes in existing design on the magnetic field strength and torque of the MR device was investigated. Park et al. (2016) designed and manufactured MR prosthetic knee integrated with a controller and tested its performance on a level ground at different walking speeds.

<div align="center">(a)   (b)   (c)</div>
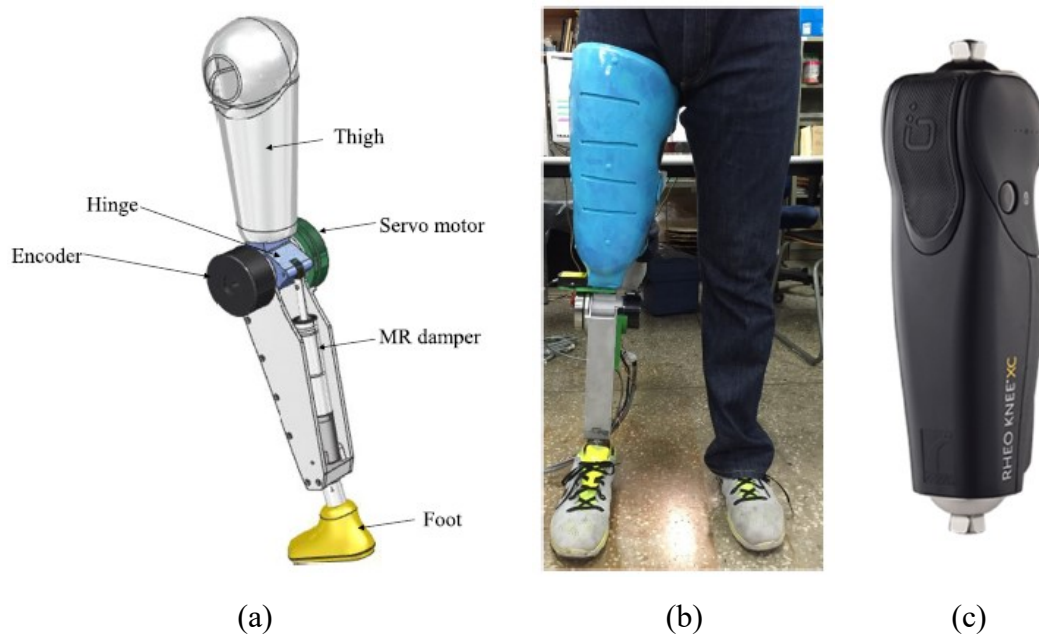
Figure 2.5 MR damper for prosthetic applications: (a) Schematic representation and (b) Photo of fitted prosthetic knee (Park et al. 2016), (c) Commercially available prosthetic Knee : Rheo Knee XC (Bellmann et al. 2019)

The configuration and the photograph of the prosthetic knee is shown in figure 2.5 (a) and 2.5 (b) respectively. It was shown that the performance of the damper was good at lower speeds while at higher walking speeds the performance got degraded due to lower response time of the damper. Bellmann et al. (2019) investigated the functional performance of microprocessor-controlled hydraulic (C-leg) and MR fluid based (Rheo Knee XC) knee joints in safety-relevant daily-life situations using biomechanical methods. Rheo Knee XC is a product Ossur Inc., Iceland as shown in figure 2.5(c).

2.3.6 Magneto-rheological fluid damper in washing machine

Spelta et al. (2009) compared the vibration and noise reduction of washing machine shown in figure 2.6 with standard passive damper and MR damper with control strategies. It was concluded that the use of MR damper significantly reduced vibration and noise as compared to passive damper.Nguyen et al. (2014) optimally designed an MR damper for a front loaded washing machine to control the vibrations of laundry mass. The objectives of optimization considered were minimization of zero field force and field induced damping force was constrained to be greater than a desired value.

Also, damper dimensions were determined by considering space constraints. Two commercially available MR fluid single and multiple coil designs were considered. Finally, the analytical results were validated with experimental test results. Ulasyar and Lazoglu (2018) optimally designed MR sponge damper for a washing machine using finite element analysis and first order derivative technique. The performance of proposed MR sponge damper were compared with those available in literature. The MR sponge damper effectively reduced the vibrations as compared to passive damper.
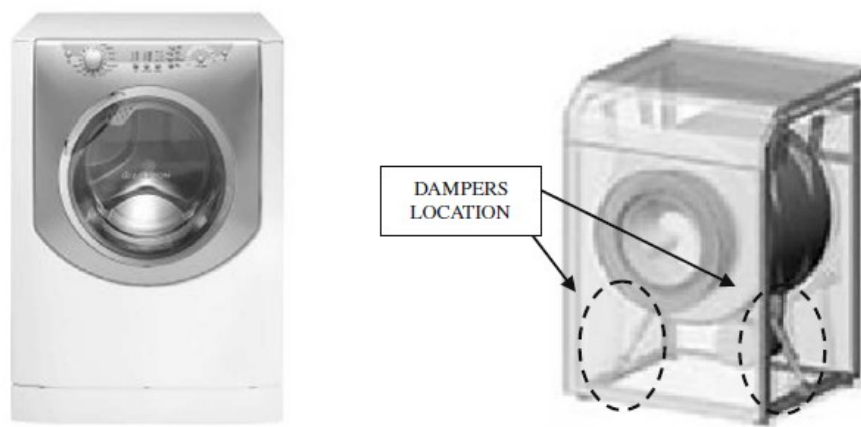
Figure 2.6 Washing machine employing MR dampers (Spelta et al. 2009)

2.3.7 Magneto-rheological fluid damper in rail vehicle suspension

Mohan and Ahmadian (2006) numerically studied the non-linear dynamics of railway bogie and proposed the use of MR dampers to increase the critical hunting velocity which significantly improves its stability. Oh et al. (2016) experimentally evaluated performance of a railway vehicle suspension equipped with magneto-rheological damper as shown in figure 2.7 using a sky-hook control and concluded that ride quality of vehicle with MR damper is significantly better than that of passive suspension. In addition, MR damper performance have been investigated to study the dynamic instability occurring in railway vehicle termed as hunting.
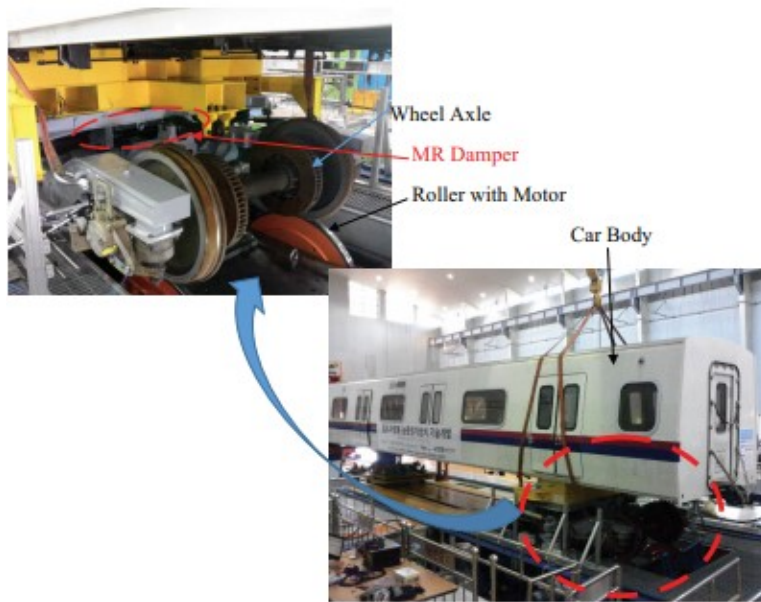
Figure 2.7 MR damper in rail car vehicle suspension (Oh et al. 2016)

2.3.8 Magneto-rheological fluid damper in seat suspension

Choi et al. (2001) designed and manufactured MR damper for seat suspension and measured the response using sky hook controller. They demonstrated that MR damper significantly reduced the vibration level of the driver seat under bump and random road excitations. Choi and Wereley (2005) studied the response of human body to vibration and blast induced shock loads using an MR seat suspension and compared its performance with passive seat suspension. It was concluded that MR seat suspension showed best vibration attenuation. Shin et al. (2015) experimentally studied the performance of MR seat suspension shown in figure 2.8 using adaptive fuzzy sliding mode controller and concluded that the MR damper provided very good ride comfort which was measured in terms of vertical acceleration under bump, random and sinusoidal excitations.

30
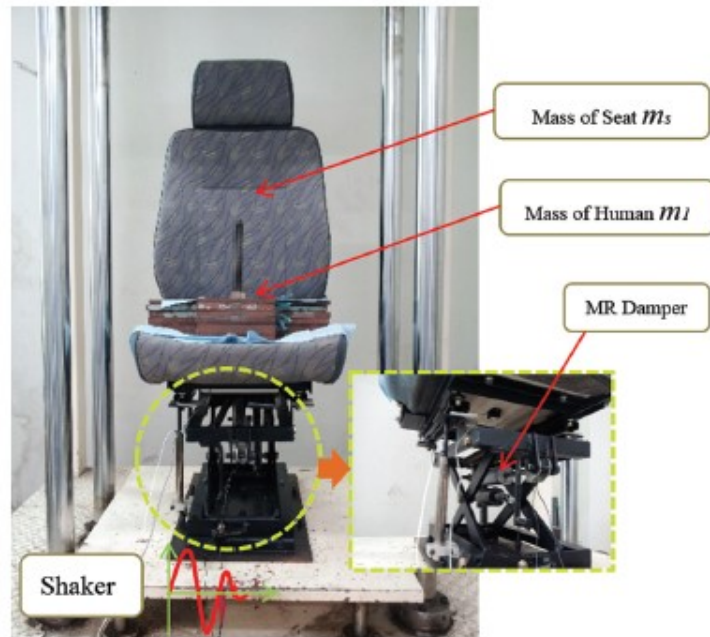
Figure 2.8 MR seat Suspension (Shin et al. 2015)

2.3.9 Magneto-rheological fluid damper in structural applications

Dyke et al. (1998) examined the effectiveness of MR dampers for seismic response reduction. A three storey test structure was subjected to earthquake tests and broad band excitation tests and concluded that MR dampers are effective in mitigation of structural response over wide range of seismic excitations. Yang et al. (2002) designed and manufactured 20 ton large scale MR damper for structural applications and validated experimental and analytical calculations. The schematic diagram of the multi-stage MR damper is shown in figure 2.9. It meets the requirement of low response time needed for a number of structural applications.
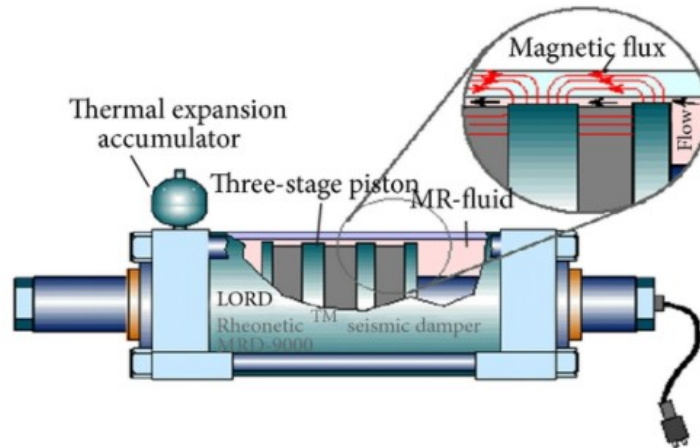
Figure 2.9 Schematic of MR damper for seismic applications (Yang et al. 2002)

2.3.10 Magneto-rheological fluid damper in stay cables of bridges

The effectiveness of MR damper for control of stay cable vibration was demonstrated after which the authorities decided to incorporate MR dampers for 20 longest cables of Shangdong Binzhou yellow river highway cable stayed bridge. The MR damper was designed by Li et al. (2005). Later, Li et al. (2007) proposed an innovative control algorithm and conducted a series of field tests to study the effectiveness of vibration control of MR dampers. It was concluded that the proposed controller can be used to determine the optimal force and MR dampers provided significant damping due to its Pseudo-negative stiffness. Wang et al. (2018) tested the damping capacity of 30 MR dampers which was used for vibration control of stay cabled bridge shown in figure 2.10 after a service of one decade. The dampers are products of Lord Corporation, USA (Model: RD-1005-3). 24 MR dampers among them could still provide considerable damping force while remaining ones failed to provide enough damping. They concluded that the performance degradation of used dampers are due to leakage of MR fluid and rough uneven surface texture of iron particles due to usage.
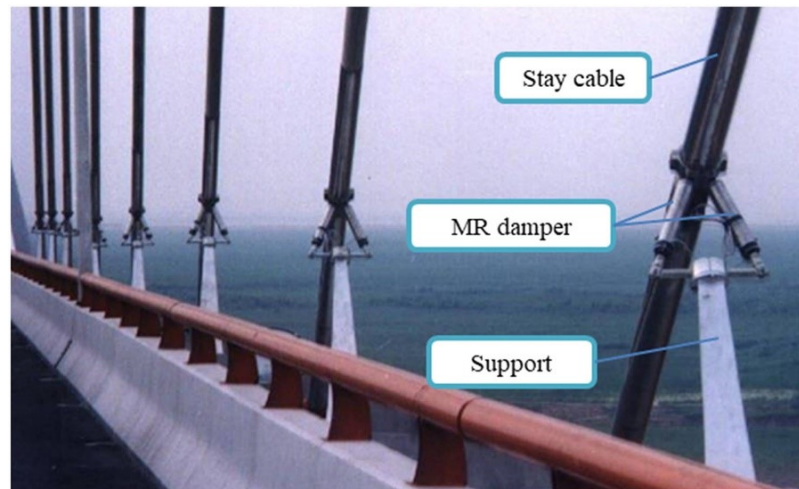
Figure 2.10 MR dampers installed in stay cable vibration control system on the Dongting Lake Bridge (Wang et al. 2018)

2.3.11 Magneto-rheological fluid damper in gun recoil control

Ahmadian and Poynor (2001) designed MR damper which can absorb large velocity impact loads which occur in gun recoil. They built a gun recoil demonstrator assembly as shown in figure 2.11. It was found that the MR damper can effectively reduce large recoil forces which occur upon firing the gun and subsequently reduce the recoil stroke.
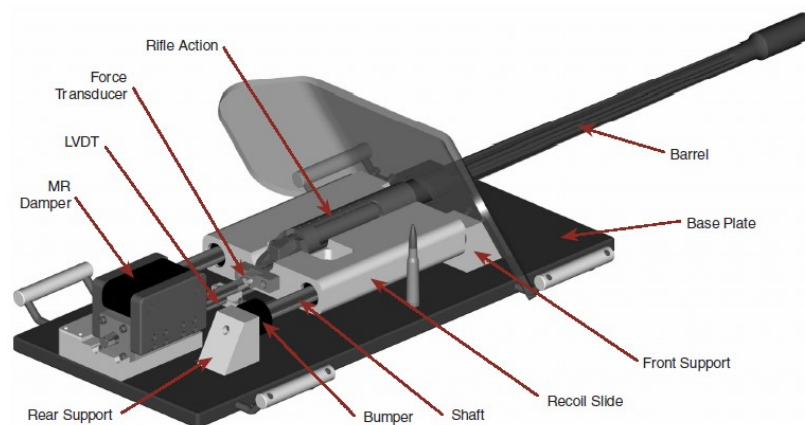
Figure 2.11 MR damper in Gun recoil systems (Ahmadian and Poynor 2001)

Li and Wang (2012) designed and manufactured MR damper for a gun recoil system and performed experiments which simulate real firing impact loading

conditions. The control method used is open loop with no feedback system due to which sensor is not required. This is advantageous for device subjected to impact loads and working in harsh environmental conditions. Singh and Wereley (2014) analytically and experimentally validated the effectiveness of MR damper for minimizing gun recoil loads and maximizing rate of fire.

2.3.12 Magneto-rheological fluid polishing devices

Extensive research has been done in the recent past for developing novel finishing technique using MR fluid. Song et al. (2011) investigated the tribological of steel, aluminium and brass materials polished by commercial Lord MR fluid in the presence and absence of magnetic fields under different test conditions using a pin-on-disc tribometer. It was observed that the wear loss and friction coefficient decreased with increase in magnetic field. Also, the wear mechanisms in materials tested were studied using scanning electron microscopy and energy dispersive X-ray spectroscopy. In another work, Song et al. (2013) performed polishing of steel, aluminium and brass on a pin-on disc tribometer using commercially available MR fluid, Lord MRF 132DG and MRF 140CG under various test conditions. It was observed that MR fluid effectively reduced surface roughness of steel surface while rough surface finish was obtained in case of brass and aluminium materials. Also, MR fluid with higher mass fraction of magnetic phase resulted in better surface finish in case of steel sample.

(a)   (b)
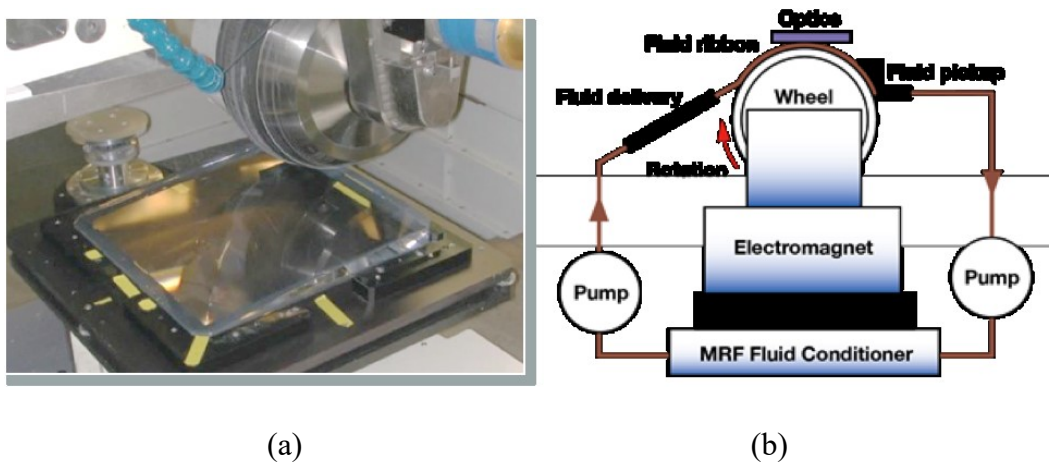
Figure 2.12 Magnetorheological finishing tool

(Courtesy: https://lasermaterials.llnl.gov/focus-areas/optical-finishing)

Lawrence Livermore National Laboratory, USA have developed Magnetorheological finishing tool for performing finishing operations in optics as shown in figure 2.12 (a). Figure 2.12 (b) shows the schematic representation of the tool. QED technologies International Inc. is an organization in North America which manufactures and markets MR fluid polishing machines for finishing optics parts. (https://qedmrf.com/en/mrfpolishing/mrf-technology/how-it-works). The company also provides MR fluids suitable for polishing tungsten carbide, aspherize optical parts, manufacturing very high surface finish parts and much more.

2.3.13 Magneto-rheological fluid damper in vehicle suspension

Major applications of MR fluid have been found in automotive suspensions. Magneto- rheological fluid-based dampers has be used in automobile suspensions for performance improvements in terms of better balance between vehicle ride, handling and stability. It has been found from experimental and modelling simulation studies that MR suspensions have better performance than that of passive suspensions. Choi et al. (2000) evaluated the performance of a full-car suspension employing MR dampers using hardware in loop simulation. It was remarked that both ride quality and steering stability can be considerably improved by incorporation of MR dampers in suspension. In 2002, Delphi Automotive Corporation introduced MagneRide^{TM} suspensions employing MR dampers and are currently used in Audi, Ferrari, General Motors and Holden Special Vehicles. (Lord Corporation product information). Figure 2.13 shows the superior performance of suspension with MR damper used in premium vehicle (Corvette) in terms of ride comfort and road holding as compared to suspension without MR damper (Goncalves 2005). Ahmadian (2017) analyzed the performance of MR damper employing hybrid control and passive damper in terms of the response of vertical sprung mass acceleration, suspension displacement and tyre deflection subjected to road input by means of simulation studies. It was concluded that performance of MR damper was significantly higher than that of passive suspensions in terms of ride comfort, handling, and road-holding (stability).

Figure 2.13 Corvette with suspension with MR damper (Goncalves 2005)

2.4 DESIGN AND CHARACTERIZATION OF MAGNETORHEOLOGICAL DAMPER

The MR damper design mainly involves material selection and determining the dimensions of the damper piston in order to realize desired performance associated objectives. The design of MR damper involves maximization of damping force while avoiding magnetic saturation in the piston core. This inturn depends on magnetic flux generated in the MR fluid gap. With this as objective, the dimensions of damper were determined by many researchers. Zhang et al. (2006) proposed damper design method such that magnetic saturation in the piston is circumvented. It was concluded that the energy dissipation and the field induced force are the chief performance measures of MR damper. Furthermore, they depend on the magnetic flux generated in the MR fluid gap. Krishna et al. (2016) obtained optimum dimensions of MR damper using response surface methodology in ANSYS software and using genetic algorithm techniques with the objective of maximization of the magnetic flux density in the MRF. Naserimojarad et al. (2018) proposed an optimum design of MR dampers by using optimization and finite element analysis and validated with experimental results. Optimal MR damper dimensions were determined by Parlak et al. (2012) computed using magnetostatic and computational fluid dynamic analyses in ANSYS software for a target damping force of 1000 N and maximization of magnetic flux density in the MRF gap. Further, dampers were manufactured as per optimized dimensions and experimental results were validated with simulation data. In another study, Parlak et al. (2013) manufactured and tested nine different configurations of MR dampers based on Taguchi experimental design approach to determine optimal configuration of MR dampers with the objectives

36

of maximizing damping force and damping ratio separately. Nguyen et al. (2008) performed a finite element analysis based optimization procedure to determine the optimum geometry for different types of MR damper pistons constrained to a specific piston radius and height which satisfies desired pressure drop with minimized power requirement. Nguyen and Choi (2009) performed multi-objective optimization with damper force, dynamic ratio and the inductive time constant of damper as objectives to determine the dimensions of MR damper for vehicle shock absorber. Nguyen et al. (2009a) suggested an analytical method to determine the optimum dimensions of single-coil and two-coil annular MR damper piston with the objective of maximization of damper force. Gurubasavaraju et al. (2017) found out optimal design of a MR damper using screening and MOGA techniques with the objective of maximization the magnetic flux density in the MRF shear gap. Desai et al. (2020) determined the dimensions and fabricated a valve mode MR damper of twin-tube construction for passenger vehicle suspension. The damper was tested at various frequencies and currents and the test results were validated with analytical calculations. Shivaram and Gangadharan (2007) designed a statistical model of MR damper using the design of experiment approach, where in various factors for experimentation such as magnetic field strength, volume fraction of the magnetic particle, shearing gap between piston and cylinder, amplitude and frequency of vibration which affects the performance of the MR damper were considered. Krishna et al. (2017) obtained optimum dimensions of MR damper using response surface methodology in ANSYS software and using genetic algorithm techniques with the objective of maximization of the magnetic flux density in the MRF. Ma et al. (2002) determined the force-displacement, force-velocity and seal friction properties of a MR damper under a wide range of control current and excitation conditions and proposed a generalized model characterizing the hysteretic force properties of a magneto-rheological damper. Facey et al. (2005) proposed an analytical optimization design method for MR valves and dampers based on the assumption of constant magnetic flux density throughout the magnetic circuit. Parlak et al. (2012) analyzed the fluid flow through the annular gap by quasi-static analysis and conducted CFD analysis of the MR damper. Mangal and Kumar (2014) conducted the optimization of geometrical parameters of MR damper to maximize the damper force by using statistical tool (Taguchi design of experiment approach) coupled with

the finite element method. Ferdaus et al. (2014) conducted studies on optimization of MR damper for different configurations of damper piston, fluid flow gap and damper housing by using finite element analysis and then validated the analysis results with experimental results. Djavareshkian et al. (2015) analytically investigated the effect of parameters such as number of turns, pole length, gap thickness and spool length of MR damper. They also conducted optimization study of these parameters for minimization of electrical power consumption and improvement of damper force by using response surface method. Hu et al. (2015) proposed a double coil MR damper which could obtain force and dynamic range though quasi-static model. They considered seven different configurations of piston head for investigating the performance of double coil damper and obtained optimal parameters. Xu et al. (2012) carried out geometric and magnetic circuit design of multistage shear-valve mode MR dam per for earthquake mitigation application. The optimal dimensions were obtained using *fmincon* optimization function for a damper force of 200 kN at 100 mm/s piston velocity and dynamic range greater than 15.

2.5 DESIGN AND CHARACTERIZATION OF MAGNETORHEOLOGICAL BRAKE

MR brakes are one of the MR devices which have grabbed the attention of researchers in the recent past owing to their bright potential in replacing conventional brakes in several applications (Karakoc et al. 2008a). The discoverer of MR fluid, Jacob Rabinow, filed the first patent on electromagnetically controlled torque-applying devices, which can be operated as a clutch or a brake (Jacob and Rabinow 1951). Later, Carlson while working in Lord Corporation filed many patents since 1994, related to MR brakes which provide controllable forces in exercise machines (Carlson and Catanzarite 1998), portable devices for rehabilitation of injured limbs, appendages and joints (David Carlson 1998), controllable brake (Carlson 2001), etc. In the early 2000 millennium, MR brakes were commercialized in aerobic exercise equipment due to their lower cost compared to their counterpart (Webb 1998). However, the temperature rise in the fluid, tremendous torque requirement and in-use thickening of MRFs (Carlson 2002) pose a major impediment for implementation of MR brakes.

Torque characteristics of MR brake filled with commercial MR fluid have been studied by many researchers. Sukhwani and Hirani (2008) studied the variation of torque characteristics of the MR brake filled with commercial MR fluid, MRF-336-AG (Make: Lord Corporation), with variation of gap and location of electromagnet. Rossa et al. (2014) analyzed single and multiple disc and drum brakes composed of commercial MR fluid, MRF-132DG (Make: Lord Corporation). They concluded that single drum brakes are more reactive and require less power compared to single disc brakes and for multiple-layered brakes, the maximum torque, the torque density and the reactivity increased with the number of fluid gaps. Li and Du (2003) studied the effects of magnetic field and rotary speed on the commercial MR fluid, MRF-132LD (Make: Lord Corporation) based MR disc brake torque and found that brake torque increased steadily with the increment of magnetic field or rotary speed. Poznic et al. (2017) obtained larger overall brake torque by combining magnetic and non-magnetic materials for fabrication of single disk MR brake compared to the conventional one with magnetic material. They used commercially available Basonetic 5030 MR fluid (Make: BASF SE, Germany). Zhou et al. (2007) designed a novel MR brake having two shearing disks with an electromagnetic coil located between them and performed electromagnetic finite element analysis to optimize the magnetic circuit. Commercial Water-based MR fluid MRF-241ES from Lord Corporation was used. On evaluation of the performance of the brake, they concluded that the compact MR brake can transmit high torque. Assadsangabi et al. (2011) performed finite element analysis of a disk-type MR brake composed of MRF-132DG fluid to analyze the magnetic field intensity distribution and then optimized braking torque capacity using Genetic Algorithm to obtain optimal design parameters. Karakoc et al. (2008) performed finite element and experimental analysis to analyze the resulting magnetic circuit and heat distribution within the MR brake containing commercial MR fluid, MRF 132DG (Lord Corporation) and obtained optimal design parameters that can generate the maximum braking torque based on multidisciplinary design optimization. Attia et al. (2017) performed theoretical and experimental analysis of braking torque of a MR brake composed of Basonetic 5030 MR fluid (Make: BASF SE) and concluded that braking torque increases gradually as input current, radius of disc and viscosity increases. Nguyen and Choi (2010) presented optimal design of a single and multiple disc MR

brake for three types of commercial MR fluid (Lord Corporation) for a middle-sized passenger vehicle based on the required braking torque, the temperature due to zero-field friction of MR fluid, the mass of the brake system and all significant geometric dimensions. Shamieh and Sedaghati (2016) formulated a multidisciplinary design optimization to identify the optimal brake geometrical parameters to maximize the dynamic range of the MR Brake based on weight, size and magnetic flux density constraints.

Sukhwani and Hirani (2008b) compared the performances of brake power output and amplification factor of MR fluid brake and MR grease brake under same operating conditions of speed and magnetic field. They concluded that MR fluid should be preferred over MR grease for application in MR brake as high MR effect is the main requirement as compared to sedimentation stability. Nguyen et al. (2014a) examined the performance characteristics of the MR brake based on a novel MR suspension with silica coated carbonyl iron particles including field dependent torque, hysteresis, time and torque tracking control responses. Sarkar (2015) characterized MR fluid composed of 85% weight fraction of iron particles at various shear rates for different magnetic fields and determined the torque characteristics of an MR brake. He concluded that dynamic yield strength increases with increase in shear rate up to particular value after which it decreases and with increase in speed, there is decrease in braking torque of MR brake. Zainordin et al. (2013) obtained performance evaluation of MR brake in terms of shaft angular velocity response, torque response and load displacement response for different currents and loads. Park et al. (2008) used three different design simulated annealing optimization procedure combined with finite element simulations involving magnetostatic, fluid flow and heat transfer analysis. Further, they studied MR fluid selection for MR brake application, magnetic circuit design and torque requirements for automotive application. MRF-132AD and MRF-241ES (Make: Lord Corporation) were used for design of the MR brake.

The torque generated by MR brake can be augmented by several methods. Reducing the gap between casing and rotor disc significantly increases the torque, as reduction in MR fluid gap reduces the reluctance of magnetic path and increases magnetic flux density (Sukhwani and Hirani, 2008; Yoo and Wereley, 2002). Selection

of magnetic and non-magnetic materials for brake components result in concentration of flux in MR fluid and consequently increases the braking torque (Acharya and Kumar 2019; Karakoc et al. 2008). Use of multi-disc rotors Nguyen and Choi (2012b) increases the torque due to more amount of fluid subjected to MR effect. Another dominant method of increasing the torque capacity of an MR brake is by incorporation of multi-pole electromagnet (Shiao and Nguyen 2013). However, the practical implementation of these methods is challenging due to the complexity involved in manufacturing. MR brakes utilizing higher yield stress fluid causes higher braking torque or reduces the dimensions of brake for realizing same value of torque. However, higher yield stress MRF consists of higher mass fraction of iron particles which leads to undesirable high viscosity and off-state torque of the brake.

The performance of a MR brake can be conveniently enhanced based on the design of the brake and the use of suitable MRF. Maximization of torque, minimization of mass and temperature were considered as objectives by many researchers (Nguyen and Choi 2010, 2012b; Sohn et al. 2015). The design of brake should ensure maximization of magnetic field strength in MRF gap which would result in higher field induced braking torque. Zhang et al. (2006) suggested design of MR damper which would focus magnetic flux in MR fluid and avoid saturation in the core and finally validated the same using experiments. Optimal dimensions of disc, cylindrical, inverted drum and T-shaped MR brakes with single and double coils were determined by Nguyen and Choi (2012b) for maximization of braking torque with torque ratio constrained to be more than required values. Finally, based on radial and axial dimensional constraints, selection of MR brake for different applications were proposed. Jonsdottir et al. (2009) investigated the influence of different parameters of MR rotary brake on the torque response by computing strength of magnetic field and flux density using magnetic finite element analysis. The parameters which had major influence on the braking torque were identified and the proposed method assists during the design stage for prioritizing key design parameters. Lijesh et al. (2018) examined the influence of brake dimensions on the torque response using magnetostatic analyses. Finally, a methodology was proposed and validated to estimate the dimensions of MR brake for specified outside dimensions, which would deliver highest braking

performance in terms of effective torque and brake cost function. Acharya et al. (2019) performed magnetostatic analysis of T-rotor MR brake for different combinations of brake dimensions to compute magnetic flux density and subsequently braking torque using analytical equations. The optimum brake parameters were obtained with the objectives of maximizing the torque ratio and minimizing brake mass by means of MOGA optimization.

Another factor which significantly affects the output of MR brake is the composition of MR fluid comprising of mass fraction of iron powder, particle size, base oil and its viscosity. Optimal composition of MRF which provided best response in MR devices have been reported in literature. (Gurubasavaraju et al. (2017); Mangal and Sharma (2017)). Wang et al. (2019) studied the effects of viscosity of silicone oil and particle size and mass fraction of CIP on yield stress of MR grease. It was concluded that viscosity of oil and mass fraction of iron powder had significant effect on the yield stress whereas particle size had a lesser effect. Gudmundsson et al. (2011) investigated the magnetorheological properties of synthesized MRF having five different particle sizes within range of 1- 8 microns and three bimodal MRFs comprising of mixture of coarse and fine powders. Three MRFs were proposed for prosthetic knee application which resulted in maximum field induced torque and minimum off-state torque. However, the effect of particle mass fraction and base oil viscosity were not considered in the study. Quoc et al. (2019) carried out simulation studies to determine the performance characteristics of an optimally designed MR brake, such as braking torque, off-state torque, and power consumption utilizing three commercial MR fluid namely MRF 122-2ED, MRF 132DG and MRF 140CG (Make: Lord Corporation). These MRF contain 72 %, 80.98 % and 85.44 % weight fraction of magnetizable particles respectively as per manufacturer's data sheet. Based on the study, commercial MR fluid, MRF 132DG (Lord Corporation) was recommended for use in MR brakes due to its optimum performance characteristics. Acharya et al. (2019) determined the optimal weight percentage and size of carbonyl iron powder in MRF for use in MR damper by means of MOGA optimization method based on characterization of MRFs comprising different weight fractions and particle size.

2.6 MAGNETORHEOLOGICAL FLUID SANDWICH BEAM

Several research works have been performed on MRF sandwich beams due to their vibration suppression capabilities and have potential applications in flexible structures such as aircraft wing, automobile hood, appendage of space robot and other structural applications (Kolekar et al. 2019). When used in structural beam applications, the MRF functions in the pre-yield regime and shows a viscoelastic behaviour with complex shear modulus relating shear stress and shear strain (Weiss et al. 1994). The vibration characteristics of a beam depends on the stiffness, mass and damping. With the usage of magnetorheological fluid sandwiched between elastic face layers and varying the magnetic field, the modal and dynamic behaviour of the beam can be altered.

The vibration controllability of MRF sandwich beams has been investigated theoretically and experimentally in many research works. Sun et al. (2003) performed oscillatory tests to determine the viscoelastic properties of MRF and forced excitation tests of MRF sandwich beam at different magnetic fields. It was found that as magnetic field is incremented, the complex shear modulus increased, the natural frequencies shifted to higher frequencies and the amplitude of vibration under forced excitation decreased. Yalcintas and Dai (1999, 2003) compared the theoretical and experimental vibration behaviour of MR sandwich beams and found that there is positive shift in natural frequencies, loss factor variation and vibration amplitude reduction. Lara-prieto et al. (2009) performed free vibration tests on MRF sandwich beams and concluded that the sandwich beam vibration response can be controlled in the form of variations in vibration peak response and shifts in natural frequency. Hu et al. (2006) analytically studied vibration behaviour of a MRF sandwich beam under changing magnetic field strength and they found out that with increase in magnetic field strength, there is an increase in the natural frequencies and the loss factors of the MRF beam while the vibration response got reduced. Fadaee (2019) studied the effects of boundary conditions, MRF layer thickness and properties of material and the magnetic field on vibration characteristics of functionally graded MRF sandwich beams through analytical approach and concluded that the effect of magnetic field on loss factor is more than that on natural frequency. Rajamohan et al. (2009) investigated the influence

of MR layer thickness on natural frequency and loss factor; effect of magnetic field intensity on natural frequency, loss factors and vibration amplitude of simply supported, cantilever and clamped-clamped MRF sandwich beams. It was determined that the natural frequencies shifted to higher frequencies and the loss factor of the MRF sandwich beams increased with increase in the magnitude of magnetic field. Kolekar and Venkatesh (2019) determined the dynamic behaviour of MRF sandwich beam under different localized magnetic fields. It was concluded that there is a shift in the natural frequency and decrease in vibration amplitude, while there is a decrease in loss factor. Allien et al. (2019; 2019a) fabricated MRF sandwich beams with face layers having different percentages of Silicon carbide (SiC) reinforced aluminium metal matrix composites (MMC). It was found that at 600 Gauss magnetic field, 20% SiC reinforced aluminium MMC MRF sandwich beam yielded maximum reduction in vibration response. Allien et al. (2016, 2020) prepared different thickness of polymer matrix composite (PMC) as face layer for MRF sandwich beams and determined their vibration suppression behaviour. It was found that at 600 Gauss magnetic field, 2 mm thick MRF core enclosed between 2 mm thick top and bottom face layers of PMC resulted in maximum percentage reduction in vibration amplitude. Srinivasa et al. (2020) performed free and forced vibration experiments of fully filled MRF sandwich beams of different core thicknesses of 2 mm, 4 mm and 6 mm and concluded that 2 mm core MRF sandwich beam yielded highest damping ratio and vibration suppression. Further, free and forced vibration studies of partially filled MRF sandwich beams of different core lengths were performed. Yeh and Shih (2006) numerically studied the effects of magnetic field, core thickness ratio and beam length on the buckling load, natural frequency, loss factor and dynamic instability of MR beam under an axial harmonic load. Kovac et al. (1971) performed theoretical and experimental study of flexural vibrations of sandwich beams clamped at its ends. Zhou and Wang (2005) studied the field dependent dynamic flexural rigidity of the simply supported beam with MR elastomers as the core. Zhou and Wang (2006) further presented the structural design aspect for enhancing the magnetic controllability of MRE-based sandwich beams using theoretical and numerical approaches. Shear thickening fluid have been used as core material into the composite structures for controlling the properties of beam. Hirunyapruk et al. (2010) developed a new type of vibration control system like

a tunable beam filled with magnetorheological fluid called tuned vibration absorber. Daniel and Abot (2000) conducted an experiment for testing and analysis of composite sandwich beams and to determine their flexural behaviour. Arvin et al. (2010) investigated and conducted experiments for composite sandwich model with composite faces and viscoelastic core. They developed finite element code for structural response analysis for the composite sandwich beam. Sapiński et al. (2010) determined the modal parameters of three-layered sandwich cantilever beam incorporating Lord Corporations' MRF 140CG fluid using experimental and computational methods and found a good agreement between the results. Sapiński et al. (2011) determined the vibration characteristics of MR beam filled with two types of commercial MR fluid and concluded that weight fraction of iron particles in the fluid has a significant effect on the natural frequency and damping coefficient of the beam. Based on the literature review, it is evident that the MRF sandwich beams can be successfully used in the control of beam vibrations. The effect of mass fraction and iron particle size in MR fluid on the vibration characteristics of beam and determination of optimal composition are scarce in literature.

2.7 OBSERVATIONS FROM LITERATURE REVIEW

- Particle shape, size and particle mass fraction have a significant effect on the shear yield stress of MR fluid and hence the performance of an MR device.

- Higher yield stresses and consequently better MR effect are obtained in the case of MR fluid with narrow particle size distribution compared to particles with broader particle size distributions.

- Generally, larger sized iron particles in MR fluid yield higher MR effect due to their larger saturation magnetization. But sedimentation stability of MR fluid containing larger sized particles is lesser compared to those containing finer sized iron particles. Also, off-state viscosity of MRF containing larger sized particles increases during passage of time due to wear and tear compared to finer sized particles. Hence, finer sized particles are preferable from wear point of view in addition to their stability.

- Higher carrier oil viscosity increases sedimentation stability while it also increases the off-state viscosity of MRF. This reduces the dynamic range of MR device. Also,

lower viscosity carrier oil has faster response to magnetic field and better redispersibility of iron particles compared to higher viscosity carrier oil.

- Different stabilizer additives have been used by many researchers to enhance the stability of MR fluids. However, most of these stabilizers decrease the MR effect or increase the off-state viscosity of the MR fluid.

- Combination of additives are added to increase sedimentation stability of MR fluid, redispersibility of iron particles, reduce oxidation, corrosion, etc.

- Temperature has detrimental effect on the rheological properties of MR fluid.

- Higher mass fraction of CIP in MR fluid yields higher yield stress of MR fluid. However, it's off-state viscosity and shear stress also increases and decreases the dynamic range of the device.

- Generally, to increase the sedimentation stability of MR fluid following methods are followed: coating magnetizable particles, use of wire-like nanoparticles, using spherical nanoparticles, using stabilizer additives and using dense carrier fluids.

- The design of MR damper involves maximization of damping force or dynamic range while avoiding magnetic saturation in the piston core. This inturn depends on magnetic flux generated in the MR fluid gap. Similarly, the design of MR brake involves maximization of torque or torque ratio.

- The MR fluid composition required for an MR device varies with application.

2.8 RESEARCH GAPS

- Commercially available MR fluid is very expensive. Although extensive research is under progress, considerable amount of work needs to be done for synthesis of In-house MR fluid having desirable properties and compare its rheological properties with that of commercially available MR fluid.

- It's necessary to design and develop low cost MR devices and compare its performance using In-house prepared MR fluid and commercially available MR fluid.

- Design of MR devices also encompasses use of suitable MR fluid in it. The strength of MR fluid depends on its composition such as particle size, shape, mass fraction, carrier fluid viscosity, additives, etc. The study of effect of mass fraction and iron particle size in In-house prepared MR fluid on the performance of MR damper, MR

brake and vibration characteristics of beam are scarce in literature and also the methodology for determination of optimal composition.

2.9 MOTIVATION

Many researchers have done considerable amount of work on enhancing the properties of magnetorheological fluid, performance of MR devices and structures. However, there is no extensive implementation of these devices owing to its high cost and limited to few high end applications. The performance of MR device should not only surpass that of passive ones, but needs to be cost effective for implementation in various devices. This requires in-house fabrication of MR devices and use of suitable MR fluid for the same. Following research which need further study were performed.

- The performance of MR device depends on the composition of MR fluid, that is, the iron particles, carrier fluid and additives. Hence, different types of iron particles and their sizes, weight fractions; carrier fluid and its viscosities; and combination of additives were used for synthesis of MR fluid. The rheological properties of these prepared fluid were compared with those of expensive commercial MR fluid, MRF 132 DG (Lord Corporation).

- The composition of MR fluid in a particular application depends on different performance indices. Determination of suitable composition of MR fluid for each of the applications was performed using MOGA optimization technique as they involved contradictory need for maximization and minimization of different factors affecting the performance of the MR device.

- The performance parameters of MR device such as MR damper, MR brake are primarily dependent on the design of the MR device. Hence, MR damper and MR brakes were designed to maximize the performance of the device while the MR beam dimensions were considered as per standards.

2.10 OBJECTIVES

1) Synthesize and characterize magnetorheological fluid of different compositions and compare the properties of in-house prepared MR fluid with commercial MR fluid (MRF 132DG, Lord Corporation).

2) Design and characterization of a MR damper and determine the optimum composition of MR fluid for use in MR damper.

3) Determine the optimum composition of MR fluid for use in brake application and to design and characterize the same.

4) Determine the dynamic characteristics of a MR fluid core sandwich beams and to find the optimum composition of MR fluid for use in MR sandwich beam.

2.11 SCOPE OF RESEARCH WORK

- Synthesize MR fluid composed of iron particles of different sizes, different carrier fluid, additives and measure their rheological properties and sedimentation stability.

- Use of multi-objective genetic algorithm (MOGA) optimization technique for determination of optimal proportion in different applications.

- Characterization of MR damper with in-house prepared fluid and commercial MR fluid.

- Determination of optimal mass fraction and iron particle size in MRF based on maximization of on-state damping coefficient and minimization of off-state damping coefficient.

- Characterization of MR brake using various MR fluid samples and determination of optimal mass fraction, iron particle size, carrier oil viscosity in MRF based on maximization of on-state torque and minimization of off-state torque.

- Determination of optimal particle size and mass fraction of iron powder in MRF for MR beam based on maximization of damping ratio and minimization of mass of MRF.

2.12 METHODOLOGY

The current study proposes to determine optimal magnetorheological fluid for different engineering applications. Overall methodology is illustrated in the flow chart shown in figure 2.14.

2.12.1 MR fluid Synthesis and Characterization

Initially, field emission scanning electron microscope images of the different powders are obtained. The particle size distribution of different powders are measured using particle size analyzer. Magnetic properties of iron powders like magnetic saturation, coercivity and retentivity are measured using Vibrating Sample Magnetometer (VSM). To synthesize MR fluid, required mass fractions of carrier fluid and additives are mixed using a mechanical stirrer. To this solution, measured quantity of iron particles are added and stirred so as to obtain a homogenous suspension. This is carried out for different combinations of particle materials and sizes, carrier fluid and additives to prepare different MR fluid. Rheological characterization of these MR fluid are done in a rotational rheometer under steady state and dynamic conditions at different currents to measure their flow curves and viscoelastic properties respectively. These are then compared with the measured rheological properties of commercially available MR fluid, MRF 132 DG fluid (Lord Corporation). Then, these fluid are filled in MR dampers, MR brake and MR sandwich beam and experiments are conducted to determine the damping force of damper, torque developed in the brake and damping ratio of the beam respectively. Based on their response for the prepared MR fluid, optimization are performed to determine the optimum composition of MR fluid suitable for respective applications using optimization techniques.
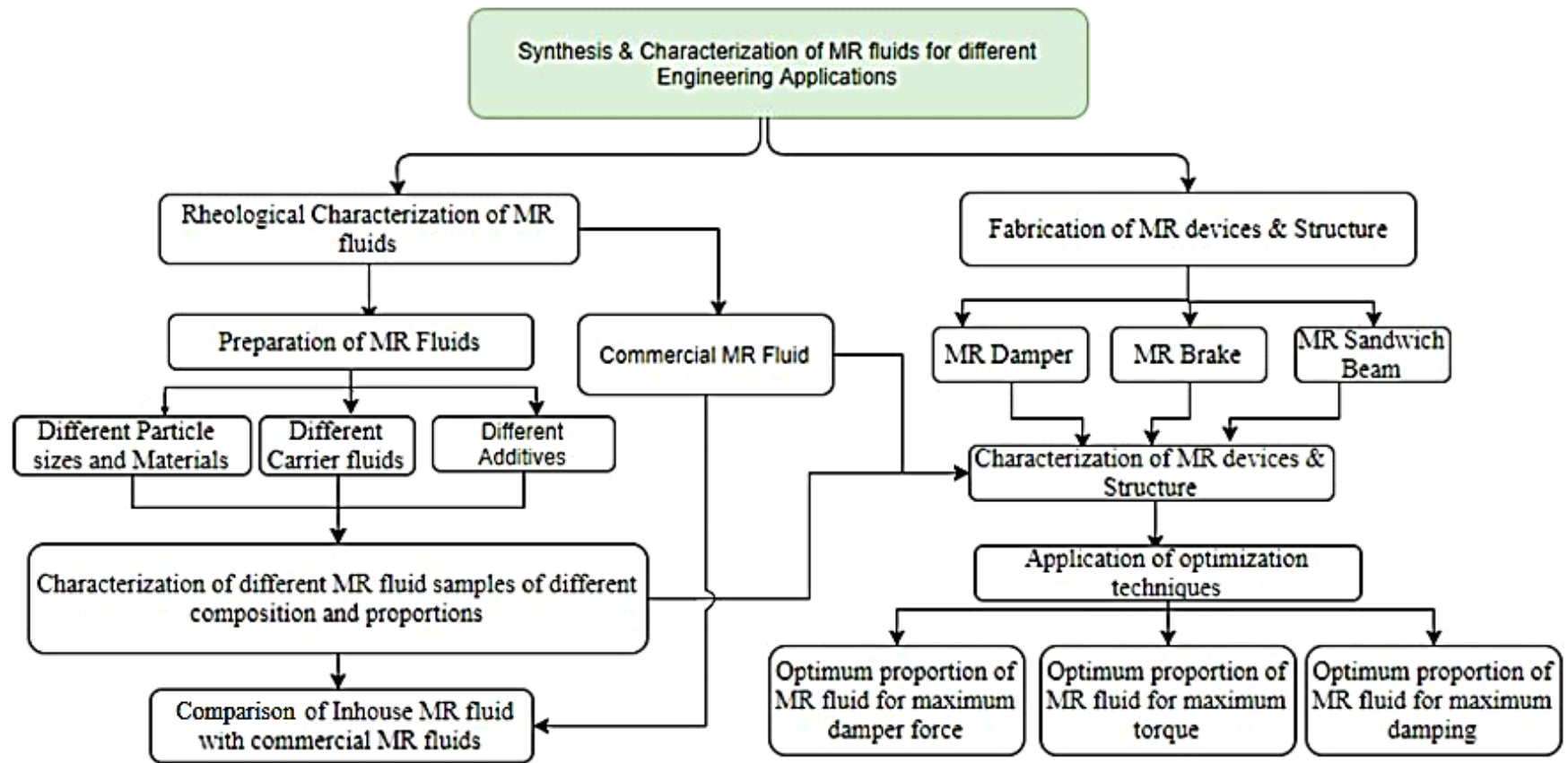
Figure 2.14 Methodology of the research work

2.12.2 Optimal composition of MR fluid for MR damper

In this study, optimum mass fraction and size of iron particles in MR fluid for use in shear mode monotube MR damper were determined based on optimization of experimentally determined damper characteristics utilizing different prepared MRF. Initially, a shear mode monotube MR damper was designed by using optimization technique for desired dynamic range and damping force. A damper was manufactured in accordance with the optimized size and was filled with commercially available MRF 132DG fluid to determine its damping characteristics using damper testing machine. Experimentally determined values were validated with computational ones. Further, iron powders of two different particle sizes were characterized to determine the morphology, particle size distribution and magnetic properties. Then, six MR fluid samples were prepared composed of combination of three different particle loadings and two sizes of iron particles. Rheological tests were conducted on these samples to determine the flow curves at off-state and on-state magnetic field conditions and they were compared with those of commercial MR fluid, MRF 132DG (Lord Corporation). In addition, the sedimentation stability of prepared fluid were measured. These MRFs were filled in the MR damper and damper characteristics were determined. The area bounded by the force-displacement graphs was used to calculate the energy dissipated which was then used to calculate equivalent damping coefficient. Finally, using MOGA optimization, based on maximization of damping coefficient in the presence of magnetic field and minimization of damping coefficient in the absence of magnetic field, the optimal mass fraction and particle size was determined.

2.12.3 Optimal composition of MR fluid for MR brake

In this study, optimal dimensions of MR brake and composition of MRF suitable for the brake application were determined. Initially, optimum parameters of MR brake were computed considering the properties of commercially available MRF132DG fluid using multi-objective genetic algorithm optimization. Maximization of field induced braking torque and minimization of off-state torque were chosen as the objectives. This was performed in MATLAB software coupled with magnetostatic

analyses in ANSYS APDL software. The braking torque of designed MR brake utilizing commercial MR fluid, MRF 132DG (Lord Corporation) was experimentally determined and validated with computational ones. Further, iron powders of three different particle sizes were characterized to determine their morphology, particle size distribution and magnetic properties prior to preparation of different MR fluid. Selection of optimal composition of MRF was done considering In-house MR fluid samples composed of different combinations of particle mass fractions, mean particle diameters and base oil viscosities. A design of experiments technique was employed and braking torque corresponding to the synthesized MR fluid samples at different speeds and current supplied along with the variation of shaft speed during braking process were measured. Grounded on the experimental results, MOGA optimization technique was used to determine optimal MR fluid composition with the objectives of maximizing field induced braking torque and minimizing off-state torque.

2.12.4 Optimal composition of MR fluid for MR fluid core sandwich beam

In this work, six MRF samples composed of combination of two particle sizes and three weight fractions of carbonyl iron powder were prepared and their viscoelastic properties were measured. The MRFs were used to fabricate different MRF core sandwich beams. Additionally, a sandwich beam with commercial MR fluid, MRF 132DG (Lord Corporation) as core was fabricated. The modal parameters of the cantilever MRF sandwich beams were determined at different magnetic fields. Further, sinusoidal sweep excitation tests were performed on these beams at different magnetic fields to investigate their vibration suppression behaviour. Finally, optimal particle size and mass fraction of CIP in MRF were determined based on maximization of damping ratio and minimization of mass of MRF used in different fabricated beams.

2.13 SUMMARY

This chapter presented various studies on synthesis and characterization of MR fluid to determine their rheological properties and sedimentation stability, MR damper design and characterization, MR brake design and characterization and dynamic characteristics of MRF sandwich beam. Based on the literature review, observations from literature, research gaps, motivation for research has been discussed. Further, the objectives of the research are listed and methodology followed to address them are discussed.

CHAPTER 3

OPTIMAL COMPOSITION OF MAGNETORHEOLOGICAL FLUID FOR MR DAMPER

3.1 INTRODCUTION

In the recent past, significant research have been carried out for the design and development of cost effective dampers. The damping force of an MR damper is the key parameter and could be suitably boosted by optimally designing the MR damper piston and the usage of appropriate MRF composition. Few literature reported optimum proportion of MR fluid which yielded maximum shear stress, damping force and on-state viscosity by using optimization techniques. The damping force increases with increase in yield stress and viscosity of MRF under the influence of magnetic field. Under zero magnetic field, the damping force and viscosity should be as low as possible while in the presence of magnetic field the damping force should be high so to increase the dynamic range of the damper. In this chapter, the dimensions of MR damper is obtained by optimization and fabricated and tested for different prepared and commercial MRF. Based on test results, optimal MR fluid composition is proposed.

3.1.1 Methodology for determination of Optimal MR Fluid Composition for MR Damper

The methodology followed for determination of optimal MR fluid suitable for a monotube MR damper is shown in figure 3.1. Initially, using constrained non-linear optimization function, a shear mode MR damper of monotube construction was designed such that it satisfies target dynamic range and damping force. A damper was manufactured in accordance with the optimized size and was filled with commercial MR fluid, MRF 132DG (Lord Corporation) to determine its damping characteristics using damper testing machine. To validate the results, magnetic field in the MR fluid gap at different current was computed by means of magnetostatic analyses in ANSYS workbench software.

The damping force was calculated based on MRF yield stress which depends on the magnetic field distribution in the shear gap. The computationally determined force values were compared with the experimental ones.
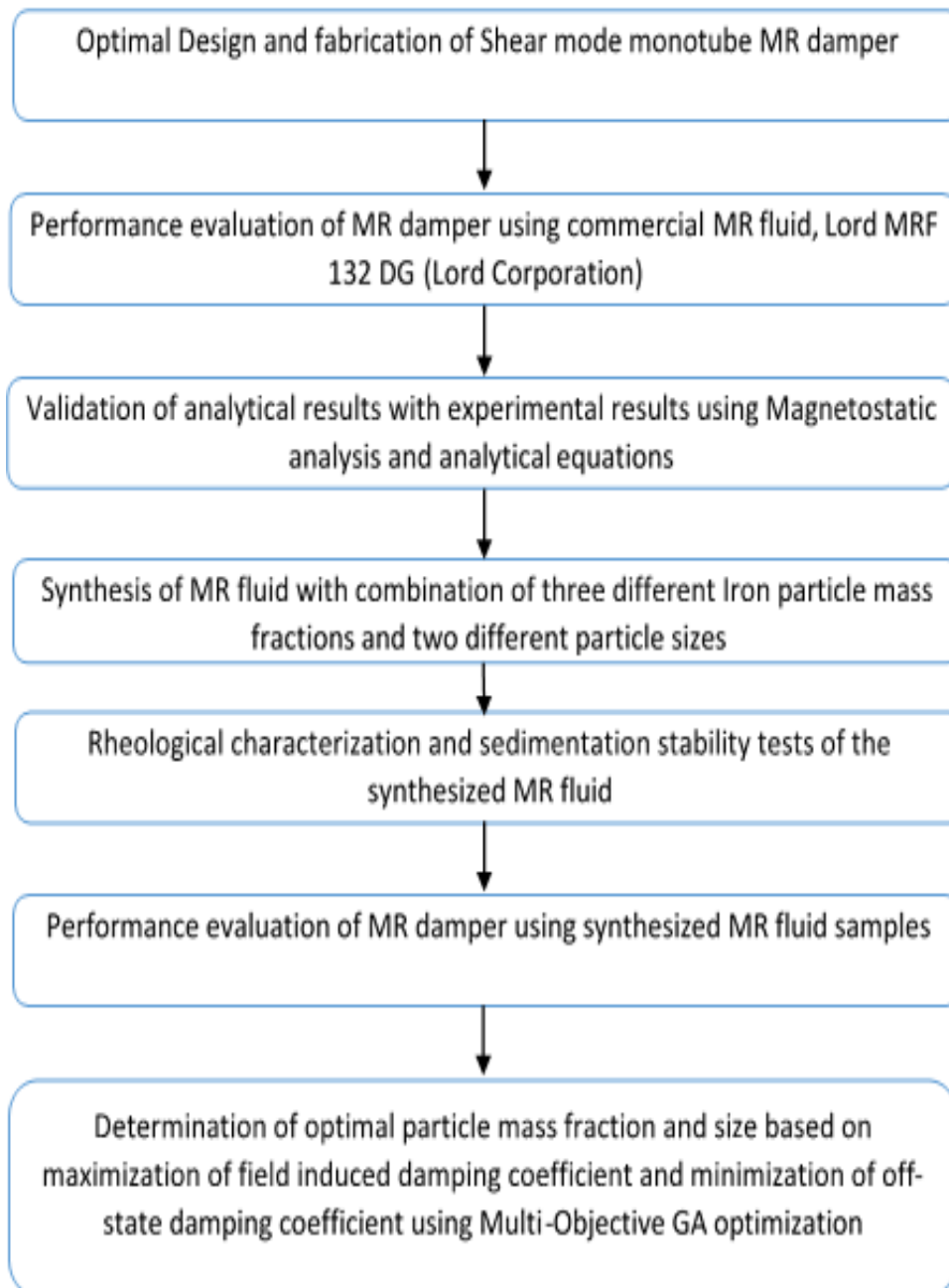
Figure 3.1: Methodology for determination of optimal MR fluid composition for MR damper

Further, MRFs were prepared composed of combinations of 60%, 70% and 80% mass fractions of iron particles and particle sizes of 2.9 μm and 8.27 μm. These were filled in the MR damper and damper characteristics were determined at sinusoidal excitation of ±10 mm piston stroke and frequencies of 0.5 Hz, 1 Hz, 2 Hz and 4 Hz without current and with DC current inputs of 1A and 2A. The area bounded by the force-displacement graphs was used to calculate the energy dissipated which was then used to calculate equivalent damping coefficient. Finally, using MOGA optimization, based on maximization of damping coefficient in the presence of magnetic field and minimization of damping coefficient in the absence of magnetic field, the optimal mass fraction and particle size of iron powder in MRF was determined.

3.2 DESIGN OF SHEAR MODE MONOTUBE MR DAMPER

A damper of monotube construction is extensively utilized in MR devices owing to its simplicity, compactness and ability to function properly in any installed orientation. It consists of single reservoir filled with MRF and piston reciprocating in it as shown in figure 3.2. The piston is wound with copper coil on its core with the lead wires taken out from piston rod end. Seal is provided at the rod end of damper housing to avoid leakage of MRF during reciprocating motion of piston rod.
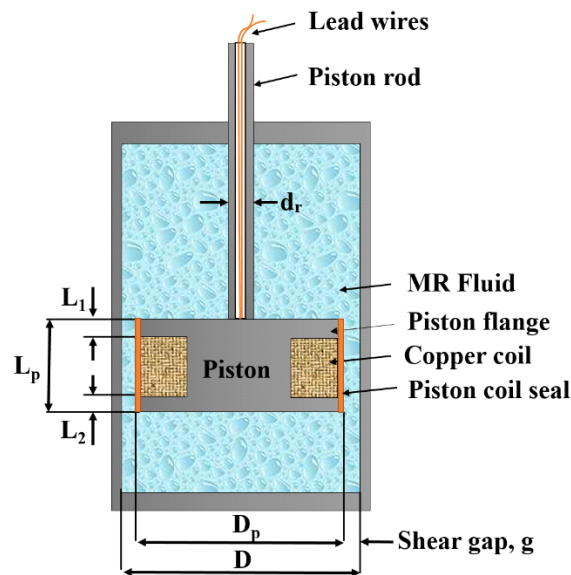
Figure 3.2 Schematic diagram of Monotube MR Damper

The total shear stress of MRF in the presence of magnetic field is expressed in terms of viscous induced shear stress and field dependent shear stress. Hence, for a shear mode MR damper of monotube construction, the total damping force (F) is the sum of viscous damping force (F_μ), field induced damping force (F_τ) and friction force (F_f) as given by equation (3.1). However, friction force is neglected and has not been considered during the design stage.

$$F = F_\tau + F_\mu + F_f. \tag{3.1}$$

Based on parallel plate Bingham model, the field dependent damping force and viscous damping force are expressed by equations (3.2) and (3.3) respectively (Choi and Wereley 2003; Yang et al. 2002).

$$F_\tau = \left(2.07 + \frac{12Q\mu}{12Q\mu + 0.4wt^2\tau_y}\right)\frac{\tau_y L A_p}{g} \tag{3.2}$$

$$F_\mu = \left(1 + \frac{wgv}{2Q}\right)\frac{12\mu Q L_p A_p}{wt^3} \tag{3.3}$$

$$A_p = \frac{\pi\left(D_p^2 - d_r^2\right)}{4} \tag{3.4}$$

$$w = \pi\left(\frac{t}{2} + D_p + \frac{t}{2}\right) \tag{3.5}$$

$$Q = vA_p \tag{3.6}$$

where, L_p is the length of piston (m), L $(= L_1 + L_2)$ is the flange height (m), w is the mean circumference of shear gap (m), D_p is the diameter of piston (m), t is the shear gap thickness (m), μ is the apparent viscosity without magnetic field (Pa-s), τ_y is the dynamic yield stress (Pa), d_r is the diameter of piston rod (m), Q is the volumetric flow rate (m^3/s), v is the relative velocity between piston and cylinder (m/s) and A_p is the piston area (m^2).

The dynamic range (K_d) is defined as the ratio of the total damping force to the uncontrollable force as given in equation (3.7). The uncontrollable force includes viscous damping force assuming negligible friction force (Hu et al. 2015).

$$K_d = \frac{F_\mu + F_\tau}{F_\mu}$$

(3.7)

The design of the damper is based on properties of commercial MR fluid, MRF 132 DG (Lord Corporation). The B-H curve of this fluid is shown in figure 3.3 (a). The apparent viscosity of this fluid is 0.114 Pa-s at 40°C as per technical data sheet provided by the company (Lord Corporation). The dynamic yield stress (τ_y in kPa) of the MRF as a function of the applied magnetic field intensity (H in kA/m) obtained by curve fitting the flow curves is given by equation (3.8), (Gao et al. 2017)

$$\tau_y = -0.8239 + 0.3668 \times H - 7 \times 10^{-4} \times H^2$$

(3.8)
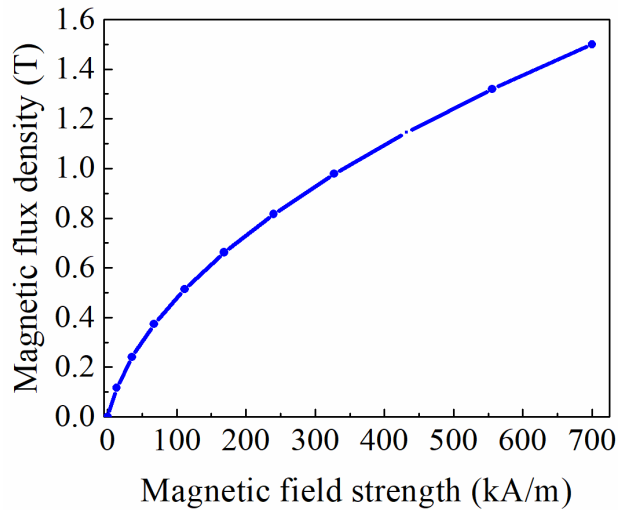
(a) Commercial MR fluid, MRF 132DG (Lord Corporation)
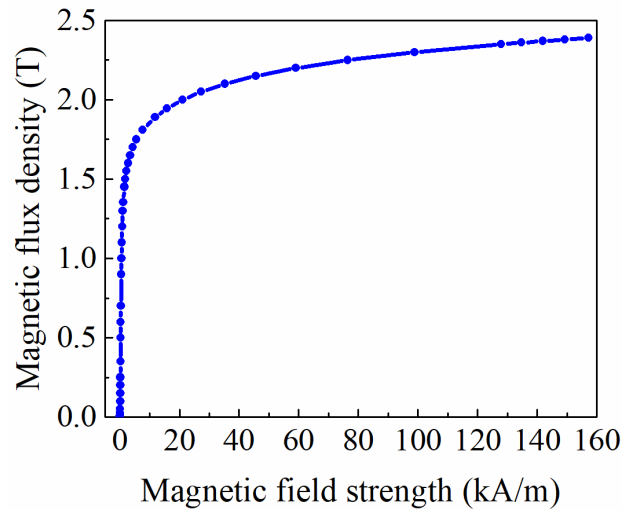
(b) SAE 1020 low carbon steel

Figure 3.3 B-H Curve of commercial MR fluid, MRF 132DG (Lord Corporation) and steel material

Commercial MR fluid, MRF 132DG (Lord Corporation) has a yield stress of 22.74 kPa at a magnetic field of 75 kA/m, obtained from equation 3.8. The design parameters are the piston diameter, piston rod diameter, piston height and its flange height. The recommended MRF gap for MR devices is in the range of 0.25 mm – 2 mm (Yoo and Wereley 2002). The MRF shear gap was chosen as 0.5 mm as smaller gap results in higher magnetic field strength and hence higher damping force. However, gap less than 0.5 mm reduces dynamic range as viscous force increases drastically compared to increase in field induced force (Hu et al. 2015). The objective was to attain damper force of 1000 N at 0.2 m/s piston velocity and dynamic range higher than 4. The constrained non-linear optimization function (*fmincon*) available in MATLAB™ software was used to design the damper piston (Xu et al. 2012). The lower and upper limits of the design parameters and the optimal dimensions of the piston are tabulated in table 3.1.

Table 3.1 Limits and optimized parameters of damper piston

Parameters	Lower limit (m)	Upper limit (m)	Optimal values (m)
Diameter of piston (D_p)	0.025	0.05	0.0287
Diameter of piston rod (d_r)	0.008	0.012	0.01
Piston height (L_p)	0.03	0.05	0.03
Total piston flange height (L)	0.006	0.012	0.012

The piston is bounded by a 1 mm thick cylindrical sheet of gun metal material which acts as a seal and avoids MRF leakage into the piston coil region. The inner diameter of cylinder was chosen as 30 mm so that when the piston is assembled into the cylinder, the shear gap between cylinder inner surface and piston outer surface is 0.5 mm. The cylinder thickness is 2 mm and the cylinder length was chosen to accommodate maximum piston stroke length of $\pm$ 20 mm. The total length of cylinder was chosen as 120 mm which provides piston eye to eye compressed length of 184 mm and 275 mm extended length. Based on available coil area, 240 turns of 26 AWG copper wire were wound on piston core having diameter of 14 mm. The current rating of 26 AWG wire is 2.2 A (Lund 2016). The piston and cylinder were chosen to be made of SAE 1020 steel owing to its high magnetic saturation, relative magnetic permeability and mechanical properties. Figure 3.3 (b) shows the B-H curve of SAE 1020 steel (Rao 2013). An MR damper was fabricated as per the design and is shown in figure 3.4.
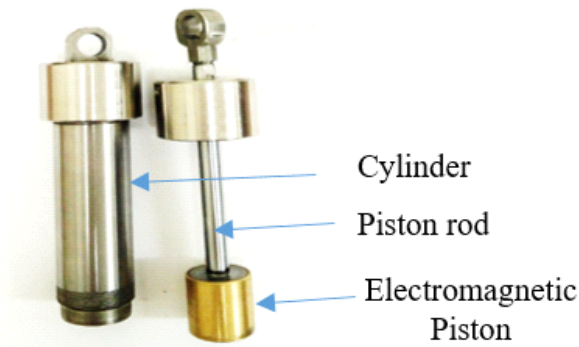
Figure 3.4 Fabricated MR damper

3.3 PERFORMANCE EVALUATION OF MR DAMPER UTILIZING COMMERCIAL MR FLUID

Dynamic behaviour of MR damper filled with commercial MR fluid, MRF 132DG (Lord Corporation) was determined experimentally by means of damper testing machine (Make: HEICO Ltd) shown in figure 3.5.The technical specifications of the machine are detailed in appendix I.6. The damper testing facility consists of hydraulic powerpack, hydraulic actuator, force transducer, position sensor, data acquisition system, software interface and servo controller. The hydraulic powerpack supplies required power to the hydraulic actuator while the frequency of excitation is governed by the servo controller (Make: Moog Ltd). The force transducer is fixed at bottom end of MR damper lower jaw and acquires the damping force. The stroke of piston, frequency of excitation and type of excitation is specified using the software interface and data acquired using position and force transducers are stored in the same for further analysis. DC power source (Make: ScientiFic) was used to supply current to damper coil.

Position sensor (hidden)
Hydraulic actuator
Movable crosshead
Upper jaw (movable)
MR damper
Lower jaw (fixed)
Force transducer
DC power supply

PC with Moog test suite

Hydraulic powerpack
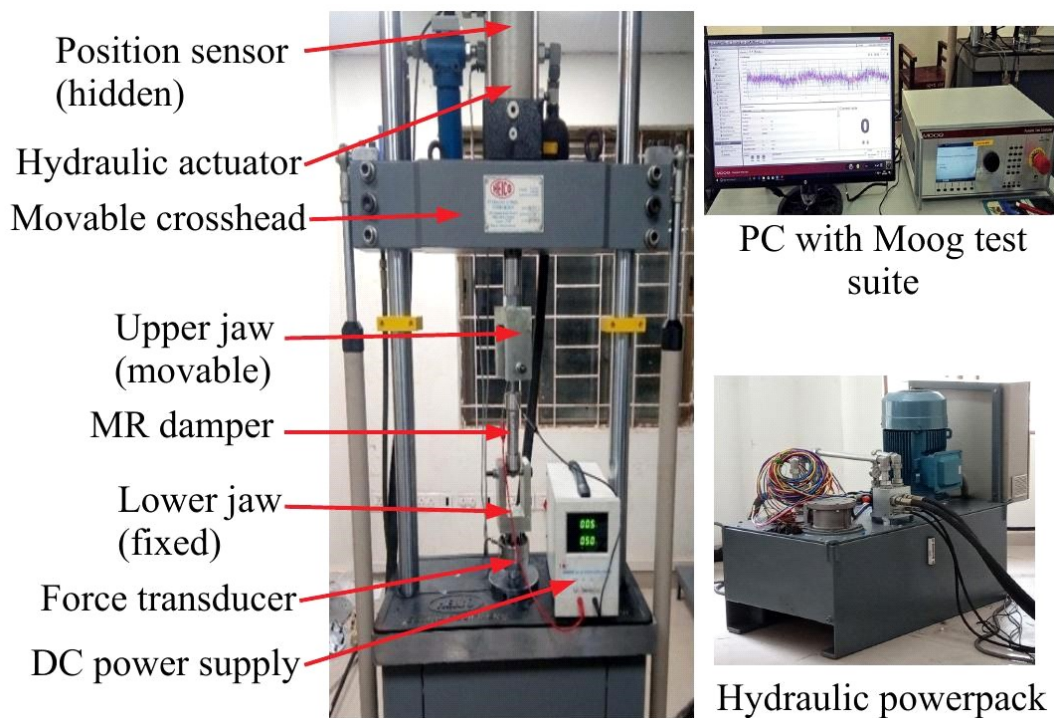
Figure 3.5 Damper testing machine

The commercial MR fluid, MRF 132DG (Lord Corporation) was filled in the damper and then firmly mounted in the damper testing machine between the upper and lower jaws of damper testing machine. Prior to performing the tests, the piston was given stroke of ± 10 mm for 10 cycles at 0.5 Hz so that MRF would be uniformly distributed in the damper cylinder. Tests were carried out for MR damper at frequencies of 0.5 Hz, 1 Hz, 2 Hz and 4 Hz without current and with DC current inputs of 1 A and 2 A and sinusoidal excitation of ± 10mm piston stroke length. Figure 3.6 (a) to (d) shows the force versus displacement curves at 0.5 Hz, 1 Hz, 2 Hz and 4 Hz frequencies at 0A, 1A and 2A current supplied to damper coil. It can be observed that with increase in frequency or current, there is increase in damping force. Maximum damping force obtained from damper testing at 4 Hz sinusoidal excitation and current magnitudes of 0A, 1A and 2A are 389.6 N, 526.4 N and 709.5 N respectively. The maximum damping force is less than designed damping force of 1000 N as required number of coils could not be wound on the piston core due to packing factor and subsequently desired magnetic field strength was not achieved in MRF shear gap.
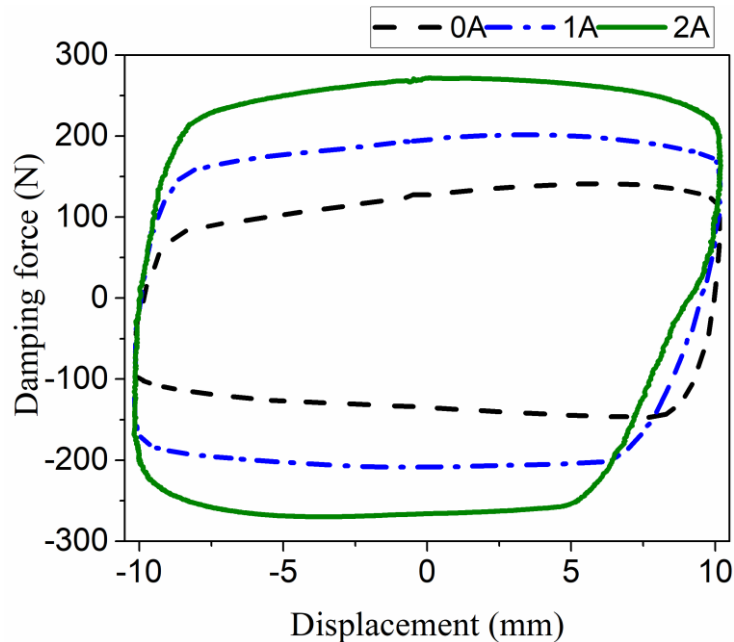
(a) 0.5 Hz sinusoidal excitation
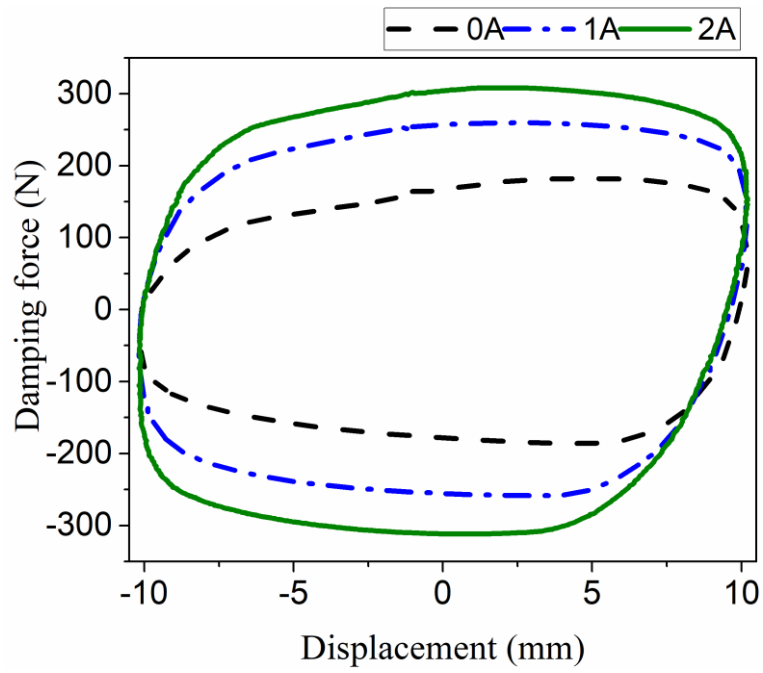
(b) 1 Hz sinusoidal excitation
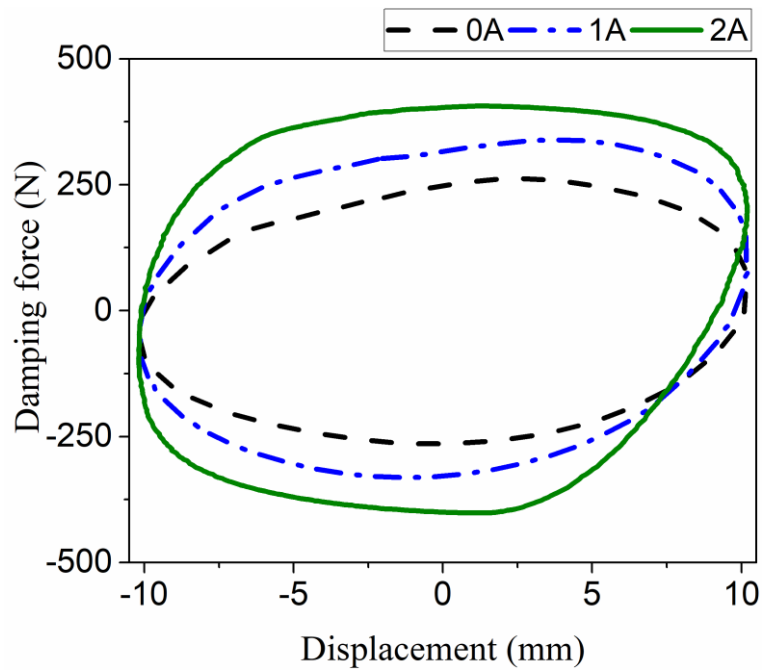
(c) 2 Hz sinusoidal excitation
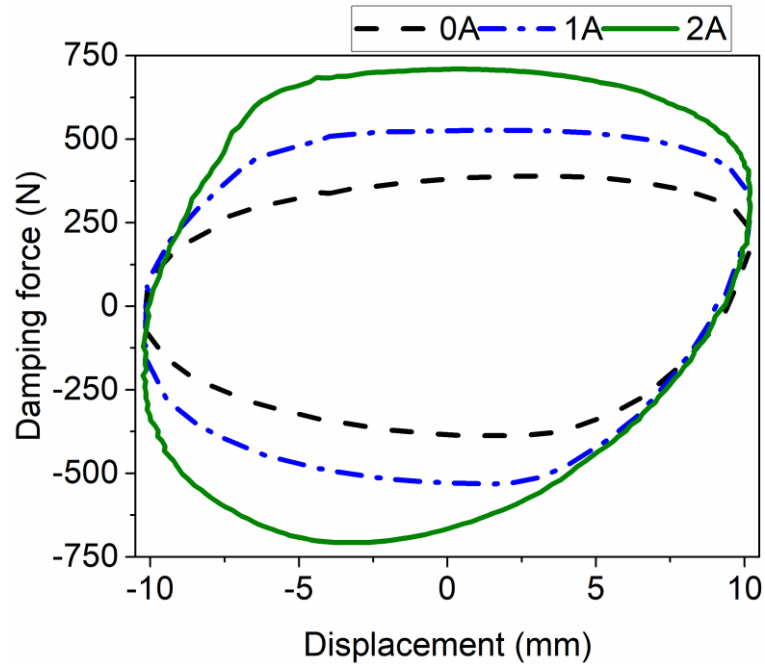
(d) 4Hz sinusoidal excitation

Figure 3.6 Force-displacement curves of commercial MR fluid, MRF 132DG (Lord Corporation)

3.4 COMPARISON OF EXPERIMENTAL AND COMPUTATIONAL RESULTS

Damping force of MR damper filled with commercial MR fluid, MRF 132DG (Lord Corporation) determined experimentally were compared with computational determined ones. Computational damping forces were determined by performing magnetostatic analyses to compute the magnetic field strength in the MRF shear gap. The analyses results were subsequently used to calculate yield stress and field induced damping force.

3.4.1 Magnetostatic Analyses of MR Damper

The damping force of MR damper is governed by the magnetic field in the MRF shear gap in the vicinity of piston flange. The magnetic field strength distribution was determined by means of magnetostatic analysis in ANSYS^{TM} Workbench software.

One fourth of axisymmetric piston was modelled and the material properties were assigned to piston core, piston rod, cylinder, copper coil, piston cover and MRF. The magnetic flux lines were specified parallel along the plane of symmetry. The analyses were performed at current amplitudes of 1 A and 2 A and constant voltage of 12 V.
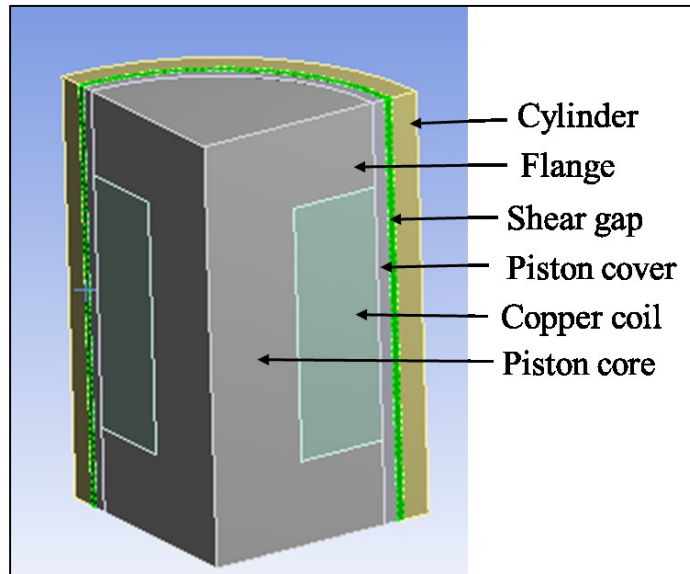
(a) Geometric model of MR damper piston
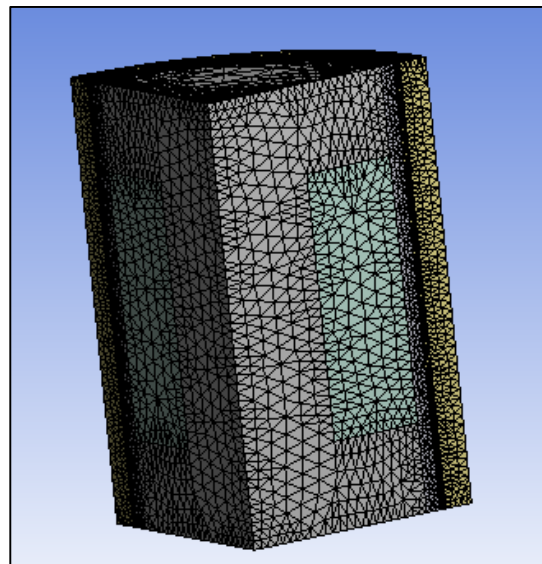
(b) Meshed model of MR damper piston

Figure 3.7 Geometric and meshed models of MR damper piston

Figure 3.7 (a) and 3.7 (b) show one-fourth geometric model of MR damper piston before and after meshing respectively. Very fine mesh was adopted in the MRF shear gap and piston flange region to capture large variation in the results. The magnetic flux density in the MR damper piston and field strength in MRF shear gap at a current of 2 A are depicted in figures 3.8 (a) and 3.8 (b) respectively. The magnetic field strength is higher in the top and bottom regions of MRF in the vicinity of piston flange. The magnetic field intensity in the vicinity of piston flange is around 43 kA/m while the maximum field value is 76 kA/m which is for very small region at the top. Similarly, magnetic field strength in the shear gap in the vicinity of flange region is obtained by performing magnetostatic analysis at 1 A current condition. The field strength distribution for a height of 6 mm from the top and bottom of piston flange are extracted to calculate the yield stress using equation (3.8) and which was then used to calculate the field induced damping force using equation (3.2).
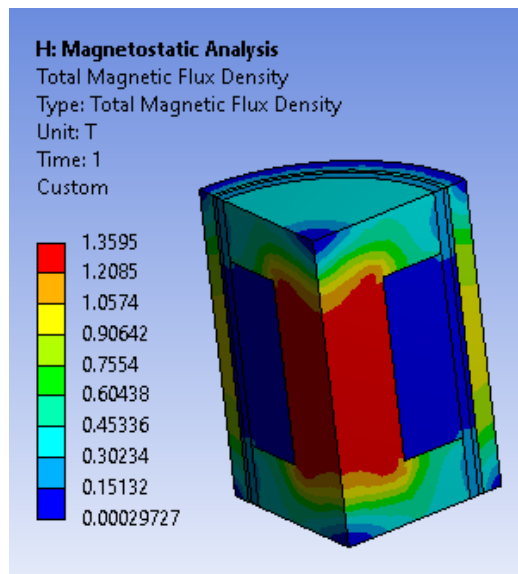
(a) Magnetic flux density in the MR damper piston
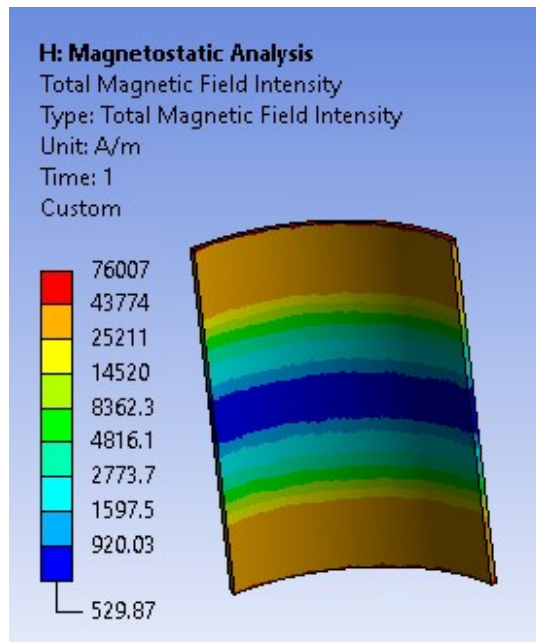
(b) Magnetic field intensity in the MRF shear gap

Figure 3.8 Magnetostatic analyses results

3.4.2 Experimental and computational damping force comparison

The off-state damping force was calculated for 4 Hz frequency (0.2512 m/s) using equation (3.3). The field induced damping forces were evaluated at 1 A and 2 A current conditions using the methodology explained in previous section. The total damping force values determined by magnetostatic analyses coupled with analytical equations were compared with experimentally determined ones at different current as tabulated in table 3.2.

Table 3.2 Computational and experimentally determined damping force

	Computationally determined force (N)			
Current (A)	Field induced force (N)	Off-state force (N)	Total damping force (N)	Experimental force (N)
0.0	0.0	313.4	313.4	389.6
1.0	177.4	313.4	490.8	526.4
2.0	438.3	313.4	751.7	709.5

The experimentally measured force values have a close agreement with those obtained using computational method in the presence and absence of magnetic field. In the absence of magnetic field, the discrepancy in the computational and experimentally determined force values can be attributed to the friction force which was not considered in analytical equations. In the presence of magnetic field, the deviation could be attributed to the variation in magnetic properties due to material imperfections. Further, the magnetic properties damper material and MRF viscosity (Karakoc et al. 2008) are affected by temperature rise which are not taken into account in the magnetostatic analysis.

3.4.3 Characterization of Iron powder

Iron powder is the key ingredient of MR fluid and should have narrow size distribution, spherical in size and should possess good magnetic properties. The particle size should be less than 10 microns to avoid sedimentation problem in MR fluid while it should be more than one micron in order to achieve higher shear stress MR fluid. The rheological properties of MRF are mainly dependent on the magnetic properties of iron particles, their size and distribution. In this work, Carbonyl iron powder (CIP) of two different mean particle sizes were used as dispersed phase for preparation of different MR fluid. The CIP of finer (C3518, Sigma Aldrich) and coarser size (44890, Sigma Aldrich) are named as SCIP and MCIP respectively. The morphology, particle size distribution and magnetic properties of iron particles were characterized.

3.4.4 Scanning Electron Microscope Images of Carbonyl Iron Particles

The scanning electron microscope images were obtained using Field Emission Scanning Electron Microscope (FESEM, Make: ZEISS SIGMA) at a magnification level of 10,000X to observe the surface morphology of iron particles (Appendix I.1). Figures 3.9 (a) and (b) depicts the FESEM images of finer and coarser sized CIP used in this study, depicting almost spherical shape of the CIP.
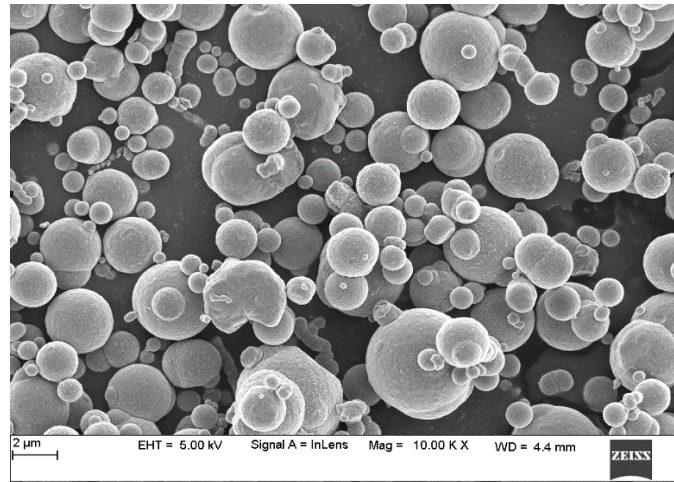
(a) Finer sized CIP
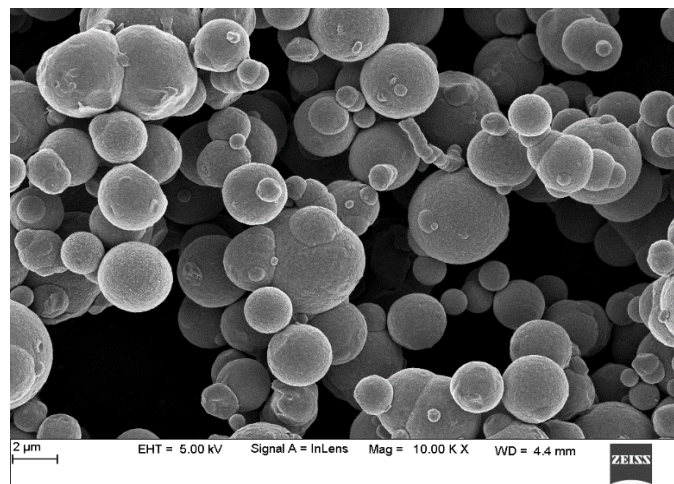
(b) Coarser sized CIP

Figure 3.9 FESEM images of iron powders

3.4.5 Particle Size Distribution

Particle size distribution has an influence on the magnetorheological effect of MRF. The size distribution of particles was determined by means of Particle Size Analyser (Make: Cilas 1064) which can be used to measure particle size ranging from 0.04 to 500 microns (Appendix I.2). Figures 3.10 (a) and 3.10 (b) depict the particle size distribution of coarser and finer sized CIP determined based on volume basis. Mean diameter of finer and coarser sized CIP was found to be 2.90 microns and 8.27 microns respectively.
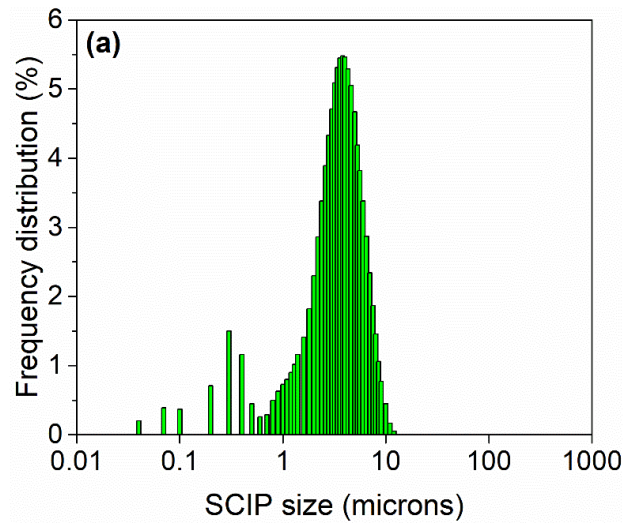
(a) Finer sized CIP
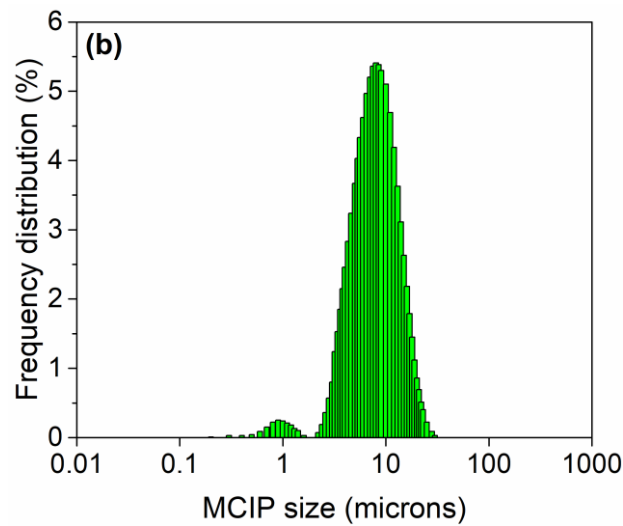
(b) Coarser sized CIP

Figure 3.10 Particle Size Distribution of iron powders

3.4.6 Magnetic properties of Carbonyl Iron powder

The magnetic hysteresis curves of the coarser and finer sized CIP shown in figure 3.11 were obtained using vibrating sample magnetometer (VSM). The VSM equipment used is Vibrating Sample Magnetometer (Make: Lakeshore, 7410) interfaced with VSM software (Appendix I.3). The test was conducted at a temperature of 25°C. The iron particles should possess high saturation magnetization and low

coercivity as well as remnant magnetization for higher yield stress of MRF and reversibility of MR effect (Genç and Phulé 2002).
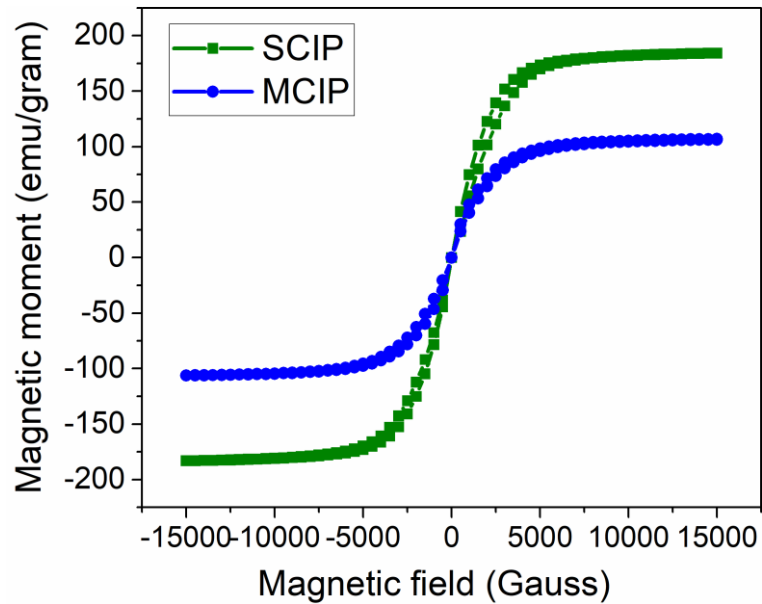
Figure 3.11 M-H curve of finer and coarser sized iron powder

From the magnetic properties of finer and coarser sized CIP listed in table 3.3, it is clear that finer sized CIP have lower retentivity, lower coercivity and higher saturation magnetization compared to coarser sized CIP. Hence, finer sized CIP have better magnetic properties compared to coarser sized CIP.

Table 3.3 Magnetic properties of iron powders

Property	Finer Sized CIP (SCIP)	Coarser Sized CIP (MCIP)
Saturation Magnetization (emu/g)	184.2	106.9
Coercivity (Gauss)	0.59	3.85
Retentivity (emu/g)	0.045	0.18

3.5 Synthesis and characterization of MR fluid

3.5.1 Synthesis of MR Fluid

Six MRF samples were prepared composed of three different particle mass fractions namely 60%, 70% and 80% composed of SCIP and MCIP. Mass fraction less than 60 % would result in lesser MR effect due to lesser number of particles for a given volume. Mass fraction more than 80% would result in higher off-state viscosity and hence higher off-state damping force which reduces the dynamic range of the damper. Further, steps of 10 % was considered to achieve noticeable difference in the shear stress of MR fluid..Polyalphaolefin (PAO, Make: Exxon Mobil) oil was used as carrier fluid having viscosity of 32 cSt (@ 40°C). A lower viscosity oil was utilized as carrier fluid since it reduces the off-state damper force which subsequently increases the MR damper dynamic range. Also, a lower viscosity base oil reduces the response time of MRF and enhances the settled particle redispersibility (Zuzhi et al., 2016). To reduce agglomeration, fumed silica (Make: Sigma Aldrich) with 3% of mass of carrier oil was added. Also, aluminium distearate (Make: Sigma Aldrich) of same proportion as fumed silica was added to enhance the suspension redispersibility (Ashtiani and Hashemabadi 2015a; López-López et al. 2006, 2008a).

Table 3.4 Composition of different MR fluid

Sl. No.	Particle type	Name of the MRF sample	Mass of CIP (gm)	Mass fraction of CIP (%)	Mass of PAO oil (gm)	Mass fraction of PAO oil (%)
1.	MCIP	MRFL60	60	60	40	40
2.	SCIP	MRFS60	60	60	40	40
3.	MCIP	MRFL70	70	70	30	30
4.	SCIP	MRFS70	70	70	30	30
5.	MCIP	MRFL80	80	80	20	20
6.	SCIP	MRFS80	80	80	20	20

During the preparation of MR Fluid, initially, carrier fluid, additives and CIP of desired mass were measured using electronic weighing balance. Fumed silica and Aluminium distearate were added to PAO oil contained in a polyethylene beaker and stirred using a mechanical stirrer for four hours to ensure proper mixing of the additives in the carrier fluid. Further, CIP was added to this solution and manually mixed and then stirred at 800 rpm for twelve hours to obtain homogenized suspension. The details of the prepared MRF samples is listed in table 3.4. The nomenclature of the prepared MRF are based on the particle mass fraction and mean size of the particles. MR fluid composed of 60%, 70% and 80% mass fraction of MCIP are termed as MRFL60, MRFL70 and MRFL80 respectively. Similarly, MR fluid composed of 60%, 70% and 80% mass fraction of SCIP are termed as MRFS60, MRFS70 and MRFS80 respectively.

3.5.2 Rheological Characterization of MR Fluid

Shear stress as a function of shear rate for the six MRF samples and commercial MR fluid, MRF 132DG (Lord Corporation) were measured using MCR-702 Anton Paar Modular Compact Parallel Plate Rheometer at different magnetic fields in a Controlled Shear Rate (CSR) mode. The rheometer along with Magnetorheological Device (MRD) cell and chiller are shown in figure 3.12. It is interfaced with Rheocompass software to give control inputs to rheometer, acquire rheological data and perform analyses. The MRD cell provides the necessary magnetic field based on the current specified in the Rheocompass software. Chiller circulates cooling water around the electromagnetic coils and parallel plates to maintain the desired temperature during rheological testing. A gap of 0.5 mm was set between the parallel plates of 20 mm diameter and temperature was maintained at 25°C during the tests. The samples were stirred to ensure homogeneity of dispersion and then very small quantity of MRF sample was poured on the stationary parallel plate. The fluid was pre-sheared for 20 seconds at 10 /s shear rate followed by 10 seconds waiting to uniformly distribute the sample, prior to testing the MRF (Gurubasavaraju et al. 2017).The samples were tested at shear rates increasing linearly from 0.1 /s to 600 /s and the properties were acquired at 12 shear rate values.

The tests were performed in the absence of current (0 A, off-state condition) and in the presence of current (on-state condition) at 1 A, 2 A and 3 A.
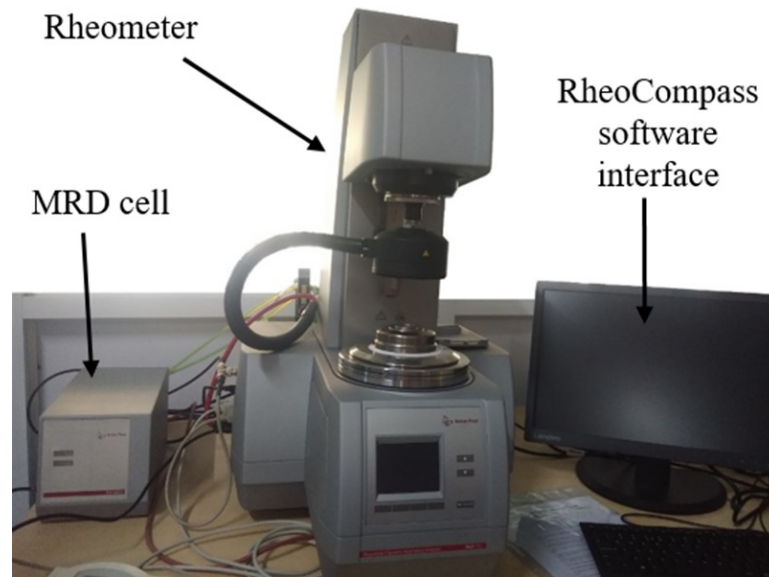
Figure 3.12 Rheometer Setup

Figure 3.13 (a) shows flow curves at zero magnetic field for commercial MR fluid, MRF 132 DG and MRFs with 60%, 70% and 80% mass fractions of fine and coarse CIP. It can be observed that MRFs composed of higher mass fraction of CIP yields higher shear stress as its viscosity is higher. Also, MRFs composed of fine CIP have greater shear stress compared to those composed of coarse CIP for all mass fractions as there would be more number of particles in MRFs containing fine sized CIP for a particular mass fraction. Commercial MR fluid, MRF 132 DG has lowest shear stress in the off-state condition. Figure 3.13 (b) shows the viscosity curves for commercial MR fluid, MRF 132 DG and in-house prepared MRF samples at no magnetic field and it can be observed that the MRF viscosity decreases with increase in shear rate i.e. the fluid exhibits shear thinning behaviour. Also, the viscosity of MRF composed of finer sized particles is higher compared to those of coarser sized particles for same particle mass fraction. Commercial MR fluid, MRF 132 DG has lowest viscosity compared to in-house prepared MRF. Figures 3.14 (a) and 3.14 (b) shows the flow curves for commercial MR fluid, MRF 132 DG and MRFs with 60%, 70% and 80% particle mass fractions composed of fine and coarse sized CIP at current of 1 A, 2

A and 3 A respectively. It is evident that for all particle mass fractions, higher shear stress is obtained for MRFs composed of fine sized CIP compared to those containing coarse CIP. This is because from magnetic property testing, it was observed that fine sized CIP have higher saturation magnetization compared to coarse sized CIP. MRF80S has higher shear stress compared to MRF 132DG at 2 A and 3 A, while at 1 A, it has comparable values.
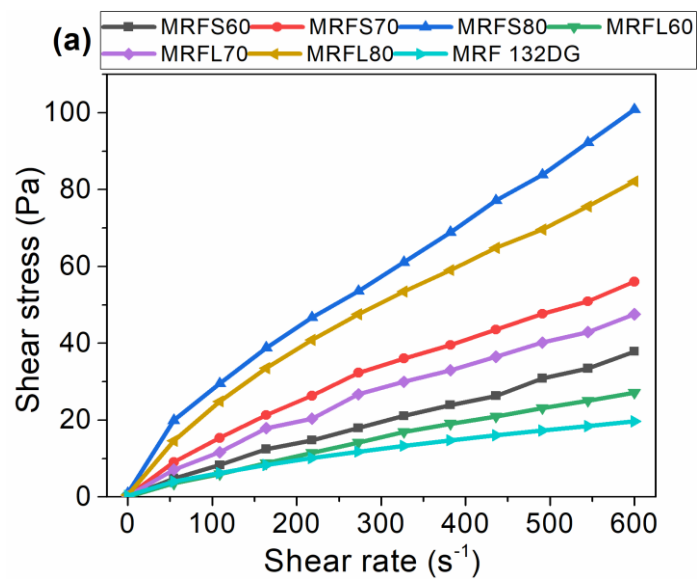
(a) Flow curves in the absence of magnetic field
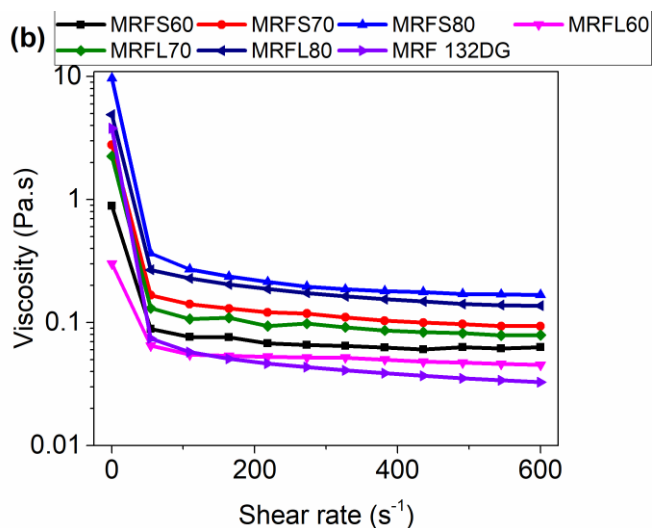
(b) Viscosity curves of in the absence of current

Figure 3.13 Rheological characterization of prepared MRFs at 0 A
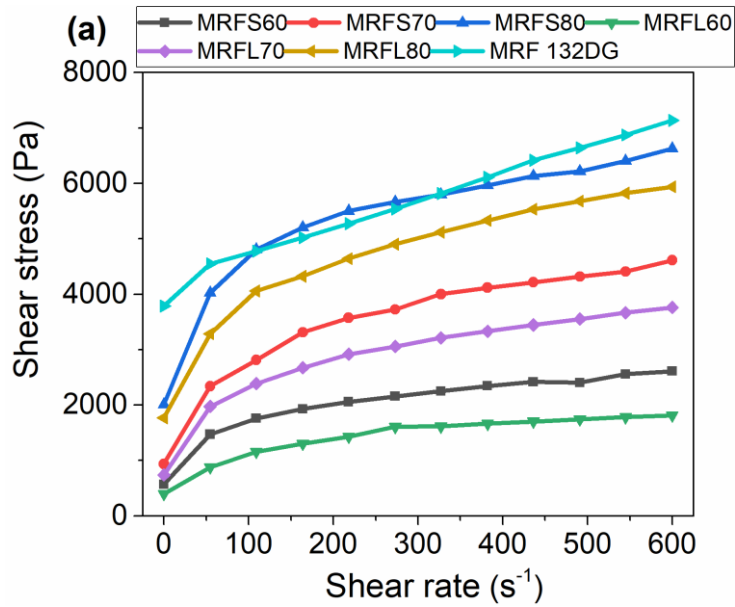
(a) Flow curves of prepared MRFs at 1 A current
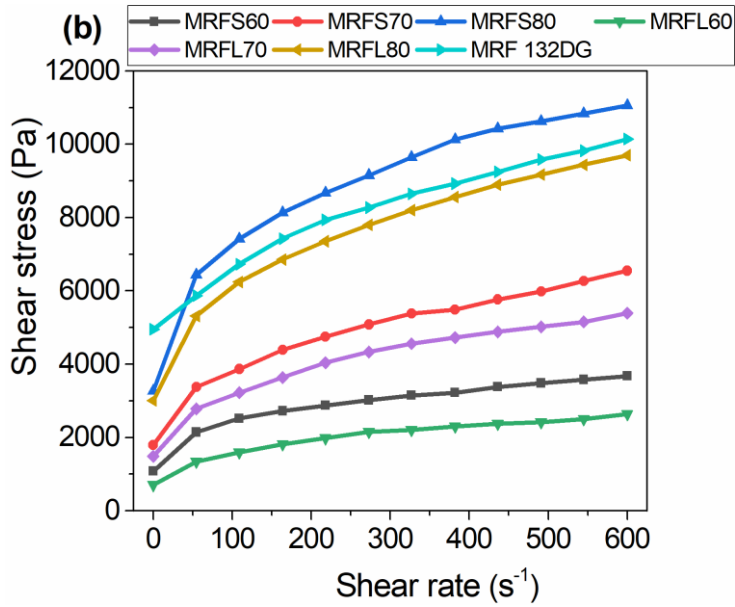
(b) Flow curves of prepared MRFs at 2 A current
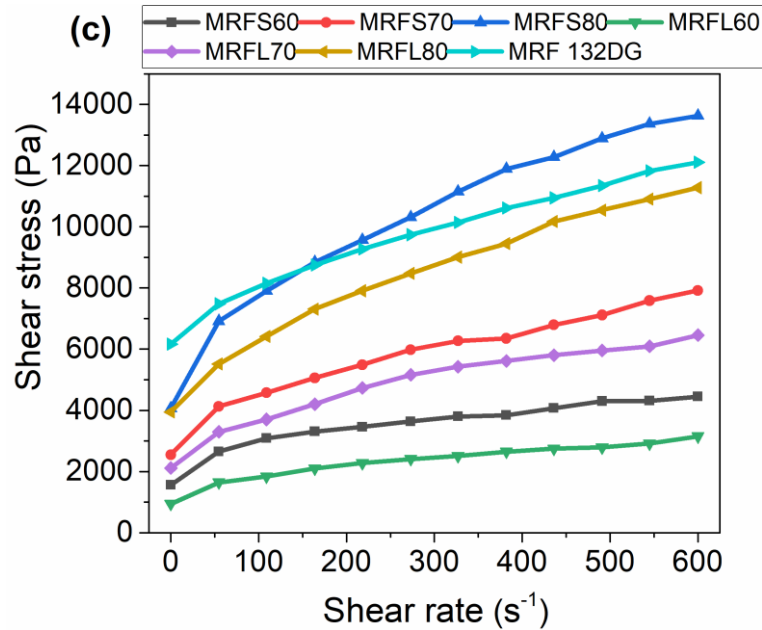
(c) Flow curves of prepared MRFs at 3 A current

Figure 3.14 Flow curves of prepared MRFs in the presence of current

3.5.3 Sedimentation Stability of MR fluid

Sedimentation stability is one of the prime factors of an MRF which affects the performance of a MR device. Sedimentation tests were performed for MRF composed of SCIP and MCIP. It was measured by visual observation of position of boundary interface between the transparent and turbid portion of the MRF. MRF were filled in 10 ml graduated polypropylene cylindrical measuring tubes. The difference in the density between the iron particles and the carrier fluid causes the iron particles to settle with time. Readings are noted periodically at intervals of three hours until there is no changes in the readings. The sedimentation stability of the fluid is quantified in terms of sedimentation ratio which is the ratio of the volume of clear or supernatant fluid to the volume of entire MRF suspension (Ashtiani and Hashemabadi 2015). Figure 3.15 (a) shows the sedimentation ratio as a function of time. Graph was plotted for time steps of twelve hours. The sedimentation ratio increases with time due to settling of particles and reaches a constant value after particle have completely settled.

Figure 3.15 (b) shows the number of hours taken by different MRF to completely settle. The sedimentation ratio increases with time due to settling of particles and reaches a constant value after particle have completely settled. It can be observed that MRF containing coarse sized iron particles have higher slope indicating faster settling rate of particles compared to those composed of fine sized iron particles for all mass fractions. MRF having SCIP have lower slope compared to LCIP based MRF and takes more time to completely settle indicating higher sedimentation stability of SCIP based MRF. This is in agreement with the results obtained by several research works published in literature. Further, MRF with higher mass fraction of iron particles in MRF yielded better stability compared to those with lower particle mass fraction as settling velocity of particles decreases with increase in particle mass fraction (Liu et al. 2013; Ngatu and Wereley 2007). Sedimentation stability of MRF with 80% mass fraction of SCIP is 72 hours which is the highest among other MRF while minimum one was observed for MRF with 60% mass fraction of LCIP i.e 27 hours. MRFL60 fluid has lowest stability as it contains lower particle mass fraction and coarse particle size of iron powder in MRF. Figure 3.15 (c) shows the photographs of graduated cylindrical measuring tubes in which MRFs have completely settled after they were poured and settling behaviour was visually observed.
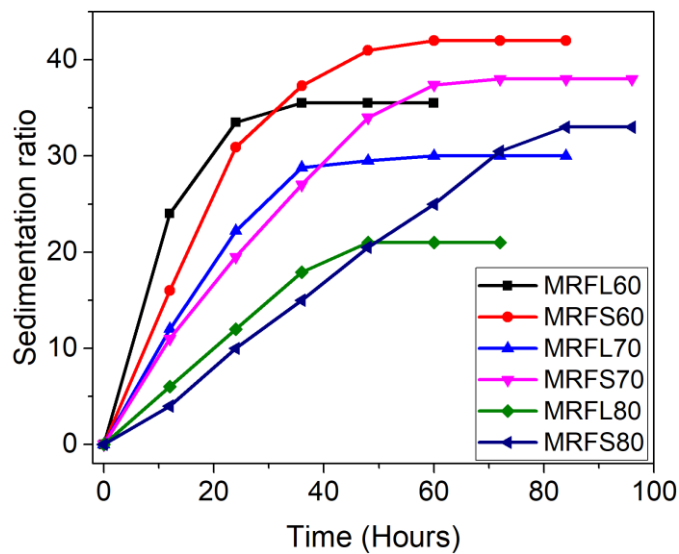
(a) Sedimentation ratio versus time of MRFs
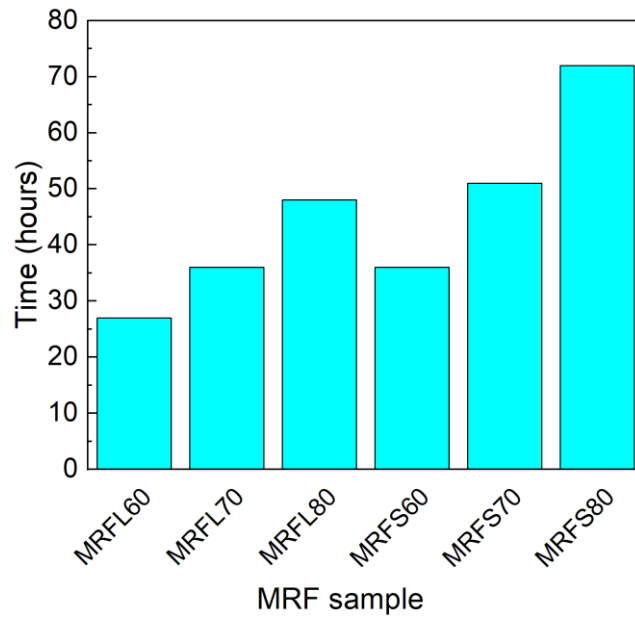
(b) Sedimentation time of different MRF
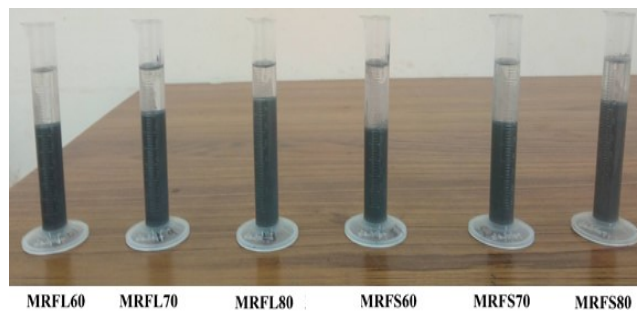
(c) MRF after complete particle settling

Figure 3.15 Sedimentation stability study of MRFs

3.6 DAMPING CHARACTERISTICS OF MR DAMPER FOR IN-HOUSE PREPARED MR FLUID

MR damper filled with different in-house prepared MRFs at frequencies of 0.5 Hz, 1 Hz, 2 Hz and 4 Hz without current and with DC current inputs of 1 A and 2 A with sinusoidal excitation of ± 10mm piston stroke length. Figures 3.16 shows the force versus displacement curves for MR damper filled with different prepared MRFs at 4 Hz frequency at 0 A, 1 A and 2 A current conditions.

80

(a) MRF with 60 % mass fraction of SCIP

(b) MRF with 60 % mass fraction of MCIP

(c) MRF with 70 % mass fraction of SCIP

(d) MRF with 70 % mass fraction of MCIP

82
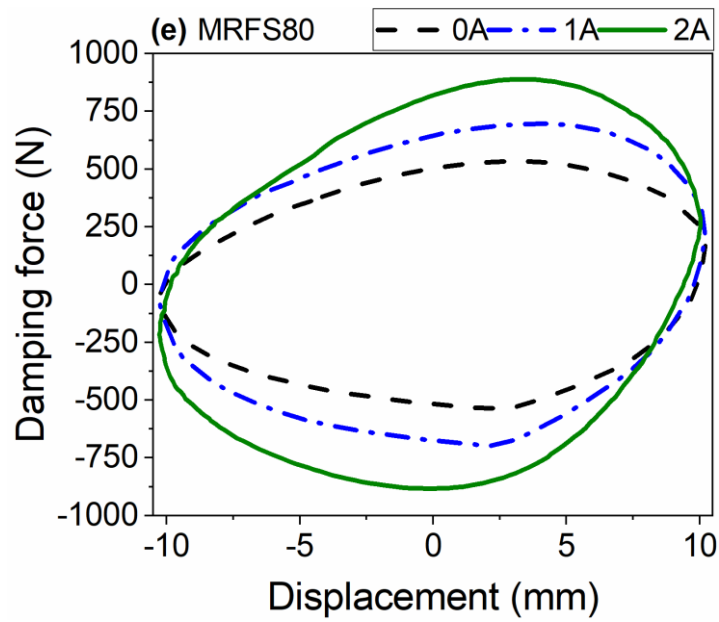
(e) MRF with 80 % mass fraction of SCIP

(f) MRF with 80 % mass fraction of MCIP

Figure 3.16 Force-displacement curves as a function of current and mass fraction for MRFs with (a),(c),(e) Finer sized CIP and (b), (d), (f) Coarser sized CIP

Figures 3.16 (a), 3.16 (c) and 3.16 (e) shows the force displacement plots for 60 %, 70 % and 80 % mass fractions of fine CIP respectively and figures 3.16 (b), 3.16 (d) and 3.16 (f) shows the force displacement plots for 60 %, 70 % and 80 % mass fractions of coarse sized CIP respectively. It can be observed that with increase in mass fraction of iron particles in MRF, there is an increase in damping force owing to more amount of iron particles. MRFs composed of finer particle size (2.9 microns) yielded higher damping force due to its higher saturation magnetization. With increase in current supplied to the electromagnetic piston, there is significant increase in damping force with respect to off-state i.e. when no current is supplied. Also, with increase in frequency of excitation, damping force increases for all mass fractions and both particle sizes. The maximum force from the force displacement curves of MRFs tested at different frequencies were plotted as function of peak velocity as shown in figures 3.17. It can be observed that with increase in velocity, there is a noticeable increase in damping force.
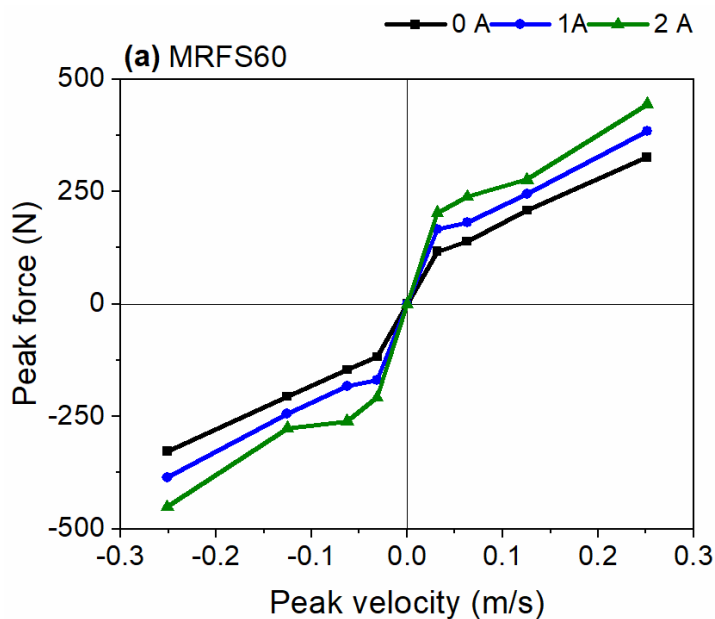
(a) MRF with 60 % mass fraction of SCIP
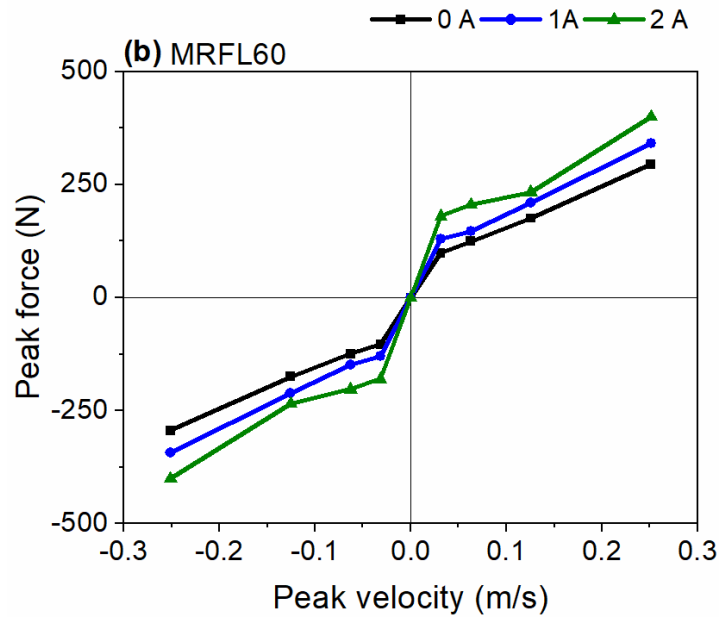
(b) MRF with 60 % mass fraction of MCIP
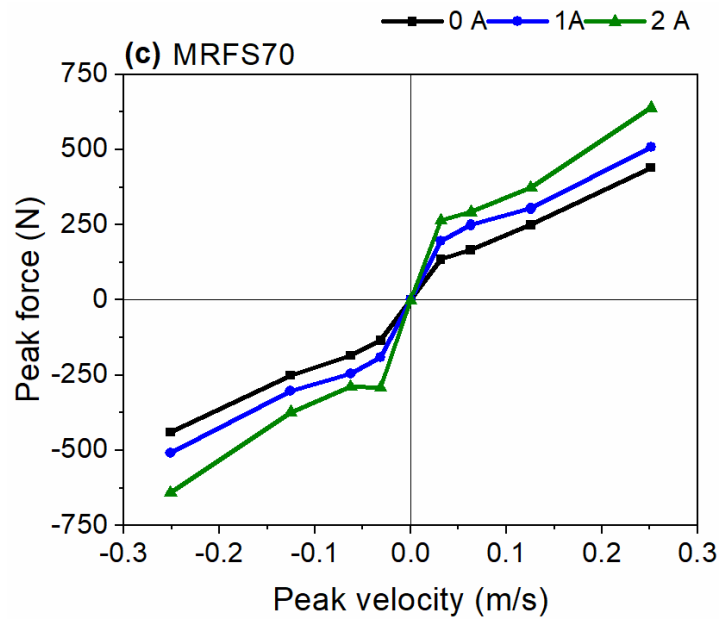
(c) MRF with 70 % mass fraction of SCIP
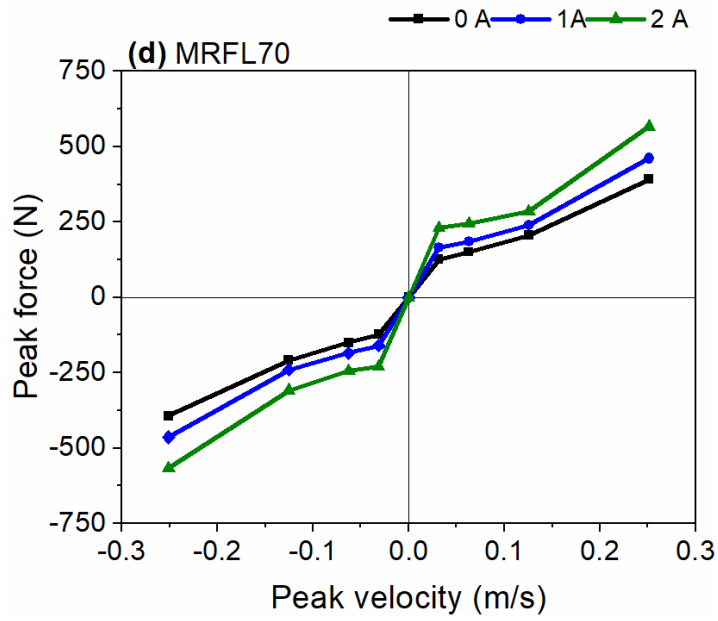
(d) MRF with 70 % mass fraction of MCIP
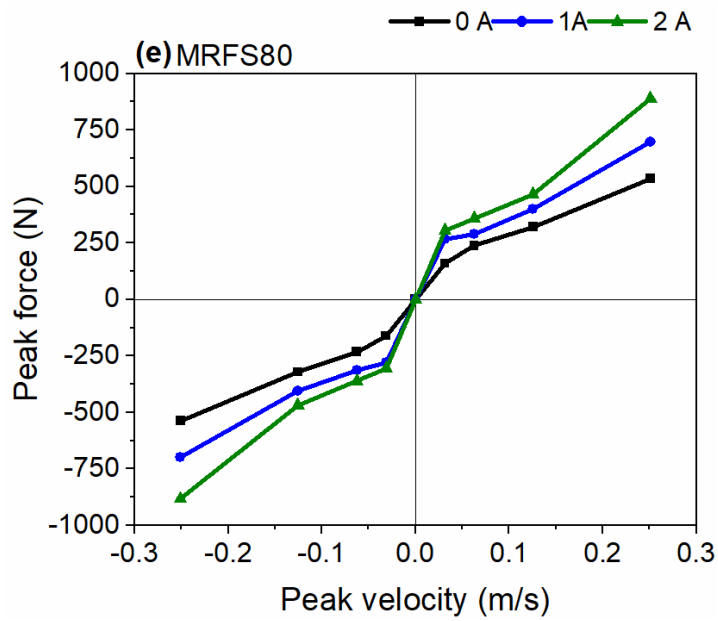
(e) MRF with 80 % mass fraction of SCIP
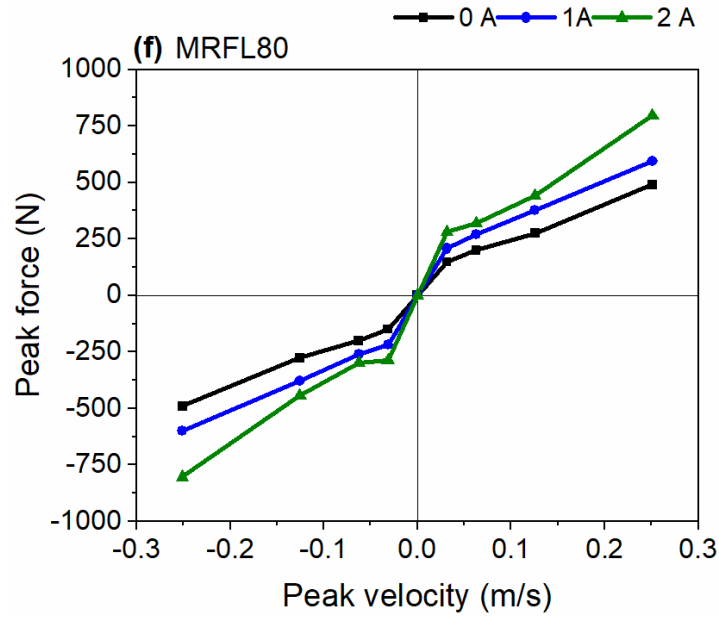
(f) MRF with 80 % mass fraction of MCIP

Figure 3.17 Peak force variation with peak velocity for MRFs with (a),(c),(e) Finer
sized CIP and (b), (d), (f) Coarser sized CIP

The area bound by the force versus displacement curve of the damper is a
measure of the energy dissipation in one cycle of upward and downward motion of
piston. The area bounded by force versus displacement curves was obtained
corresponding to 4 Hz frequency at off-state condition (0A) and on-state condition
(2A). Further, using equation (3.9), the equivalent damping coefficient (C_{eq}) of the
damper was evaluated (Rao 2017), where, E is the energy dissipated in each cycle, X is
the excitation amplitude and f is the excitation frequency.

$$C_{eq} = \frac{E}{2.\pi^2.f.X^2} \tag{3.9}$$
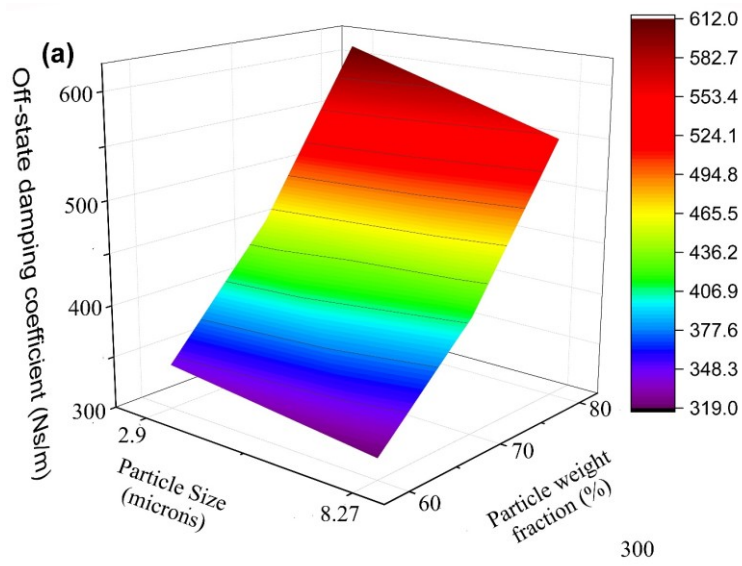
(a) Effect of particle size and mass fraction on 'off state damping Coefficient'
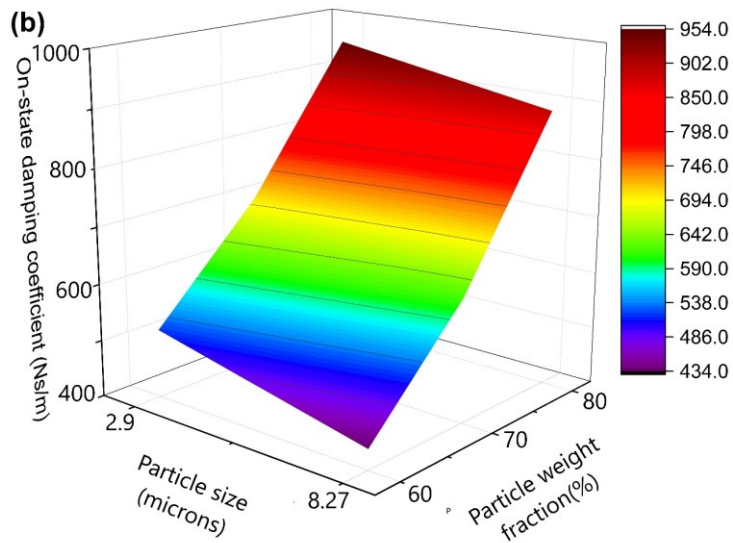
(b) Effect of particle size and mass fraction on 'on-state damping coefficient'

Figure 3.18 Effect of independent factors on 'off-state and on-state Damping Coefficients'

Figure 3.18 (a) shows the effect of CIP size and its mass fraction on the off-state damping coefficient. The off-state damping coefficient increases substantially with increase in CIP mass fraction while there is a minor decrease in off-state damping coefficient with increase in particle size. Figure 3.18 (b) shows the effect of CIP size and its mass fraction on the on-state damping coefficient. The on-state damping coefficient increases considerably with increase in particle mass fraction. MRFs composed of fine CIP have higher damping coefficient in comparison to those composed of coarse CIP due to higher shear stress of MRFs composed of fine CIP and higher saturation magnetization. Hence, particle mass fraction in MRF has significant effect on the damping coefficient compared to particle size.

3.7 DETERMINATION OF OPTIMAL PARTICLE MASS FRACTION AND PARTICLE SIZE

A damper with high on-state damping coefficient and low off-state damping coefficient is essential to realize higher dynamic range. Hence, maximization of on-state damping coefficient and minimization of off-state damping coefficient were chosen as the objective functions. MOGA technique was used to compute optimal particle size and mass fraction which satisfies conflicting criteria of objective functions. The relationship between independent and response factors were obtained using regression analyses using MATLAB^{TM} software. The response factors are on-state damping coefficient and off-state damping coefficient while the independent factors are the particle size (PS) and particle mass fraction (MF). The regression model for off-state damping coefficient with R-square and adjusted R-square values of 1 and 0.9999 is given by equation (3.10),

$$\text{Off-state damping coefficient} = 598.9 + 16.75 \times PS - 17.92 \times MF - 0.353 \times$$
$$PS \times MF + 0.2312 \times MF \times MF \qquad (3.10)$$

The regression model for on-state damping coefficient of damper having an R-Square and adjusted R-square: values of 0.9999 and 0.9994 is given by equation (3.11),

$$\text{On-state Damping coefficient} = 1143 - 26.39 \times PS - 32.57 \times MF + 0.1662 \times PS \times MF + 0.3837 \times MF \times MF \qquad (3.11)$$

MOGA optimization performed in MATLAB^{TM} software gives a set of solutions satisfying the objective functions known as pareto front graph as shown in figure 3.19. MRF composed of particle size of 3.03 μm and 73.56 % particle mass fraction was selected as it produces on-state damping coefficient of 780.5 N.s/m and off-state damping coefficient of 503.8 N.s/m. Also, a lower particle size is preferable as it yields better sedimentation stability and lower particle wear.
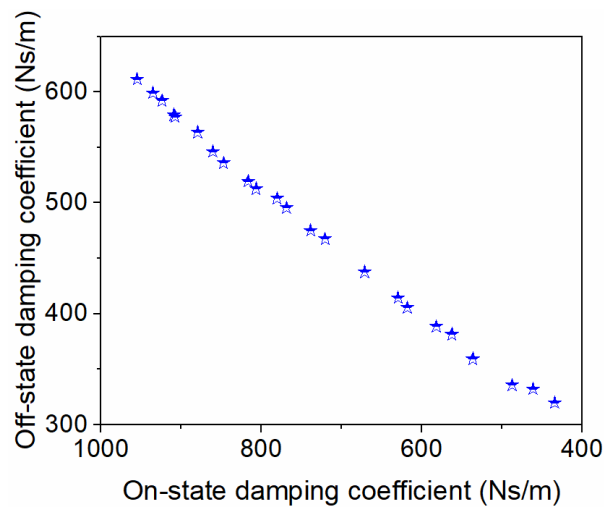
Figure 3.19 Pareto front graph

3.8 SUMMARY

Using constrained non-linear optimization method, a shear mode MR damper was designed to attain target damping force and dynamic range. A damper was manufactured based on the optimal dimensions and was filled with commercial MR fluid, MRF 132DG (Lord Corporation) to determine its damping characteristics and validated with analytical results. The optimally designed and fabricated MR damper filled with commercial MR fluid, MRF 132DG (Lord Corporation) produced maximum damping force of 709.5 N at 2A current and 4 Hz frequency of sinusoidal excitation.

However, the designed damping force of 1,000 N was not achieved as required number of coils could not be wound on the piston core due to packing factor and subsequently the desired magnetic field strength was not generated in the MRF shear gap. The computationally determined damping force based on magnetostatic analyses and analytical equation is 751.7 N. Hence, a close agreement in the results between the two was observed. Further, MRFs were prepared composed of 60 %, 70 % and 80 % mass fractions of iron particles and particle sizes of 2.9 µm and 8.27 µm. The flow curves of the MR fluid were measured at 1A, 2 A and 3 A. MRFs with fine sized CIP produced higher shear stress with variation of shear rate due to higher saturation magnetization of fine sized CIP. Also, the shear stress of MRF with 80% mass fraction of CIP were comparable with those of Lord MRF 132DG fluid. The sedimentation stability tests were performed and it was confirmed that MRFs composed of fine sized CIP have lower settling rate compared to those composed of coarse sized CIP and settles after longer duration of time indicating greater sedimentation stability of fine sized CIP based MRFs. Maximum sedimentation stability of 3 days was observed for MRF with 80% mass fraction of SCIP.

Further, MR fluid were filled in the MR damper and its damping characteristics were determined at sinusoidal excitation of ±10 mm piston stroke and frequencies of 0.5 Hz, 1 Hz, 2 Hz and 4 Hz without current and with DC current inputs of 1A and 2A. Higher mass fraction of CIP in the MRF resulted in higher damping force. Also, with increase in current delivered to MR damper piston, the damping force increased. Damping force also increased as frequency of excitation was increased. The area bounded by the force displacement graphs was used to calculate the energy dissipated which was then used to calculate damping coefficient. MRFs composed of fine sized CIP yielded higher damping force and equivalent damping coefficient in comparison to those composed of coarse CIP due to its higher saturation magnetization and shear stress compared to its counterpart. CIP mass fraction in MRF has significant effect on the equivalent damping coefficient when compared to particle size. Finally, by means of MOGA optimization, based on maximization of damping coefficient in the presence of magnetic field and minimization of damping coefficient in the absence of magnetic

field, the optimal mass fraction and particle size was determined. MRF composed of 3.03 μm average particle size and particle mass fraction of 73.56 % was chosen which yields on-state damping coefficient of 780.5 N.s/m and off-state damping coefficient of 503.8 N.s/m.

CHAPTER 4

OPTIMAL COMPOSITION OF MAGNETORHEOLOGICAL FLUID FOR MR BRAKE

4.1 INTRODUCTION

The torque capacity of a MR brake is very important factor and can be conveniently enhanced by optimal design of the brake. Another factor which significantly affects the performance of MR brake is the composition of MRF, viz. mass fraction of iron powder, particle size, type of base oil and its viscosity. While much of research work is performed in developing novel MR brakes to produce high torque and the use of commercial MRFs for experimental characterization, there is lack of research to determine the optimal composition of MRF suitable for brake application (Attia et al. 2017; Li and Du 2003; Sohn et al. 2018; Song et al. 2018; Wu et al. 2020; Zhou et al. 2007).

4.1.1 Methodology for determination of Optimal MR Fluid Composition for MR Brake

This work focusses mainly on two aspects namely optimal design of MR brake as well as determination of optimal composition of MRF for use in MR brake as they have major effect on the performance of the MR brake. The methodology followed in this work is shown in figure 4.1. MOGA optimization technique was used to determine optimum dimensions of MR brake which would maximize field induced braking torque and minimize off-state torque. This was performed in MATLAB software integrated with magnetostatic analyses in ANSYS APDL software. The torque was constrained to be greater than 10 Nm and magnetic flux density within the core material to be less than 2.0 T. The magnetic saturation limit of the core material (SAE 1020 steel) is 2.39 T. However, a lower value was used considering factor of safety. Variation of magnetic field in the MRF, in the radial direction was considered for calculation of braking torque rather than the average values. The pareto optimal solution which yielded a braking

torque close to 20 Nm was selected based on trade-off between the objective functions. The test setup was developed, MR brake was fabricated as per the optimal dimensions and its braking characteristics were determined for commercial MR fluid, MRF 132DG (Lord Corporation) fluid at different speeds and currents. The experimentally determined braking torques were compared with those obtained by computational results. Further, the morphology and magnetic properties of different iron particles used for synthesis of MRF were characterized. MRF composed of different combinations of different particle mass fractions, base oil viscosities and mean particle diameters were synthesized and their braking characteristics were determined to propose the optimal composition of MRF using MOGA optimization. To end with, the effect of different particle mass fractions, base oil viscosities and mean particle diameters on the sedimentation stability of SCIP and MRIP based MRFs were examined.
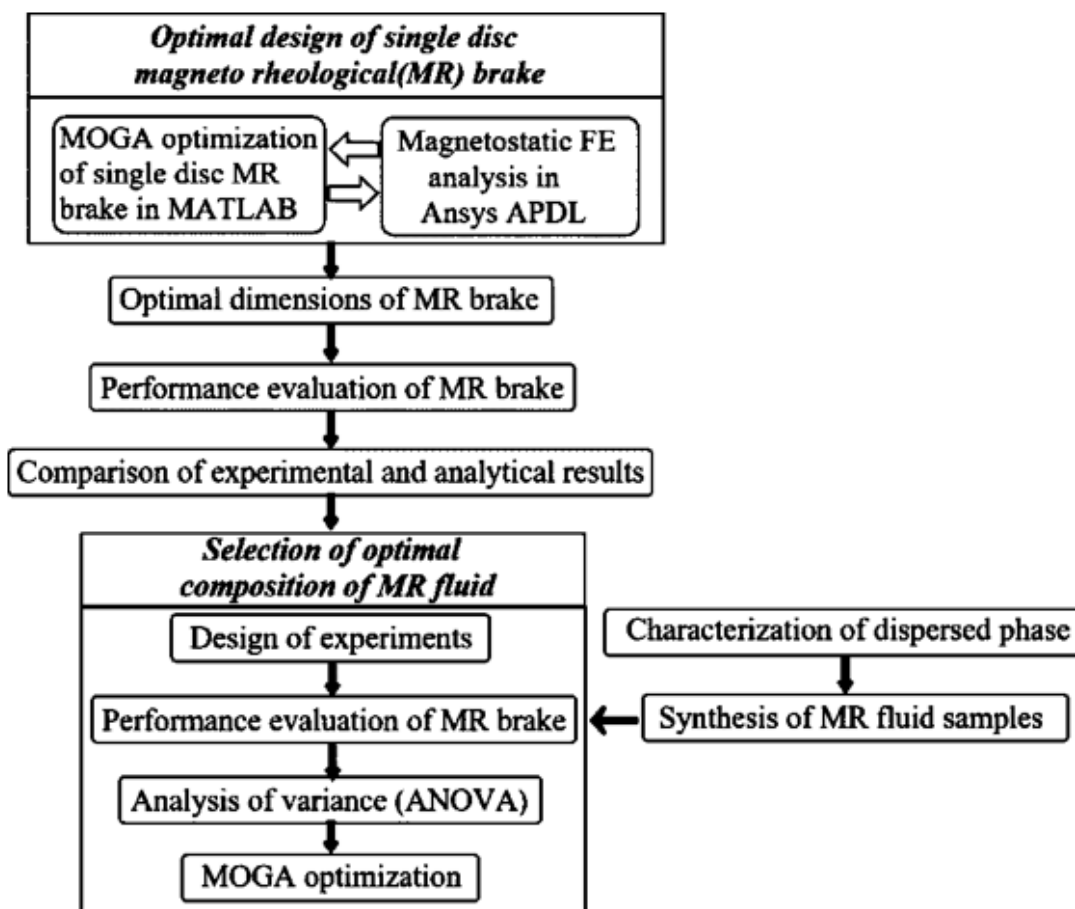
Figure 4.1 Methodology flowchart

4.2 OPTIMAL DESIGN OF SINGLE DISC MAGNETORHEOLOGICAL BRAKE
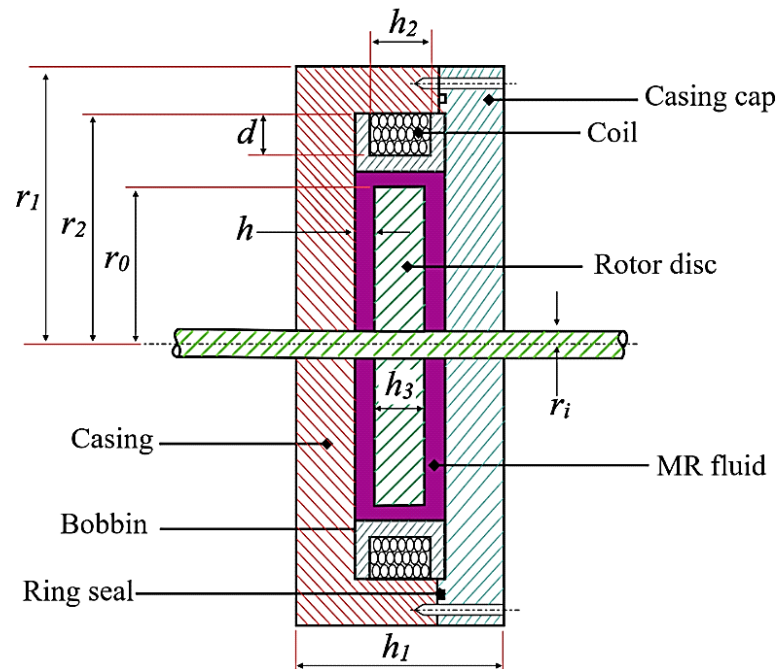
Figure 4.2 Cross-sectional view of MR brake with geometrical parameters

The cross-sectional view of single disc MR brake showing different components and geometrical parameters are shown in figure 4.2. The different parts of MR brake are casing, casing cap, single disc rotor mounted on a shaft, MRF, bobbin and seals. The stationary housing is made of two parts termed as casing and casing cap. Copper coil wound on a bobbin forms the electromagnet of the brake and bobbin is press-fit into the casing. The magnetic field induced by the electromagnet has to pass through the MRF in the gap between casing and rotor for producing braking resistance. Hence, the casing, casing cap and rotor which form path for magnetic field should have high magnetic permeability to ensure concentration of flux density in the MRF. Therefore, based on the availability, cost and superior magnetic properties, SAE 1020 steel was chosen as material for these components. In order to prevent magnetic flux leakages, the rotor shaft is made of non-magnetic material. The bobbin plays no part in the magnetic flux and braking torque generation and thus is also selected to be made of non-magnetic material. Table 4.1 shows the different materials used for the components of MR brake.

Table 4.1 Material of brake components

Part Name	Material
Casing & Casing cap	SAE 1020 steel
Rotor	SAE 1020 steel
Bobbin	316 Stainless steel (Non-magnetic)
Rotor shaft	SS 304 Stainless steel (Non-magnetic)
MR Fluid	Commercial MR fluid, MRF 132 DG (Lord Corporation)
Coil winding	24 AWG copper wire

A MR brake operates in shear mode. The braking torque produced by the MR brake can be obtained as the sum of off-state or viscous torque (T_η) and the controllable field induced torque (T_{MR}) neglecting friction effects and is given by equation (4.1).

$$T_B = T_\eta + T_{MR} \tag{4.1}$$

Assuming Bingham fluid flow in the radial gap region, the braking torque for single disc MR brake can be calculated using equation (4.2) (Gudmundsson et al., 2011b; Park et al., 2008; Phillips, 1969).

$$T_B = n\pi\eta\omega\left(\frac{r_0^4 - r_i^4}{2h}\right) + 2\pi n \int_{r_i}^{r_o} \tau(H,r)r^2 dr \tag{4.2}$$

where, η : apparent viscosity of the fluid (without magnetic field)

n : number of surfaces in contact with MRF

ω : angular velocity of the disc (value corresponding to 500 rpm was considered for design)

$\tau(H,r)$: yield stress which is a function of magnetic field intensity in the MRF and varies with radius.

The design of the MR brake was performed on the basis of commercially available MR fluid, MRF 132DG properties (Lord Corporation). The magnetization curve of this fluid is shown in figure 3.3 (a) of chapter 3 and its apparent viscosity at 40°C is 0.114 Pa-s. The relation between dynamic yield stress (of the MRF and the magnetic field intensity (*H in kA/m*) obtained by curve fitting the flow curves of MRF is given by equation (4.3),(Gao et al. 2017)

$$\tau_y = -0.8239 + 0.3668 \times H - 7 \times 10^{-4} \times H^2 \qquad (4.3)$$

The design variables of MR brake are rotor disc radius, casing outer radius, casing width, coil height and coil width. The shaft diameter was chosen as 10 mm. The bobbin thickness was chosen as 2 mm based on fabrication limitations, although lower value of the same would be beneficial. Typically, 0.25 to 2 mm MRF gap has been recommended for MR devices (Yoo and Wereley 2002). Though smaller MRF gap yields higher braking torque, it causes greater heating of MRF and subsequent reduction in braking torque. Also, the wear rate is higher in smaller MRF gap (Song et al. 2018). In this study, MRF gap of 1 mm was considered as smaller MRF gap is difficult to achieve due to manufacturing limitations (Nguyen et al.,2019; Lijesh et al., 2018; Sukhwani and Hirani, 2008a). 24 AWG copper wire which has diameter of 0.5105 mm (without insulation layer) and current carrying capacity of 3.5 A was selected (Lund 2016). The wires used for the MR brake winding are enamel coated or insulated. The thickness of insulation varies with manufacturer and application. Hence, a packing factor of 0.5 was considered for winding to account for wire insulation, winding imperfections, etc. The lower and upper bounds of the design parameters of the MR brake are given in table 4.2. The upper bound for casing outer radius was chosen based on the availability of the largest diameter of SAE 1020 steel raw material. Remaining bounds were set relative to the bounds of casing outer radius.

Table 4.2 Bounds of design parameters

Parameter	Lower Bound (mm)	Upper Bound (mm)
Casing outer radius, r_1	70	120
Rotor radius, r_0	40	80
Casing width, h_1	25	50
Coil height, d	5	35
Coil width, h_2	5	35

The methodology shown in figure 4.3 was used to optimally design the single disc MR brake. The braking torque mainly depends on the magnetic field strength in MRF gap which in turn depends on electromagnetic coil dimensions, dimensions of brake components and choice of materials. The relationship between them in the form of analytical equation is not possible. Genetic algorithm (GA) doesn't need a closed form analytical equation to obtain solution. It belongs to a class of evolutionary algorithms and has been previously used in many studies (Assadsangabi et al. 2011; Shamieh and Sedaghati 2017) due to its remarkable performance. Hence, GA was chosen as optimization method in this study.
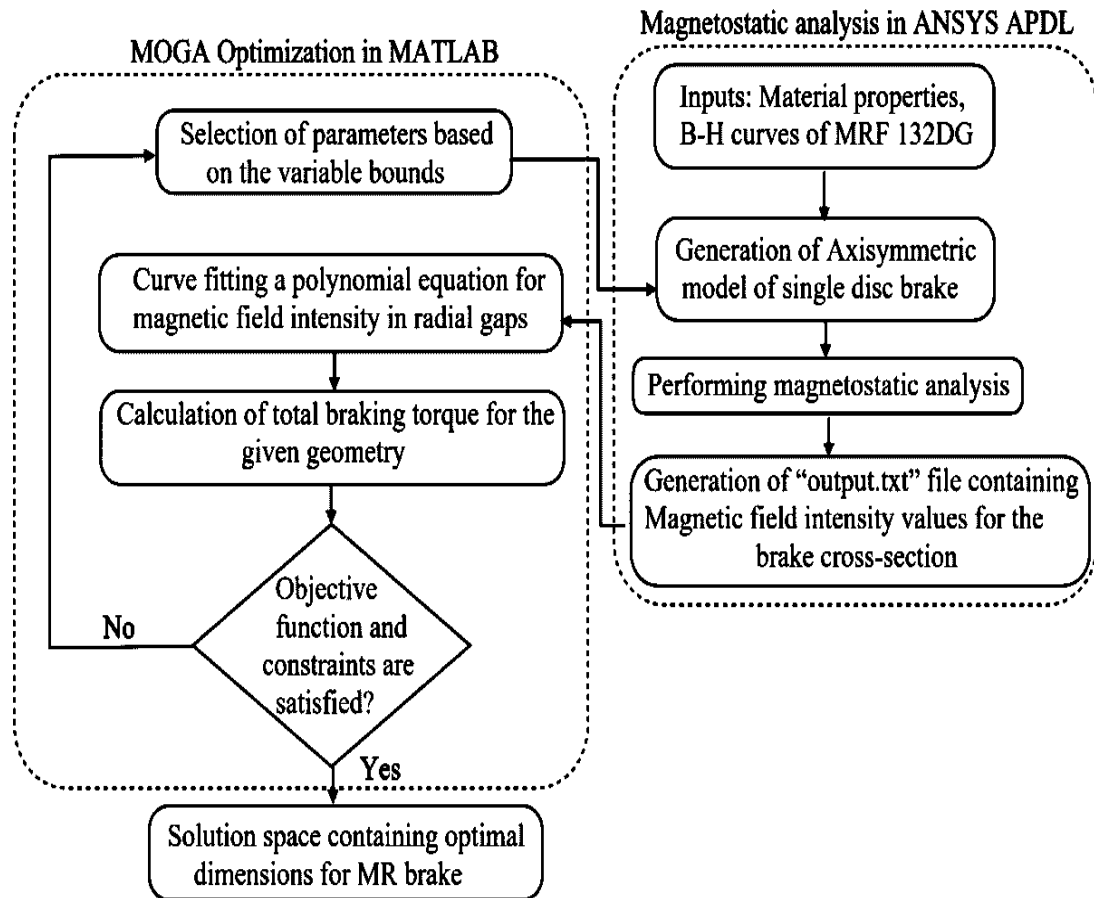
Figure 4.3 Methodology for Optimal Design for single disc MR brake

The optimization problem was defined as follows. Minimization of off-state torque, T_η and maximization of field induced braking torque, T_{MR} subject to constraints namely braking torque, $T_B \geq 10\text{ Nm}$ and magnetic flux density, $B_{max} \leq 2\text{ T}$. Also, the bounds for the MR brake dimensions were defined as listed in table 4.2. The optimization parameters used for Genetic algorithm were specified as follows. A population count of 30 and number of generations as 100 were specified. Further, the crossover, mutation, selection schemes and other relevant parameters were specified similar to the study by Assadsangabi et al. (2011). For the optimization, off-state torque and field induced braking torque were considered as separate objective functions instead of torque ratio which considers both of them in single variable due to following reasons. The off-state torque which is synonymous to off-state damping force in a damper, has different effects. The off-state damping force of a damper can still be a

desirable property when used in a suspension system since it provides the system with a nominal viscous damping. Contrary to this, off-state damping torque in a MR brake is not a desired property. For instance, in a vehicular brake application, the off-state damping torque should be maintained as low as possible so as to avoid any power wastage and quicker heating of MRF. Although, the MR brake design in the present study is not application oriented, the objectives were chosen similar to previous study on MR brake design, which considered off-state braking torque also as a design objective (Gudmundsson et al. 2010).

The optimal design was obtained by means of MOGA optimization technique. The optimization was performed in MATLAB software coupled with magnetostatic analyses in ANSYS APDL software. Initially, the MOGA algorithm choses the values of design variables which are limited within the bounds specified. MATLAB creates an input file, "Input.txt" which contains all the design parametric information of the MR brake and sends the data to the ANSYS ".bat" file which executes the APDL code. The APDL code creates the axi-symmetric model of the MR brake according to the data received, assigns material properties of different components of MR brake and discretizes the problem domain with variable mesh sizes using Plane 53 element. This element type is a two dimensional, eight noded element with four degrees of freedom per node. The B-H curve of SAE 1020 steel (Rao 2013) is assigned to rotor disc, casing and casing cap material and that of commercial MR fluid, MRF 132DG (Lord Corporation) is also specified. A current of 2.5 A was chosen for analyses. The ANSYS program will generate an "output.txt" file containing the analysis results and communicates to MATLAB software. The magnetic field intensity varies in the radial direction in the MRF and hence it is not reasonable to assume average value throughout the radius of the rotor disc. Eventually, the MATLAB software evaluates the yield stress at discrete radial location in MRF based on the computed values of magnetic field distribution using equation (4.3) and the integral $\int_{r_i}^{r_o} \tau(H,r) r^2 dr$ to calculate the field induced braking torques by summing up the torque generated by the individual elements. The algorithm performs the analyses iteratively for all possible values within the bounds specified.
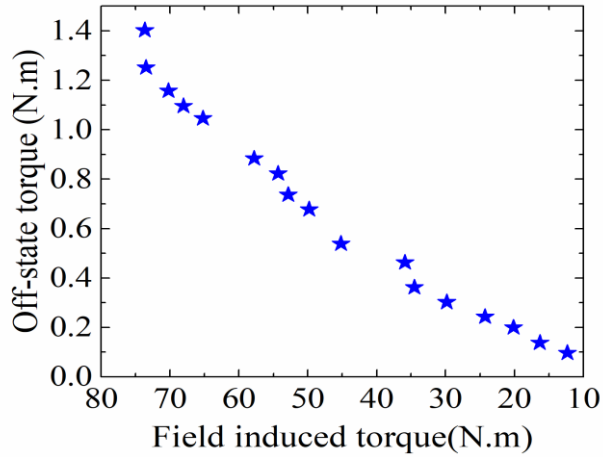
Figure 4.4 Pareto Optimal solutions

The algorithm generated eighteen optimal solutions which satisfy the chosen objective functions and the Pareto front graph is shown in the figure 4.4 and tabulated in table 4.3. It can be observed that the field induced and off state torques increases with increase in rotor radius owing to more amount of MRF in contact with it and subjected to MR effect. However, an opposite behaviour is observed in case of torque ratio with increase in rotor radius due to increase in off-state torque too. Highest torque ratio is obtained for lowest rotor radius of 40.26 mm due to very low off-state torque though field induced torque is 12.31 Nm which is the lowest among other solutions. Maximum torque rating of torque sensor available for measuring torque characteristics of MR brake is 50 Nm and hence a design torque of less than 40 Nm has to be chosen for safety operation of torque sensor. Hence, based on this constraint, any one of the optimal solutions 1,5,10,13,16 or 18 could be selected. Optimal solutions 10 and 18 provide very low braking torque while solutions 1, 5 and 13 yield high torque which could result in significant temperature effects on braking performance especially at higher speeds of testing. Very few papers have reported fabrication and testing of brakes with high braking torque capacity and it necessitates incorporation of cooling water jacket in the brake (Wang et al. 2019b). Hence, based on the dimensional, thermal and experimental constraints, a lower braking torque design point close to 20 Nm was selected. The corresponding off-state torque is 0.2 Nm and has a very high torque ratio of 100.65. The chosen optimal dimensions of the MR brake are shown in table 4.4.

101

Table 4.3 Pareto front solutions for optimal MR brake design

Solution	Rotor radius (mm)	Casing radius (mm)	Total width (mm)	Coil height (mm)	Coil width (mm)	Field induced torque (Nm)	Off state torque (Nm)	Torque ratio
1	59.54	106.53	44.99	12.45	13.07	35.90	0.46	77.54
2	78.55	108.23	46.43	10.95	7.73	73.67	1.40	52.51
3	65.49	102.57	47.36	9.47	8.57	49.82	0.68	73.51
4	76.35	105.33	49.67	10.43	7.33	73.49	1.25	58.71
5	50.69	105.42	42.10	18.53	12.26	24.26	0.24	99.79
6	69.99	99.55	46.24	11.44	7.92	57.80	0.88	65.37
7	74.86	105.66	48.20	11.68	7.72	70.24	1.16	60.69
8	72.99	106.24	48.25	11.60	9.26	65.21	1.05	62.34
9	73.85	106.19	48.63	10.40	7.43	68.05	1.10	62.09
10	43.99	110.92	38.04	26.76	11.52	16.30	0.14	118.18
11	78.55	108.23	46.43	10.95	7.73	73.67	1.40	52.51
12	66.88	103.71	47.15	10.46	8.24	52.84	0.74	71.68
13	53.52	104.47	45.30	11.25	9.11	29.82	0.30	98.65
14	68.75	99.04	45.50	11.43	8.34	54.32	0.82	65.99
15	61.84	103.46	48.06	13.54	8.84	45.19	0.54	83.87
16	48.25	109.35	36.96	25.21	9.54	20.13	0.20	100.65
17	56.00	107.45	48.33	10.82	9.66	34.51	0.36	95.26
18	40.26	111.74	44.38	29.18	12.31	12.31	0.10	127.19

Table 4.4 Optimum dimensions of single disc MR brake

Parameter	Value (mm)
Rotor radius, r_o	48.25
Casing outer radius, r_1	109.35
Casing width, h_1	36.96
Coil height, d	25.21
Coil width, h_2	9.54

The fabricated MR brake is shown in figure 4.5. The rotor disc thickness was calculated as 11.5 mm based on the optimal dimensions. Although, a packing factor of 0.5 was considered, use of insulation material on bobbin reduced the available space for coil. Thus, only 385 turns of copper coil were possible to be wound on the bobbin instead of 588 turns as predicted by the optimal dimensions. The resistance of the coil was measured to be 10.2 Ohms using multi-meter due to which the maximum current allowed by the coil is 1.2 A for supply voltage of 12 V. Further, due to heat generated in brake at higher torques, speeds, MRFs with higher particle mass fraction and higher base oil viscosity, the allowable current got slightly reduced during experimentation upto 1.15 A. Therefore, a nominal value of 1.0 A was chosen such that all experiments could be safely performed and under same maximum current condition.
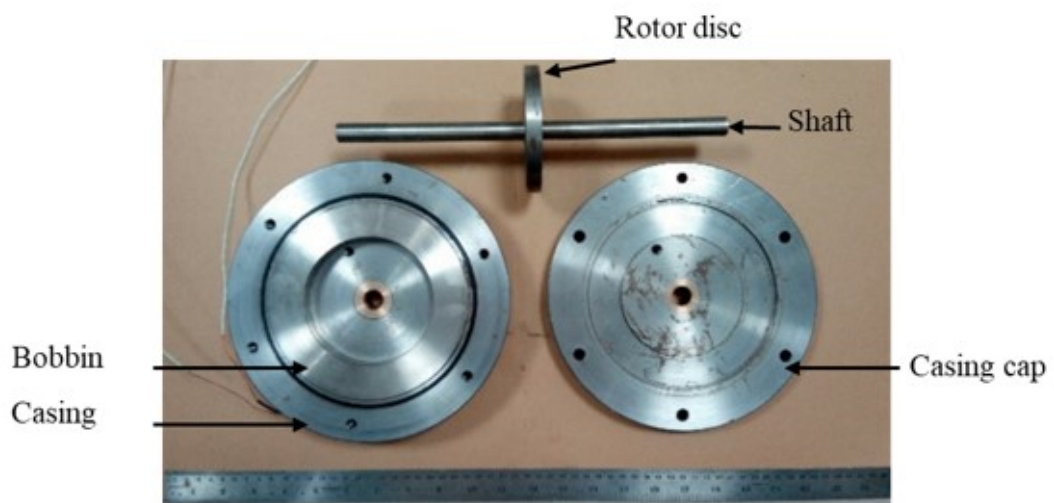
Figure 4.5 Fabricated MR brake components

4.3 PERFORMANCE EVALUATION OF MR BRAKE UTILIZING COMMERCIAL MR FLUID

The MR brake performance is measured in terms field induced and off-state braking torques, torque ratio, hysteresis time, torque tracking control characteristics, speed reduction, etc. (Li and Du, 2003; Nguyen et al., 2014; Rossa et al., 2014; Sukhwani and Hirani, 2008a; Sukhwani and Hirani, 2008b; Dai et al.,2019). In the current study, the field induced and off-state braking torques, speed reduction and torque ratio of MR brake were investigated.
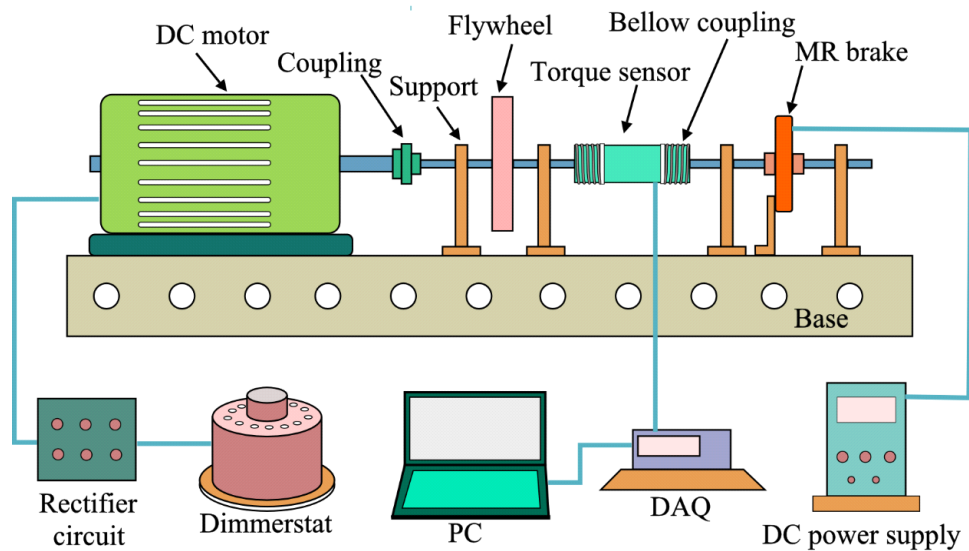
Figure 4.6 Schematic diagram of the MR brake test setup

The schematic diagram of the MR brake test set up is shown in figure 4.6. It comprises of a DC Motor sequentially connected to the MR brake through lovejoy coupling, flywheel, bellow couplings and torque sensor. A DC motor was used as speed control in case of DC motor is easier and much precise compared to that in an AC motor. The DC motor is connected to rectifier circuit which in turn obtains power from the dimmerstat. The dimmerstat receives power from 220 V mains. Dimmerstat is used for varying the speed of the motor by controlling the current to be supplied to the DC motor. The output of dimmerstat is connected to rectifier circuits which will convert alternating current to direct current and supplies to the DC motor. One rectifier circuit consists of a diode which connects between the dimmerstat and armature windings of

DC motor. Another rectifier circuit consists of full wave bridge rectifier which is connected between dimmerstat and field winding of DC motor. A flywheel is connected between torque sensor and DC motor for maintaining uniform speed of rotation without much fluctuations. A torque sensor measures the difference in the torque between input and output shafts during braking. The torque data acquired by the sensor is sent to data acquisition device which communicates it to a software interface. The flywheel and MR brake shafts are supported on ball bearings having a bore diameter of 10 mm. A DC power supply is utilized to supply different magnitudes of direct current to the electromagnet of MR brake.
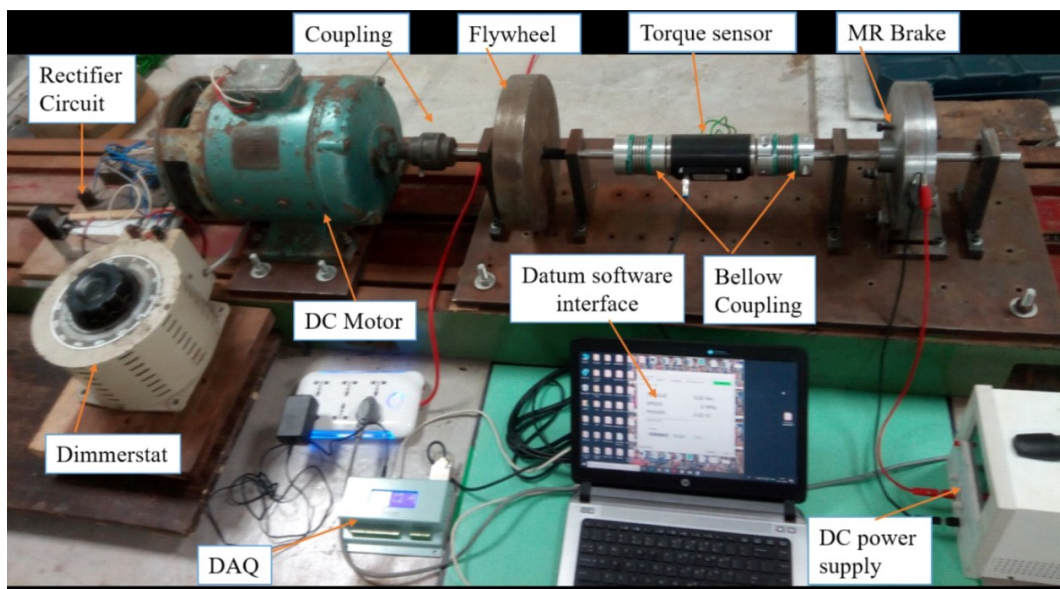
Figure 4.7 MR brake experimental test setup

Figure 4.7 shows the experimental setup for testing of MR brake. A 3 HP DC motor with maximum speed rating of 1440 rpm was used as prime mover to drive the MR brake rotor at desired speeds. A Cast iron disc type flywheel having a mass and mass moment of inertia of 19.6 kg and 0.165 kg.m^2 respectively, was used. The torque and speed of the brake were measured using a torque sensor which has a measuring range of 0-50 Nm with an accuracy of 0.1 %. The signals were acquired through Universal Torque Transducer Interface data acquisition device (DAQ) and interfaced with Datum^{TM} software. The torque sensor (M425), data acquisition device and Datum software package is a product of Datum Electronics limited, UK. The torque sensor is

connected between flywheel shaft and MR brake shaft by means of bellow couplings. The bellow couplings are keyed to the torque sensor on one side and flywheel or MR brake shaft on other side. A cable connects the torque sensor and Universal Torque Transducer Interface data acquisition device. The motor and remaining parts of the test setup are bolted to base plates which have provision for properly fixing them to a rigid base. The MR brake outer casing is fixed to an L-shaped fixture which in turn is bolted to the base plate to prevent the rotation of MR brake during testing. Seals are provided in the brake to prevent leakage of MRF. The MR brake has a pair of screwed holes on either side of its casing to ensure proper filling of MRF between the rotor and casing surfaces. Once the MRF is filled in the MRF gap, the screw is tightened to close the hole.

Initially, the torque and speed reduction characteristics were measured for commercial MR fluid, MRF 132DG (Lord Corporation) based MR brake using the following procedure. The MR brake was filled with commercial MR fluid and connected to experimental setup. The motor was run at 100 rpm for 5 minutes to ensure uniform distribution the MRF in the fluid gap. The DC Motor was run at the required speed of 100 rpm to 500 rpm in steps of 100 rpm and corresponding off-state torques (without application of current to the MR brake electromagnet) were measured. Next, the motor speed is set to 100 rpm and direct current of different magnitudes were supplied to MR brake electromagnet, i.e. 0.25 A, 0.5 A, 0.75 A and 1.0 A. The field induced torques and reduced speed of the MR brake at different supplied currents were acquired using torque sensor and sent to Datum software through data acquisition device. At every supplied current, after a waiting time of 15 seconds, data were acquired for 5 seconds at a sampling rate of 100 samples per second. Tests were performed twice in a random manner for each combination of speed and current at different instances of time to ensure repeatability of readings and eliminate the effect of earlier readings (Sukhwani and Hirani, 2008a).The procedure was repeated for other test speeds. The experiments were performed at different test speeds and braking torque and speed reduction at different currents were acquired.
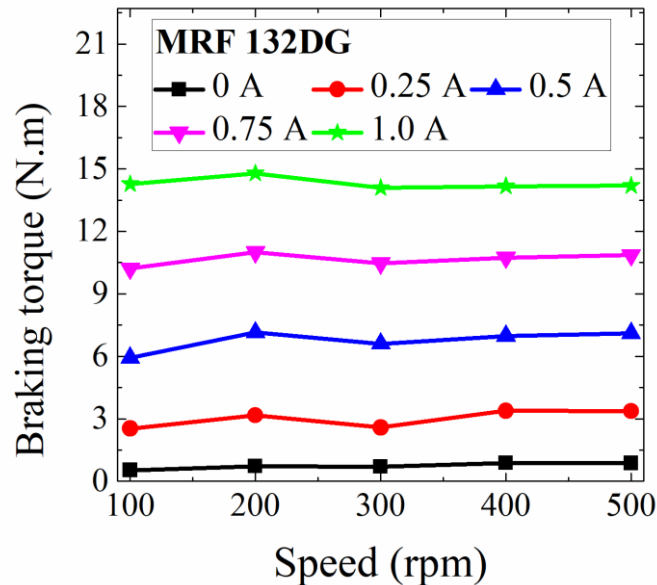
Figure 4.8 Braking torque for commercial MR fluid based brake

The braking torque insignificantly varies with increase in speed of the rotor as can be observed in figure 4.8. The maximum torque generated in case of commercial MR fluid, MRF 132DG (Lord Corporation) is 14.8 Nm at a speed of 200 rpm and current of 1.0 A. With increase in speed there is a slight drop in the torque obtained due to shear thinning behaviour of MRFs (Sukhwani and Hirani, 2008a) and a torque of 14.2 Nm is obtained at 500 rpm. The design torque of 20 Nm was not attained as the design using magnetostatic analysis was carried out at current of 2.5 A and also required number of coils could not be wound on bobbin due to packing factor.

4.4 VALIDATION OF EXPERIMENTAL RESULTS WITH COMPUTATIONAL RESULTS

Experimentally determined torque values of commercial MR fluid based brake were compared with computational results. Computational braking torques were determined by performing magnetostatic analyses to compute the magnetic field strength in the MRF. The analyses were also performed at same magnitude of currents supplied to MR brake during experimentation. The analyses results were subsequently used to calculate torques by means of torque equations.

107

4.4.1 Magnetostatic analyses of MR brake

The field induced torque of a MR brake at a particular supplied current is a function of magnetic field strength and flux density generated in the MRF located in-between rotor disc and casing. The flow of magnetic field and its distribution is non-linear due to the differences in the magnetic properties of different components of brake which form magnetic path and also flux leakages. Hence, magnetostatic analysis was performed in ANSYS^{TM} Workbench software to determine magnetic field strength and flux density in the brake components and essentially in the MRF. Analyses involves creation of the MR brake geometry, meshing, specifying material properties, boundary conditions and loads. One-fourth axisymmetric 3D model of MR brake was created in design modeler as shown in figure 4.9 (a) owing to symmetry in the brake geometry, material properties and boundary conditions. This would substantially reduce the time for computation without affecting the solution accuracy (Piłat 2004). The model created comprises of rotor disc, MRF, bobbin, coil and casing which is based on the computed optimized dimensions. Additionally, ambient air having permeability of unity is modelled surrounding the MR brake casing. The number of turns of 24 AWG copper coil is specified as 385. The model was meshed with relatively finer element size in the vicinity of MRF and electromagnetic coil to capture the drastic variation in the solution that occurs in those regions (Hartman and Rimmer 2001; Piłat 2004). Mesh dependence study was performed to select suitable mesh size which does not affect the solution accuracy. The element type chosen by the software is Solid 117 which has 20 nodes and can model 3-D magnetic fields. The material properties were specified in terms of magnetic hysteresis curves. The B-H curve of SAE 1020 steel is assigned to rotor disc, casing and casing cap material and that of commercial MR fluid, MRF 132DG (Lord Corporation) is also specified. Relative permeability of unity was specified for rotor shaft and bobbin made of non-magnetic stainless steel material. Magnetic flux parallel boundary condition is applied and the analysis was performed at 12 V and 1.0 A current. The current specified in the analyses was restricted to 1.0 A as compared to 2.5 A specified during the design of MR brake. This is based on the

maximum current that was supplied to the MR brake electromagnetic coil during experimentation. The magnetic flux density distribution in the MR brake at the current of 1.0 A is shown in figures 4.9 (b). The maximum flux density of 1.473 T occurs in the casing in the vicinity of coil and rotor periphery and is well within the magnetic saturation limit of the casing material which is 2.39 T (Rao 2013; Seid et al. 2018).
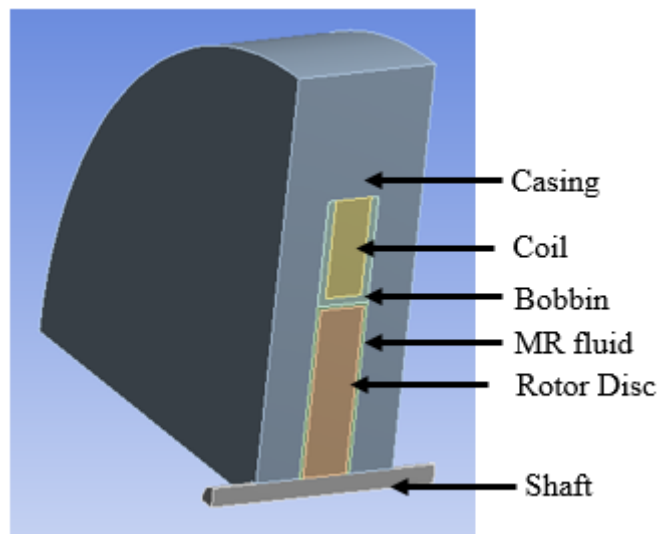
(a) Axisymmetric quarter model of MR Brake
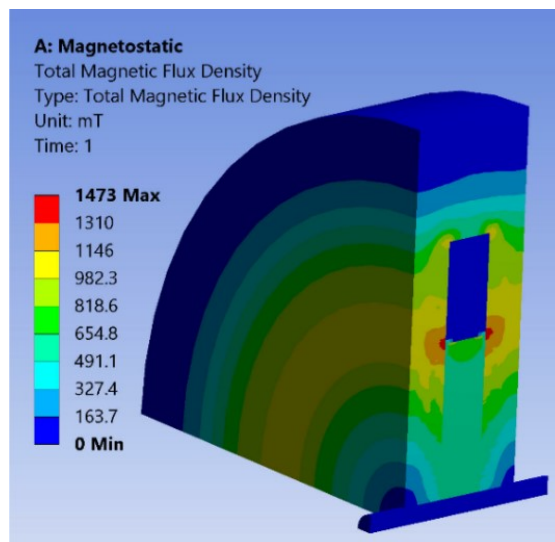
(b) Magnetic flux density in the MR brake

Figure 4.9 Geometric model and magnetic flux density of the MR brake

The magnetic field intensity in the MR brake and MRF are shown in figures 4.10 (a) and 4.10 (b) respectively. The field strength is maximum in the casing with a maximum magnitude of 210.4 kA/m as shown in figure 4.10 (a). The field strength in the MRF varies in the radial direction and is highest near the periphery of the rotor and is 121.38 kA/m. Similarly, magnetostatic analyses were carried out for 0.25A, 0.5 A and 0.75 A to compute the distribution of magnetic field intensity in the MRF.
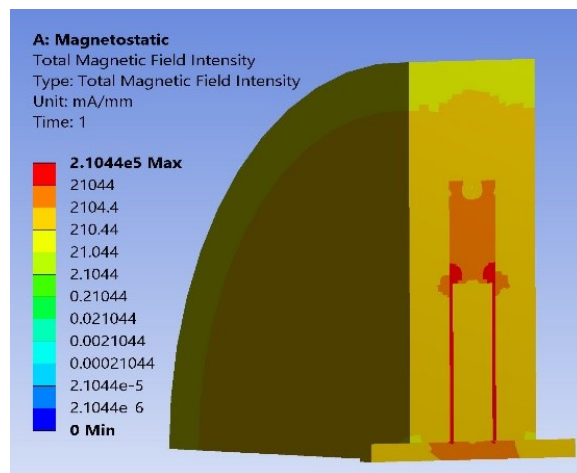
(a) Magnetic field strength distribution in the MR brake
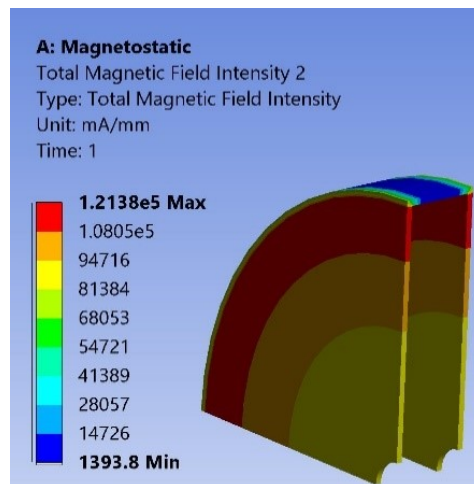
(b) Magnetic field strength distribution in the MR fluid

Figure 4.10 Magnetic field strength distribution in the MR brake and MR fluid

4.4.2 Comparison of experimental and computational braking torques

The magnetic field strength distribution computed in the MRF was used to calculate the yield stress using equation (4.3) and subsequently field induced braking torque using second term of equation (4.2). The off-state torque was calculated corresponding to maximum rotor speed of 500 rpm using first term of equation (4.2). The total analytically determined torque value was obtained by summing up field induced and off-state torque values at different currents. The results were compared with experimentally determined torque values at different supplied currents as shown in table 4.5.

Table 4.5 Computational and experimentally determined braking torque

Sl. No.	Current (A)	Computational torque (Nm)			Experimental torque, T_E (Nm)	Error $(T_E - T_B)$ (Nm)
		Field induced torque (Nm)	Off-state torque (Nm)	Total braking torque, T_B (Nm)		
1	0	--	0.197	0.197	0.864	+ 0.667
2	0.25	2.317	0.197	2.514	3.368	+ 0.854
3	0.50	6.852	0.197	7.049	7.109	+ 0.060
4	0.75	11.015	0.197	11.212	10.853	- 0.359
5	1.00	14.562	0.197	14.759	14.195	- 0.564

It can be observed that the torque calculated using analytical equations coupled with magnetostatic analysis and the experimentally determined ones show a good agreement. The maximum difference between the experimental and computational torque values is 0.854 Nm. The deviation in the results could be due to the friction torque which is neglected in design process and also any form of defects in the material used for fabrication that may have affected its magnetic properties. Also, the temperature rise has an effect on both the magnetic properties of materials and viscosity of fluid (Karakoc et al.,2008) which are not accounted in the finite element analyses.

4.5 SYNTHESIS AND CHARACTERIZATION OF MR FLUID

The selection of optimal composition of MRF suitable for use in MR brake was done by means of MOGA optimization. MR fluid with Iron powder of different particle sizes and mass fractions in base oil with different viscosities were considered. Initially, particles were characterized to determine their shape and sizes followed by synthesis of different MRFs.

4.5.1 Characterization of iron powder

The rheological properties of MRF are mainly dependent on the magnetic properties of iron particles, their size and distribution. In this work, iron particles of three different particle sizes were used as dispersed phase for preparation of MRF. Carbonyl iron powders were procured from BASF (CN grade) and Sigma Aldrich (C3518) and reduced iron powder was procured from Sigma Aldrich (12310,fine).

4.5.1.1 Particle size distribution

Sherman and Wereley (2013) studied the influence of particle size distribution on properties of MRF by means of simulation. It was established that the particle size distribution has a substantial effect on the yield stress of MRF since it greatly changes the chain structures of iron particles in MRF under influence of magnetic field. Also, a narrow size distribution yielded higher MR effect. The particle size distribution of different powders were obtained using Particle Size Analyser (Make: Cilas 1064) which has particle size measuring range from 0.04 to 500 microns. Figures 4.11 (a)-(c) depicts the volume basis particle size distribution of smaller, medium and larger sized iron particles denoted as SCIP, MRIP and LCIP respectively. The nomenclature is based on the mean particle diameter of the powders. Mean diameter of SCIP, MRIP and LCIP were found to be 2.9 microns, 6.71 microns and 9.68 microns respectively.
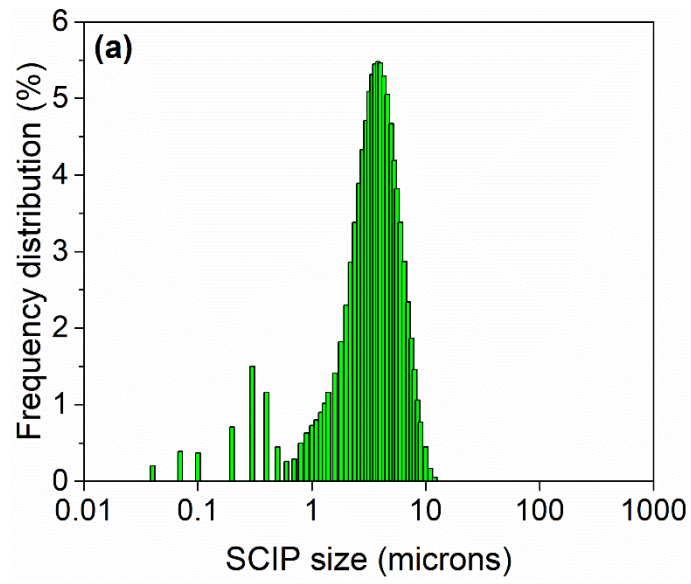
(a) Particle Size Distribution of SCIP
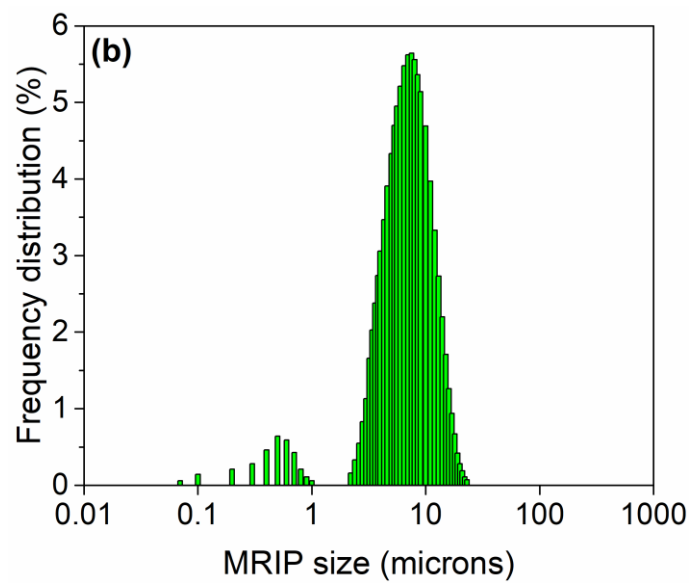
(b) Particle Size Distribution of MRIP

113
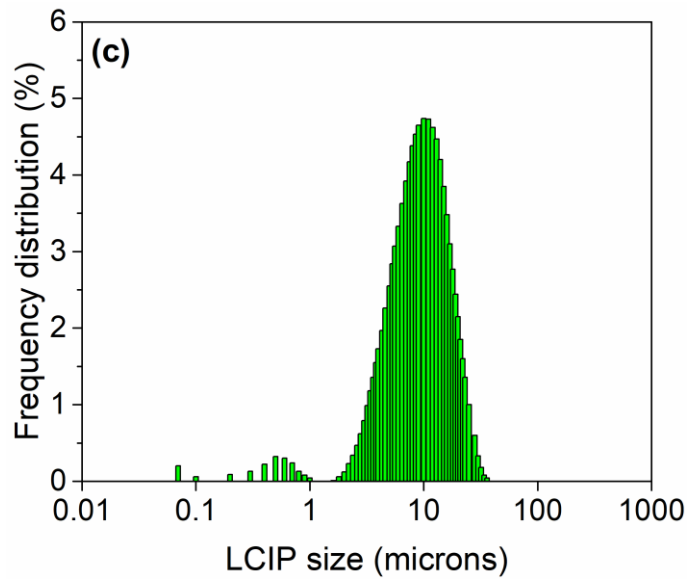
(c) Particle Size Distribution of LCIP

Figure 4.11 Particle Size Distribution of iron powders (a) SCIP (b) MRIP and (c) LCIP

The volume weighted D-values of particle size distribution provided by the software interface are listed in table 4.6, which describe the particle size distribution. For example, D (0.9) is the diameter at which 90% of the sample's mass is composed of particles with a diameter less than this value.

Table 4.6 Particle size distribution of Iron powders

Size of iron powder	Mean particle diameter (microns)	D-Values of Particle Size Distribution (microns)		
		D (0.1)	D (0.5)	D (0.9)
SCIP	2.90	≤ 0.18	≤ 2.80	≤ 5.84
MRIP	6.71	≤ 0.66	≤ 6.34	≤ 11.89
LCIP	9.68	≤ 3.33	≤ 8.76	≤ 17.56

4.5.1.2 FESEM Images

Figures 4.12 (a) - (c) depicts the scanning electron microscope images of SCIP, MRIP and LCIP obtained using Field Emission Scanning Electron Microscope (FESEM, Make: ZEISS SIGMA) at magnification of 10,000X. All the powders have nearly spherical shape which are essential from standpoint of tribological properties of MRF (Genç and Phulé 2002).
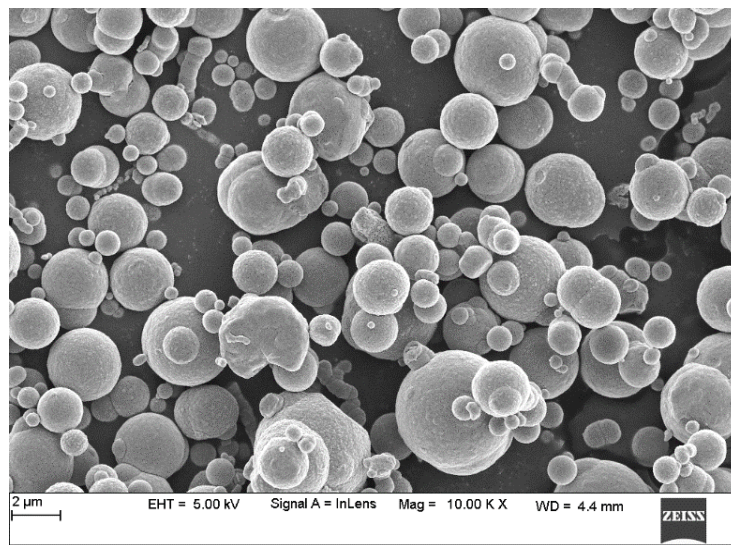
(a) SCIP
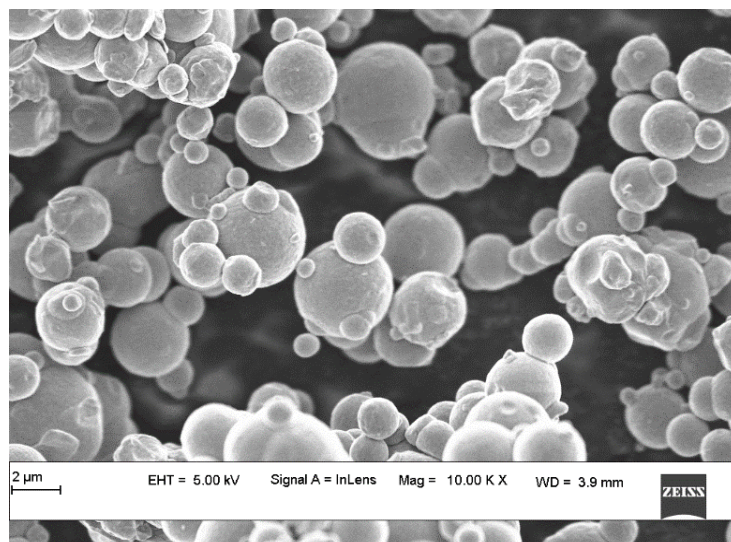
(b) MRIP
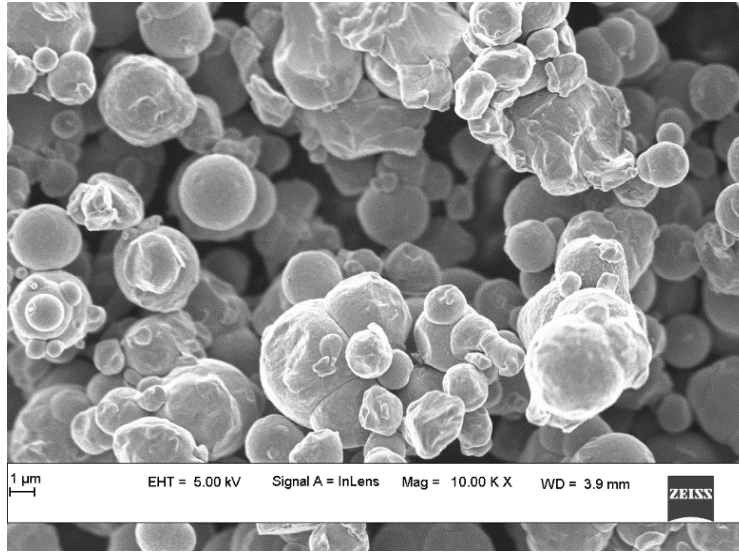
(c) LCIP

Figure 4.12. FESEM images iron powders

4.5.1.3 Magnetic properties of iron powder

The yield stress of MRF is more dependent on magnetic properties and saturation magnetization of iron particles than on its size and its distribution (Ginder and Davis 1994). Iron powder having high saturation magnetization results in higher strength of MRF. It should possess lower coercivity and remnant magnetization for reversible magnetorheological response. Vibrating Sample Magnetometer (Make: Lakeshore) was used to obtain the magnetization curves of the SCIP, MRIP and LCIP and are shown in figure 4.13. The testing was performed on 20 mg of samples at a temperature of 25°C. A total of 151 data points were acquired with field increment of 500 Gauss. The equipment has magnetic field measurement range of $\pm$ 2.5 Tesla, magnetic field accuracy of $\pm$ 0.05 %, magnetic field resolution of $\pm$ 0.001 % and sensitivity of 10^{-7} emu.
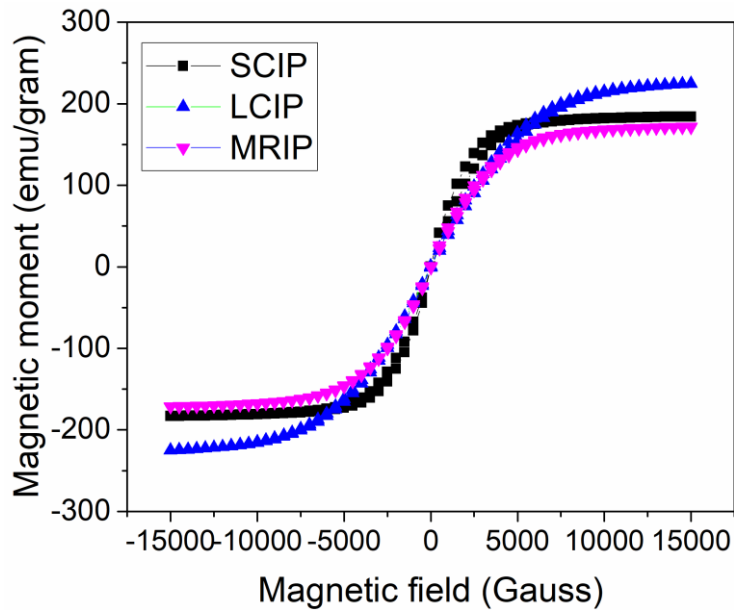
Figure 4.13 Magnetization curves of SCIP, MRIP and LCIP at 25°C

The magnetic properties of different sized iron powders determined are listed in table 4.7. LCIP has highest saturation magnetization compared to SCIP and MRIP. SCIP has slightly higher saturation magnetization than MRIP. However, at low magnetic fields upto 5000 Gauss (0.5 T), SCIP has higher slope or permeability compared to MRIP and LCIP. This means that it gets magnetized by higher value for given amount of magnetic field strength. The permeability of MRIP and LCIP are almost same but the saturation magnetization of LCIP is the highest among all. Further, the coercivity and retentivity of SCIP is lowest which is advantageous for MR effect and hence SCIP possesses superior magnetic properties compared to other powders though it has lowest particle size.

Table 4.7 Magnetic properties of different Iron powders

Magnetic Property	SCIP	MRIP	LCIP
Saturation Magnetization (emu/g)	184.2	171.4	224.6
Coercivity (Gauss)	0.59	15.7	18.8
Retentivity (emu/g)	0.045	0.79	0.84

117

4.5.2 Synthesis of MR fluid

In this study, twelve MRFs were synthesized composed of two different mass fraction of iron powder namely 75 % and 85 %, silicone oils of two different viscosities and iron powder of three different mean particle diameters. High mass fractions considered for composition of MR fluid is based on the fact that MR brakes require high strength fluids for braking action. Silicone oil (Supreme Silicones Limited, Pune), having specific gravity of 0.96 and viscosities of 50 cSt (SF 50, 48.4 cPs) and 100 cSt (SF 100, 104 cPs) (@ 25°C) were used as base oil. Reduced iron powder and carbonyl iron powder of two different grades were used as dispersed phase. Nano Bentonite clay and Aluminium distearate procured from Sigma Aldrich with 5% of mass of base oil were used for the synthesis of different MRF samples. Bentonite clay is a thickener which imparts thixotropic properties to the magnetorheological liquid and increases the stability of the suspension with regard to settling (Munoz et al. 2001). Aluminium distearate improves the redispersibility of iron particles in MRF (López-López et al. 2008).

Prior to MRF synthesis, desired mass of silicone oil, iron powder and additives were weighed using electronic weighing balance. Initially, Bentonite clay was mixed with base oil for one hour at 400 rpm and then aluminium distearate was added and mixed for another one hour. Later, iron powder was added to this solution and stirred for 8 hours at 400 rpm to obtain homogeneous suspension. The twelve different synthesized MRF samples are named as listed in table 4.8 along with their compositions. For instance, MRFs with 85 % mass fraction of SCIP, MRIP and LCIP in 100 cSt silicone oil are designated as MF85S100, MF85M100 and MF85L100 respectively.

Table 4.8 Constituents of synthesized MRFs

Sl. No.	MRF Sample	Mass of Iron powder (gm)	Mass fraction of Iron powder(%)	Viscosity of base oil @ 25 °C (cSt)	Mass of Base oil (gm)	Mass fraction of Base oil (%)
1	MF75S50	75	75	50	25	25
2	MF75M50	75	75	50	25	25
3	MF75L50	75	75	50	25	25
4	MF85S50	85	85	50	15	15
5	MF85M50	85	85	50	15	15
6	MFF85L50	85	85	50	15	15
7	MF75S100	75	75	100	25	25
8	MF75M100	75	75	100	25	25
9	MF75L100	75	75	100	25	25
10	MF85S100	85	85	100	15	15
11	MF85M100	85	85	100	15	15
12	MF85L100	85	85	100	15	15

4.5.3 Characterization of MR fluid

Shear stress as a function of shear rate for the twelve MRF samples and commercial MR fluid, MRF 132DG (Lord Corporation) were measured using MCR-702 Anton Paar Modular Compact Parallel Plate Rheometer at different magnetic fields in a CSR mode. A gap of 1 mm was set between the parallel plates of 20 mm diameter and temperature was maintained at 25°C during the tests. The samples were stirred to ensure homogeneity of dispersion and then very small quantity of MRF sample was placed on the stationary parallel plate. Before measuring the response, the fluid were subjected to pre-shear for 20 seconds at shear rate of 10 s^{-1} followed by waiting time of 10 seconds to obtain uniformity in the sample. The fluid was subjected to shear rate

increasing logarithmically from 0.1 to 1000 s^{-1} and the fluid response was measured at 21 shear rate values. The flow curves were determined at 2A current which produce a magnetic field strength of 65 kA/m.
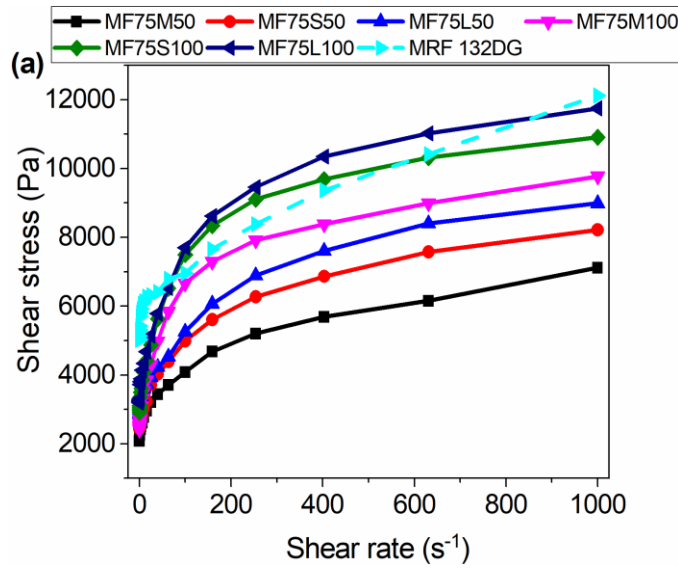
Figure 4.14 Flow curves of different prepared fluid with 75 % mass fraction of iron powder
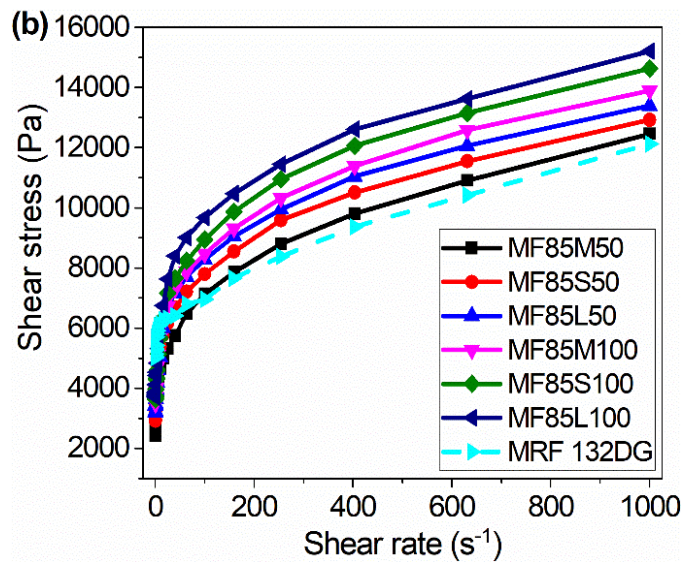
Figure 4.15 Flow curves of different prepared fluid with 85 % mass fraction of iron powder

Figure 4.14 and 4.15 shows the shear stress plotted as a function of shear rate for commercial MR fluid, MRF 132 DG and MRFs with 75% and 85% mass fractions of SCIP, MRIP and LCIP at magnetic field strengths of 65 kA/m respectively. It is evident that with increase in particle weight fraction of iron powder, there is an increase in shear stress of MRF. However, MRF containing LCIP have higher shear stress compared to those containing SCIP and MRIP for all weight fractions. This is attributed to the higher saturation magnetization of coarser sized particles compared to smaller sized ones. In case of commercial MR fluid, MRF 132 DG, except at very low shear rates, it has lower shear stress compared to MRFs composed of 85 % mass fraction of iron powder in 50 cSt and 100 cSt base oil. However, it has higher shear stress compared to MRFs with composed of 75 % mass fraction of iron powder in 50 cSt base oil. MRFs with composed of 75 % mass fraction of SCIP and LCIP in 100 cSt base oil have higher shear at shear rates lower than 600 /s.

4.5.4 Sedimentation Stability of MRF

Sedimentation tests were performed for MRFs composed of SCIP and MRIP. It was measured by visual observation of position of boundary interface between the transparent and turbid portion of the MRF. MRFs were filled in 10 ml graduated polypropylene cylindrical measuring tubes. The difference in the density between the iron particles and the carrier fluid causes the iron particles to settle with time. Readings are noted periodically at intervals of three hours until there is no changes in the readings. The sedimentation stability of the fluid is quantified in terms of sedimentation ratio which is the ratio of the volume of clear or supernatant fluid to the volume of entire MRF suspension (Ashtiani and Hashemabadi 2015b).

Figure 4.16 (a) shows the sedimentation ratio as a function of time of MRFs composed of SCIP and MRIP dispersed in 50 cSt and 100 cSt base oil. Graph was plotted for time steps of twelve hours. Figure 4.16 (b) shows the number of days taken by different MRFs to completely settle. The sedimentation ratio increases with time due to settling of particles and reaches a constant value after particle have completely settled. It can be observed that MRFs containing 50 cSt oil have higher slope indicating

121

faster settling rate of particles compared to those composed of 100 cSt base oil. This is because higher viscosity oil offers more resistance to settling of iron particles, increasing the sedimentation time. MRFs based on 100 cSt base oil viscosity have minimum and maximum sedimentation stability of 5.5 days and 12 days respectively while that for 50 cSt base oil based MRFs are 1 day and 4 days respectively. Sedimentation stability of MRF with 85% mass fraction of SCIP dispersed in 100 cSt silicone oil is 12 days (288 hours) which is the highest among other MRFs while minimum one was observed for MRF with 75% mass fraction of MRIP dispersed in 50 cSt base oil, i.e.1 day (24 hours). MF75M50 fluid has lowest stability as it contains lower base oil viscosity and coarser particle size of iron powder in MRF. However, a lower oil viscosity causes faster response time of MRF and better redispersibility of iron particles after the particles have settled (Zuzhi et al. (2016). MRFs having SCIP have lower slope compared to MRIP based MRFs and takes more time to completely settle indicating higher sedimentation stability of SCIP based MRFs. This is in agreement with the results obtained by several research works published in literature. Further, MRFs with higher mass fraction of iron particles in MRF yielded better stability compared to those with lower particle mass fraction as settling velocity of particles decreases with increase in particle mass fraction (Liu et al. 2013b; Ngatu and Wereley 2007b). Figure 4.16 (c) shows the photographs of graduated cylindrical measuring tubes in which MRFs have completely settled after they were poured and settling behaviour was visually observed. The first four tubes from the left contain MRFs with 75 % mass fraction of iron particles while the remaining ones contain MRFs with 85 % mass fraction of iron particles. Similarly, MRFs composed of LCIP will have lower sedimentation stability than those containing MRIP and SCIP due to its higher particle size as reported in literature. The optimal MRF consists of 80.95 % mass fraction of SCIP dispersed in 50 cSt base oil. MRFs based on 50 cSt base oil and SCIP include MF75S50 and MF85S50 which have a sedimentation stability of three and four days respectively. Hence, the optimal MRF would have a stability within this time range. Although it has lower sedimentation stability, it would not be a major problem as MR brakes are highly efficient mixing devices (Carlson 2002).
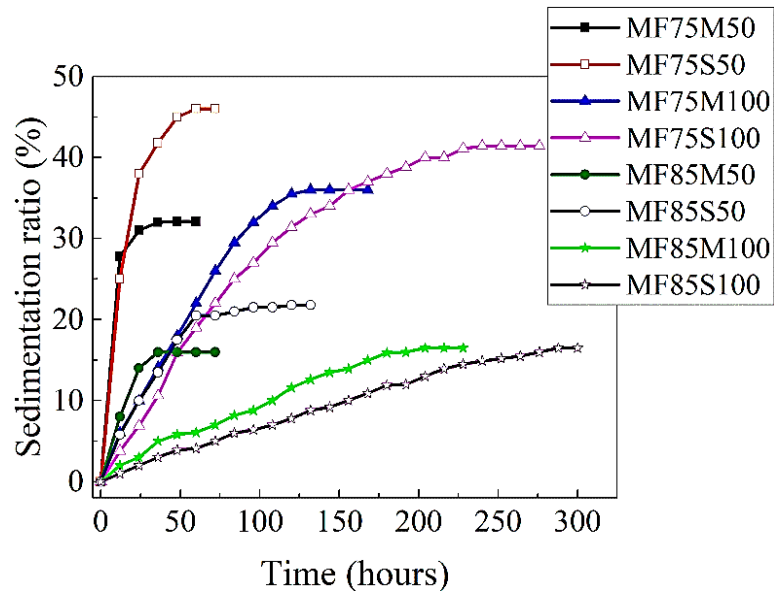
(a) Sedimentation ratio versus time of MRFs
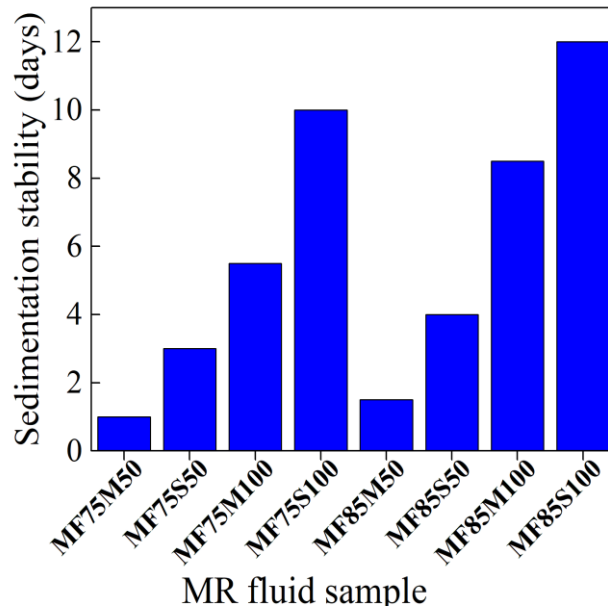
(b) Sedimentation time of different MRFs
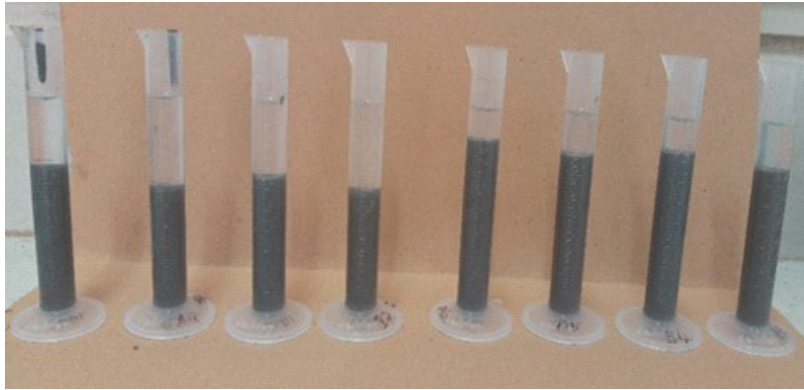
(c) MRFs after complete settling of particles

Figure 4.16 Sedimentation stability of prepared MRFs

4.6 PERFORMANCE EVALUATION OF MR BRAKE FOR SYNTHESIZED MRFs

Torque and speed reduction characteristics of the MR brake were measured for all the synthesized MRFs individually using the procedure detailed in section 4.3. Figures 4.17 (a) to 4.17 (f) depicts the braking torque generated at different speeds and current supplied to MR brake containing synthesized MRFs. Figures 4.17 (a), 4.17 (c) and 4.17 (e) shows the braking torque of MR brake composed of 75% mass fraction of SCIP, MRIP and LCIP based MRFs respectively. Similarly, figures 4.17 (b), 4.17 (d) and 4.17 (f) shows the braking torque of MR brake composed of 85% mass fraction of SCIP, MRIP and LCIP based MRFs respectively. Torque increases significantly with increase in current for all synthesized MRFs. Brake utilizing MRFs having 50 cSt viscosity base oil yielded higher torque compared to those containing 100 cSt base oil. This could be due to better particle chain formation and higher MR effect in lower viscosity oil. Also, base oil having low viscosity results in quicker response time and easier redispersibility of particles (Zuzhi et al. 2016). Also, the difference in torque values obtained for 50 cSt and 100 cSt based MRFs increases with increase in current supplied. Nevertheless, off-state torque (corresponding to zero current) of brake utilizing 100 cSt base oil based MRFs are higher than those employing 50 cSt base oil due to their higher viscosity. The braking torque increases gradually with increase in speed upto 300 rpm and then slightly decreases for most of the MRFs. This is attributed to the shear thinning behaviour of fluid at high shear rates.

124

Further, SCIP based MRFs generated higher torque for all input speeds, mass fraction and almost all applied currents compared to their counterparts. This is because at lower magnetic field strengths, magnetic permeability is highest for SCIP compared to MRIP and LCIP, which has been discussed in section 4.5.1.3, and hence stronger chains of particles are formed. However, the difference in the value of torque is smaller for SCIP and LCIP based MRFs due to higher saturation magnetization of LCIP. Also, MRFs composed of MRIP produced lower braking torque compared to those containing LCIP due to their lower saturation magnetization. The torque produced by LCIP based MRFs are closer to those of composed of SCIP due to its higher saturation magnetization, though its permeability is lesser than that of SCIP. It was discussed previously in section 4.3 that the maximum torque generated in case of commercial MR fluid, MRF 132DG (Lord Corporation) is 14.8 Nm at current of 1.0 A. This is lesser than that obtained for synthesized MRFs having 85% particle mass fraction, since the particle mass fraction of commercial MR fluid, MRF 132DG (Lord Corporation) is 80.98 % as per company material data sheet. However, synthesized MRFs having 75 % particle mass fraction produce comparable braking torque to that of MRF 132DG fluid. The SCIP based MRF, MF75S50, produces higher braking torque than that of commercial MR fluid, MRF 132DG (Lord Corporation) even though it has lower mass fraction as can be seen in figure 4.17 (a).
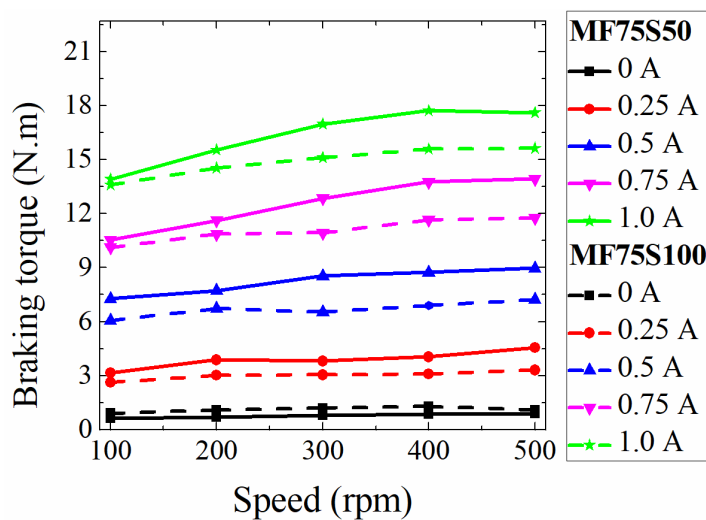
(a) 75 % mass fraction of SCIP in 50 cst and 100 cSt silicone oil
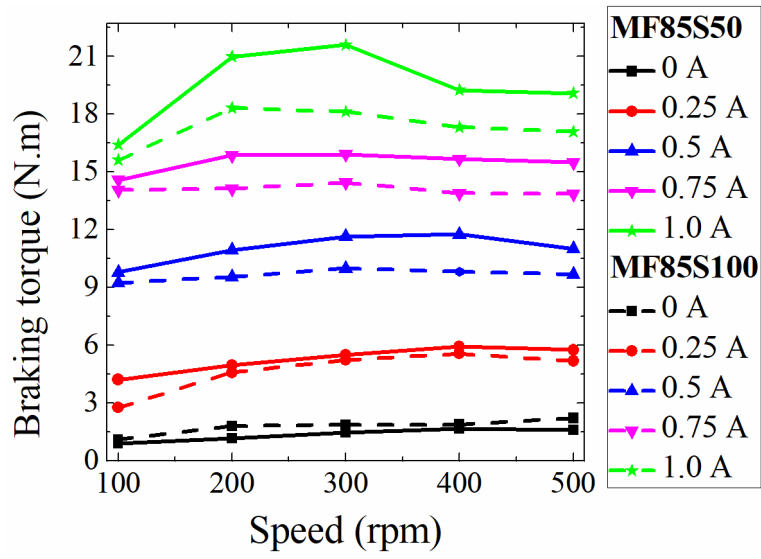
(b) 85 % mass fraction of SCIP in 50 cst and 100 cSt silicone oil
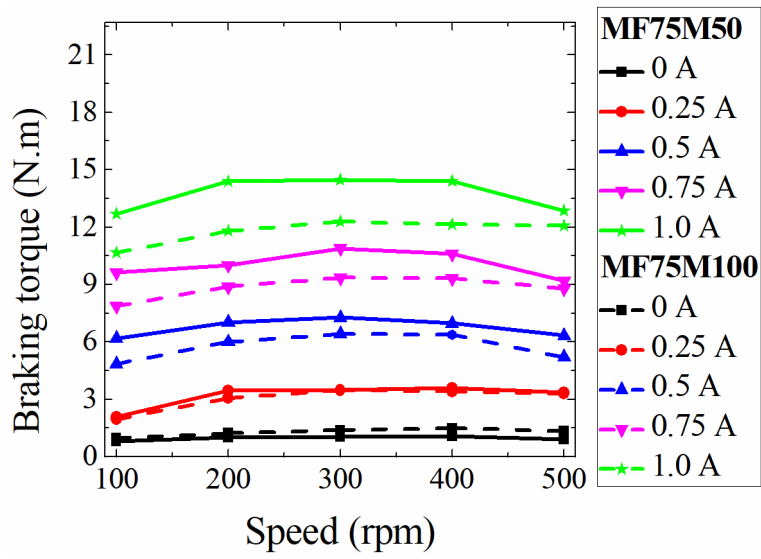
(c) 75 % mass fraction of MRIP in 50 cst and 100 cSt silicone oil

126
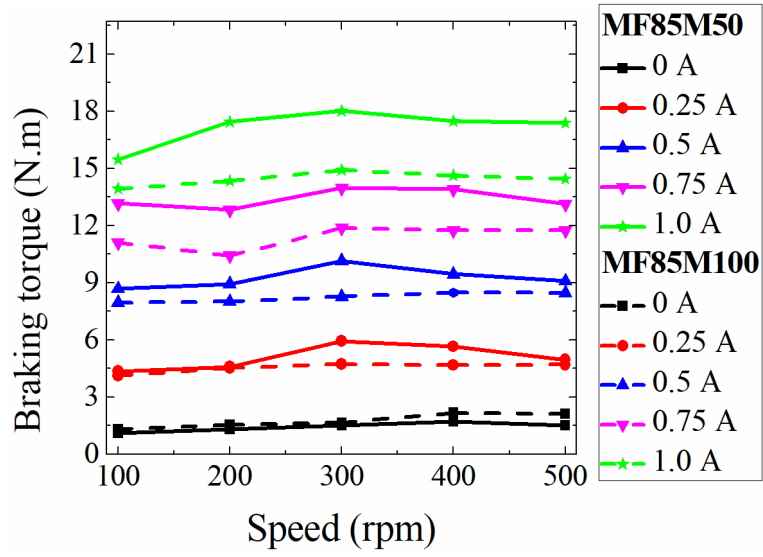
(d) 85 % mass fraction of MRIP in 50 cst and 100 cSt silicone oil
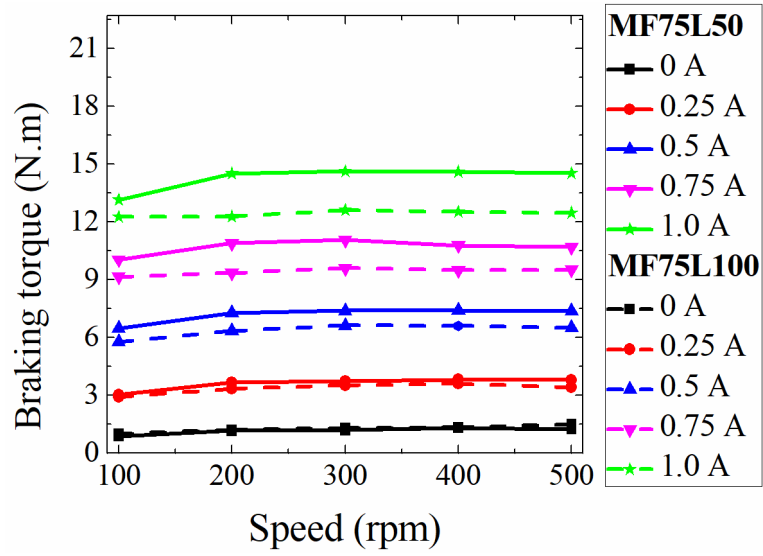
(e) 75 % mass fraction of LCIP in 50 cst and 100 cSt silicone oil
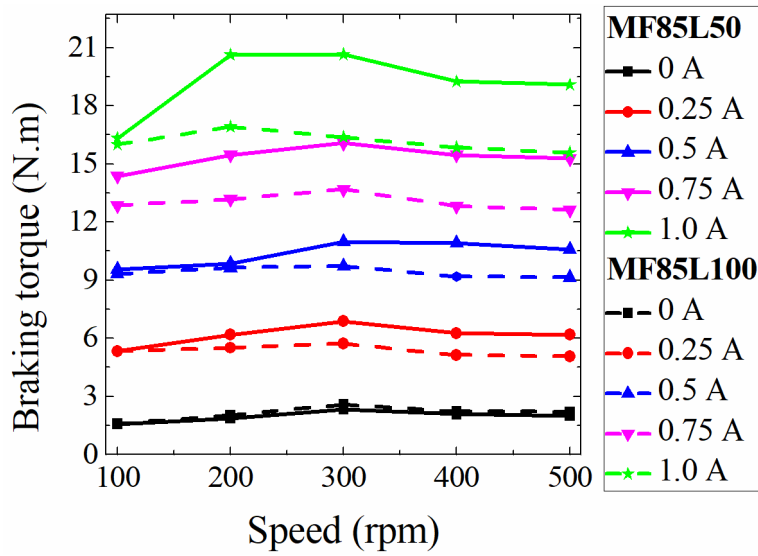
(f) 85 % mass fraction of LCIP in 50 cst and 100 cSt silicone oil

Figure 4.17 Experimentally determined braking torque for synthesized MRFs

In addition, the speed characteristics of the MR brake were measured with increase in current from 0.25 A to 1.0 A. During testing, the motor speed was set to initial speed, say 100 rpm when no current is supplied and then direct current of different magnitudes were supplied to MR brake electromagnet, i.e. 0.25 A, 0.5 A, 0.75 A and 1A. Due to MR effect, the reduction in speed with current supplied were noted at each current. This procedure was repeated for other speeds i.e. 200 rpm, 300 rpm, 400 rpm and 500 rpm. Figure 4.18 (a) and 4.18 (b) shows speed reduction with increase in current supplied for 75% and 85% mass fraction of SCIP based MRFs respectively, for different initial speeds of 100 rpm to 500 rpm in steps of 100 rpm. The speed reduction for MRFs containing 50 cSt and 100 cSt base oil viscosities and for MRF 132DG are also shown. There is a significant speed reduction with increase in applied current for all MRFs. The 50 cSt oil based MRFs have higher speed reduction in the presence of magnetic field compared to those containing 100 cSt oil for any particular current supplied as they produce higher torque. Further, speed reduction of brake composed of MRF 132DG is higher compared to MRFs containing 75% mass fraction of iron powder while it is lower compared to MRFs containing 85% mass fraction of iron powder as mass fraction of iron powder in MRF 132DG fluid is 80.98%. Similar

behaviour is observed in case of MR brakes employing MRIP and LCIP based MRFs. However, MF75S50 resulted in higher speed reduction as it has very high field induced torque compared to MRF 132DG fluid. MRFs composed of SCIP generated highest speed reduction compared to those composed of MRIP and LCIP due to its higher torque generation.
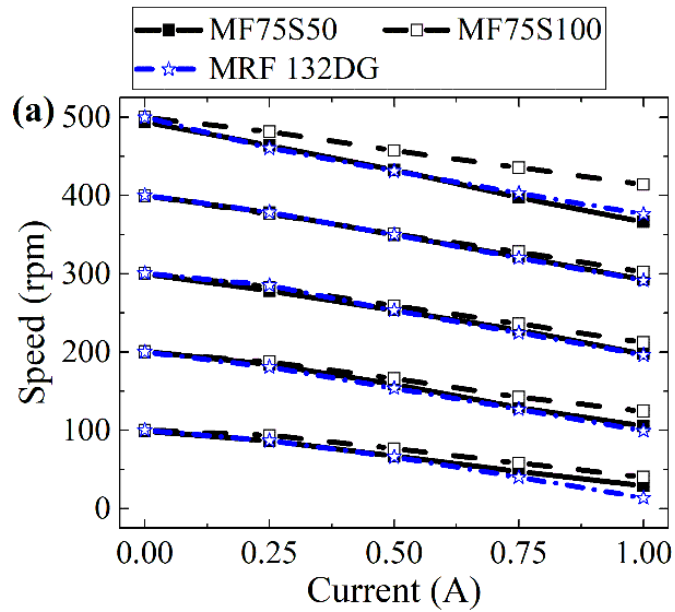
(a) 75 % mass fraction of SCIP in 50 cst and 100 cSt silicone oil & MRF 132 DG
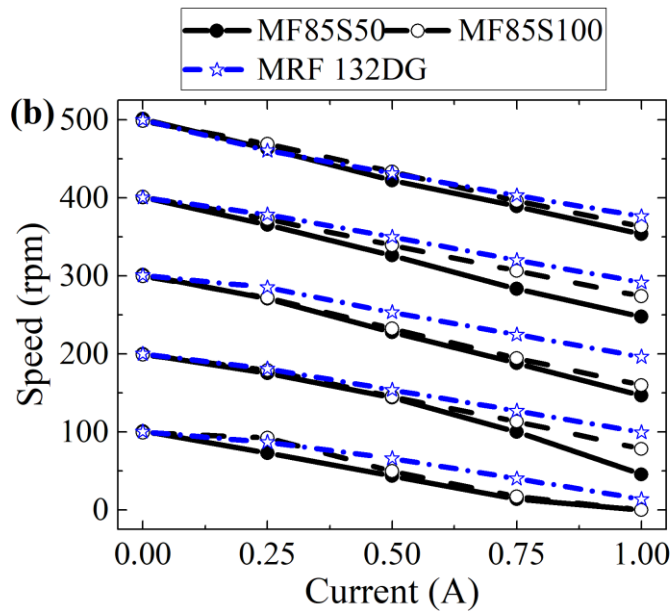
(b) 85 % mass fraction of SCIP in 50 cst and 100 cSt silicone oil & MRF 132 DG

Figure 4.18 Speed reduction with current for different initial test speeds

Figures 4.19 (a), 4.19 (b) and 4.19 (c) depict the torque ratio at different speeds of MR brake composed of SCIP, MRIP and LCIP based MRFs. Torque ratio is the ratio of field induced braking torque to off-state torque and signifies the controllable range of the MR brake (Gudmundsson et al. 2011b; Jolly et al. 1999). These values were calculated based on torques at maximum current with respect to that at no current supplied at a particular speed. It can be observed that torque ratios of brake employing SCIP based MRFs are the highest at all speeds compared to those containing MRIP and LCIP. This is due to the high field induced torque and low off-state torque compared to MRFs containing MRIP and LCIP. The torque ratio of MRIP and LCIP based MRFs are comparable as MRIP based fluid have slightly lower off-state torque while the field induced torques of LCIP based MRFs are higher. Also, the 50 cSt base oil based MRFs have higher torque ratio than 100 cSt based MRFs as lower viscosity base oil results in lower off-state torque compared to 100 cSt oil based MRFs leading to higher torque ratio. The torque ratio of MRF 132DG is higher compared to SCIP, MRIP and LCIP based MRFs due to very low viscosity of MRF132DG fluid. However, MF75S50 has higher torque ratio than MRF132DG fluid except at 100 rpm, as it possess lowest off-

130

state torque compared to all synthesized fluid and very high field induced torque. Further, for given mean particle diameter and base oil viscosity, the torque ratio of MRFs with 85 % particle mass fraction have lower value compared those with 75 % particle mass fraction due to higher off-state viscosity of MRFs with 85 % mass fraction.
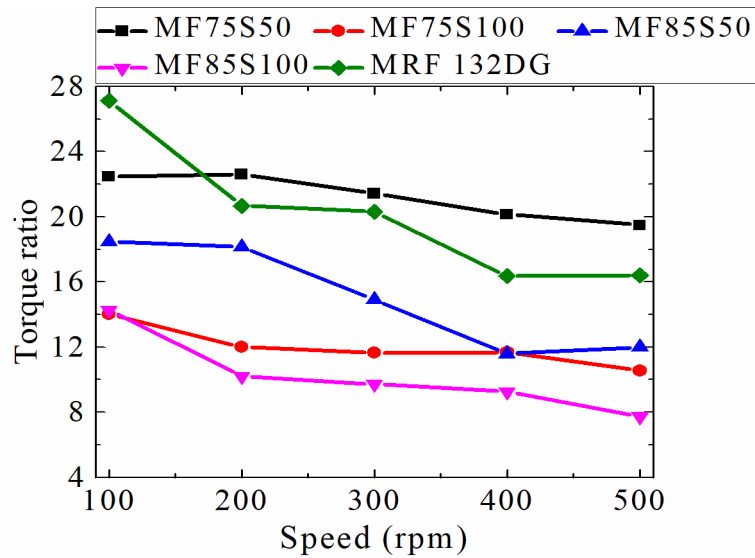
(a) SCIP based MRFs and MRF 132DG
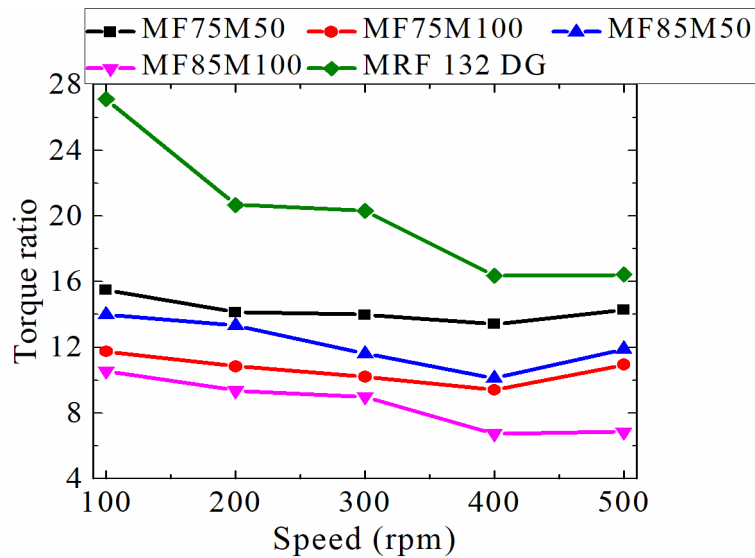
(a) MRIP based MRFs and MRF 132DG
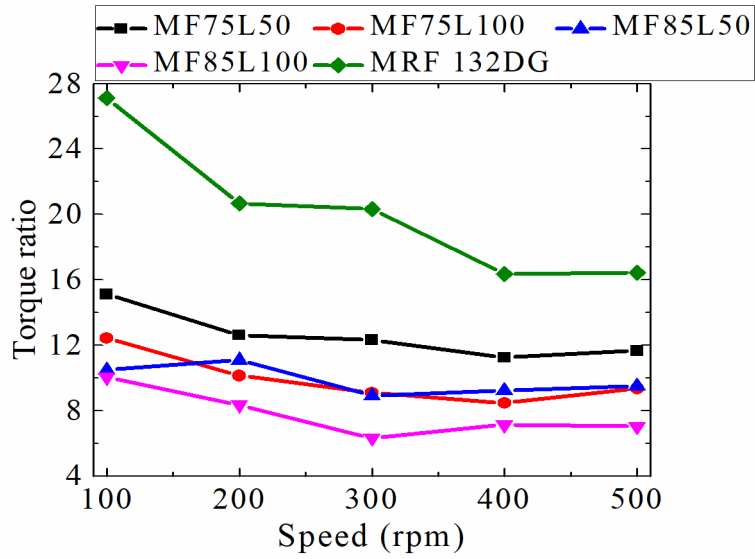
(a) LCIP based MRFs and MRF 132DG

Figure 4.19 Torque ratio of brakes utilizing MRF 132 DG and different synthesized MRFs containing (a) SCIP, (b) MRIP (c) LCIP

4.7 DESIGN OF EXPERIMENTS (DOE)

Factorial DOE is utilized to study the influence of several parameters and their interaction effects simultaneously and also to reduce the number of tests in understanding the system behaviour. The response factors considered in this work are field induced torque and off-state torque, while the independent factors studied are mean particle diameter, particle mass fraction of iron powder and base oil viscosity. The independent factors and their levels are shown in table 4.9.

Table 4.9 Factors and their levels

Factors	Level 1	Level 2	Level 3
Mean Particle diameter (microns)	2.9	6.71	9.68
Particle mass fraction of Iron powder (%)	75	85	--
Base oil Viscosity (cSt)	50	100	--

Table 4.10 Field induced, off-state braking torques and torque ratio for L-12 orthogonal array

Sl. No.	Mean particle diameter (microns)	Particle mass fraction (%)	Base oil viscosity (cSt)	Average off-state braking torque (Nm)	Average Field induced Braking Torque (Nm)	Torque ratio
1	2.9	75	50	0.78	16.35	20.96
2	6.71	75	50	0.97	13.76	14.18
3	9.68	75	50	1.15	14.28	12.42
4	2.9	75	100	1.26	14.89	11.82
5	6.71	75	100	1.12	11.80	10.53
6	9.68	75	100	1.28	12.42	9.70
7	2.9	85	50	1.35	19.78	14.65
8	6.71	85	50	1.43	17.15	11.99
9	9.68	85	50	1.97	19.19	9.74
10	2.9	85	100	1.77	17.29	9.76
11	6.71	85	100	1.76	14.45	8.21
12	9.68	85	100	2.13	16.15	7.58

The L_{12} ($3 \times 2 \times 2$) orthogonal array was employed for conducting the tests in order to analyze the effects on field induced and off-state braking torques and to determine the optimum mass fraction, mean particle diameter and base oil viscosity. The off-state torques and field induced braking torques at 1.0 A for different synthesized MRFs measured at different test speeds from 100 to 500 rpm in steps of 100 rpm were considered for analyses. It was be observed that the variation of braking torque with test speeds from 100 to 500 rpm is not significant. Hence, average value of field induced braking torque at current of 1.0 A and off-state braking torque of different MRFs over the test speed range were considered to determine the optimal MRF composition and are tabulated in table 4.10.

The optimal brake dimensions should theoretically provide a braking torque of 20 Nm at current of 2.5 A and rotor speed of 500 rpm for commercial MR fluid, MRF 132DG (Lord Corporation). However, the braking torque obtained at 1.0 A current is 14.2 Nm. The discrepancy is attributed to lower permissible current that could be supplied to coils and lower number of turns that was possible to be wound on the bobbin. Conversely, the braking torque calculated for synthesized fluid are in the range of 11.8 Nm to 19.8 Nm depending on the particle size, particle mass fraction and base oil viscosity at supply current of 1.0 A. Maximum average braking torque of 19.78 Nm is obtained for MF85S50 sample and nearly same value is obtained in case of MF85L50. However, the torque ratio for MF85S50 is higher due to its lower off-state torque. The torque ratio for MF75S50 sample is highest due to lowest off-state torque though it has lower field induced torque compared to MF85S50 sample. It can also be observed that though field induced torque of MRFs having MRIP are lower compared to those containing LCIP, their torque ratios are higher due to their lower off-state torques. With increase in mass fraction of iron powder from 75% to 85%, there is increase in off-state braking torque due to higher amount of iron particles which would have reduced the torque ratio though the field induced braking torque is also increased. Further, MRFs having higher base oil viscosities have lower torque ratio compared to those consisting of lower base oil viscosity. This is attributed to the fact that higher base oil viscosity results in higher MRF viscosity and consequently higher off-state torque which reduces the torque ratio.

4.7.1 Analysis of field induced and off-state torques

Analysis of variance (ANOVA) is a statistical method which is widely utilized to examine the relative significance of all the independent factors on the response factors. In this work, ANOVA technique was used to study the individual and interaction effects of mean particle diameter, particle mass fraction and base oil viscosity on the field induced and off-state braking torque of MR brake. The effect of independent factors on the field induced and off-state braking torque are tabulated in tables 4.11 and 4.12 respectively. 95% confidence level was considered for analyses. In order to get better R^2 value, regression model chosen was quadratic.

Table 4.11 Analysis of variance for field induced torque of MR brake

Source	DF	Adj SS	Adj MS	F-Value	P-Value	Contribut -ion rate (%)
Model	7	67.721	9.6745	114.40	< 0.0001	99.50
Linear	3	54.406	18.1354	214.45	< 0.0001	79.93
Mean particle diameter	1	4.9141	4.9141	58.11	0.002	7.22
Particle mass fraction	1	34.432	34.4322	407.15	< 0.0001	50.59
Base oil Viscosity	1	15.059	15.0598	178.08	< 0.0001	22.12
Square	1	9.6701	9.6701	114.35	< 0.0001	14.20
Mean particle diameter ×Mean particle diameter	1	9.6701	9.6701	114.35	< 0.0001	14.20
2-Way Interaction	3	1.7521	0.5840	6.91	0.046	2.57
Mean particle diameter × Particle mass fraction	1	0.9148	0.9148	10.82	0.030	1.34
Mean particle diameter × Base oil Viscosity	1	0.1171	0.1171	1.38	0.305	0.17
Particle mass fraction × Base oil Viscosity	1	0.7203	0.7203	8.52	0.043	1.05
Error	4	0.3383	0.0846			
Total	11	68.059				

Table 4.12 Analysis of variance for off-state torque of MR brake

Source	DF	Adj SS	Adj MS	F-Value	P-Value	Contrib-ution rate (%)
Model	7	1.84506	0.26358	43.15	0.001	98.69
Linear	3	1.68695	0.56232	92.06	< 0.0001	90.24
Mean particle diameter	1	0.23461	0.23461	38.41	0.003	12.55
Particle mass fraction	1	1.20980	1.20980	198.06	< 0.0001	64.71
Base oil Viscosity	1	0.24254	0.24254	39.71	0.003	12.97
Square	1	0.07003	0.07003	11.46	0.028	3.75
Mean particle diameter ×Meanparticle diameter	1	0.07003	0.07003	11.46	0.028	3.75
2-Way Interaction	3	0.08963	0.02988	4.89	0.080	4.79
Mean particle diameter × Particle Mass fraction	1	0.04002	0.04002	6.55	0.028	2.14
Mean particle diameter × Base oil Viscosity	1	0.04773	0.04773	7.81	0.049	2.55
Particle Mass fraction × Base oil Viscosity	1	0.00187	0.00187	0.31	0.609	0.10
Error	4	0.02443	0.00611			
Total	11	1.86949				

Since the *P* values are less than 0.05, it is clear that the mean particle diameter, mass fraction and base oil viscosity have substantial influence on the field induced braking torque as can be seen in table 4.11. The contribution rate of mean particle diameter, particle mass fraction and base oil viscosity on the field induced braking torque are 7.22 %, 50.59 % and 22.12 %, respectively. Hence, particle mass fraction is highly significant factor which affects the field induced braking torque of MR brake. Further, base oil viscosity has more influence than mean particle diameter which is also evident from their F-values.

Similarly, it can be observed that the mean particle diameter, mass fraction and base oil viscosity have major effect on the off-state braking torque of MR brake as their P-values are lower than 0.05 as shown in table 4.12. Further, square effect of mean particle diameter, interaction effects of mean particle diameter with particle mass fraction and base oil viscosity have significant influence on the off-state torque. The contribution rates of mean particle diameter, particle mass fraction and base oil viscosity on off-state braking torque are 12.55 %, 64.71 % and 12.97 %, respectively. Yet again, particle mass fraction has maximum influence on the off-state torque while the mean particle diameter and base oil viscosity have almost same effect. Thus, the particle mass fraction is the parameter having highest effect on the field induced and off-state braking torque of MR brake followed by base oil viscosity and mean particle diameter.

4.8 OPTIMAL SELECTION OF CONSTITUENTS OF MRF FOR MR BRAKE

The constituents of MRF influences the field induced braking torque and off-state braking torque. Both parameters were considered as separate objective functions rather than torque ratio as single objective of optimization due to following reasons. Lower mass fraction of iron powder in MRF leads to lower field induced torque and lower off-state torque. A small decrease in the value of the off-state torque leads to large increase in the torque ratio and hence MRFs having lower mass fraction produce higher torque ratio though the field induced torque is lower, as can be observed in table 4.10. Similarly, MRF having higher mass fraction of iron powder leads to higher off-

state torque as well as higher field induced torque. This would decrease the torque ratio as the off-state torque is also higher. Optimal constituents of MRF namely mean particle diameter, mass fraction of iron particles and base oil viscosity that yielded maximum field induced torque and minimum off-state torque were determined using MOGA optimization technique. The first step in the optimization process is to determine regression model for the response parameters in terms of independent parameters. The response parameters are the field induced and off-state braking torques, whereas the independent parameters are the mean particle diameter (MPD), particle mass fraction of dispersed phase (PMF) and base oil viscosity (BOV). The maximization of field induced braking torque and minimization of off-state braking torque were chosen as objective functions. The regression models were obtained using MINITAB^{TM} software and the equation for field induced braking torque with R^2 value of 0.995 is given by equation (4.4),

$$\text{Field induced torque} = -3.71 - 3.839 \times \text{MPD} + 0.3610 \times \text{PMF} + 0.1209 \times \text{BOV} + 0.1687 \times \text{MPD} \times \text{MPD} + 0.01990 \times \text{MPD} \times \text{PMF} - 0.00142 \times \text{MPD} \times \text{BOV} - 0.001960 \times \text{PMF} \times \text{BOV} \tag{4.4}$$

Equation (4.5) gives the regression model for off-state braking torque with R^2 value of 0.9869,

$$\text{Off-state torque} = -1.70 - 0.395 \times \text{MPD} + 0.0299 \times \text{PMF} + 0.0034 \times \text{BOV} + 0.01436 \times \text{MPD} \times \text{MPD} + 0.00416 \text{ MPD} \times \text{PMF} - 0.000909 \times \text{MPD} \times \text{BOV} + 0.000100 \times \text{PMF} \times \text{BOV} \tag{4.5}$$

MOGA optimization was performed in MATLAB^{TM} software by specifying following optimization parameters and limits. Population size, number of iterations and crossover value of 50, 100 and 80 % were specified for optimization (Puneet et al. 2015; 2019). Objective functions are maximization of field induced torque defined by regression equation 4.4 and minimization of off-state torque defined by regression equation 4.5. Limits of Independent parameters are mean particle diameter (microns): [2.9 9.68], Particle mass fraction of Iron powder (%): [75 85] and Base oil Viscosity (cSt): [50 100].
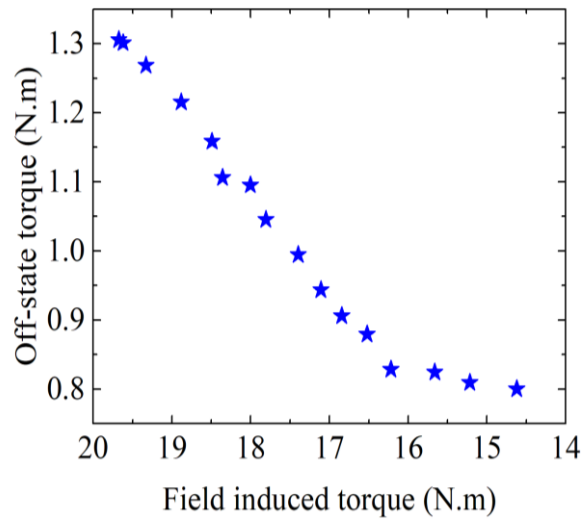
Figure 4.20 Pareto front solution from MOGA optimization

The result of MOGA optimization is Pareto front solution shown in figure 4.20 and table 4.13 which provides a number of alternate solutions depending on the weightage given to the response parameters. All the optimal solutions of Pareto front yielded base oil having viscosity of 50 cSt which demonstrated that MRF composed of lower viscosity base oil is beneficial compared to that composed of higher viscosity base oil as it yields lower off-state torque and higher torque ratio as well. Further, optimal mean particle diameter is close to that of SCIP since higher field induced torques are produced due to higher magnetic properties of SCIP. Also, the off-state torque is lower for SCIP based MRF which leads to higher torque ratio. The particle mass fraction varies between 75 % and 85 %, the corresponding field induced torque varies between 14.62 Nm and 19.67 Nm, the corresponding off-state torque varied between 0.8 Nm and 1.31 Nm and subsequently the torque ratio varies between 18.27 and 15.07 respectively. The variation in the field induced torque, off-state torque and torque ratio for this range are 5.05 Nm, 0.51 Nm and 3.2 respectively. Lower particle mass fraction results in lower field induced torque whereas higher particle mass fraction results in higher off-state torque causing generation of fluid frictional resistance and heat, wastage of power, etc.

Table 4.13 Pareto front solutions for optimal MRF composition

Optimal Solution	Mean particle diameter (microns)	Particle mass fraction (%)	Base oil viscosity (cSt)	Field induced torque (Nm)	Off-state torque (Nm)	Torque ratio
1	4.47	75.00	50.00	14.62	0.80	18.27
2	2.90	85.00	50.02	19.67	1.31	15.07
3	2.90	85.00	50.02	19.67	1.31	15.07
4	4.47	75.00	50.00	14.62	0.80	18.27
5	2.97	79.49	50.05	17.81	1.05	17.04
6	3.57	75.25	50.00	15.66	0.82	19.00
7	2.99	76.56	50.04	16.84	0.91	18.59
8	3.91	75.08	50.02	15.22	0.81	18.80
9	3.05	83.11	50.05	18.88	1.22	15.53
10	2.98	77.35	50.01	17.11	0.94	18.13
11	2.91	80.95	50.03	18.35	1.10	16.68
12	3.03	78.45	50.04	17.40	0.99	17.50
13	3.05	81.91	50.04	18.49	1.16	15.96
14	2.98	84.22	50.04	19.33	1.27	15.23
15	3.10	80.59	50.08	18.00	1.10	16.44
16	3.08	75.01	50.01	16.22	0.83	19.58
17	2.92	84.91	50.02	19.62	1.30	15.08
18	3.11	76.09	50.07	16.52	0.88	18.79

Hence, based on trade-off between off-state torque, field induced torque and torque ratio, an optimal solution having mean particle diameter of 2.91 microns, particle mass fraction of 80.95 % and base oil viscosity of 50.03 cSt was selected which produces a field induced torque of 18.35 Nm, off-state torque of 1.1 Nm and torque ratio of 16.68. There is a meagre difference of 1.32 Nm in the field induced torque for selected MRF with respect to the maximum value in the pareto front. The difference in the off-state torque with respect to the minimum value in the pareto front is 0.3 Nm. Also, the difference in the torque ratio with respect to the maximum value in the pareto front is 1.59. That is, the field induced torque is given more weightage compared to the off-state torque and torque ratio. Smallest particle size was preferred as it has superior sedimentation stability and beneficial from tribological point of view. The particle mass fraction of this MRF is almost same as that in commercial MR fluid, MRF 132DG (Lord Corporation). However, its off-state torque is 27.3 % higher than that of commercial one having an off-state torque of 0.864 Nm. Nevertheless, its field induced torque is 29.2 % higher than that obtained for commercial MRF.

4.9 SUMMARY

In this study, optimum dimensions of MR brake utilizing commercial MR fluid, MRF 132DG (Lord Corporation) were obtained using MOGA optimization. Experiments were performed on the designed MR brake utilizing commercial MR fluid, MRF 132DG (Lord Corporation) and validated using analytical results. The morphology and magnetic properties of three different iron powders were characterized. A DOE technique was employed to determine the optimal composition of MRF. Experiments were performed on the MR brake utilizing twelve synthesized MRFs composed of combinations of different particle mass fractions, base oil viscosities and mean particle diameters. Torque characteristics and speed reduction performance of MR brake utilizing different MRFs were determined. Optimal MRF was selected by means of MOGA optimization. Finally, the sedimentation stability of SCIP and MRIP based MRFs were studied. Following were the main conclusions drawn from the current study.

- The design torque of 20 Nm was not attained as the design using magnetostatic analysis was carried out at current of 2.5 A while the maximum current supplied to coil was limited to 1 A due to coil resistance. Also, required number of coils could not be wound on bobbin due to packing factor. However, a close agreement was found between experimentally determined and computationally determined values of braking torque for optimally designed MR brake utilizing commercial MR fluid, MRF 132DG (Lord Corporation).

- Based on magnetization curves, smaller sized carbonyl particles (2.9 microns) possess superior magnetic properties among other iron particles in terms of higher permeability at lower magnetic fields upto 5000 Gauss, lower coercivity and remnant magnetization. It has higher saturation magnetization than that of medium sized (6.71 microns) reduced iron particles while lower saturation magnetization than that of large sized (9.68 microns) carbonyl iron particles.

- Sedimentation stability tests also confirmed the superiority of smaller sized iron particles based MRFs and that the optimal MRF would have sedimentation stability between three to four days. This would not be a problem as MR brakes are highly efficient mixing devices.

- Smaller sized iron particles based MRFs produced higher braking torque, speed reduction and torque ratio compared to medium and large sized iron particles based MRFs for several speeds, mass fractions and current supplied. This is due to higher magnetic permeability of the smaller sized iron particles at lower magnetic field as could be observed from its magnetization curve which results in higher MR effect. This confirms that not only the size and magnetic saturation of iron particles, but the initial magnetic permeability also has major effect on the rheological properties and subsequent performance of the MR brake.

- Mass fraction of iron particles has the highest effect on the field induced and off-state braking torque followed by base oil viscosity and mean particle diameter which were evident from analysis of variance (ANOVA) study.

- MRFs composed of lower viscosity base oil (50 cSt) resulted in higher field induced torque compared to those containing higher viscosity base oil (100 cSt) for all mean particle diameters and particle mass fractions. Further, 50 cSt oil based MRFs have

lower off-state torques compared to those containing 100 cSt oil due to lower viscosity. This results in higher torque ratio when a low viscous base oil is utilized.

- Based on MOGA optimization, pareto front solution having mean particle diameter of 2.91 microns, particle mass fraction of 80.95 % and base oil viscosity of 50.03 cSt was recommended as optimal composition of MRF for designed MR brake which yields a field induced torque of 18.35 Nm, off-state torque of 1.1 Nm and torque ratio of 16.68. The composition was chosen based on trade-off between response factors namely field induced torque and off-state torque which in turn is influenced by the mean particle diameter, particle mass fraction and base oil viscosity.

CHAPTER 5

OPTIMAL COMPOSITION OF MAGETORHEOLOGICAL FLUID FOR SANDWICH BEAM

5.1 INTRODUCTION

An MRF core beam consists of MRF sandwiched between two constraining face layers, sealed using adhesive. Its vibration behaviour can be altered by the application of magnetic field due to controllability in the properties of MRF. The effect of constituents of MRF such as particle size, mass fraction of carbonyl iron powder, base oil viscosity, additives on the performance of MR devices were investigated, such as MR dampers (Acharya et al. 2019b; Gurubasavaraju et al. 2017b) MR brakes (Nguyen et al. 2019), MR rotary brakes (Gudmundsson et al. 2011b) and the optimal composition of MRF which yielded best performance for those MR devices were determined. Sapiński et al. (2011) determined the vibration characteristics of MR beam filled with two types of commercial MRFs and concluded that mass fraction of iron particles in the fluid has a major effect on the natural frequency and damping coefficient of the beam. The study on the vibration behaviour of MRF sandwich beams involving In-house prepared MRFs having different proportions of iron particle mass fractions and particle sizes are scarce in literature. In this work, the effect of mass fraction and particle size on the natural frequencies and damping ratio characteristics of MR fluid core sandwich beams have been investigated. Further, the optimal composition of MR fluid for MR fluid core sandwich beam have been proposed.

5.1.1 Methodology for determination of Optimal MR Fluid Composition for MR fluid core sandwich Beam

The methodology followed for determination of optimal composition of MR fluid for sandwich beam is depicted in figure 5.1. Six different MRFs having combination of two different particle size and three mass fractions of CIP were used to manufacture different MRF sandwich beams. The free vibration tests of MRF sandwich

beams at different magnetic fields were performed to compare their natural frequencies and damping ratio. Further, sinusoidal sweep excitation tests were performed on these beams to determine the reduction in the amplitude of vibration for MRFs with different particle mass fractions, particle sizes at different magnetic fields. Finally, optimal CIP particle size and its mass fraction in MRF was determined using multi-objective genetic algorithm (MOGA) optimization method based on maximization of damping ratio and minimization of mass of MRF as objectives.

Characterization of iron particle size and its distribution, morphology and magnetic properties

↓

Synthesis of Magnetorheological fluid (MRF) with combination of three Iron particle weight fractions and two particle sizes

↓

Measurement of viscoelastic properties of the in-house prepared MRF and a commercial MRF in the presence and absence of magnetic field

↓

Fabrication of MRF sandwich beams with in-house prepared MRF and commercial MRF as core

↓

Determination of natural frequencies and damping ratios of MRF sandwich beams at different magnetic fields using Impact hammer tests

↓

Vibration suppression behaviour of MRF sandwich beams at different magnetic fields using sinusoidal sweep excitation tests

↓

Determination of optimal iron particle mass fraction and size using optimization based on maximization of damping ratio and minimization of MRF mass

Figure 5.1 Methodology

5.2 CHARACTERIZATION OF IRON POWDER

The viscoelastic properties of MRF depend on the magnetic properties of iron particles, their size and distribution. CIP of different mean particle sizes namely finer sized CIP (SCIP) and coarser sized CIP (LCIP) were used as dispersed phase for the preparation of MRF and they are products of Sigma Aldrich (C3518) and BASF (CN grade) respectively. The morphology, size distribution and magnetic properties of CIP were characterized. These have been reported in section 4.5.1 of chapter 4 of this thesis. Field emission scanning electron micrographs of CIP depicted their near spherical shape. From the particle size distribution measurement, the mean sizes of fine and coarse CIP obtained are 2.9 microns and 9.68 microns respectively. Also, using vibrating sample magnetometer, the saturation magnetization of fine and coarse CIP was measured to be 184.2 emu/g and 224.6 emu/g. LCIP has higher saturation magnetization compared to SCIP which means the LCIP get magnetized upto higher magnetic field than SCIP which is beneficial for MR effect.

5.3 PREPARATION OF MR FLUID

Six MRFs were prepared composed of SCIP (2.9 microns) and LCIP (9.68 microns) and having three different particle mass fractions namely 60%, 70% and 80%. Polyalphaolefin (PAO) oil (Make: Exxon Mobil) was used as the carrier fluid. It has 32 cSt kinematic viscosity (@ 40°C) and specific gravity of 0.824. Initially, electronic weighing balance was used to weigh desired mass of PAO oil and CIP. Using a mechanical stirrer, CIP was mixed in PAO oil at 500 rpm for eight hours to properly mix the powder in the oil. The constituents of the prepared MRFs is listed in table 5.1. The prepared MRFs are named on the basis of particle mass fraction and particle size. MF60L and MF60S are composed of 60% mass fraction of LCIP and SCIP respectively.

Table 5.1 Constituents of prepared MRFs.

Sl. No.	MRF sample	CIP Mass fraction (%)	PAO oil Mass fraction (%)
1.	MF60L	60	40
2.	MF60S	60	40
3.	MF70L	70	30
4.	MF70S	70	30
5.	MF80L	80	20
6.	MF80S	80	20

5.4 VISCOELASTIC PROPERTIES OF MRFs

The viscoelastic properties are measures of the materials ability to store and dissipate energy. The MRF exhibits viscoelastic nature within the pre-yield region under external magnetic field (Li et al. 1999). The storage modulus is a measure of the elastic property and the loss modulus is a measure of the viscous property of MRF. These two quantities are combined and expressed as complex shear modulus. The viscoelastic properties of the six MRFs and commercial MR fluid, MRF 132DG (Lord Corporation) were measured by performing oscillatory rheology tests using Modular Compact Parallel Plate Rheometer (MCR-702 Anton Paar). During the tests, a small amount of MRF was poured on the bottom stationary plate, the gap between 20 mm parallel plates was set to 1 mm and temperature was set to 25°C. Prior to measuring the viscoelastic properties, the MRF was pre-sheared at shear rate of 10 s^{-1} for 10 seconds followed by 5 seconds waiting time to ensure uniform distribution of iron powder in the sample. The tests were performed at strain amplitude of 0.1% and frequency logarithmically increasing from 0.1 Hz to 100 Hz (Hemmatian et al. 2018). Strain amplitude was chosen as 0.1% (0.001) to ensure that the MRF operates in pre-yield regime (Li et al. 1999). The storage, loss and complex moduli were measured at 16 distinct frequency values. The viscoelastic properties were measured in the absence of current (Off-state condition), that is, 0 A (0 Gauss) and with the application of current (On-state condition), i.e. 0.38 A which produce magnetic fields of 745 Gauss.
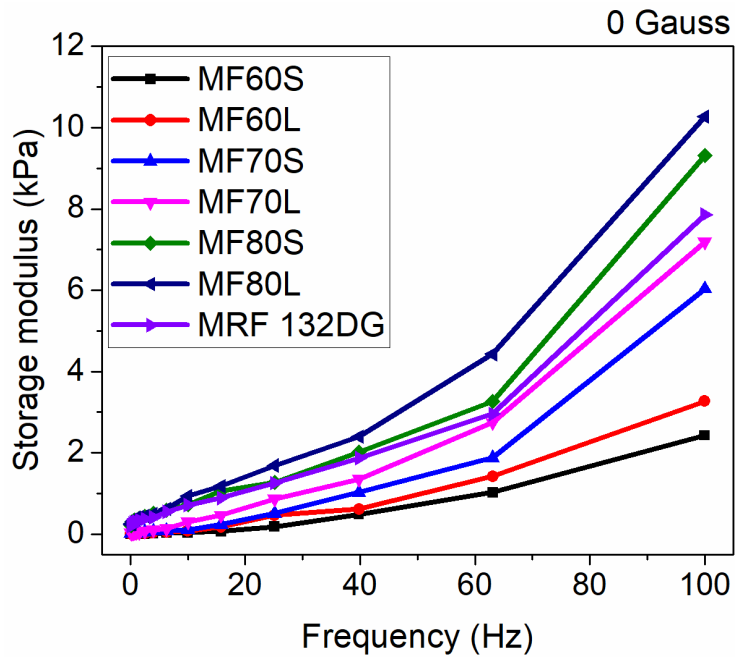
(a) In-house prepared and commercial MRFs at 0 Gauss
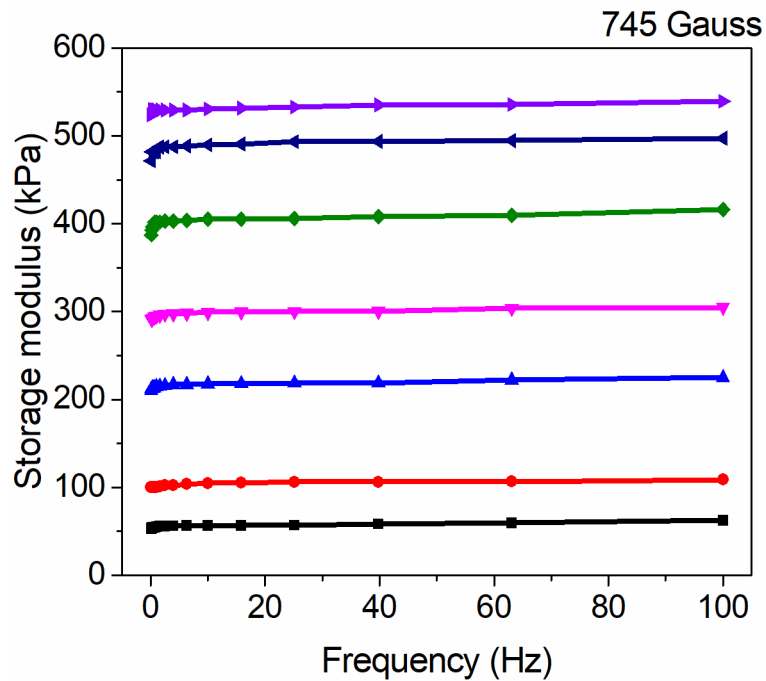
(b) In-house prepared and commercial MRFs at 745 Gauss

Figure 5.2 Storage Modulus of MRFs in the absence and presence of magnetic field
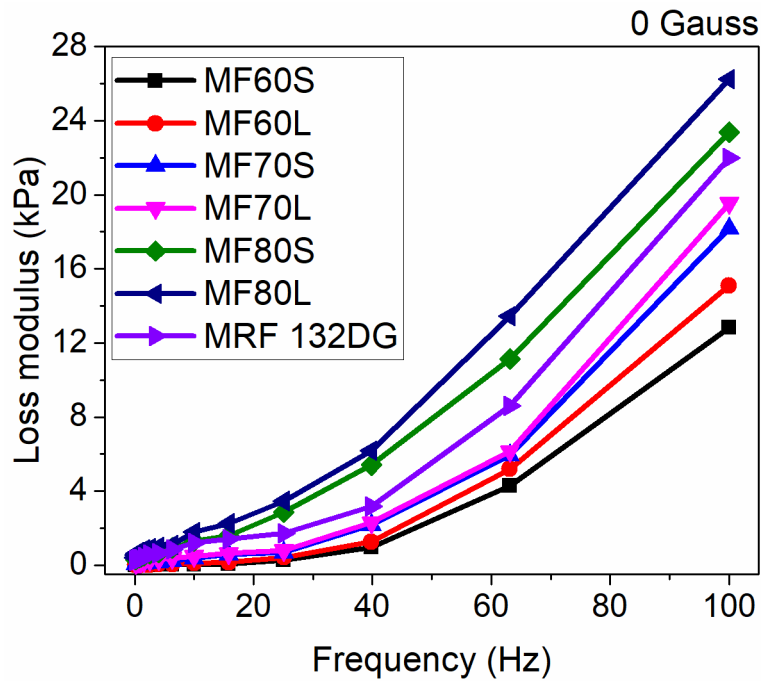
149

(a) In-house prepared and commercial MRFs at 0 Gauss

(b) In-house prepared and commercial MRFs at 745 Gauss

Figure 5.3 Loss Modulus of MRFs in the absence and presence of magnetic field
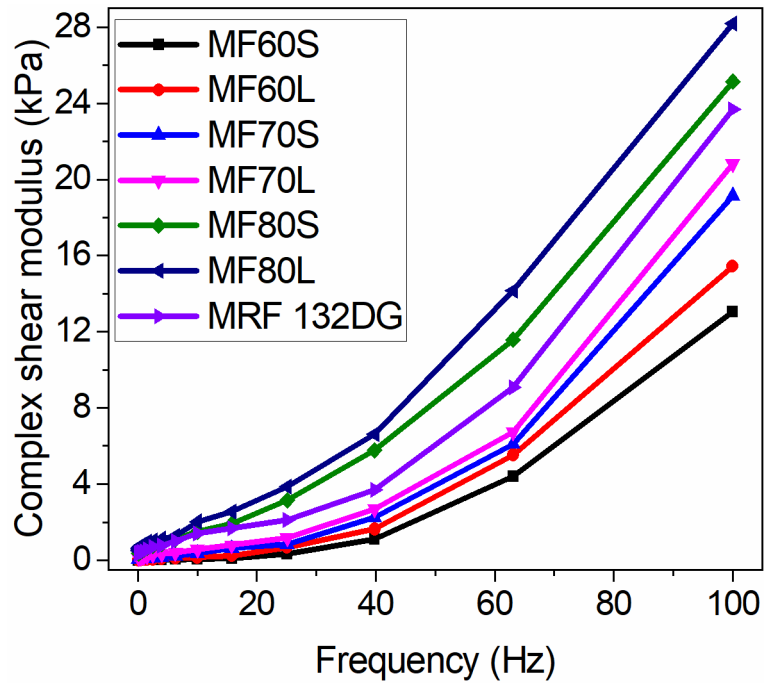
(a) In-house prepared and commercial MRFs at 0 Gauss
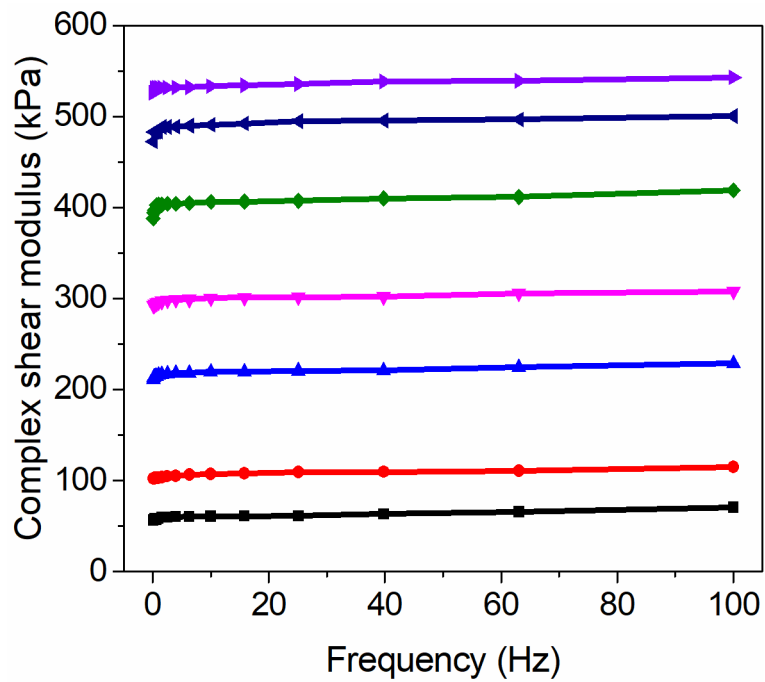
(b) In-house prepared and commercial MRFs at 745 Gauss

Figure 5.4 Complex Shear Modulus of MRFs in the absence and presence of magnetic field

The variation of storage modulus with frequency for prepared and commercial MR fluid, MRF 132DG (Lord Corporation) at 0 Gauss and 745 Gauss are shown in figures 5.2 (a) and 5.2 (b) respectively. Figures 5.3 (a) and 5.3 (b) show the variation of loss modulus with frequency for different MRFs at 0 Gauss and 745 Gauss respectively. Figures 5.4 (a) and 5.4 (b) illustrates the variation of complex shear modulus with frequency for different MRFs at 0 Gauss and 745 Gauss respectively. It can be seen that in off-state condition (0A), the storage, loss and complex shear moduli increase with frequency. The loss modulus is considerably higher than storage modulus in the off-state condition indicating that the MRF has more viscous behaviour than elastic one. An opposite behaviour is observed in the on-state condition, as MRF changes to semi-solid which in turn increases the storage modulus more compared to the loss modulus. Viscoelastic properties increase with mass fraction of CIP in MRF in both on-state and off-state conditions. Also, MRFs having LCIP have higher viscoelastic properties compared to those containing SCIP due to higher saturation magnetization of LCIP. The viscoelastic properties are enhanced when magnetic field is applied (Chooi and Oyadiji 2005; Hemmatian et al. 2018; Li et al. 1999). In the off-state condition, the viscoelastic properties of commercial MR fluid, MRF 132DG (Lord Corporation) are lower than MF80S and MF80L among the prepared MRFs. Though, these MRFs have same mass fractions of iron powder, commercial MR fluid, MRF 132DG (Lord Corporation) has a very low apparent viscosity of 0.114 Pa-s at 40°C (LORD Corporation Technical Data Sheet, 2003). Commercial MR fluid, MRF 132DG (Lord Corporation) has 80.98 % mass fraction of magnetic particle phase in the MRF. Nevertheless, the viscoelastic properties of commercial MR fluid, MRF 132DG (Lord Corporation) in the on-state condition are higher compared to those of the prepared MRFs which indicates that it is more responsive to the magnetic field.

5.5 GEOMETRY OF MRF SANDWICH BEAM

MRF sandwich cantilever beam having dimensions shown in figure 5.5 (a) was used in this study. The aluminium beam is 260 mm long, 25 mm wide and 6 mm thick. MRF layer of 2 mm was chosen based on the study performed by Srinivasa et al. (2020). Using wire cut electric discharge machining (Appendix I.14), central cavity of 2 mm height and length of 220 mm was created in solid aluminium material, leaving 2 mm each top and bottom face layers of aluminium material.
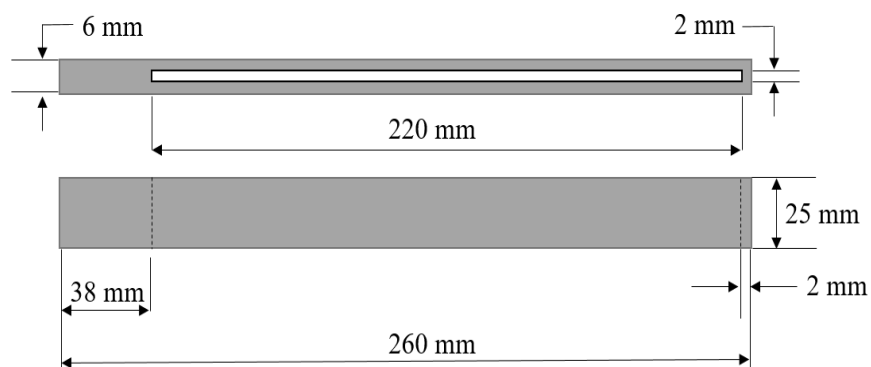
(a) Beam dimensions

(b) Fabricated MRF sandwich beams

Figure 5.5 Beam dimensions and Fabricated MRF sandwich beams.

Seven aluminium beams with cavity for filling MRF were manufactured using wire EDM machining. The periphery of cavity was sealed with silicone sealant to avoid MRF leaks. A small portion (hole) was not sealed at each end of the beam so as to fill the MRF. The MRF was poured into the cavity through one of the holes while the beam is held vertical. The other hole helps in pushing out the trapped air present in the cavity of the beam when MRF is poured. After filling the beam with MRF, the small holes were properly sealed with silicone sealant. Figure 5.5 (b) shows six beams filled with prepared MRFs and one beam filled with commercial MR fluid, MRF 132DG (Lord Corporation). The MRF sandwich beams are named as MRB60S, MRB70S, MRB80S, MRB60L, MRB70L and MRB80L based on the mass fraction of iron powder and particle size in the MRF. The beam filled with commercial MR fluid, MRF 132DG (Lord Corporation) is named as MRB 132DG.

5.6 MODAL PARAMETERS OF THE MRF SANDWICH BEAMS

Free vibration tests of MRF beams at different magnetic fields were performed as per ASTM E756-05 standards (Thomas M Lewis 2007) using the set up shown in figure 5.6. It consists of stainless steel rigid base with provisions to hold the beam and the permanent magnet fixtures. Beam fixture is used for mounting the beams whereas permanent magnet fixtures are used to mount the permanent magnets. The permanent magnet fixtures are screwed to a vertical plate and can be moved to vary the distance between the permanent magnets so as to obtain desired magnetic field induced on the beam. Miniature accelerometer (Make: PCB Piezotronics; Model: 352A25)) was used to acquire acceleration signals and sent to LabVIEW software through NI 9234 data acquisition device (DAQ, Make: National Instruments). An impact hammer (Make: Kistler) was utilized to apply impact excitation to the beam. One end of the MRF beam was fixed to the fixture such that 38 mm of the beam was fixed and remaining beam length containing MRF was free and could be exposed to magnetic field. The distance between the permanent magnets which are mounted on the top and bottom fixtures was adjusted such that it produced a desired magnetic fields of 250 Gauss, 500 Gauss and 750 Gauss. The MRF beams were given impact excitation at 20 mm from its clamped

end and acceleration signals were acquired using accelerometer mounted 25 mm from the beam's free end.
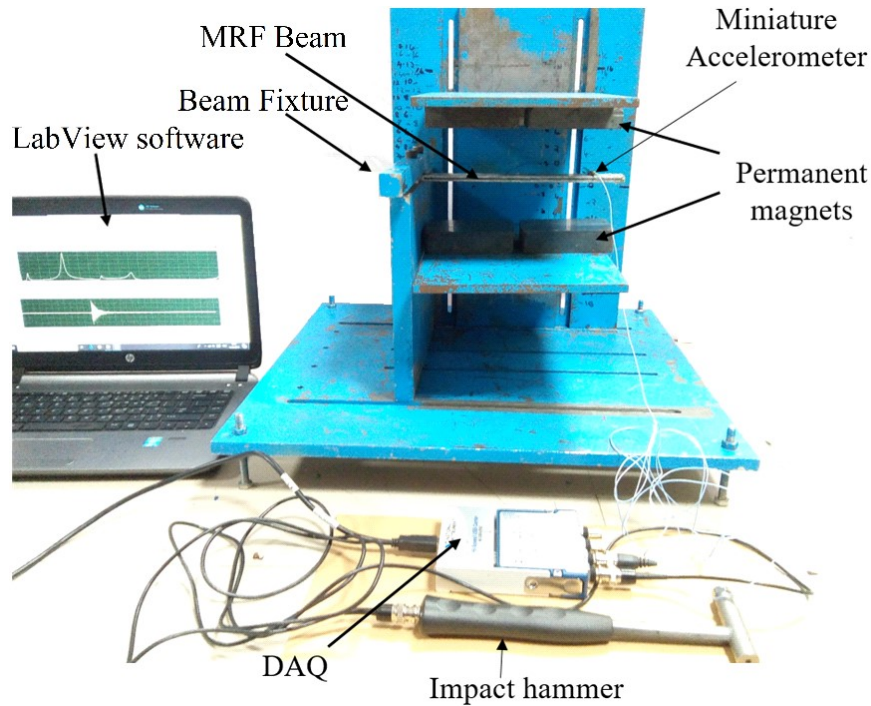
Figure 5.6 Free vibration test setup

Free vibration tests using Impact hammer were performed on the MRF sandwich beams to determine the first three natural frequencies and their corresponding damping ratios. The first three natural frequencies of the beams were identified from peaks in the free vibration test results. Using half power bandwidth technique, the damping ratio at the first three natural frequencies of the beam were calculated (Eshaghi et al. 2015; Yalcintas and Dai 2003). In this method, the peak amplitude at a particular natural frequency (ω_n) is noted. The peak amplitude is divided by $\sqrt{2}$ and the frequencies (ω_1, ω_2) at this amplitude are identified. The ratio of the difference between these frequencies to the twice the natural frequency is termed as damping ratio and is given by equation (5.1).

$$\zeta = \frac{\omega_2 - \omega_1}{2\omega_n}$$

(5.1)

155
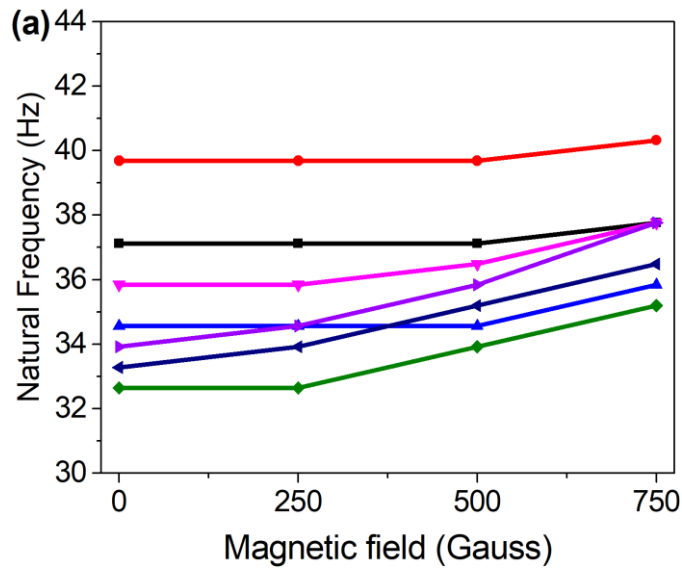
(a) Variation of first natural frequency with magnetic field
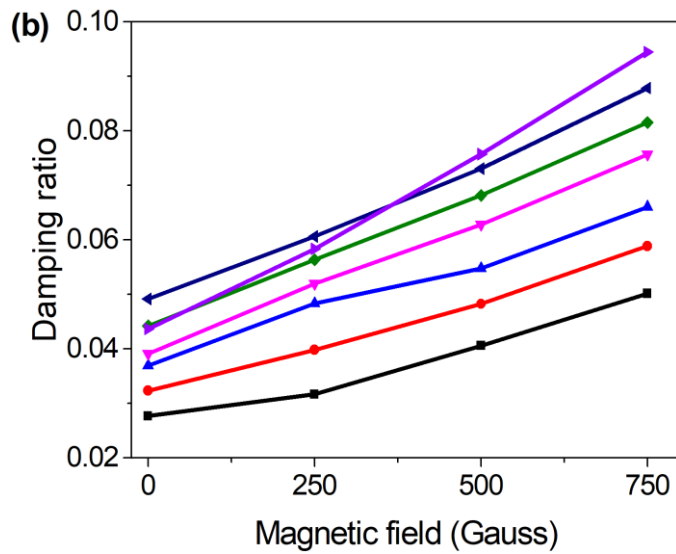
(b) Variation of damping ratio with magnetic field

Figure 5.7 Effect of magnetic fields natural frequency and damping ratio of MRF sandwich beams at first mode
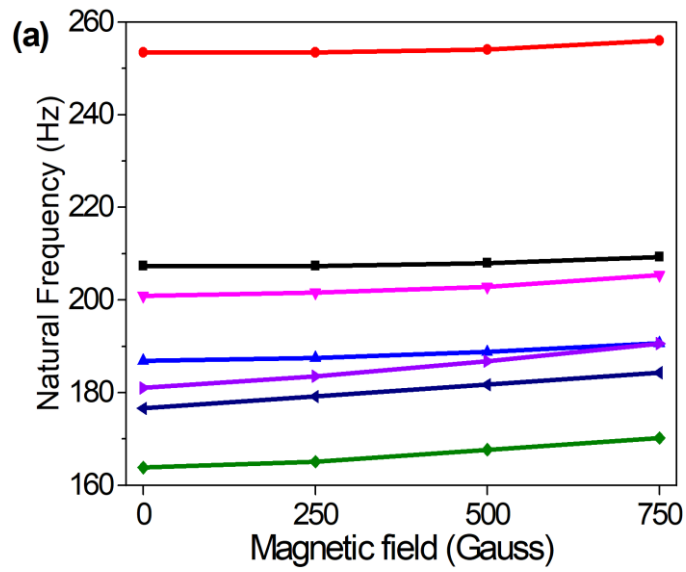
(a) Variation of second natural frequency with magnetic field

(b) Variation of damping ratio with magnetic field

MRB60S —— MRB60L —— MRB70S —— MRB70L —— MRB80S —— MRB80L —— MRB 132DG
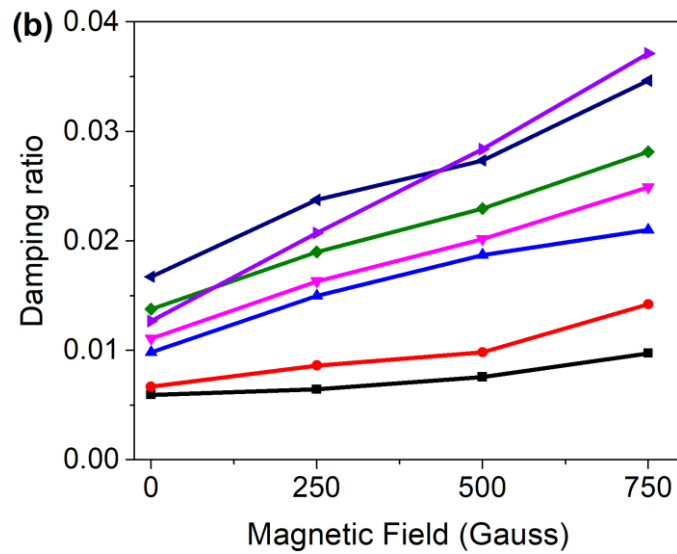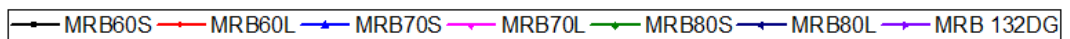
Figure 5.8 Effect of magnetic fields natural frequency and damping ratio of MRF
sandwich beams at second mode
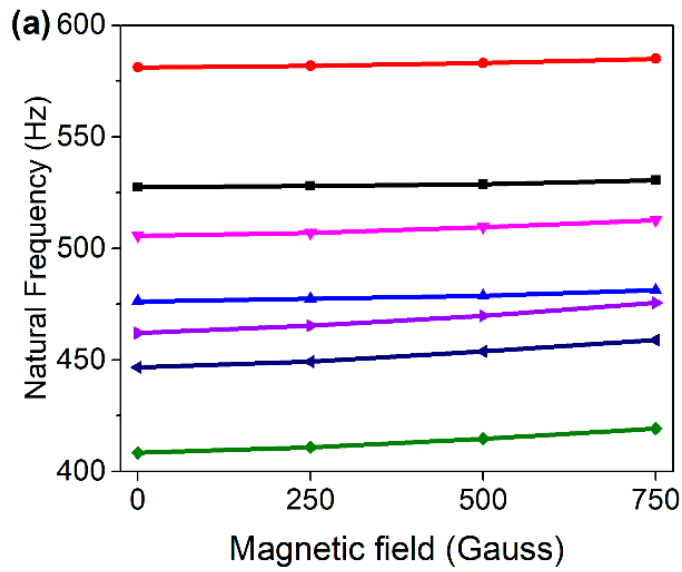
(a) Variation of third natural frequency with magnetic field
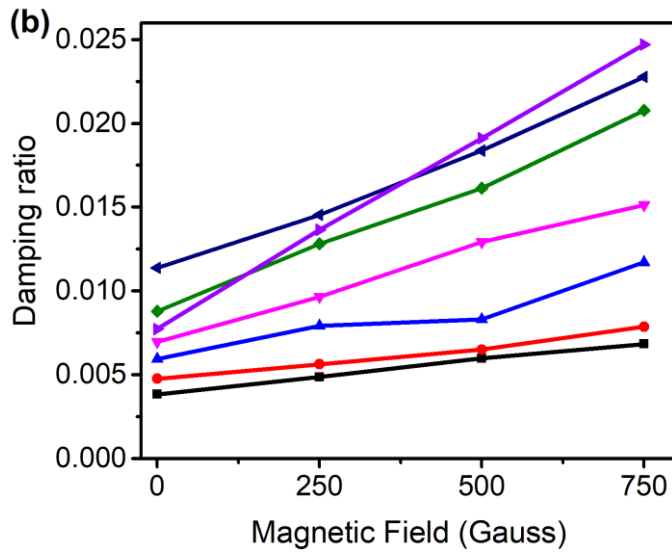
(b) Variation of damping ratio with magnetic field

| MRB60S | MRB60L | MRB70S | MRB70L | MRB80S | MRB80L | MRB 132DG |

Figure 5.9 Effect of magnetic fields natural frequency and damping ratio of MRF sandwich beams at third mode

Figures 5.7 to 5.9 show the variation of first three natural frequencies and damping ratios of beams filled with prepared MRFs and commercial MR fluid, MRF 132DG (Lord Corporation). Damping ratio increases with increase in applied magnetic field. Also, there is upward shift in the natural frequency with increase in magnetic field and is higher at second and third natural frequencies compared to that at first natural frequency. This is attributed to the increase in storage modulus with increase in magnetic field and subsequently the stiffness of the beam (Chooi and Oyadiji 2005; Fadaee 2019). Natural frequencies of MRFs with higher mass fractions of CIP are lower especially at higher modes. This is due to the increase in mass of the beam with increase in mass fractions which would reduce the frequency. Further, with increase in mass fraction of CIP, there is significant increase in damping ratio due to more iron particles which cause higher MR effect. Damping ratio of beams with LCIP MRFs are higher compared to those with SCIP at all magnetic fields due to higher saturation magnetization of LCIP and subsequent higher complex shear modulus compared to SCIP MRFs. In the absence of magnetic field, beam with commercial MR fluid, MRF 132DG (Lord Corporation) core has lower damping ratio compared to MF80S and MF80L MRFs, which is due to its lower loss modulus and complex shear modulus compared to them. However, with increase in applied magnetic field, the damping ratio of beam with commercial MR fluid, MRF 132DG (Lord Corporation) increases at a higher rate compared to beams with MF80S and MF80L MRF cores and its value is higher at magnetic fields of 500 Gauss and 750 Gauss. Hence, beam with commercial MR fluid, MRF 132DG (Lord Corporation) core showed superior damping properties compared to all the fabricated MRF sandwich beams especially at higher magnetic fields.

5.7 FORCED VIBRATION RESPONSE

Figure 5.10 shows the experimental setup for performing forced vibration testing of MRF sandwich beams which consists of function generator (Make: Tektronix, AG 1022), power amplifier (Make: Saraswati Dynamics), electrodynamic shaker (Make: Saraswati Dynamics), data acquisition device (NI 9234, Make: National Instruments), accelerometer (Make: PCB Piezotronics), load cell (Make: Kistler), structure for mounting the permanent magnets and stinger with fixture for holding the beam. A Labview program was interfaced with function generator and sensors by means of DAQ. The beam was subjected to sinusoidal sweep excitation from a start frequency to end frequency for desired duration of time. The start and end frequency, time duration for sweep excitation and number of iterations can be varied in the Labview program. The start and end frequencies were set to 1 Hz and 600 Hz, time duration as 20 seconds and the sweep excitation was repeated four times and average value was plotted. Based on input received from Labview program, the function generator produces sinusoidal excitation frequency ranging from 1 Hz to 600 Hz and sends it to amplifier. The amplifier output gain was set to 5% and it amplifies the voltage and sends it to electrodynamic shaker. This causes excitation of the beam which is held in the fixture mounted on a rod. Bottom end of the stinger rod is screwed tightly to the shaker while the other end holds the beam fixture. A load cell is screwed to the stinger rod near the fixture end. The load cell located in the stinger rod measures the input force acting on the beam while the accelerometer mounted on the beam acquires acceleration data and sends them to Labview program through DAQ device. The permanent magnets are moved away or towards each other equidistant from the beam to produce desirable magnetic field over the entire beam length. The frequency response function is obtained, which is the ratio of acceleration response (output) and the force (input), as a function of frequency.
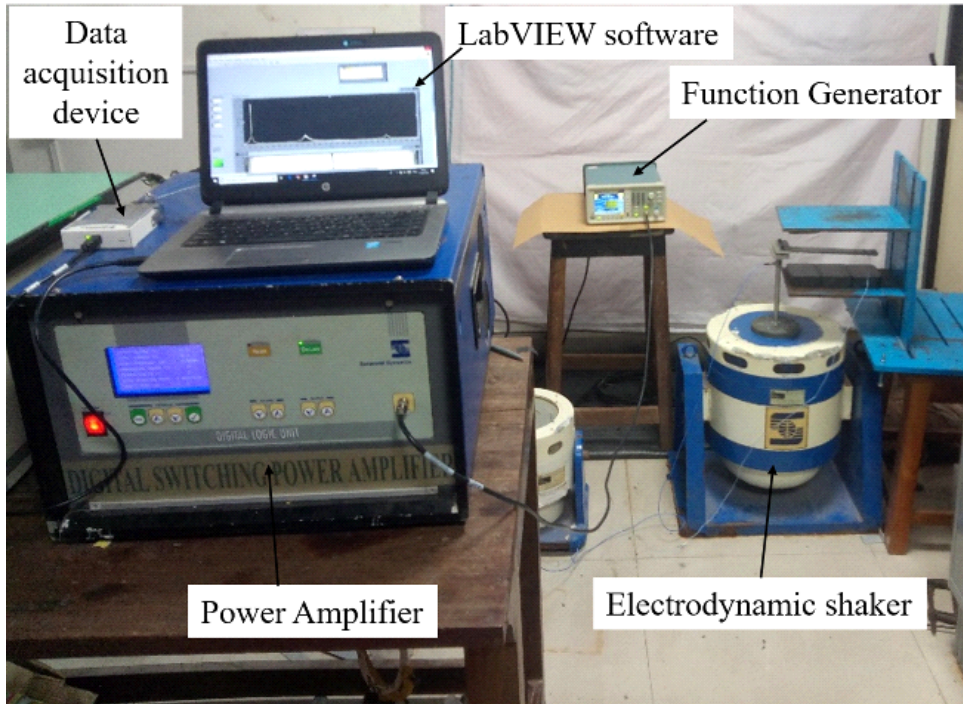
(a) Whole Forced vibration test set up
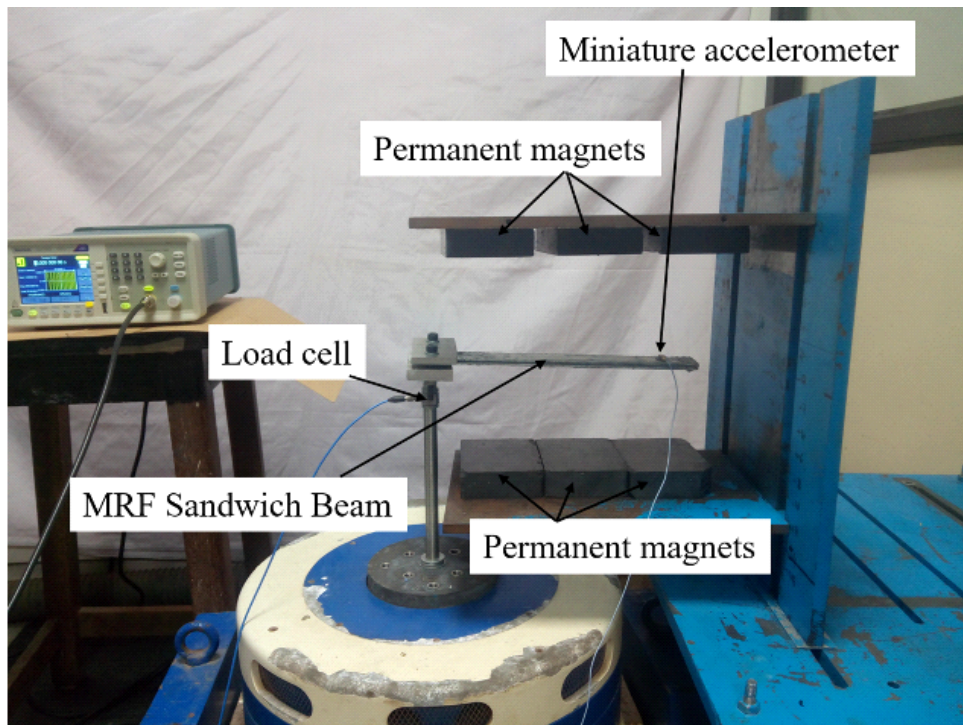
(b) Closer view of the MRF Sandwich beam mounted on fixture

Figure 5.10 Forced vibration test setup

The frequency response function for sandwich beams containing MF80S, MF80L and commercial MR fluid, MRF 132DG (Lord Corporation) as core at different magnetic fields are depicted in figures 5.11 (a)-(c) respectively. It can be observed that there is significant reduction in vibration amplitude response of the beams at natural frequencies with increase in magnetic fields due to increase in damping ratio, especially at first natural frequencies. Also, MRF beam comprising of LCIP (MRB80L) has higher vibration suppression capability compared to beam having SCIP (MRB80S) and this behaviour is observed for other mass fractions too. This could be explained by their higher complex shear modulus obtained in oscillatory tests and also higher damping ratio obtained from free vibration tests. However, the reduction in peak amplitude is lesser for sandwich beams with MRF having lower mass fractions of CIP as they possess lower damping ratio. MRF sandwich beam composed of commercial MR fluid, MRF 132DG (Lord Corporation) (MRB 132DG) produced highest amplitude reduction compared to all other beams due to their superior viscoelastic properties and damping ratio.
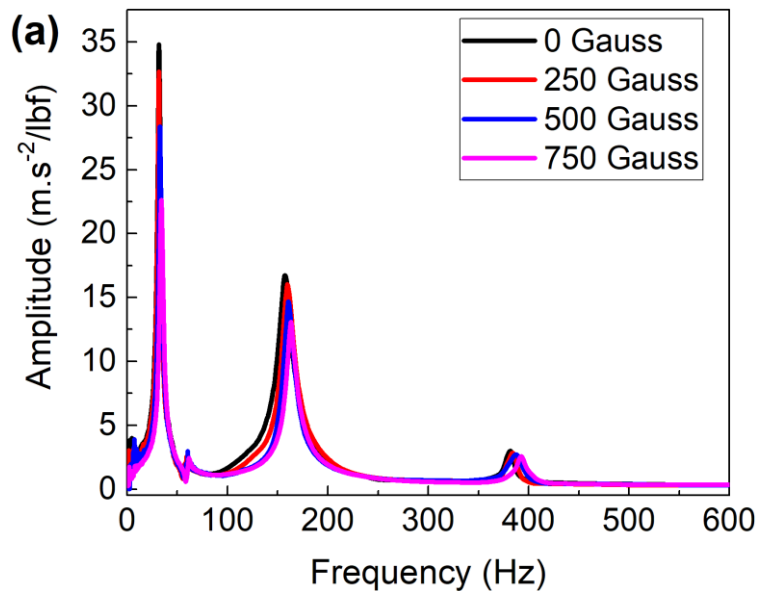
(a) FRF of MRB80S sandwich beams at different magnetic fields
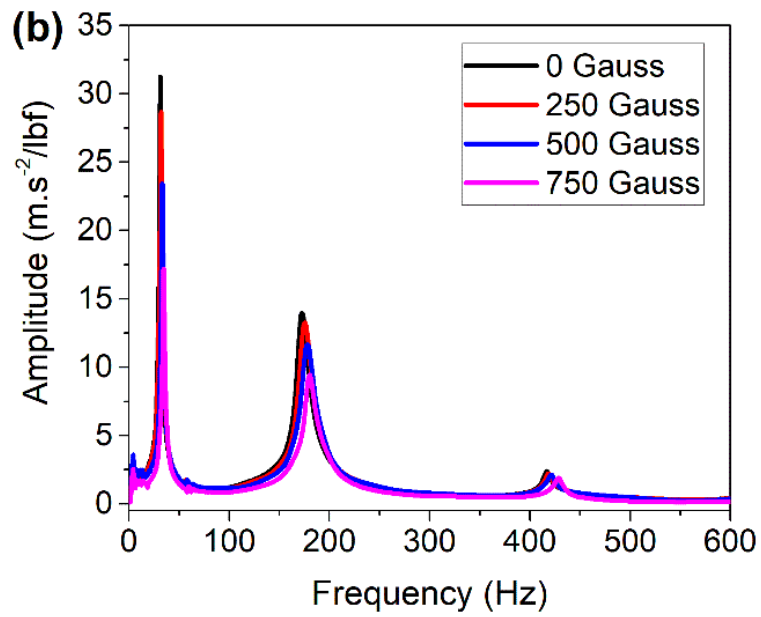
(a) FRF of MRB80L sandwich beams at different magnetic fields
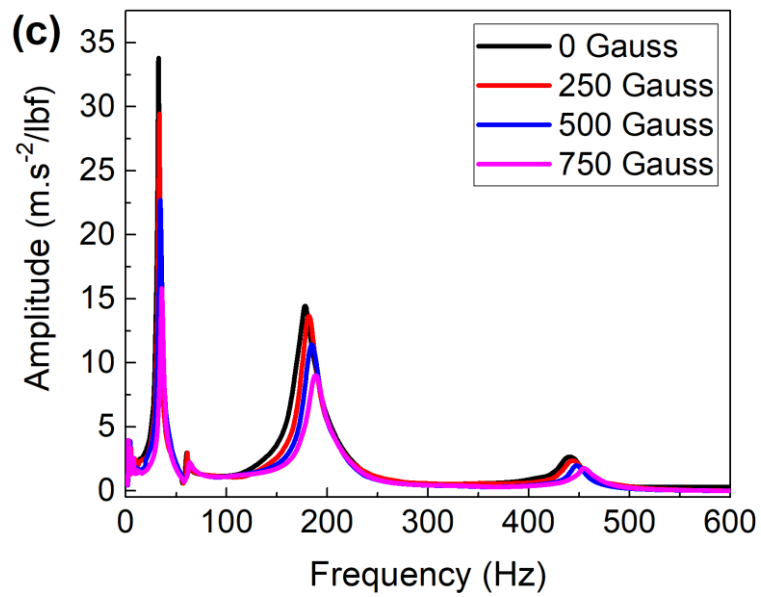
(a) FRF of MRB 132 DG sandwich beams at different magnetic fields

Figure 5.11 Frequency response functions (FRF) of MRF Sandwich beams at different magnetic fields

163

Figure 5.12 shows the percentage amplitude reduction at the first natural frequency for the sandwich beams containing prepared MRFs and commercial MR fluid, MRF 132DG (Lord Corporation) fluid as core at different magnetic fields. It can be observed that at 250 Gauss, 500 Gauss and 750 Gauss, the MRB80L sandwich beam yielded highest percentage peak amplitude reduction of 8.2%, 18.2% and 26.6% respectively compared to all fabricated beams. This is attributed to its superior viscoelastic properties and highest damping ratios among fabricated beams containing prepared MRFs. Further, the sandwich beam consisting of commercial MR fluid, MRF 132DG (Lord Corporation) has highest vibration suppression of 12.9%, 22.8 % and 30.3% at 250 Gauss, 500 Gauss and 750 Gauss respectively. Hence, the forced vibration analyses reveals the vibration control capability of sandwich beams with MRF core by application of appropriate magnetic field. In this study, permanent magnets were used to apply magnetic field. In real time application, electromagnets must be used and using suitable control strategy, the current supplied to the electromagnet should be varied to produce desired magnetic field on the beam. This in turn would alter the dynamic behaviour of beam when it is subjected to excitation.
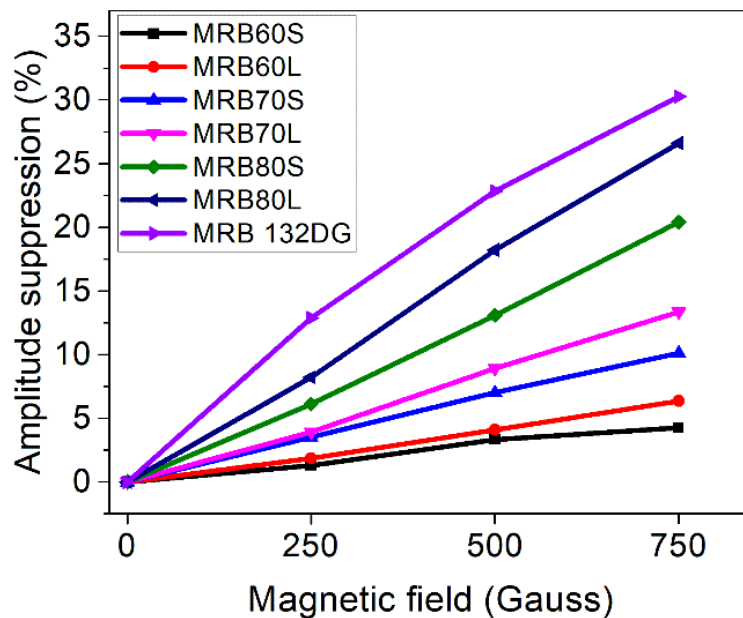
Figure 5.12 Vibration amplitude reduction with applied magnetic fields at first natural frequency

5.8 DETERMINATION OF OPTIMAL PARTICLE SIZE AND MASS FRACTION OF CIP IN MRF

The damping ratio for a sandwich beam should be high in order to achieve higher vibration suppression. Damping ratio is higher for higher mass fraction of CIP in MRF and vice versa. However, higher mass fraction of CIP results in higher mass of MRF and that of the sandwich beam. This also reduces the natural frequency of the beam especially in the higher modes. This conflicting criteria was solved using MOGA optimization technique. Maximization of damping ratio and minimization of mass of the MRF in the sandwich beam were specified as objectives of optimization to determine optimum particle size and mass fraction. The orthogonal array L6 (2×3) was used for conducting the experiments to analyse the effects on damping force and off-state viscosity of MRF and to determine the optimal particle size and mass fraction of iron powder.

Table 5.2 Response factors of prepared MRFs

Sl. No.	MRF Sample	Damping ratio	Mass of MRF (grams)
1	MF60L	0.0588	26.46
2	MF60S	0.0501	27.78
3	MF70L	0.0756	29.36
4	MF70S	0.0660	30.90
5	MF80L	0.0878	32.26
6	MF80S	0.0815	34.02

Regression analysis were performed using MATLAB^{TM} software to determine the relation between independent and response factors. The results of the damping ratios determined in accordance with L6 (2×3) orthogonal array and the mass of different prepared MRFs are tabulated in table 5.2. Damping ratio (corresponding to 750 Gauss) and mass of MRF are considered as the response factors while particle size (S_p) and particle mass fraction (MF_p) are the independent parameters.

The regression model for damping ratio (ζ) is given by equation (5.2) and has R-square, adjusted R-square and root mean square error values of 0.9986, 0.993 and 0.001198 respectively.

$$\zeta = -0.1119 + 0.002446 \times S_p + 0.003382 \times MF_p - 1.763 \times e\text{-}5 \times S_p \times MF_p - 1.258e\text{-}5 \times MF_p \times MF_p \tag{5.2}$$

The regression model for mass of MRF (M) is given by equation (5.3) and has R-square, adjusted R-square and root mean square error values of 1, 1 and 2.487e-14 respectively.

$$M = 9.064 - 2.502 \times e\text{-}15 \times S_p + 0.3214 \times MF_p - 0.003245 \times S_p \times MF_p + 1.077 \times e\text{-}16 \times MF_p \times MF_p \tag{5.3}$$

Pareto front solutions obtained from MOGA optimization using MATLAB^{TM} software which satisfies the objectives of optimization is shown in figure 5.13. A set of solutions are obtained depending on more weightage given to each of the response factors. The selection of optimal result depends on higher weightage given to the magnitude of damping ratio. Also, the mass of MRF should be preferably lower. Pareto front solution with particle size of 9.65 microns and 74.92% particle mass fraction was selected as it yields damping ratio of 0.0817 and mass of MRF as 30.79 grams.
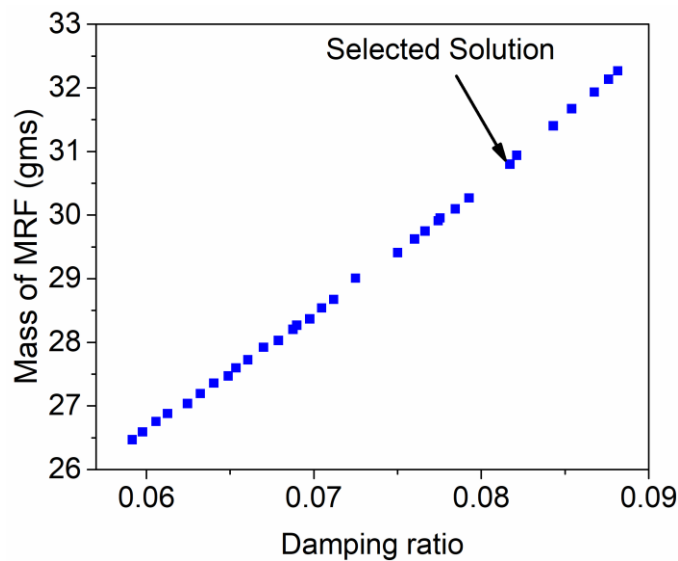
Figure 5.13 Optimal solutions from Pareto front

5.9 SUMMARY

Initially, combination of two iron particle sizes and three mass fractions of iron powder were used to prepare six MRFs. The viscoelastic properties of the prepared MRFs and commercial MR fluid, MRF 132DG (Lord Corporation) were determined using oscillatory tests performed by means of a Rheometer. Seven MRF sandwich beams were fabricated filled with six prepared MRFs and commercial MR fluid, MRF 132DG (Lord Corporation). Impact hammer tests of MRF sandwich beams were performed at different magnetic fields to evaluate the natural frequencies and damping ratio of the cantilever MRF sandwich beams. Further, response of the MRF sandwich beams under sinusoidal sweep excitations were also measured to investigate their vibration suppression capability. Following were the conclusions drawn from this study.

- The viscoelastic properties increase with increase in mass fraction of CIP in MRF, both in the presence and absence of magnetic field. Also, viscoelastic properties of MRFs having coarser sized CIP (9.68 microns) are higher compared to those containing smaller sized CIP (2.9 microns) due to the higher saturation magnetization of LCIP compared to SCIP.

- The shift in the natural frequency with applied magnetic field is insignificant at first natural frequency. However, at second and third modes, the shift in frequency with magnetic field is significant for MRF sandwich beams with higher mass fraction of CIP. The shift in natural frequency is due to increase in storage modulus of MRF with magnetic field.

- There is a significant increase in damping ratio with increase in mass fraction of CIP compared to particle size in MRF.

- The damping ratio of beams with LCIP are higher compared to those with SCIP at all magnetic fields due to higher loss modulus and complex shear modulus of LCIP which is evident from oscillatory rheology tests.

- There is a significant reduction in forced vibration amplitude of the beams at the natural frequencies with increase in magnetic fields due to increase in damping ratio. Beams with higher mass fractions resulted in higher reduction in peak amplitude due to higher damping ratio, loss modulus and complex shear modulus.

- Amongst the MRF sandwich beams composed of prepared MRF, beam with 80% mass fraction of LCIP in MRF yielded highest damping ratio and vibration suppression. At first natural frequency, for an applied magnetic field of 750 Gauss, the percentage reduction in the peak amplitude of 26.6% was observed.

- Sandwich beam with commercial MR fluid, MRF 132DG (Lord Corporation) core showed superior damping properties and vibration suppression capability compared to all fabricated MRF core sandwich beams. At first natural frequency for an applied magnetic field of 750 Gauss, it yielded highest percentage reduction in the peak amplitude of 30.3%.

- MOGA optimization was used to obtain optimal particle mass fraction and particle size in MRF which maximizes damping ratio and minimizes mass of MRF. MRF with particle size of 9.65 microns and 74.92% particle mass fraction was selected as it produced damping ratio of 0.0817 and MRF mass of 30.79 grams. This method would be predominantly useful for optimal selection of constituents of MRF for MRF sandwich beam considering different combinations of magnetic particles, carrier fluid, additives and their mass fractions.

- This controllability of stiffness and damping properties and hence the dynamic behaviour of sandwich beams has prospective vibration control applications in aircraft and automobile structures.

CHAPTER 6

SUMMARY & CONCLUSIONS

6.1 SUMMARY

6.1.1 Determination of Optimal Composition of Magnetorheological Fluid for MR Damper

A shear mode monotube MR damper was optimally designed for desired damping force and dynamic range. A damper was manufactured based on the optimal dimensions and was filled with commercial MR fluid, MRF 132DG (Lord Corporation) to determine its damping characteristics and validated with computational results. Further, MRFs were prepared composed of 60 %, 70 % and 80 % mass fractions of iron particles and particle sizes of 2.9 microns and 8.27 microns. The flow curves of the MR fluid were measured in the presence and absence of current. Further, In-house prepared MR fluid were filled in the MR damper and their damping characteristics were determined at sinusoidal excitation at different frequencies and DC current inputs. The area bounded by the force displacement graphs was used to calculate the energy dissipated which was then used to calculate damping coefficient. By means of MOGA optimization, based on maximization of on-state damping coefficient and minimization of off-state damping coefficient, the optimal mass fraction and particle size was determined.

6.1.2 Determination of Optimal Composition of Magnetorheological Fluid for MR Brake

Initially, optimum dimensions of MR brake were obtained using MOGA optimization. Experiments were performed on the designed MR brake utilizing commercial MR fluid, MRF 132DG (Lord Corporation) and validated with computational results. A DOE technique was employed to determine the optimal composition of MRF. Experiments were performed on the MR brake utilizing twelve synthesized MRFs composed of combinations of different particle mass fractions, base

oil viscosities and mean particle diameters. Torque characteristics and speed reduction performance of MR brake utilizing different MRFs were determined. Optimal MRF was selected by means of MOGA optimization. Finally, the sedimentation stability of SCIP and MRIP based MRFs were studied.

6.1.3 Determination of Optimal Composition of Magnetorheological Fluid for MRF Core Sandwich Beam

Combination of two iron particle sizes and three weight fractions of iron powder were used to prepare six MRFs. The viscoelastic properties of the prepared MRFs and commercial MR fluid, MRF 132DG (Lord Corporation) were determined using oscillatory tests performed by means of a Rheometer. Seven MRF sandwich beams were fabricated filled with six prepared MRFs and commercial MR fluid, MRF 132DG (Lord Corporation). Impact hammer tests of MRF sandwich beams were performed at different magnetic fields to evaluate the natural frequencies and damping ratio of the cantilever MRF sandwich beams. Further, response of the MRF sandwich beams under sinusoidal sweep excitations were also measured to investigate their vibration suppression capability.

6.2 CONCLUSIONS

Following were the conclusions drawn from the study on determination of optimal composition of MR fluid for MR damper, MR brake and MR fluid core sandwich beam.

- The optimally designed and fabricated MR damper filled with commercial MR fluid, MRF 132DG (Lord Corporation) produced maximum damping force of 709.5 N at 2A current and 4 Hz frequency of sinusoidal excitation. However, the designed damping force of 1,000 N was not achieved as required number of coils could not be wound on the piston core due to packing factor and subsequently the desired magnetic field strength was not generated in the MRF shear gap. The computationally determined damping force based on magnetostatic analyses and analytical equation is 751.7 N. Hence, a close agreement in the results between the two was observed.

170

- The damper force of MR damper filled with commercial MR fluid, MRF 132DG (Lord Corporation) was found to be lesser than those obtained for In-house prepared MRFs with 80 % weight fraction of iron powder. This could be attributed lesser concentration of magnetic field in the MR fluid gap while in case of In-house prepared fluid, the viscous damping force is having more contribution on the total damping force.

- MRFs with fine sized CIP produced higher shear stress with variation of shear rate due to higher saturation magnetization of fine sized CIP. MRFs composed of fine sized CIP (SCIP, 2.9 microns) have lower settling rate compared to those composed of coarse sized CIP (MCIP, 8.27 microns) and settles after longer duration of time indicating greater sedimentation stability of fine sized CIP based MRFs. Maximum stability of three days was observed for 80% mass fraction of SCIP based MRF.

- MRF composed of SCIP yielded higher damping force compared to those containing MCIP due to its higher saturation magnetization and shear stress. Higher mass fraction of CIP in the MRF resulted in higher damping force. Also, increasing current delivered to MR damper piston increased the damping force. Damping force also increases as frequency of excitation is increased. CIP mass fraction in MRF has significant effect on the equivalent damping coefficient when compared to particle size.

- MRFs composed of fine sized CIP yielded equivalent damping coefficient in comparison to those composed of coarse CIP due to its higher damping force. CIP mass fraction in MRF has significant effect on the equivalent damping coefficient when compared to particle size.

- MRF composed of 3.03 μm average particle size and particle weight fraction of 73.56 % was chosen which yields on-state damping coefficient of 780.5 Ns/m and off-state damping coefficient of 503.8 Ns/m.

- The design torque of 20 Nm was not attained as the MR brake design using magnetostatic analysis was carried out at current of 2.5 A while the maximum current supplied to coil was limited to 1 A due to coil resistance. Also, required number of coils could not be wound on bobbin due to packing factor. However, a close agreement was found between experimentally determined and

computationally determined values of braking torque for optimally designed MR brake utilizing commercial MR fluid, MRF 132DG (Lord Corporation).

- Sedimentation stability tests also confirmed the superiority of smaller sized iron particles based MRFs and that the optimal MRF would have sedimentation stability between three to four days. This would not be a problem as MR brakes are highly efficient mixing devices.

- Fine sized CIP (SCIP, 2.9 microns) based MRFs produced higher braking torque, speed reduction and torque ratio compared to medium (MRIP, 6.71 microns) and large sized CIP (LCIP, 9.68 microns) based MRFs. This is due to higher magnetic permeability of SCIP at lower magnetic field as could be observed from its magnetization curve which results in higher MR effect. This confirms that not only the size and magnetic saturation of iron particles, but the initial magnetic permeability also has major effect on the rheological properties and subsequent performance of the MR brake.

- Mass fraction of iron particles has the highest effect on the field induced and off-state braking torque followed by base oil viscosity and mean particle diameter which were evident from analysis of variance (ANOVA) study.

- MRFs composed of lower viscosity base oil (50 cSt) resulted in higher field induced torque compared to those containing higher viscosity base oil (100 cSt) for all mean particle diameters and particle mass fractions. However, 50 cSt oil based MRFs have lower off-state torques compared to those containing 100 cSt oil due to lower viscosity. This results in higher torque ratio when a low viscous base oil is utilized.

- The braking torque of MR brake filled with commercial MR fluid, MRF 132DG (Lord Corporation) was found to be lesser than those obtained for In-house prepared MR fluid composed of 85% weight fraction of iron powder, while it was higher than those with 75% weight fraction of iron powder. This is because the mass fraction of magnetic particles in Lord MRF 132DG fluid is 80.98%.

- Based on MOGA optimization, pareto front solution having mean particle diameter of 2.91 microns, particle mass fraction of 80.95 % and base oil viscosity of 50.03 cSt was recommended as optimal composition of MRF for designed MR brake

which yields a field induced torque of 18.35 Nm, off-state torque of 1.1 Nm and torque ratio of 16.68. The composition was chosen based on trade-off between response factors namely field induced torque and off-state torque which in turn is influenced by the mean particle diameter, particle mass fraction and base oil viscosity.

- The viscoelastic properties enhance with increase in mass fraction of CIP in MRF, both in the presence and absence of magnetic field. Also, viscoelastic properties of MRFs having LCIP (9.68 microns) are higher compared to those containing fine sized SCIP (2.9 microns) due to the higher saturation magnetization of LCIP compared to SCIP.

- The shift in the natural frequency with applied magnetic field is insignificant at first natural frequency. However, at second and third modes, the shift in frequency with magnetic field is significant for MRF sandwich beams with higher mass fraction of CIP. The shift in natural frequency is due to increase in storage modulus of MRF and stiffness of the beam with increase in magnetic field.

- There is a significant increase in damping ratio with increase in mass fraction of CIP compared to particle size in MRF. The damping ratio of beams with LCIP are higher compared to those with SCIP at all magnetic fields due to higher loss modulus and complex shear modulus of LCIP which is evident from oscillatory rheology tests.

- There is a significant reduction in forced vibration amplitude of the beams at the natural frequencies with increase in magnetic fields due to increase in damping ratio. Beams with higher CIP mass fractions resulted in higher reduction in peak amplitude due to higher damping ratio and complex shear modulus.

- Amongst the MRF sandwich beams composed of prepared MRF, beam with 80% mass fraction of LCIP in MRF yielded highest damping ratio and vibration suppression. At first natural frequency, for an applied magnetic field of 750 Gauss, the percentage reduction in the peak amplitude of 26.6% was observed.

- Sandwich beam with commercial MR fluid, MRF 132DG (Lord Corporation) core showed superior damping properties and vibration suppression capability compared to all fabricated MRF core sandwich beams. At first natural frequency for an applied

magnetic field of 750 Gauss, it yielded highest percentage reduction in the peak amplitude of 30.3%.

- MOGA optimization was used to obtain optimal particle mass fraction and particle size in MRF which maximizes damping ratio and minimizes mass of MRF. MRF with particle size of 9.65 microns and 74.92% particle weight fraction was selected as it produced damping ratio of 0.0817 and MRF weight of 30.79 grams. This method would be predominantly useful for optimal selection of constituents of MRF for MRF sandwich beam considering different combinations of magnetic particles, carrier fluid, additives and their mass fractions.

6.3 CONTRIBUTIONS

- The proposed methodology in this study can be used for optimal design of MR damper and MR brake considering different performance indices.
- The methodology can be followed for optimal determination of composition of MRF for MR damper, MR brake, MR beam or any other MR device considering several blends of dispersed iron particles, base oil, additives and their proportions.
- In case of MR damper, MRF composed of smaller sized iron particles (SCIP) yielded maximum damping force compared to that containing larger sized iron particles (MCIP). Hence, it can be concluded that damping force depends more on saturation magnetization than on particle size of iron powder.
- In case of MR brake, MRF composed of smaller sized iron particles (SCIP) yielded maximum braking torque compared to that containing medium (MRIP) and larger sized iron particles (LCIP). Though the saturation magnetization of LCIP is more than that of SCIP, SCIP has higher permeability at lower magnetic fields upto 5000 Gauss, lower coercivity and remnant magnetization. Hence, initial permeability is also a major factor affecting the performance of MR brake.
- In case of MRF sandwich beam, MRF composed of larger sized iron particles (LCIP) yielded maximum damping ratio and vibration suppression compared to that containing smaller sized iron particles (SCIP). The MR fluid operates in the pre-yield regime in case of MRF sandwich beams and also not subjected to thermal effects as in the case of MR brake.

174

6.4 SCOPE FOR FUTURE WORK

- MR damper was designed to achieve a target damping force and dynamic range using *fmincon* optimization. The design could be further improved by performing computational fluid dynamic and magnetostatic analyses of the MR damper and optimize the dimensions to reduce cost, increase dynamic range and damper force.

- For MR damper, the optimal mass fraction and particle size iron powder in MRF was obtained by means of MOGA optimization. Three mass fractions of iron powder and two average particle sizes were considered. This could be further extended by considering different base oil and their viscosities and additives of different types and mass fractions.

- The optimal dimensions of MR brake was determined based on MOGA optimization combined with magnetostatic analysis with the maximization of on-state torque and minimization of off-state torque. The design can be incorporated with provision for cooling of brake as temperature rise is significant and has detrimental effect on the braking torque of MR brake. Also, multi disk MR brake can be designed and its performance can be investigated.

- In case of MR brake, the optimal mass fraction and particle size iron powder and base oil viscosity in MRF was obtained by means of MOGA optimization. Three mass fractions of iron powder, three average iron particle sizes and two base oil viscosities were considered. This could be further extended by considering different base oils and additives of different types and mass fractions.

- In case of MRF core sandwich beam, two iron particle sizes and three mass fractions of iron powder were considered for determination of optimal mass fraction and particle size iron powder in MRF was obtained by means of MOGA optimization. This could be further extended by considering different base oils and their viscosities and additives of different types and mass fractions.

- Design of controller for MR damper, MR brake and MR beam in place of manually supplying the current to the coil.

175

REFERENCES

Acharya, S., and Kumar, H. (2019). "Investigation of magnetorheological brake with rotor of combined magnetic and non-magnetic materials." *SN Appl. Sci.*, 1(9), 997.

Acharya, S., Saini, T. R. S., and Kumar, H. (2019a). "Optimal design and analyses of T-shaped rotor magnetorheological brake." *IOP Conf. Ser. Mater. Sci. Eng.*, IOP Publishing, 12024.

Acharya, S., Saini, T. R. S., and Kumar, H. (2019b). "Determination of optimal magnetorheological fluid particle loading and size for shear mode monotube damper." *J. Brazilian Soc. Mech. Sci. Eng.*, 41(10), 392.

Ahamed, R., Choi, S. B., and Ferdaus, M. M. (2018). "A state of art on magneto-rheological materials and their potential applications." *J. Intell. Mater. Syst. Struct.*, 29(10), 2051–2095.

Ahmadian, M. (2017). "Magneto-rheological suspensions for improving ground vehicle's ride comfort, stability, and handling." *Veh. Syst. Dyn.*, 55(10), 1618–1642.

Ahmadian, M., and Poynor, J. C. (2001). "An evaluation of magneto rheological dampers for controlling gun recoil dynamics." *Shock Vib.*, 8(3–4), 147–155.

Allien, J. V., Kumar, H., and Desai, V. (2019a). "Semi-active vibration control of SiC-reinforced Al6082 metal matrix composite sandwich beam with magnetorheological fluid core." *Proc IMechE Part L J Mater. Des. Appl.*, 243(3), 408–424.

Allien, J. V., Kumar, H., and Desai, V. (2020). "Semi-active vibration control of MRF core PMC cantilever sandwich beams : Experimental study." *Proc. Inst. Mech. Eng. Part L J. Mater. Des. Appl.*, 234(4), 574–585.

Allien, V. J., Kumar, H., and Desai, V. (2019b). "Dynamic analysis and optimization of SiC reinforced Al6082 and Al7075 MMCs Dynamic analysis and optimization of SiC reinforced Al6082 and Al7075 MMCs." *Mater. Res. Express*, 6(5), 056528.

Allien, V., Kumar, H., and Desai, V. (2016). "An Investigation on Characteristics and Free Vibration Analysis of Laminated Chopped Glass Fiber Reinforced Polyester Resin

Composite." *An Investig. Charact. Free Vib. Anal. laminated chopped Glas. fiber Reinf. Polyest. resin Compos.*, 11(18), 11016–11022.

Arvin, H., Sadighi, M., and Ohadi, A. R. (2010). "A numerical study of free and forced vibration of composite sandwich beam with viscoelastic core." *Compos. Struct.*, 92(4), 996–1008.

Ashtiani, M., and Hashemabadi, S. H. (2015a). "The effect of nano-silica and nano-magnetite on the magnetorheological fluid stabilization and magnetorheological effect." *J. Intell. Mater. Syst. Struct.*, 26(14), 1887–1892.

Ashtiani, M., and Hashemabadi, S. H. (2015b). "The effect of nano-silica and nano-magnetite on the magnetorheological fluid stabilization and magnetorheological effect." *J. Intell. Mater. Syst. Struct.*, 26(14), 1887–1892.

Ashtiani, M., Hashemabadi, S. H., and Ghaffari, A. (2015). "A review on the magnetorheological fluid preparation and stabilization." *J. Magn. Magn. Mater.*, 374, 716–730.

Assadsangabi, B., Daneshmand, F., Vahdati, N., Eghtesad, M., and Bazargan-Lari, Y. (2011). "Optimization and design of disk-type MR brakes." *Int. J. Automot. Technol.*, 12(6), 921–932.

Attia, E. M., Elsodany, N. M., and Elgohary, M. A. (2017). "Theoretical and experimental study of magneto-rheological fluid disc brake." *Alexandria Eng. J.*, 56(2), 189–200.

Avraam, M., Horodinca, M., Romanescu, I., and Preumont, A. (2010). "Computer controlled rotational MR-brake for wrist rehabilitation device." *J. Intell. Mater. Syst. Struct.*, 21(15), 1543–1557.

B Swaminathan, and Raj, M Srinu, A. (2016). "A Study And characterization Of magnet or heological Fluid For Damper In Automobile Suspension." *Int. J. Eng. Invent.*, 5(5), 74–81.

Batterbee, D. C., Sims, N. D., Stanway, R., and Rennison, M. (2007a). "Magnetorheological landing gear: 2. Validation using experimental data." *Smart Mater. Struct.*, 16(6), 2441–2452.

Batterbee, D. C., Sims, N. D., Stanway, R., and Wolejsza, Z. (2007b). "Magnetorheological landing gear: 1. A design methodology." *Smart Mater. Struct.*, 16(6), 2429–2440.

Bellmann, M., Köhler, T. M., and Schmalz, T. (2019). "Comparative biomechanical evaluation of two technologically different microprocessor-controlled prosthetic knee joints in safety-relevant daily-life situations." *Biomed. Tech.*, 64(4), 407–420.

Bicchi, A., Raugi, M., Rizzo, R., and Sgambelluri, N. (2005). "Analysis and design of an electromagnetic system for the characterization of magneto-rheological fluids for haptic interfaces." *IEEE Trans. Magn.*, 41(5), 1876–1879.

Bombard, A. J. F., Antunes, L. S., Balestrassi, P. P., and Paiva, A. P. (2009). "Magneto-rheological fluids redispersibility – a factorial design study of phosphate shell on carbonyl iron powder with dispersing additives." *J. Phys. Conf. Ser.*, 149, 012036.

Bombard, A. J. F., and Teodoro, J. V. R. (2011). "Magnetorheological Fluids With Carbonyl and Water Atomized Iron Powders." *Int. J. Mod. Phys. B*, 25(07), 943–946.

Bompos, Dimitrios A, Nikolakopoulos, P, G. (2014). "Experimental and Analytical Investigations of Dynamic Characteristics of Magnetorheological and Nano Magnetorheological Fluid Film Journal Bearing." *Proc. ASME Turbo Expo 2014 Turbine Tech. Conf. Expo. , Ger.*, 1–8.

Bompos, D. A., and Nikolakopoulos, P. G. (2016). "Rotordynamic Analysis of a Shaft Using Magnetorheological and Nanomagnetorheological Fluid Journal Bearings." *Tribol. Trans.*, 59(1), 108–118.

Bucchi, F., Forte, P., and Frendo, F. (2015). "Temperature effect on the torque characteristic of a magnetorheological clutch." *Mech. Adv. Mater. Struct.*, 22(1–2), 150–158.

Bucchi, F., Forte, P., and Frendo, F. (2017). "Geometry optimization of a magnetorheological clutch operated by coils." *Proc. Inst. Mech. Eng. Part L J. Mater. Des. Appl.*, 231(1–2), 100–112.

Bucchi, F., Forte, P., Frendo, F., Musolino, A., and Rizzo, R. (2014). "A fail-safe magnetorheological clutch excited by permanent magnets for the disengagement of automotive auxiliaries." *J. Intell. Mater. Syst. Struct.*, 25(16), 2102–2114.

Carlson, J. D. (2001). "Magnetorheological brake with integrated flywheel." U.S. Patent 6,186,290.

Carlson, J. D. (2002). "What makes a good MR fluid?" *J. Intell. Mater. Syst. Struct.*, 431–435.

Carlson, J. D., and Catanzarite, D. M. (1998). "Magnetorheological fluid devices and process of controlling force in exercise equipment utilizing same." U.S. Patent No. 5,816,372.

Chand, M., Shankar, A., Noorjahan, Jain, K., and Pant, R. P. (2014). "Improved properties of bidispersed magnetorheological fluids." *RSC Adv.*, 4(96), 53960–53966.

Cheng, H., Zhang, X., Liu, G., Ma, W. and Wereley, N.M. (2016). "Measuring the sedimentation rate in a magnetorheological fluid column via thermal conductivity monitoring." *Smart mat. Struct.*, 25(5), 055007.

Chiriac, H., and Stoian, G. (2009). "Influence of the particles size and size distribution on the magnetorheological fluids properties." *IEEE Trans. Magn.*, 45(10), 4049–4051.

Choi, S. B., and Han, Y. M. (2012). *Magnetorheological fluid technology: Applications in vehicle systems. Magnetorheol. Fluid Technol. Appl. Veh. Syst.*, CRC press.

Choi, S. B., Lee, H. S., Hong, and Cheong. (2000). "Control and response characteristics of a magneto-rheological fluid damper for passenger vehicles." *J. Intell. Mater. Syst. Struct.*, 11(1), 80–87.

Choi, S. B., Nam, M. H., and Lee, B. K. (2001). "Vibration control of a MR seat damper for commercial vehicles." *J. Intell. Mater. Syst. Struct.*, 11(12), 936–944.

Choi, Y. T., and Wereley, N. M. (2005). "Mitigation of biodynamic response to vibratory and blast-induced shock loads using magnetorheological seat suspensions." *Proc. Inst. Mech. Eng. Part D J. Automob. Eng.*, 219(6), 741–753.

Chooi, W. W., and Oyadiji, S. O. (2005). "Characterizing the effect of temperature and magnetic field strengths on the complex shear modulus properties of magnetorheological (MR) fluids." *Int. J. Mod. Phys. B*, 19(7–9), 1318–1324.

Dai, S., Du, C., and Yu, G. (2013). "Design, testing and analysis of a novel composite magnetorheological fluid clutch." *J. Intell. Mater. Syst. Struct.*, 24(14), 1675–1682.

Daniel, I. M., and Abot, J. L. (2000). "Fabrication, testing and analysis of composite sandwich beams." *Compos. Sci. Technol.*, 60(12–13), 2455–2463.

De Vicente, J., Klingenberg, D. J., and Hidalgo-Alvarez, R. (2011). "Magnetorheological fluids: a review". *Soft matter*, 7(8), 3701-3710.

Djavareshkian, M. H., Esmaeili, A., and Safarzadeh, H. (2015). "Optimal Design of Magnetorheological Fluid Damper Based on Response Surface Method." *Int. J. Eng.*, 28(9 (C)), 1359–1367.

Do, X. P., and Choi, S. B. (2015). "High Loaded Mounts for Vibration Control Using Magnetorheological Fluids: Review of Design Configuration." *Shock Vib.*, 2015(2).

Dodbiba, G., Park, H. S., Okaya, K., and Fujita, T. (2008). "Investigating magnetorheological properties of a mixture of two types of carbonyl iron powders suspended in an ionic liquid." *J. Magn. Magn. Mater.*, 320(7), 1322–1327.

Dyke, S. J., Spencer, B. F., Sain, M. K., and Carlson, J. D. (1998). "An experimental study of MR dampers for seismic protection." *Smart Mater. Struct.*, 7(5), 693–703.

Eshaghi, M., Rakheja, S., and Sedaghati, R. (2015). "An accurate technique for pre-yield characterization of MR fluids." *Smart Mater. Struct.*, 24(6), 1–13.

Facey, W. B., Rosenfeld, N. C., Choi, Y.-T., Wereley, N. M., Choi, S. B., and Chen, P. (2005). "Design and Testing of a Compact Magnetorheological Damper for High Impulsive Loads." *Int. J. Mod. Phys. B*, 19(7–9), 638–644.

Fadaee, M. (2019). "A new reformulation of vibration suppression equations of functionally graded magnetorheological fluid sandwich beam." *Appl. Math. Model.*, 74, 469–482.

Fang, C., Zhao, B. Y., Chen, L. S., Wu, Q., Liu, N., and Hu, K. A. (2005). "The effect of the green additive guar gum on the properties of magnetorheological fluid." *Smart Mater. Struct.*, 14(1).

Fei, C., Zuzhi, T., and Xiangfan, W. (2015). "Novel process to prepare high-performance magnetorheological fluid based on surfactants compounding." *Mater. Manuf. Process.*, 30(2), 210–215.

Ferdaus, M. M., Rashid, M. M., Hasan, M. H., and Rahman, M. A. (2014). "Optimal design of Magneto-Rheological damper comparing different configurations by finite element analysis." *J. Mech. Sci. Technol.*, 28(9), 3667–3677.

Forte, P., Paternò, M., and Rustighi, E. (2004). "A magnetorheological fluid damper for rotor applications." *Int. J. Rotating Mach.*, 10(3), 175–182.

Gao, F., Liu, Y. N., and Liao, W. H. (2017). "Optimal design of a magnetorheological damper used in smart prosthetic knees." *Smart Mater. Struct.*, 26(3), 35034.

Genc, S., and Phule, P. P. (2002). "Rheological properties of magnetorheological fluids." *Smart Mater. Struct.*, 11(1), 140–146.

Genç, S., and Phulé, P. P. (2002). "Rheological properties of magnetorheological fluids." *Smart Mater. Struct.*, 11(1), 140–146.

Gertzos, K. P., Nikolakopoulos, P. G., and Papadopoulos, C. A. (2008). "CFD analysis of journal bearing hydrodynamic lubrication by Bingham lubricant." *Tribol. Int.*, 41(12), 1190–1204.

Gilbert, R., and Jackson, M. (2005). "Magnetic Ride Control." *GM Tech Link*, 4(1), 1–2.

Ginder, J. M., Davis, L. C. , Elie, L. D. (1996). "Rheology of magnetorheological fluids: models and measurements." *Int. J. Mod. Phys. B*, 10(23), 32.

Ginder, J. M., and Davis, L. C. (1994). "Shear stresses in magnetorheological fluids: Role of magnetic saturation." *Appl. Phys. Lett.*, 65(26), 3410–3412.

Gołdasz, J., and Bogdan, S. (2014). *Insight into Magnetorheological Shock Absorbers*. Switzerland: Springer International Publishing.

Goncalves, F. D. (2005). *Characterizing the Behavior of Magnetorheological Fluids at High Velocities and High Shear Rates*. Blacksburg, Virginia.

Goncalves, F. D., and Carlson, J. D. (2009). "An alternate operation mode for MR fluids—magnetic gradient pinch." *J. Phys. Conf. Ser.*, 149, 012050.

Gudmundsson, K. H., Jonsdottir, F., and Thorsteinsson, F. (2010). "A geometrical optimization of a magneto-rheological rotary brake in a prosthetic knee." *Smart Mater. Struct.*, 19(3), 035023.

Gudmundsson, K. H., Jonsdottir, F., and Thorsteinsson, F. (2011a). "Field-on versus field-off characteristics of magnetorheological fluids with an application in prosthetic devices." *ASME 2011 Conf. Smart Mater. Adapt. Struct. Intell. Syst. SMASIS 2011*, 1(6), 275–280.

Gudmundsson, K. H., Jonsdottir, F., Thorsteinsson, F., and Gutfleisch, O. (2011b). "An experimental investigation of unimodal and bimodal magnetorheological fluids with an application in prosthetic devices." *J. Intell. Mater. Syst. Struct.*, 22(6), 539–549.

Gurubasavaraju, T. M., Kumar, H., and Arun, M. (2017a). "Evaluation of optimal parameters of MR fluids for damper application using particle swarm and response surface optimisation." *J. Brazilian Soc. Mech. Sci. Eng.*, 39(9), 3683–3694.

Gurubasavaraju, T. M., Kumar, H., and Arun, M. (2017b). "Evaluation of optimal parameters of MR fluids for damper application using particle swarm and response surface optimisation." *J. Brazilian Soc. Mech. Sci. Eng.*, 39(9), 3683–3694.

Hartman, N., and Rimmer, R. A. (2001). "Electromagnetic, thermal, and structural analysis of RF cavities using ANSYS." *PACS2001. Proc. 2001 Part. Accel. Conf. (Cat. No. 01CH37268)*, IEEE, 912–914.

Hemmatian, M., Sedaghati, R., and Rakheja, S. (2018). "Linear and nonlinear viscoelastic behavior of MR fluids: Effect of temperature." *ASME 2018 Conf. Smart Mater. Adapt. Struct. Intell. Syst. SMASIS 2018*, 1, 6–10.

Herold, Z., Libl, D., and Deur, J. (2010). "Design and testing of an experimental magnetorheological fluid clutch." *Strojarstvo*, 52(6), 601–614.

Hesselbach, J., and Abel-Keilhack, C. (2003). "Active hydrostatic bearing with magnetorheological fluid." *J. Appl. Phys.*, 93(10 3), 8441–8443.

Hirunyapruk, C., Brennan, M. J., MacE, B. R., and Li, W. H. (2010). "A tunable magneto-rheological fluid-filled beam-like vibration absorber." *Smart Mater. Struct.*, 19(5), 055020.

Hong, S. R., and Choi, S. B. (2005). "Vibration control of a structural system using magneto-rheological fluid mount." *J. Intell. Mater. Syst. Struct.*, 16(11–12), 931–936.

Hu, B., Wang, D., Xia, P., and Shi, Q. (2006). "Investigation on the vibration characteristics of a sandwich beam with smart composites — MRF." *World J. Model. Simul.*, 2(3), 201–206.

Hu, G., Xie, Z., and Li, W. (2015). "Optimal design of a double coil magnetorheological fluid damper with various piston profiles." *11th World Congr. Struct. Multidiscip. Optim. Sydney*, 2–7.

Iglesias, G. R., López-López, M. T., Durán, J. D. G., González-Caballero, F., and Delgado, A. V. (2012). "Dynamic characterization of extremely bidisperse magnetorheological fluids." *J. Colloid Interface Sci.*, 377(1), 153–159.

J. David Carlson. (1998). "Portable Controllable Fluid Rehabilitation Devices." *United States Patents 5,711,746*.

Jacob, R., and Rabinow, J. (1951). "Magnetic fluid torque and force transmitting device." *United States Patents 2,575,360*.

Jang, I. B., Kim, H. B., Lee, J. Y., You, J. L., Choi, H. J., and Jhon, M. S. (2005). "Role of organic coating on carbonyl iron suspended particles in magnetorheological fluids."

J. Appl. Phys., 97(10), 8–11.

Jiang, W., Zhang, Y., Xuan, S., Guo, C., and Gong, X. (2011). "Dimorphic magnetorheological fluid with improved rheological properties." *J. Magn. Magn. Mater.*, 323(24), 3246–3250.

Jolly, M. R., Bender, J. W., and Carlson, J. D. (1999). "Properties and Applications of Commercial Magnetorheological Fluids." *J. Intell. Mater. Syst. Struct.*, 10(1), 5–13.

Jonsdottir, F., Thorarinsson, E. T., Palsson, H., and Gudmundsson, K. H. (2009a). "Influence of parameter variations on the braking torque of a magnetorheological prosthetic knee." *J. Intell. Mater. Syst. Struct.*, 20(6), 659–667.

Jonsdottir, F., Thorarinsson, E. T., Palsson, H., and Gudmundsson, K. H. (2009b). "Influence of parameter variations on the braking torque of a magnetorheological prosthetic knee." *J. Intell. Mater. Syst. Struct.*, 20(6), 659–667.

Kamble, V. G., Kolekar, S., and Madivalar, C. (2015). "Preparation of Magnetorheological Fluids Using Different Carriers and Detailed Study on Their Properties." *Am. J. Nanotechnol.*, 6(1), 7–15.

Karakoc, K., Park, E. J., and Suleman, A. (2008). "Design considerations for an automotive magnetorheological brake." *Mechatronics*, 18(8), 434–447.

Kim, J., Ko, J., Liu, Y., Kim, I., and Choi, H. (2012). "CV-03 Effect of medium oil on magnetorheology of soft magnetic carbonyl iron particles." *IEEE Trans. Magn.*, 48(11), 3442–3445.

Klingenberg, D. J. (2001). "Magnetorheology: Applications and challenges." *AIChE J.*, 47(2), 246–249.

Kolekar, S., Kurahatti, R. V, K, P. P., Kamble, V., and Reddy, N. (2014). "Preparation of a Silicon oil based Magneto Rheological Fluid and an Experimental Study of its Rheological Properties using a Plate and Cone Type Rheometer." *Inst. Smart Struct. Syst.*, 3(2), 23–26.

Kolekar, S., and Venkatesh, K. (2019). "Experimental Investigation of Damping Effect

in Semi - active Magnetorheological Fluid Sandwich Beam Under Non - Homogeneous Magnetic Field." *J. Vib. Eng. Technol.*, 7(2), 107–116.

Kolekar, S., Venkatesh, K., Oh, J., and Choi, S. (2019). "Vibration Controllability of Sandwich Structures with Smart Materials of Electrorheological Fluids and Magnetorheological Materials : A Review." *J. Vib. Eng. Technol.*, 7(4), 359–377.

Kovac, E. J., Anderson, W. J., and Scott, R. A. (1971). "Forced non-linear vibrations of a damped sandwich beam." *J. Sound Vib.*, 17(1), 25–39.

Krishna, H., Kumar, H., and Gangadharan, K. (2016). "Optimization of Magneto-Rheological Damper for Maximizing Magnetic Flux Density in the Fluid Flow Gap Through FEA and GA Approaches." *J. Inst. Eng. Ser. C*, 98(4), 533–539.

Kumar, J. S., Paul, P. S., Raghunathan, G., and Alex, D.G. (2019). "A review of challenges and solutions in the preparation and use of magnetorheological fluids." *Int. J. Mech. Mater. Eng.,* 14(1), 1-18.

Lara-prieto, V., Parkin, R., and Jackson, M. (2009). "Vibration characteristics of MR cantilever sandwich beams : experimental study." *Smart Mater. Struct.*, 19(1), 015005.

Lee, D. Y., Nam, Y. J., Yamane, R., and Park, M. K. (2009). "Performance evaluation on vibration control of MR landing gear." *J. Phys. Conf. Ser.*, 149, 012068.

Lee, J. H., and Choi, H. J. (2018). "Synthesis of core-shell formed carbonyl iron/polydiphenylamine particles and their rheological response under applied magnetic fields." *Colloid Polym. Sci.*, 296(11), 1857-1865.

Leong, S. A. N., Mazlan, S. A., Mohamad, N., Aziz, S. A. A., and Ubaidillah. (2016). "An overview of nanoparticles utilization in magnetorheological materials." *AIP Conf. Proc.*, 1710.

Li, H., Ph, D., Liu, M., Li, J., Guan, X., Ph, D., Ou, J., and Ph, D. (2007). "Vibration Control of Stay Cables of the Shandong Binzhou Yellow River Highway Bridge Using Magnetorheological Fluid Dampers." *J. Bridg. Eng.*, 12(4), 401–409.

Li, W. H., Chen, G., and Yeo, S. H. (1999). "Viscoelastic properties of MR fluid."

Smart Mater. Struct., 8, 460–468.

Li, W. H., and Du, H. (2003). "Design and experimental evaluation of a magnetorheological brake." *Int. J. Adv. Manuf. Technol.*, 21(7), 508–515.

Li, Z. C., and Wang, J. (2012). "A gun recoil system employing a magnetorheological fluid damper." *Smart Mater. Struct.*, 21(10).

Lijesh, K. P., Kumar, D., and Gangadharan, K. V. (2018). "Design of magneto-rheological brake for optimum dimension." *J. Brazilian Soc. Mech. Sci. Eng.*, 40(3), 161.

Lim, S. T., Cho, M. S., Choi, H. J., and Jhon, M. S. (2005). "Magnetorheological characterization of organoclay added carbonyl-iron suspensions." *Int. J. Mod. Phys. B*, 19(10), 1142–1148.

Lim, S. T., Cho, M. S., Jang, I. B., and Choi, H. J. (2004). "Magnetorheological characterization of carbonyl iron based suspension stabilized by fumed silica." *J. Magn. Magn. Mater.*, 282, 170–173.

Liu, X., Lu, H., Chen, Q., Wang, D., and Zhen, X. (2013a). "Study on the preparation and properties of silicone oil-based magnetorheological fluids." *Mater. Manuf. Process.*, 28(6), 631–636.

Liu, X., Lu, H., Chen, Q., Wang, D., Zhen, X., Liu, X., Lu, H., Chen, Q., Wang, D., and Zhen, X. (2013b). "Study on the Preparation and Properties of Silicone Oil-Based Magnetorheological Fluids Study on the Preparation and Properties of Silicone Oil-Based Magnetorheological Fluids." *Mater. Manuf. Process.*, 28(6), 631–636.

López-López, M. T., Durán, J. D. G., Delgado, A. V., and González-Caballero, F. (2005). "Stability and magnetic characterization of oleate-covered magnetite ferrofluids in different nonpolar carriers." *J. Colloid Interface Sci.*, 291(1), 144–151.

López-López, M. T., Kuzhir, P., Bossis, G., and Mingalyov, P. (2008a). "Preparation of well-dispersed magnetorheological fluids and effect of dispersion on their magnetorheological properties." *Rheol. Acta*, 47(7), 787–796.

López-López, M. T., Zugaldia, A., Gómez-Ramirez, A., González-Caballero, F., and Durán, J. D. G. (2008b). "Effect of particle aggregation on the magnetic and magnetorheological properties of magnetic suspensions." *J. Rheol.*, 52(4), 901–912.

López-López, M. T., Zugaldía, A., González-Caballero, F., and Durán, J. D. G. (2006). "Sedimentation and redispersion phenomena in iron-based magnetorheological fluids." *J. Rheol.*, 50(4), 543–560.

Lund, M. W. (2016). "Wire Gauge and Current Limits Including Skin Depth Strength." *PowerStream Technol. USA*, https://www.powerstream.com/Wire_Size.html (May 30, 2019).

Ma, X. Q., Wang, E. R., Rakheja, S., and Su, C. Y. (2002). "Modeling hysteretic characteristics of MR-fluid damper and model validation." *Proc. IEEE Conf. Decis. Control*, 1675–1680.

Madhavrao Desai, R., Acharya, S., Jamadar, M. E. H., Kumar, H., Joladarashi, S., and Sekaran, S. R. (2020). "Synthesis of magnetorheological fluid and its application in a twin-tube valve mode automotive damper." *Proc. Inst. Mech. Eng. Part L J. Mater. Des. Appl.*, 234(7), 1001–1016.

Madhavrao, R., Mohibb, D., Jamadar, E. H., Kumar, H., and Joladarashi, S. (2019). "Design and experimental characterization of a twin - tube MR damper for a passenger van." *J. Brazilian Soc. Mech. Sci. Eng.*, 41(8), 1–21.

Mangal, S. K., and Kumar, A. (2014). "Experimental and Numerical Studies of Magnetorheological (MR) Damper." *Chinese J. Eng.*, 2014, 1–7.

Mangal, S. K., and Sharma, V. (2017). "Multi-parameter optimization of magnetorheological fluid with high on-state yield stress and viscosity." *J. Brazilian Soc. Mech. Sci. Eng.*, 39(10), 4191–4206.

Moghadam, M. G. E., Shahmardan, M. M., and Norouzi, M. (2020). "Magneto-rheological damper modeling by using dissipative particle dynamics method." Comput. Part. Mech., 7(3), 567-592.

Mohan, A., and Ahmadian, M. (2006). "Nonlinear Investigation of the Effect of Suspension Parameters." *Proc. 2006 IEEE/ASME Jt. Rail Conf.*, 327–336.

Morillas, J. R., and de Vicente, J. (2020). "Magnetorheology: a review." *Soft Matter*, 16(42), 9614-9642.

Muhammad, A., Yao, X., and Deng, Z. (2006). "Review of magnetorheological (MR) fluids and its applications in vibration control." *J. Mar. Sci. Appl.*, 5(3), 17–29.

Munoz, B. C., Adams, G. W., and Kitchin, J. R. (2001). "Stable magnetorheological fluids." US Patents 6203717B1.

Naserimojarad, M. M., Moallem, M., and Arzanpour, S. (2018). "A comprehensive approach for optimal design of magnetorheological dampers." *J. Intell. Mater. Syst. Struct.*, 29(18), 3648–3655.

Ngatu, G. T., and Wereley, N. M. (2007a). "Viscometric and sedimentation characterization of bidisperse magnetorheological fluids." *IEEE Trans. Magn.*, 43(6), 2474–2476.

Ngatu, G. T., and Wereley, N. M. (2007b). "Viscometric and Sedimentation Characterization of Bidisperse Magnetorheological Fluids." 43(6), 2474–2476.

Nguyen, P.-B. B., Do, X.-P. P., Jeon, J., Choi, S.-B. B., Liu, Y. D., and Choi, H. J. (2014a). "Brake performance of core–shell structured carbonyl iron/silica based magnetorheological suspension." *J. Magn. Magn. Mater.*, 367, 69–74.

Nguyen, Q., and Choi, S. (2009). "Optimal design of a vehicle magnetorheological damper considering the damping force and dynamic range." *Smart Mater. Struct.*, 18(1), 015013.

Nguyen, Q. H., and Choi, S. B. (2010). "Optimal design of an automotive magnetorheological brake considering geometric dimensions and zero-field friction heat." *Smart Mater. Struct.*, 19(11), 115024.

Nguyen, Q. H., and Choi, S. B. (2012a). "Selection of magnetorheological brake types via optimal design considering maximum torque and constrained volume." *Smart

Mater. Struct., 21(1), 15012.

Nguyen, Q. H., and Choi, S. B. (2012b). "Optimal design of a novel hybrid MR brake for motorcycles considering axial and radial magnetic flux." *Smart Mater. Struct.*, 21(5), 055003.

Nguyen, Q. H., Choi, S. B., Lee, Y. S., and Han, M. S. (2009a). "An analytical method for optimal design of MR valve structures." *Smart Mater. Struct.*, 18(9), 095032.

Nguyen, Q. H., Choi, S. B., and Wereley, N. M. (2008). "Optimal design of magnetorheological valves via a finite element method considering control energy and a time constant." *Smart Mater. Struct.*, 17(2), 025024.

Nguyen, Q. H., Choi, S. B., and Woo, J. K. (2014b). "Optimal design of magnetorheological fluid-based dampers for front-loaded washing machines." *Proc. Inst. Mech. Eng. Part C J. Mech. Eng. Sci.*, 228(2), 294–306.

Nguyen, T., Ciocanel, C., and Elahinia, M. (2009b). "Analytical modeling and experimental validation of a magnetorheological mount." *Proc. SPIE Act. Passiv. Smart Struct. Integr. Syst. 2009*, 72881D.

Nguyen, V. Q., Tuan, L. D., Hiep, L. D., Quoc, H. N., and Choi, S. B. (2019). "Material characterization of MR fluid on performance of MRF based brake." *Front. Mater.*, 6, 125.

Oh, J. S., Shin, Y. J., Koo, H. W., Kim, H. C., Park, J., and Choi, S. B. (2016). "Vibration control of a semi-active railway vehicle suspension with magneto-rheological dampers." *Adv. Mech. Eng.*, 8(4), 1–13.

Park, B. J., Song, K. H., and Choi, H. J. (2009). "Magnetic carbonyl iron nanoparticle based magnetorheological suspension and its characteristics." *Mater. Lett.*, 63(15), 1350–1352.

Park, E. J., Luz, L. F. F. da, and Suleman, A. (2008). "Multidisciplinary design optimization of an automotive magnetorheological brake design." *Comput. Struct.*, 86(3–5), 207–216.

Park, J., Yoon, G. H., Kang, J. W., and Choi, S. B. (2016). "Design and control of a prosthetic leg for above-knee amputees operated in semi-active and active modes." *Smart Mater. Struct.*, 25(8), 1–13.

Parlak, Z., Engin, T., and Çalli, I. (2012). "Optimal design of MR damper via finite element analyses of fluid dynamic and magnetic field." *Mechatronics*, 22(6), 890–903.

Parlak, Z., Engin, T., and Şahin, I. (2013). "Optimal magnetorheological damper configuration using the taguchi experimental design method." *J. Mech. Des. Trans. ASME*, 135(8), 1–9.

Patel, R. (2011). "Mechanism of chain formation in nanofluid based MR fluids." *J. Magn. Magn. Mater.*, 323(10), 1360–1363.

Phillips, R. W. (1969). "Engineering applications of fluids with a variable yield stress." *Theol. Today*, University of California, Berkeley.

Phule, P. P., and Ginder, J. M. (1998). "Materials science of field-responsive fluids." *MRS Bull.*, 23(8), 19–22.

Phulé, P. P., Mihalcin, M. P., and Genc, S. (1999). "Role of the dispersed-phase remnant magnetization on the redispersibility of magnetorheological fluids." *J. Mater. Res.*, 14(7), 3037–3041.

Piłat, A. (2004). "FEMLab Software Applied to Active Magnetic Bearing Analysis." *Int. J. Appl. Math. Comput. Sci.*, 14, 497–501.

Pisetskiy, S., and Kermani, M. R. (2018). "Development of MR Clutch for a Prospective 5 DOF Robot*." *IEEE/RSJ Int. Conf. Intell. Robot. Syst. Madrid*, 5900–5905.

Plachy, T., Kutalkova, E., Sedlacik, M., Vesel, A., Masar, M., and Kuritka, I. (2018). "Impact of corrosion process of carbonyl iron particles on magnetorheological behavior of their suspensions." *J. Ind. Eng. Chem.*, 66, 362-369.

Portillo, M. A., and Iglesias, G. R. (2017). "Magnetic Nanoparticles as a Redispersing Additive in Magnetorheological Fluid." *J. Nanomater.*, 2017.

Powell, L. A., Hu, W., and Wereley, N. M. (2013). "Magnetorheological fluid composites synthesized for helicopter landing gear applications." *J. Intell. Mater. Syst. Struct.*, 24(9), 1043–1048.

Poznic, A., Miloradovic, D., and Juhas, A. (2017). "A new magnetorheological brake`s combined materials design approach." *J. Mech. Sci. Technol.*, 31(3), 1119–1125.

Puneet, N. P., Hegale, A., Kumar, H., and Gangadharan, K. V. (2019). "Multi objective optimization of quarter car parameters for better ride comfort and road holding." *AIP Conf. Proc.*, AIP Publishing LLC, 20046.

Puneet, N. P., Srinivasa, P. P., and D'mello, G. (2015). "Optimization techniques in Turning–A review." *Manuf. Technol. Today*, 14(5), 3–21.

Rabbani, Y., Ashtiani, M., and Hashemabadi, S. H. (2015). "An experimental study on the effects of temperature and magnetic field strength on the magnetorheological fluid stability and MR effect." *Soft Matter*, 11(22), 4453–4460.

Rajamohan, V., Sedaghati, R., and Rakheja, S. (2009). "Vibration analysis of a multi-layer beam containing magnetorheological fluid." *Smart Mater. Struct.*, 19(1), 015013.

Rao, D. (2013). "Free B(H) & Core Loss Curves." *MagWeb USA*, http://magweb.us/free-bh-curves/ (May 30, 2019).

Rao, S. S. (2017). *Mechanical Vibrations*. *Pearson, Glob. Ed.*

Rosenfeld, N., and Wereley, N. M. (2002). "Behavior of magnetorheological fluids utilizing nanopowder iron." *nternational J. Mod. Phys. B,* 16(17), 2392–2398.

Rossa, C., Jaegy, A., Lozada, J. J., and Micaelli, A. (2014a). "Design considerations for magnetorheological brakes." *IEEE/ASME Trans. Mechatronics*, 19(5), 1669–1680.

Rossa, C., Jaegy, A., and Micaelli, A. (2014b). "Design Considerations for Magnetorheological Brakes." *IEEE/ASME Trans. MECHATRONICS*, 19(5), 1669–1680.

Sapiński, B., Pakuła, S., Snamina, J., and Romaszko, M. (2011). "Vibration parameters of sandwich beams with two types of MR fluid." *Mech. Control*, 30(3), 151–156.

Sapiński, B., Snamina, J., and Romaszko, M. (2010). "Identification of model parameters of a sandwich beam incorporating magnetorheological fluid." *XXIV Symp. Vib. Phys. Syst. Pozn. – Bedlewo*, 349–354.

Sarkar, C. (2015). "Shear Behavior of Magnetorheological Fluid and its effect on MR brake performance." *Int. J. Curr. Eng. Technol.*, 5(2), 1104–1108.

Sarkar, C., and Hirani, H. (2015). "Effect of Particle Size on Shear Stress of Magnetorheological Fluids." *Smart Sci.*, 3(2), 65–73.

Seid, S., Chandramohan, S., and Sujatha, S. (2018). "Optimal design of an MR damper valve for prosthetic knee application." *J. Mech. Sci. Technol.*, 32(6), 2959–2965.

Seung-Bok Choi, Y. M. H. (2013). *Magnetorhological Fluid Technology*. Boca Raton: CRC Press.

Shah, K., Upadhyay, R. V., and Aswal, V. K. (2012). "Influence of large size magnetic particles on the magneto-viscous properties of ferrofluid." *Smart Mater. Struct.*, 21(7), 075005.

Shamieh, H., and Sedaghati, R. (2016). "Design optimization of a magneto-rheological fluid brake for vehicle applications." *ASME 2016 Conf. Smart Mater. Adapt. Struct. Intell. Syst.*, American Society of Mechanical Engineers Digital Collection, V002T03A008.

Shamieh, H., and Sedaghati, R. (2017). "Multi-objective design optimization and control of magnetorheological fluid brakes for automotive applications." *Smart Mater. Struct.*, 26(12).

Sherman, S. G., and Wereley, N. M. (2013). "Effect of particle size distribution on chain structures in magnetorheological fluids." *IEEE Trans. Magn.*, 49(7), 3430–3433.

Shiao, Y., and Nguyen, Q. A. (2013). "Development of a multi-pole magnetorheological brake." *Smart Mater. Struct.*, 22(6), 65008.

Shin, D. K., Phu, D. X., Choi, S., and Choi, S. (2015). "An adaptive fuzzy sliding mode control of magneto-rheological seat suspension with human body model." *J. Intell.*

Mater. Syst. Struct., 27(7), 925–934.

Shivaram, A. C., and Gangadharan, K. V. (2007). "Statistical modeling of a magneto-rheological fluid damper using the design." *Smart Mater. Struct.*, 16(4), 1310–1314.

Singh, H. J., and Wereley, N. M. (2014). "Optimal control of gun recoil in direct fire using magnetorheological absorbers." *Smart Mater. Struct.*, 23(5).

Sohn, J. W., Gang, H. G., and Choi, S. B. (2018). "An experimental study on torque characteristics of magnetorheological brake with modified magnetic core shape." *Adv. Mech. Eng.*, 10(1), 1–8.

Sohn, J. W., Jeon, J., Nguyen, Q. H., and Choi, S.-B. B. (2015). "Optimal design of disc-type magneto-rheological brake for mid-sized motorcycle: Experimental evaluation." *Smart Mater. Struct.*, 24(8), 85009.

Song, W. L., Choi, S. B., Cai, Q. C., Choi, J. Y., and Lee, C. H. (2013). "Finishing performance of magneto-rheological fluid under magnetic field." *Mech. Adv. Mater. Struct.*, 20(7), 529–535.

Song, W. L., Choi, S. B., Choi, J. Y., and Lee, C. H. (2011). "Wear and friction characteristics of magnetorheological fluid under magnetic field activation." *Tribol. Trans.*, 54(4), 616–624.

Song, W., Wang, S., and Choi, S. (2018). "Thermal and Tribological Characteristics of a Disc-Type Magnetorheological Brake Operated by the Shear Mode." *J. Intell. Mater. Syst. Struct.*, 30(5), 722–733.

Spaggiari, A., Castagnetti, D., Golinelli, N., Dragoni, E., and Scirè Mammano, G. (2019). "Smart materials: Properties, design and mechatronic applications." *Proc. Inst. Mech. Eng. Part L J. Mater. Des. Appl.*, 233(4), 734–762.

Spelta, C., Previdi, F., Savaresi, S. M., Fraternale, G., and Gaudiano, N. (2009). "Control of magnetorheological dampers for vibration reduction in a washing machine." *Mechatronics*, 19(3), 410–421.

Srinivasa, N., Gurubasavaraju, T. M., Kumar, H., and Arun, M. (2020). "Vibration

analysis of fully and partially filled sandwiched cantilever beam with magnetorheological fluid." *J. Eng. Sci. Technol.*, 15(5), 3163–3177.

Sukhwani, V. K., and Hirani, H. (2007). "Synthesis and characterization of low cost magnetorheological (MR) fluids." *Proc. SPIE Behav. Mech. Multifunct. Compos. Mater.*, 65262R.

Sukhwani, V. K., and Hirani, H. (2008a). "A comparative study of magnetorheological-fluid-brake and magnetorheological-grease-brake." *Tribol. Online*, 3(1), 31–35.

Sukhwani, V. K., and Hirani, H. (2008b). "Design, development, and performance evaluation of high-speed magnetorheological brakes." *Proc. Inst. Mech. Eng. Part L J. Mater. Des. Appl.*, 222(1), 73–82.

Sun, Q., Zhou, J. X., and Zhang, L. (2003). "An adaptive beam model and dynamic characteristics of magnetorheological materials." *J. Sound Vib.*, 261(3), 465–481.

Thomas M Lewis. (2007). *Characterization of the Dynamic Mechanical Properties of Materials using the Vibrating Beam Technique*. Mishavaka Indiana.

Turczyn, R., Kciuk, M., Materials, F., and Technologies, P. (2008). "Preparation and Study of Model Magnetorheological Fluids." *J. Achivements Mater. Manuf. Eng.*, 27(2), 131–134.

Ulasyar, A., and Lazoglu, I. (2018). "Design and analysis of a new magneto rheological damper for washing machine." *J. Mech. Sci. Technol.*, 32(4), 1549–1561.

Utami, D., Mazlan, S. A., Imaduddin, F., Nordin, N. A., Bahiuddin, I., Aziz, A., and Choi, S. B. (2018). "Material characterization of a magnetorheological fluid subjected to long-term operation in damper." *Mater.*, 11(11), 2195

Vicente, J. De, Vereda, F., Segovia-gutiérrez, J. P., Puerto, M., and Hidalgo-álvarez, R. (2012). "Effect of particle shape in magnetorheology." *J. Rheol.*, 54(6), 1337-1362.

Wang, J., and Meng, G. (1948). "Magnetorheological fluid devices : principles , characteristics and applications in mechanical engineering." *Proc. Inst. Mech. Eng. Part L J. Mater. Des. Appl.*, 215(3), 165–175.

Wang, K., Dong, X., Li, J., Shi, K., and Li, K. (2019a). "Effects of silicone oil viscosity and carbonyl iron particleweight fraction and size on yield stress for magnetorheological grease based on a new preparation technique." *Materials (Basel).*, 12(11), 1778.

Wang, N., Liu, X., Królczyk, G., and Li, Z. (2019b). "Effect of temperature on the transmission characteristics of high-torque magnetorheological brakes." *Smart Mater. Struct.*, 28(5), 057002.

Wang, W., Xugang, H., Xiuyong, W., Jiali, W., Hongxin, S., and Song, G. (2018). "Mechanical behavior of magnetorheological dampers after long-term operation in a cable vibration control system." *Struct. Control Heal. Monit.*, 26(1), e2280.

Webb, G. M. (1998). "Exercise apparatus and associated method including rheological fluid brake." US patent 5810696.

Weiss, K. D., Carlson, J. D., and Nixon, D. A. (1994). "Viscoelastic properties of magneto- and electro-rheological fluids." *J. Intell. Mater. Syst. Struct.*, 5(6), 772–775.

Wereley, N. M., Chaudhuri, A., Yoo, J. H., John, S., Kotha, S., Suggs, A., Radhakrishnan, R., Love, B. J., and Sudarshan, T. S. (2006). "Bidisperse magnetorheological fluids using Fe particles at nanometer and micron scale." *J. Intell. Mater. Syst. Struct.*, 17(5), 393–401.

Wu, J., Hu, H., Li, Q., Wang, S., and Liang, J. (2020). "Simulation and experimental investigation of a multi-pole multi-layer magnetorheological brake with superimposed magnetic fields." *Mechatronics*, 65, 102314.

Wu, J., Pei, L., Xuan, S., Yan, Q., and Gong, X. (2016a). "Particle size dependent rheological property in magnetic fluid." *J. Magn. Magn. Mater.*, 408, 18–25.

Wu, W. P., Zhao, B. Y., Wu, Q., Chen, L. S., and Hu, K. A. (2006). "The strengthening effect of guar gum on the yield stress of magnetorheological fluid." *Smart Mater. Struct.*, 15(4), N94.

Wu, X. F., Xiao, X., Tian, Z. Z., and Chen, F. (2016b). "Study on the preparation

process and properties of magnetorheological fluid treated by compounding surfactants." *J. Magn.*, 21(2), 229–234.

Xu, Z.-D., Sha, L.-F., Zhang, X.-C., and Ye, H.-H. (2012). "Design, performance test and analysis on magnetorheological damper for earthquake mitigation." *Struct. Control Heal. Monit.*, 20(6), 956–970.

Xu, J., Li, J., and Cao, J. (2018). "Effects of fumed silica weight fraction on rheological properties of magnetorheological polishing fluids." *Colloid Polym. Sci.*, 296(7), 1145-1156.

Yalcintas, M., and Dai, H. (1999). "Magnetorheological and electrorheological materials in adaptive structures and their performance comparison." *Smart Mater. Struct.*, 8(5), 560.

Yalcintas, M., and Dai, H. (2003). "Vibration suppression capabilities of magnetorheological materials based adaptive structures." *Smart Mater. Struct.*, 13(1), 1.

Yang, G. (2002). "Large-scale MR fluid dampers : modeling and dynamic performance considerations." *Eng. Struct.*, 24(3), 309–323.

Yang, J., Yan, H., Wang, X., and Hu, Z. (2016). "Enhanced yield stress of magnetorheological fluids with dimer acid." *Mater. Lett.*, 167, 27–29.

Yeh, Z. F., and Shih, Y. S. (2006). "Dynamic characteristics and dynamic instability of magnetorheological material-based adaptive beams." *J. Compos. Mater.*, 40(15), 1333–1359.

Yoo, J.-H. H., and Wereley, N. M. (2002). "Design of a high-efficiency magnetorheological valve." *J. Intell. Mater. Syst. Struct.*, 13(10), 679–685.

Yoon, J. Y., Kang, B. H., Kim, J. H., Choi, S. B. (2020). "New control logic based on mechanical energy conservation for aircraft landing gear system with magnetorheological dampers." *J. Biomol. Struct. Dyn.*, 29(8), 084003.

Zainordin, A. Z., Abdullah, M. A., and Hudha, K. (2013). "Experimental Evaluations

on Braking Responses of Magnetorheological Brake." *Int. J. Mining, Metall. Mech. Eng.*, 1(3), 195–199.

Zhang, H. H., Liao, C. R., Chen, W. M., and Huang, S. L. (2006). "A magnetic design method of MR fluid dampers and FEM analysis on magnetic saturation." *J. Intell. Mater. Syst. Struct.*, 17(8–9), 813–818.

Zhang, J. Q., Zhang, J. Q., and Jing, Q. (2009). "Effect of seven different additives on the properties of MR fluids." *J. Phys. Conf. Ser.*, 149, 012086.

Zhang, Q., Liu, X., Ren, Y., Wang, L., and Hu, Y. (2016). "Effect of Particle Size on the Wear Property of Magnetorheological Fluid." *Adv. Mater. Sci. Eng.*, 2016, 1–8.

Zhang, X., Liu, X., Ruan, X., Zhao, J., and Gong, X. (2021). "The Influence of Additives on the Rheological and Sedimentary Properties of Magnetorheological Fluid." *Front. Mater. Sci.,* 7

Zhang, X. J., Farjoud, A., Ahmadian, M., Guo, K. H., and Craft, M. (2011). "Dynamic testing and modeling of an MR squeeze mount." *J. Intell. Mater. Syst. Struct.*, 22(15), 1717–1728.

Zhou, G. Y., and Wang, Q. (2005). "Magnetorheological elastomer-based smart sandwich beams with nonconductive skins." *Smart Mater. Struct.*, 14(5), 1001.

Zhou, G. Y., and Wang, Q. (2006). "Study on the adjustable rigidity of magnetorheological-elastomer-based sandwich beams." *Smart Mater. Struct.*, 15(1), 59–74.

Zhou, W., Chew, C., Hong, G., Zhou, W., Chew, C., and Hong, G. (2007). "Development of a compact double-disk magneto-rheological fluid brake." *Robotica*, 25(4), 493–500.

Zhu, C., Robb, D. A., and Ewins, D. J. (2001). "Magnetorheological fluid dampers for rotor vibration control." *19th 1 Am. Inst. Aeronaut. Astronaut. Appl. Aerodyn. Conf.*, 1469.

Zhu, W., Dong, X., Huang, H., and Qi, M. (2021). "Enhanced magnetorheological

effect and sedimentation stability of bimodal magnetorheological fluids doped with iron nanoparticles." *J. Intell. Mater. Syst. Struct.,* 32(12), 1271-1277.

Zuzhi, T., Fei, C., Xiangfan, W., and Jian, W. (2016). "A Novel Preparation Process for Magnetorheological Fluid with High Sedimentation Stability." *Mater. Manuf. Process.,* 31(15), 2030–2036.

Appendix I

1. Field Emission Scanning Electron Microscope (Make: Zeiss Sigma)
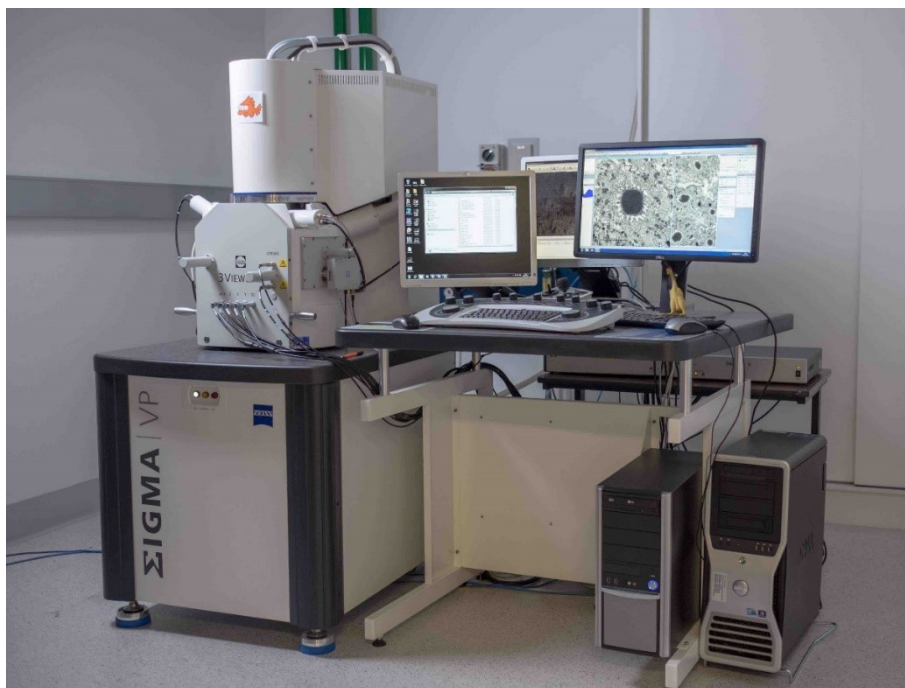
Parameter	Specification
Electron Source	Schottky Thermal Field Emitter
Resolution* at 30 kV (STEM)	1.0 nm
Resolution* at 15 kV	1.0 nm
Resolution* at 1 kV	1.6 nm
Resolution* at 30 kV (VP Mode)	2.0 nm
Maximum Scan Speed	50 ns/pixel
Accelerating Voltage	0.02 – 30 kV
Magnification	10× – 1,000,000×
Probe Current	3 pA - 20 nA (100 nA optional)
Image Framestore	32 k × 24 k pixels

2. Particle Size Analyzer (Make: Cilas 1064 Particle size analyzer)

Parameter	Specification
Particle size range	0.04 to 500 μm
Number of lasers	2
Laser source	Fiber and collimated laser diodes
Wavelength	635 and 830 nm
Power	3/7 mW
Beam diameter	2 and 20 mm
Repeatability	± 0.5 %
Reproducibility	< 2 %

3. Vibrating sample Magnetometer Make: Lakeshore 7407 ; System Software: Lakeshore Cryotronics Inc.

Parameter	Specification
Magnetic field measurement range	± 2.5 Tesla
Magnetic field accuracy	± 0.05 %
Magnetic field resolution	± 0.001 %
Sensitivity	10^{-7} emu

4. Electronic Weighing Balance

Parameter	Specification
Maximum capacity	1 Kg
Accuracy	0.1 gram
Power supply	230V AC, 50Hz

5. Mechanical Stirrer

Parameter	Specification
Max. stirring Capacity	5 litres
Speed range	50-1500 rpm
Power	10 watt
Supply voltage	220-240 V
Line frequency	50 Hz, single phase

6. Damper testing machine (Make: Heico)

- **Hydraulic power pack**

Parameter	Specification
Flow of the pump	64 LPM
Max. Operating Pressure	210 bar
Oil tank capacity	200 ltr.
Power rating of motor	40 HP
Length of hoses	5 m. (each)
Electric power supply	440V, 3 phase (AC supply)

- **Hydraulic actuator**

Parameter	Specification
Type	Double acting double ended
Capacity	+/- 20 kN
Stroke	150 mm (+/- 75 mm)
Max. working pressure	210 bar
Max. sustained velocity	0.8 m/s
Peak velocity	1.2 m/s
Servo valve	63 LPM
Pressure line filter	180 LPM with 3 microns filtration
Accumulator (2 No.)	0.36 ltr. capacity

- **Force transducer**

Parameter	Specification
Capacity	+/- 30 kN
Resolution	0.001 kN
Full scale output	2 mV/V
Excitation Voltage	10 Volts DC
Non-linearity	< +/- 0.15 % FSO
Safe overload	150 %
Operating temperature	0 to +60 deg. C
Accuracy	0.5% of indicated value as per ISO7500-1

- **Position sensor/ Displacement transducer**
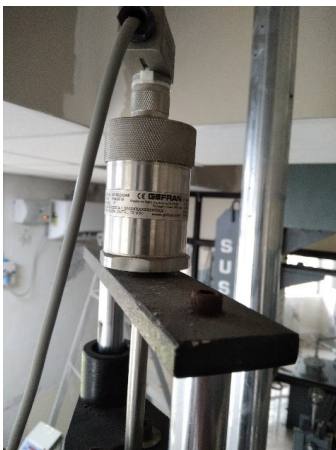
Parameter	Specification
Range	200 mm
Make	Gefran/Balluff
Full scale output	10 volts
Repeatability	<0.01 mm
Pressure withstand	Upto 600 bar
Excitation voltage	24 volts DC
Sampling rate	2 kHz
Operating temperature	-30 to +75 deg. C

- **Signal conditioning and controlling unit**

Specifications of controller

- Auto PID operation with auto zeroing, auto tuning and auto-adjustment feature servo operation.
- Digital signal processing (DSP) based closed loop servo controller with closed loop update rate of 10 kHz.
- Number of control channels - 4 (Load/Displacement/External channel strain 1 and strain2).
- Demand wave generation - Sine, Triangular, Square and ramp signal.
- High speed 32 bit data acquisition with 6 kHz sampling rate on all primary channels.
- Auto calibration and digital auto zero capability.

7. Rheometer
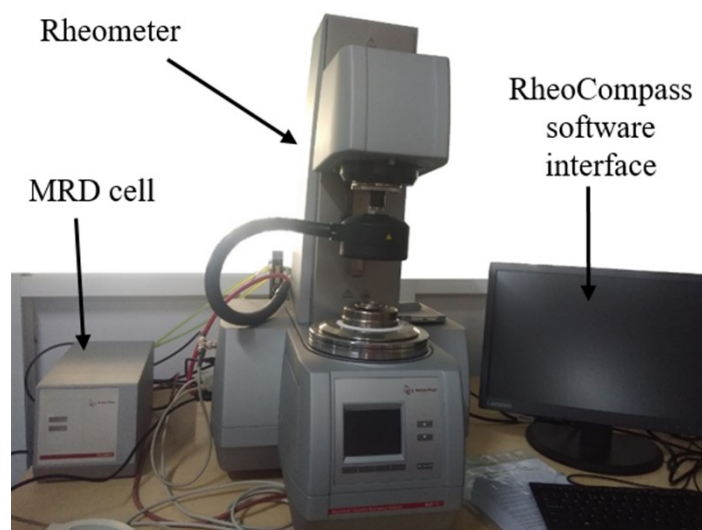
Parameter	Specification
Minimum torque, rotation	1 nNm
Maximum torque, rotation	230 mNm
Minimum torque, oscillation	0.5 nNm
Maximum angular frequency	628 rad/s
Normal force range	0.005 to 50 N
Maximum temperature range	160 to +1000 °C
Pressure range	up to 1000 bar
Rheometer Software RheoCompass^{TM} Professional	Running under Microsoft Windows 7/8/8.1/10 (64 bit versions only)
Magnetorheological Device Cell	Magnetic Flux density upto 1Tesla Temperature range -10 to 170°C
Hood With Peltier Heating/Cooling	Temperature range: -40 to 200 °C
Compressor	230/50 V/Hz, 55 l/min, OILFREE Motor Power: 0.55 kW Output (5 bar): 55 l/min max. Pressure: 8 bar Tank Volume: 10 l Weight: 59 kg Dimensions: 510x530x515 mm
Peltier Temperature Control Device	Temperature range: -5 to 200 °C
Power Supply Magneto Cell	230V HCP 14-12500,12.5,1 mA

8. Commercial MR Fluid, MRF 132 DG (Lord Corporation, USA)

Parameter	Specification
Appearance	Dark Gray Liquid
Viscosity, Calculated as slope 800-1200 sec-1 , Pa-s @ 40°C (104°F)	0.112 ± 0.02
Density, g/cm^3 (lb/gal)	2.95-3.15 (24.6-26.3)
Solids Content by Weight, %	80.98
Flash Point, °C (°F)	>150 (>302)
Operating Temperature, °C (°F)	-40 to +130 (-40 to +266)

9. DC Power supply (Make: Scientific Instruments, PSD3005 30V)

Parameter	Specification
DC output	0 to 30V / 5A
Settling resolution	V: 10 mV, I : 5 mA
Load Regulation	<= +/-(0.05% + 10 mV)
Input Supply	230 AC +/- 10% / 50-60 Hz
Internal resistance	<=10 milli Ohms

10. Torque Sensor : Make: Datum Electronics

Parameter	Specification
Range	0 Nm to 50 Nm
Accuracy	0.1%
Non-Linearity	0.1%
Repeatability	0.05%
Sample Rate	1 to 4000 samples per second
Operating Range	-10 to +70°C
Power Supply	10-24Vdc 250mA

Data Acquisition Device: DAQ for Torque sensor (Datum Electronics)

- Universal Torque Transducer Interface
- Power Supply 15-24V DC
- Calibrated Display of Torque in Nm or lb/ft
- Display of Speed (rpm) and Display of Power in kW or HP

11. Electric Motor

Make : Khalsa Foundry & Workshop, Kanpur
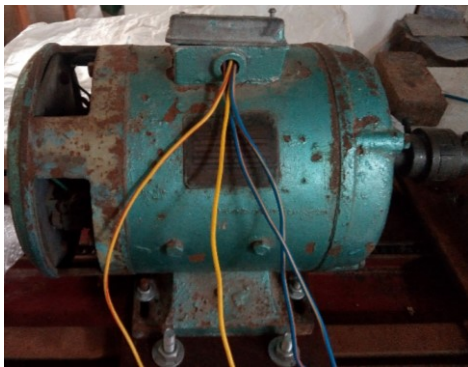
Parameter	Specification
Rated Power	3 hp
Rated Voltage	230 V DC
Max Current	12 A
Max speed	1440 rpm

12. Dimmerstat
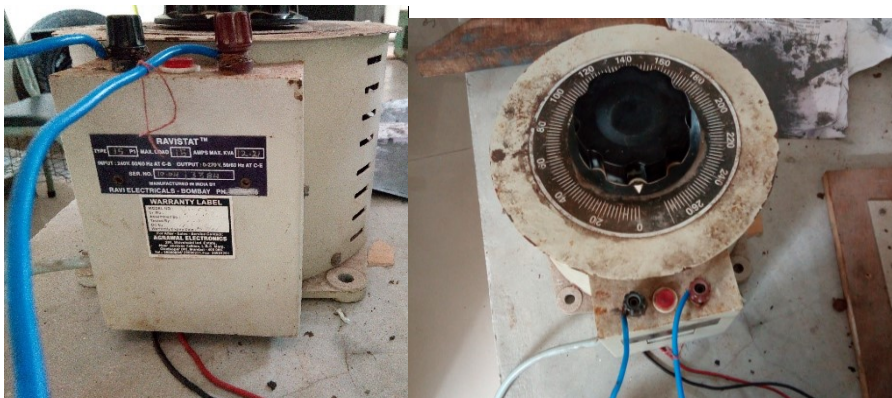
Make : Ravistat

Parameter	Specification
Rated Input voltage	230 V AC
Output Voltage range	0 – 260 V AC
Max Load	12.21 kVA
Max Current	15 A

13. NI 9234 C- series sound and vibration Input module IEPE

Parameter	Specification
IEPE channels	4 channel sound and
Resolution	24-bit resolution
Operational	±5 V, 0 to 20mA Input
Connectivity	BNC connectivity only
Sampling rate	51.2 kS/s

14. Wire cut electric discharge machine (Make: Concord United Pvt Ltd.)

Technical Specifications : Model name: DK7732VC	
	DK7732
Table Travel X,Y Axis (mm)	320 x 400
Work Table Size L x W (mm)	415 x 635
Maximum Work Piece Thickness (mm)	500
Maximum Work Piece Weight (kgs)	400
Machine Weight (kgs)	1800

Controller Specifications	
Display	LCD Display
Control System	CNC
PC	Industrial PC [#]
Axis Control	4 - axes (X,Y,U,V)
X, Y Axis Guide Ways	Linear motion guide ways for X, Y axis
Resolution	0.001 mm
Wire Dia	0.18mm (Std.)
Interpolation	Linear and Circular
Programming	Incremental
Least Input Increment	0.001 mm
Least Command Input	± 0.001mm
Data Input / Output System	USB Port , Regular Keyboard and Mouse; Can read AutoCAD .dxf format
Total Machine Load	1.5 KVA
Graphic Display	Graphic display of part showing wire position
Processing and Data Entry	Dual Screen, New programs can be entered while cutting previous programme
Dielectric Fluid	Soft water (D.M Water) + Gel
Dielectric Tank Capacity	55 Litres

15. Load cell (Force sensor)

Parameter	Specification
Force range	-50 lbf to 50 lbf
Threshold	0.001 lbf
Sensitivity	100 mV/lbf
Non-linearity	1% FSO
Natural frequency	70 kHz
Temperature range	-60 to 250 °F
Output voltage	5V (full scale)
Output Impedance	<100 Ω
Sensing element	Quartz
Sealing	Hermetic
Weight	19 grams

16. Function generator

Parameter	Specification
Number of channels	02
Signal types	Continuous, sweeping, burst, and modulation modes
Frequency range of Sinusoidal waveform	1 μHz to 25 MHz
Frequency counter	200 MHz counter with 6-digit resolution
Frequency resolution	1 μHz or 12 digits
Sweep time	1 ms to 500 s

17. Miniature accelerometer (Make: PCB Piezotronics; Model: 352A25)

Parameter	Specification
Sensitivity (± 15 %)	2.5 mV/g
Measurement Range	± 2000 g pk
Broadband Resolution (1 to 10,000 Hz)	0.01 g rms
Frequency Range (± 5 %)	1.0 to 10,000 Hz
Resonant Frequency	≥ 80 kHz
Temperature range	-54 to 121 °C
Mounting	Adhesive
Size	3.6 mm x 11.4 mm x 6.4 mm
Sensing element	Ceramic
Sealing	Epoxy
Weight	0.6 grams

LIST OF PUBLICATIONS

INTERNATIONAL JOURNALS

1) **Subash Acharya**, Saini, T. R. S., Sundaram, V., Kumar, H. (2020). "Selection of optimal composition of MR fluid for a brake designed using MOGA optimization coupled with magnetic FEA analysis", Journal of Intelligent Material Systems and Structures, Sage Publication, 1045389X20977905. **(SCI and Scopus Indexed, Impact factor: 2.41,Q1 Journal)** https://doi.org/10.1177/1045389X20977905

2) **Subash Acharya**, Tak Radhe Shyam Saini, Hemantha Kumar. (2019) "Determination of optimal magnetorheological fluid particle loading and size for shear mode monotube damper", Journal of the Brazilian Society of Mechanical Sciences and Engineering, Springer Publication. 41(10), 392. **(SCI and Scopus Indexed, Impact factor: 1.755, Q2 Journal)** https://doi.org/10.1007/s40430-019-1895-4

3) **Subash Acharya**, Vipin J. Allien, Puneeth N P, Hemantha Kumar. (2021) "Dynamic behavior of sandwich beams with different compositions of magnetorheological fluid core", International Journal of Smart and Nano Materials, Taylor & Francis Publication, 12(1), 88-106. (**SCIE and Scopus Indexed, Q2 Journal)** https://doi.org/10.1080/19475411.2020.1871104

4) **Subash Acharya** and Hemantha Kumar. (2019) "Investigation of Magneto-rheological Brake with Rotor of Combined magnetic and non-magnetic materials", SN Applied Sciences, Springer International Publishing, 1(9): 997. **(Scopus Indexed)** https://doi.org/10.1007/s42452-019-1029-8

5) **Subash Acharya**, Puneet N P, Rangaraj M Desai, Vishal Sundaram, Hemantha Kumar. "Synthesis, characterization and selection of optimal composition of Magnetorheological fluid for a Damper application", Proceedings of the Institution of Mechanical Engineers, Part L: Journal of Materials: Design and Applications, Sage Publication. **(Under Review) (SCI and Scopus Indexed, Impact factor: 2.311, Q2 Journal)**

CONFERENCE PROCEEDINGS

1) **Acharya, S.**, Saini, T. R. S., Kumar, H. (2019, October). "Optimal design and analyses of T-shaped rotor magnetorheological brake". First International Conference on Mechanical Power Transmission (ICMPT 2019), IIT Madras, Chennai, India, 11-13 July 2019. Published in IOP Conference Series: Materials Science and Engineering, (Vol. 624, No. 1, p. 012024), IOP Publishing. **(Scopus indexed)** https://doi.org/10.1088/1757-899X/624/1/012024

2) **Acharya, S.**, Tak, R. S. S., Singh, S. B., Kumar, H. (2020, March). "Characterization of magnetorheological brake utilizing synthesized and commercial fluid", International Mechanical Engineering Congress (IMEC-2019), National Institute of Technology, Tiruchirappalli, 29th Nov to 1st December, 2019. Published in Materials Today: Proceedings, (Vol. 46, No.19, p. 9419-9424) Elsevier Publisher. **(Scopus indexed)** https://doi.org/10.1016/j.matpr.2020.03.061
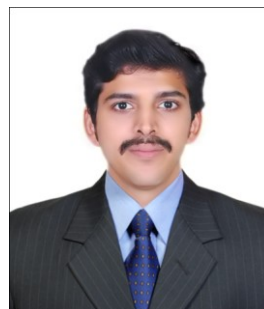
BIO-DATA

Name	SUBASH ACHARYA
Date of Birth	12-06-1983
Mobile Number	+91 8105760122
Email Id	subhashacharya12@gmail.com
Address	S/o Govinda Acharya, Govinda Nivas, D. No. 4-389, Hayagreeva Nagar, Near Indrali Bus-stop, Kunjibettu post, Udupi-576102.

Qualification

Degree	Institute/Board	Year	Percentage/CGPA
Ph.D (Course Work)	NITK, Surathkal	2016	8.92/10
M.Tech (Computer Aided Mechanical Design & Analysis)	MIT.Manipal	2006-2008	8.47/10
B.E. (Mechanical Engg.)	NMAMIT, Nitte	2001-2005	73.6 %

Experience

Sl. No.	Name of the Institute	Designation	From	To
1.	Manipal Institute of Technology, Manipal	Assistant Professor	2009	2014
2.	Manipal Institute of Technology, Manipal	Assistant Professor-Senior Scale	2014	Currently working

Journal Publications: 04

Conferences: 02